Numerical evaluation of Mellin-Barnes integrals in Minkowskian regions and their application to two-loop bosonic electroweak contributions to the weak mixing angle of the $\mathrm{Z}\bar{\mathrm{b}}\mathrm{b}$-vertex

Dissertation
zur Erlangung des akademischen Grades

doctor rerum naturalium
(Dr. rer. nat.)

im Fach Physik
Spezialisierung: Theoretische Physik

eingereicht an der
Mathematisch-Naturwissenschaftlichen Fakultät
der Humboldt-Universität zu Berlin

von
Herrn M.Sc. Johann Usovitsch

Präsident der Humboldt-Universität zu Berlin:
Prof. Dr.-Ing. Dr. Sabine Kunst

Dekan der Mathematisch-Naturwissenschaftlichen Fakultät:
Prof. Dr. Elmar Kulke

Gutachter/innen:

1. *Prof. Dr. Peter Uwer*
2. *Prof. Dr. habil. Johannes Blümlein*
3. *Prof. Dr. Charalampos Anastasiou*

Tag der mündlichen Prüfung: *29.05.2018*

Acknowledgements

I would like to thank Tord Riemann for the given opportunity to be part of a fruitful project, which is built up on a collaboration with great scientists including Ievgen Dubovyk, Ayres Freitas and Janusz Gluza. For the great support during the final stage of this work I would like to thank Bas Tausk and Peter Uwer.

My thanks belong to my wife Julia for the steady support in the last three years of my PhD and for providing me with the best self made tartlets and cakes. I would like to give thanks to my two little children Mara and Maxim whose appearance in my life gave me the biggest drive to accomplish this work. Also during the final stage of this work I was quite busy to take care of my newborn baby Mara and to organize the moving to a new country, while Maxim stayed very brave during this time. Due to these circumstances it would be impossible to finalize this work without the great support of my parents, Nataly Usovitsch and Sergey Usovitsch and in-laws, Petra Kaeding and Lothar Kaeding.

I greatly acknowledge the hospitality of DESY Zeuthen. I thank Peter Uwer and his group "Phenomenology of Elementary Particle Physics beyond the Standard Model" at Humboldt-Universität zu Berlin for providing computer resources. This work is supported by Graduiertenkolleg 1504 "Masse, Spektrum, Symmetrie" of Deutsche Forschungsgemeinschaft (DFG).

Abstract

In the Z-boson resonance physics several precision observables, like the mass and width of the Z-boson and the effective weak mixing angle for leptons and bottom quarks are in a perfect state, where the theory uncertainty is lower than the present experimental uncertainty. The ambitious concepts for the future colliders, like International Linear Collider (ILC), Future Circular Collider (FCC) or Circular Electron-Positron Collider (CEPC), aim for an improvement of measurements for the precision observables by one to two significant digits. This will put the Electroweak Standard Model predictions in a situation where complete two-loop corrections together with the leading three-loop corrections will become mandatory. The complete two-loop corrections for effective weak mixing angle for bottom quarks $\sin^2\theta^b_{\text{eff}}$ were reported recently, by providing the missing *bosonic* two-loop corrections. The difficult task in this computation is the calculation of the corresponding two-loop vertex Feynman integrals which include several massive particles. At present the analytic evaluation for most of these integrals is out of reach and purely numerical techniques were applied. Only two methods are known to extract infrared and ultraviolet singularities in a systematic way for a general Feynman integral with fully automatized algorithms. Namely the sector decomposition approach and the Mellin-Barnes integral approach. It was not known until recently how to treat Mellin-Barnes integral representations in Minkowskian regions numerically. To address this problem we introduce and discuss in detail a variety of one- and multi-dimensional techniques, which are part of a new program `MBnumerics.m` developed in this thesis work. As a result, the Mellin-Barnes integral representations of the two-loop vertex Feynman integrals can be evaluated numerically in Euclidean and Minkowskian regions with unprecedented accuracy. Furthermore the two techniques, sector decomposition and Mellin-Barnes integral approach, are complementary and together sufficient to treat electroweak two-loop corrections to the precision observables for the e^+e^- annihilation into two fermions at the Z-boson resonance. This leads to the most precise prediction at present for the effective weak mixing angle for bottom quarks: $\sin^2\theta^b_{\text{eff}} = 0.232312$.

Zusammenfassung

In der Z -Boson-Resonanzphysik sind mehrere Präzisionsobservablen, wie die Masse und Breite des Z -Bosons und der effektive schwache Mischungswinkel für Leptonen und bottom Quarks in einem perfekten Zustand, bei dem die theoretische Unsicherheit niedriger ist als die gegenwärtige experimentelle Unsicherheit. Die Konzepte für die zukünftigen Teilchenbeschleuniger, wie International Linear Collider (ILC), Future Circular Collider (FCC) oder Circular Electron-Positron Collider (CEPC), wollen eine Verbesserung der Messungen für die Präzisionsobservablen um ein bis zwei signifikante Stellen erreichen. Damit werden die Vorhersagen des elektroschwachen Standardmodells in eine Situation versetzt, in der vollständige Zweischleifenkorrekturen zusammen mit den führenden Dreischleifenkorrekturen obligatorisch werden. 2016 wurden die vollständigen Zweischleifenkorrekturen für den effektiven schwachen Mischungswinkel für die bottom Quarks $\sin^2\theta^b_{\text{eff}}$ berechnet, indem die fehlenden *bosonischen* Zweischleifenkorrekturen bereitgestellt wurden. Dabei liegt die Schwierigkeit in der Berechnung der entsprechenden Zwei-Schleifen Vertex-Feynman-Integrale, die mehrere massive Teilchen einschließen. Gegenwärtig ist die analytische Rechnung der meisten dieser Integrale schwierig deswegen werden rein numerische Techniken angewandt. Für ein allgemeines Feynman-Integral sind nur zwei Verfahren bekannt um Infrarot- und Ultraviolett-Singularitäten auf systematische Weise mit vollautomatisierten Algorithmen zu extrahieren. Das sind der Sektorzerlegungsansatz und der Integralansatz nach Mellin-Barnes. Es war bis vor kurzem nicht bekannt, wie Mellin-Barnes-Integraldarstellungen in den minkowskischen Integrationsgebieten numerisch behandelt werden können. Um dieses Problem anzugehen, stellen wir eine Vielzahl von ein- und mehrdimensionaler Techniken vor, die ein Teil des neuen Programms `MBnumerics.m` sind, welches in dieser Dissertation entwickelt wurde. Als Ergebnis können die Mellin-Barnes-Integraldarstellungen der Zwei-Schleifen Vertex-Feynman-Integrale numerisch in euklidischen und minkowskischen Integrationsgebieten mit einer hohen Genauigkeit ausgerechnet werden. Darüber hinaus sind der Sektorzerlegungsansatz und der Integralansatz nach Mellin-Barnes, komplementär und zusammen ausreichend, um elektroschwache Zweischleifenkorrekturen für die Präzisionsobservablen der Annihilation von e^+e^- in zwei Fermionen in der Z -Bosonresonanz auszurechnen. Aktuell führt dies zu der genauesten Vorhersage für den effektiven elektroschwachen Mischungswinkel für bottom Quarks $\sin^2\theta^b_{\text{eff}} = 0.232312$.

Contents

Chapter 1

Introduction

In this work we cover the so far unresolved subjects in the study of the Z-boson resonance in e^+e^- annihilation,

$$e^+e^- \to (\gamma, Z) \to \bar{f}f \ (+ n\gamma), \tag{1.1}$$

where f can be a lepton or quark, except the top quark. The writing (γ, Z) in Eq. (1.1) indicates an s-channel exchange of an intermediate photon γ or Z-boson. The symbol n stands for multiple photons in the final state of the reaction. This process has been analyzed with high precision at LEP 1 and SLC [1]. The mass and width of the Z-boson, $\tilde{M}_Z$ and $\tilde{\Gamma}_Z$ and the effective weak mixing angle for leptons $\sin^2\theta^l_{\text{eff}}$ and bottom quarks $\sin^2\theta^b_{\text{eff}}$, which are defined by the ratios of vector and axial couplings v_l, a_l and v_b, a_b of the Z-boson, are precisely measured.

The theoretical analysis is usually not based on cross sections as measured in reaction (1.1), including non-observed additional photons (and gluons), but on the so-called pseudo-observables, which correspond to the hard process

$$e^+(q_1)e^-(q_2) \to (\gamma, Z) \to \bar{f}(p_1)f(p_2). \tag{1.2}$$

For the theoretical prediction of the effective weak mixing angle at electroweak two-loop accuracy at the Z-boson resonance, as we will soon see, it is sufficient to study the simpler process

$$Z(k) \to \bar{f}(p_1)f(p_2). \tag{1.3}$$

In the Standard Model, the prediction of the effective weak mixing angle for leptons $\sin^2\theta^l_{\text{eff}}$ is known including the one-loop corrections $\mathcal{O}(\alpha)$ [2, 3], the complete two-loop corrections $\mathcal{O}(\alpha\alpha_s)$[4] and $\mathcal{O}(\alpha^2)$[5, 6, 7, 8, 9], as well as leading three loop [10, 11, 12] and four loop [13, 14, 15] results. Only the *fermionic* electroweak two-loop corrections [16] were known for the effective weak mixing angle for bottom quarks $\sin^2\theta^b_{\text{eff}}$. Where *fermionic* means diagrams with one or two closed fermion loops. The complete two-loop corrections for $\sin^2\theta^b_{\text{eff}}$ were reported recently in [17], by providing the missing *bosonic* two-loop corrections. At the Z-boson resonance, the theoretical prediction of the effective weak mixing angle for leptons $\sin^2\theta^l_{\text{eff}}$ is in perfect agreement with the experiment. The theoretical uncertainty is smaller than the experimental uncertainty. On the other hand the effective weak mixing angle

for bottom quarks $\sin^2\theta^b_{\text{eff}}$ shows a discrepancy to its Standard Model expectation, at the level of 2.8 standard deviations.

The study of Z-boson resonance physics is planned with a much improved precision at proposed future e^+e^- colliders: International Linear Collider (ILC)[18], Circular Electron-Positron Collider (CEPC)[19] or Future Circular Collider (FCC)[20]. The later mentioned, which is a 100 km circular collider, would deliver the highest integrated luminosities compared to the previous concepts. Conceptually the FCC is supposed to be run first in the FCC-ee mode which would deliver e^+e^- collisions to study the Z, W, and Higgs bosons, and the top quark, but also the bottom and charm quarks, and the tau lepton. The FCC-ee would become a new Z-factory, because the produced number of Z-bosons is envisaged to be up to 5×10^{12}, which would be almost six orders of magnitude larger than the number of Z-bosons collected at LEP, 2×10^7. If this collider is going to be realized, the Standard Model predictions will have to match the experimental uncertainties with an improvement of one-to-two orders of magnitude. Roughly speaking exact two-loop and leading three-loop vertex corrections will be needed.

This is in particular a problem for the electroweak predictions, which involve several particles with different non-negligible masses, because it becomes more and more difficult to find analytic solutions for their calculations with increasing order of perturbation theory or with increasing number of independent mass and momentum scales. Significant progress is made by considering numerical techniques. In this context we want to point out the recent developments in the sector decomposition technique [21, 22] and Mellin-Barnes integral approach [23, 24, 25, 26, 27]. To make predictions for electroweak observables, the Zff vertex in Z-boson resonance production, the calculations must be done in the Minkowskian regions. The sector decomposition technique may be used [28]. So far only for some rare classes of Feynman integrals the Mellin-Barnes integral approach could also be applied to integrals in Minkowskian regions [29]. In this thesis we cover the subject on how to treat Mellin-Barnes integrals in Minkowskian regions for a general class of Feynman integrals. We show that the sector decomposition and Mellin-Barnes integral approaches are complementary and well suited to calculate the *bosonic* two-loop electroweak predictions to the effective weak mixing angle for bottom quarks $\sin^2\theta^b_{\text{eff}}$.

This thesis is organized as follows. In Chap. 2 we introduce the electroweak sector of the Standard Model. Chap. 3 describes the Z-boson resonance physics tailored to the calculation of the effective weak mixing angle. In particular this chapter emphasizes that within the Electroweak Standard Model the prediction of the pseudo-observables relies on the calculation of two-loop vertex Feynman integrals. In Chap. 4 we cover in detail the loop-momenta representation and the Feynman parameter representation. We keep the notations used as general as possible. For example the notations for scalar Feynman integrals are extended to Feynman integrals with non-trivial numerators. It is then straightforward to introduce the sector decomposition technique in Chap. 5. We cover in Chap. 6 the construction of the Mellin-Barnes integrals by two different methods, the loop-by-loop approach and the global approach and recapitulate how to derive formally well defined Mellin-Barnes integrals by means of analytic continuation. In order to evaluate Mellin-Barnes integrals in Minkowksian regions we study in Chap. 7 the asymptotic behavior of Mellin-Barnes integrals. We find that it is worth to study the polynomial

asymptotic behavior of a Mellin-Barnes integral. In Chap. 8 we introduce and discuss in detail a variety of one- and multi-dimensional techniques, which are part of the new program `MBnumerics`, developed in this thesis. In Chap. 9 we cover the application of the sector decomposition technique and the Mellin-Barnes integral approach to selected examples stemming from the calculation of the *bosonic* electroweak two-loop vertex Feynman integrals, which show the strengths of both techniques. Finally we conclude with a summary and outlook in Chap. 10.

Chapter 2

The Electroweak part of the Standard Model

The Glashow-Salam-Weinberg [30, 31, 32] theory first realized the unification of the electromagnetic with the charged and neutral weak interactions which is now called the Electroweak Standard Model. It is a non-abelian gauge theory with the gauge group SU(2)×U(1). This theory includes the gauge coupling constants g_2 for the SU(2) related to the weak-isospin and g_1 for the U(1) related to the weak-hypercharge. The three generators of the weak-isospin are I^a, $a = 1, 2, 3$, the generator of the weak-hypercharge is Y. Furthermore, the Gell-Mann-Nishijima relation holds:

$$Q = I^3 + \frac{Y}{2}. \tag{2.1}$$

Fermionic part

The corresponding Lagrangian for the fermionic part is

$$\mathcal{L}_{\mathrm{F}} = \sum_i^3 \bar{L}_i^L i\gamma^\mu D_\mu L_i^L + \bar{Q}_i^L i\gamma^\mu D_\mu Q_i^L + \bar{l}_i^R i\gamma^\mu D_\mu l_i^R + \bar{u}_i^R i\gamma^\mu D_\mu u_i^R + \bar{d}_i^R i\gamma^\mu D_\mu d_i^R. \tag{2.2}$$

The left handed lepton and quark doublets are

$$L_i = \begin{pmatrix} \nu_i^L \\ l_i^L \end{pmatrix}, \quad Q_i^L = \begin{pmatrix} u_i^L \\ d_i^L \end{pmatrix}, \tag{2.3}$$

where $i = 1, 2, 3$ is the fermion generation index. Each symbol ν, l, u and d represents neutrinos, leptons, up-type quarks and down-type quarks respectively. The right handed fermion singlets are l^R, u^R and d^R. For a global gauge symmetry D_μ is the derivative ∂_μ with respect to x^μ.

Gauge part

Imposing the local gauge symmetry introduces additional gauge fields. The Lagrangian for the gauge fields reads

$$\mathcal{L}_{\mathrm{G}} = -\frac{1}{4}(\partial_\mu B_\nu - \partial_\nu B_\mu)^2 - \frac{1}{4}(\partial_\mu W_\nu^a - \partial_\nu W_\mu^a + g_2 \varepsilon^{abc} W_\mu^b W_\nu^c)^2, \tag{2.4}$$

where ε^{abc} are the antisymmetric structure constants of the SU(2) group: $[I^a, I^b] = i\varepsilon^{abc} I^c$. The gauge fields W^a_μ, $a = 1, 2, 3$, belong to the weak-isospin group SU(2) and the gauge field B_μ belongs to the weak-hypercharge group U(1). The symbol D_μ is now promoted to the covariant derivative which involves the interaction of the matter fields:

$$D_\mu = \partial_\mu - ig_2 I^a W^a + ig_1 \frac{Y}{2} B_\mu. \tag{2.5}$$

Higgs part

The gauge invariant Lagrangian for the complex scalar Higgs field $\Phi = (\phi^+, \phi^0)$ [33, 34, 35, 36, 37] is

$$\mathcal{L}_{\rm H} = (D_\mu \Phi)^\dagger (D^\mu \Phi) - V(\Phi), \tag{2.6}$$

where the Higgs potential is

$$V(\Phi) = -\mu^2 \Phi^\dagger \Phi + \frac{\lambda}{4} (\Phi^\dagger \Phi)^2. \tag{2.7}$$

The vacuum expectation value for the Higgs field is:

$$|\langle \Phi \rangle|^2 = \frac{2\mu^2}{\lambda} = \frac{v^2}{2}. \tag{2.8}$$

This non vanishing vacuum expectation value will introduce masses to the gauge bosons in the Standard Model within the covariant derivative in Eq. (2.5). We parameterize the Higgs field using

$$\Phi = \begin{pmatrix} \phi^+ \\ \frac{1}{\sqrt{2}}(v + H + i\chi) \end{pmatrix}, \quad \phi^- = (\phi^+)^\dagger, \tag{2.9}$$

this way the fields H, χ, $\phi^\pm$ have vanishing vacuum expectation value. The fields χ, ϕ^+, ϕ^- are would-be Goldstone fields, which are unphysical degrees of freedom and can be eliminated by the transition to the unitary gauge. The only remaining physical part is the Higgs boson H.

The physical content of the Electroweak Standard Model is most easily extracted in the unitary gauge, where $\phi^\pm = \chi = 0$. From the quadratic part of the Higgs potential the Higgs boson gets its mass $M_H = \sqrt{2}\mu$. The mass eigenstates of the physical gauge bosons are obtained by the mixing of the gauge fields belonging to the weak-isospin group SU(2) and the weak-hypercharge group U(1):

$$W^\pm_\mu = \frac{1}{\sqrt{2}} (W^1_\mu \mp i W^2_\mu), \tag{2.10}$$

and

$$\begin{pmatrix} A_\mu \\ Z_\mu \end{pmatrix} = \begin{pmatrix} c_w & -s_w \\ s_w & c_w \end{pmatrix} \begin{pmatrix} B_\mu \\ W^3_\mu \end{pmatrix}, \tag{2.11}$$

with

$$c_W \equiv \cos\theta_W = \frac{g_2}{\sqrt{g_1^2 + g_2^2}}, \tag{2.12}$$

$$s_W \equiv \sin\theta_W = \frac{g_1}{\sqrt{g_1^2 + g_2^2}}, \tag{2.13}$$

and the weak mixing angle θ_W. We identify the $W^{\pm}$-Boson, the Z-boson and the photon A. By requiring that the photon-fermion couplings equal those in Quantum Electrodynamics we can identify

$$e = \frac{g_1 g_2}{\sqrt{g_1^2 + g_2^2}} = g_2 s_W = g_1 c_W. \tag{2.14}$$

The masses of physical gauge bosons can then be written as:

$$M_W = \frac{ev}{2s_W}, \quad M_Z = \frac{M_W}{c_W}, \quad M_\gamma = 0. \tag{2.15}$$

It is possible to relate the fermion masses with the Yukawa couplings to the Higgs field:

$$\mathcal{L}_Y = -\sum_{i,j}^{3} \bar{L}_i^L G_{ij}^l l_j^R \Phi + \bar{Q}_i^L G_{ij}^u u_j^R \Phi^c + \bar{Q}_i^L G_{ij}^d d_j^R \Phi + h.c., \tag{2.16}$$

where the G_{ij} are the coupling constants and $\Phi^c = (\phi^{0*}, -\phi^-)$. Again due to the non vanishing vacuum expectation value of the Higgs field the fermion mass matrices can be written for leptons, up-type quarks and down-type quarks as

$$M_{ij}^l = \frac{G_{ij}^l v}{\sqrt{2}}, \quad M_{ij}^u = \frac{G_{ij}^u v}{\sqrt{2}}, \quad M_{ij}^d = \frac{G_{ij}^d v}{\sqrt{2}}. \tag{2.17}$$

These can be diagonalized by bi-unitary transformations with $U_{ik}^{f,L}$ and $U_{ik}^{f,R}$ for left-handed and right-handed fermion fields respectively, resulting in the fermion mass eigenstates

$$f'^L_i = \sum_k U_{ik}^{f,L} f_k^L, \quad f'^R_i = \sum_k U_{ik}^{f,R} f_k^R, \tag{2.18}$$

and the fermion masses,

$$m_{f,i} = \frac{1}{\sqrt{2}} \sum_{k,m} U_{ik}^{f,L} G_{km}^f U_{mi}^{f,R\dagger} v. \tag{2.19}$$

The matrices $U_{ik}^{f,L}$ and $U_{ik}^{f,R}$ drop out of the interaction terms between fermions and neutral gauge bosons, but in the quark-W-boson interaction terms a non-trivial quark-mixing matrix remains:

$$V = U^{u,L} U^{d,L\dagger}. \tag{2.20}$$

The complete Lagrangian can be written in terms of the classical fields, A_μ, Z_μ, $W_\mu^{\pm}$, H, l, ν, u, d, the would-be Goldstone fields $\phi^{\pm}$ and χ and the physical parameters describing the Standard Model e, M_W, M_Z, M_H, m_f and V :

$$\mathcal{L}_{Cl} = \mathcal{L}_F + \mathcal{L}_G + \mathcal{L}_H + \mathcal{L}_Y. \tag{2.21}$$

The quantization of the Electroweak Standard Model requires for higher order calculations the introduction of the gauge-fixing term and the Fadeev-Popov fields. Which together with a suitable gauge will ensure that the gauge-boson propagators behave as $1/k^2$ for large k^2. This gauge is called 't Hooft gauge, see for example [38].

Chapter 3

The Z-boson resonance

In the Z-boson resonance the Z-boson propagator is ill defined. The work around is to re-sum the selected self energy corrections [39]. Here the Z-boson propagator mixes with the photon propagator. The transverse parts of the renormalized two-point functions are put in the matrix

$$\Gamma^{VV'}(k^2) = i(G^{VV'})^{-1} = -\begin{pmatrix} k^2 + \Sigma^{AA}(k^2) & \Sigma^{AZ}(k^2) \\ \Sigma^{AZ}(k^2) & k^2 - M_Z^2 + \Sigma^{ZZ}(k^2) \end{pmatrix}. \tag{3.1}$$

The inversion of $\Gamma^{VV'}$ gives the re-summed propagator matrix

$$G^{VV'} = \begin{pmatrix} G^{AA} & G^{AZ} \\ G^{AZ} & G^{ZZ} \end{pmatrix}, \tag{3.2}$$

with

$$G^{AA} = \frac{i}{s + \Sigma^{AA} - \frac{(\Sigma^{AZ})^2}{s - M_Z^2 + \Sigma^{ZZ}}}, \tag{3.3}$$

$$G^{ZZ} = \frac{i}{s - M_Z^2 + \Sigma^{ZZ} - \frac{(\Sigma^{AZ})^2}{s + \Sigma^{AA}}}, \tag{3.4}$$

$$G^{AZ} = -\frac{\Sigma^{AZ}}{s + \Sigma^{AA}} G^{ZZ}. \tag{3.5}$$

and $s = k^2$. In the Z-boson resonance for $s \approx M_Z^2$ we may neglect the terms $(\Sigma^{AZ})^2$. In the on-shell scheme we require

$$\Re e\, \Sigma^{AZ}(M_Z^2) = 0, \quad \Re e\, \Sigma^{ZZ}(M_Z^2) = 0, \quad \frac{\mathrm{d}\Re e\, \Sigma^{ZZ}}{\mathrm{d}s}|_{s=M_Z^2} = 0. \tag{3.6}$$

Neglecting the fermion masses

$$\Im m\, \Sigma^{ZZ}(M_Z^2) = \frac{s}{M_Z^2} \Im m\, \Sigma^{ZZ}(M_Z^2), \tag{3.7}$$

together with the optical theorem

$$M_Z \Gamma_Z = \Im m\, \Sigma^{ZZ}(M_Z^2), \tag{3.8}$$

we derive the denominator of the Z-boson propagator for $s \approx M_Z^2$:

$$s - M_Z^2 + \Sigma^{ZZ} = s - M_Z^2 + i\Im m\, \Sigma^{ZZ} + \mathcal{O}((s - M_Z^2)^2) \tag{3.9}$$

$$\approx s - M_Z^2 + is\frac{\Gamma_Z}{M_Z}. \tag{3.10}$$

With this approximation the s-dependence of a cross section is parameterized by a Breit-Wigner function with a running (energy-dependent) width, $\sigma \propto ((s - M_Z^2)^2 + s^2\Gamma_Z^2/M_Z^2)^{-1}$. It has been shown in Ref. [40] that the approximation going from Eq. (3.9) to Eq. (3.10) leads to significant numerical effects, which need to be taken into account given the accuracy reached at LEP. This is achieved by the following manipulations:

$$s - M_Z^2 + is\frac{\Gamma_Z}{M_Z} = \left(1 + i\frac{\Gamma_Z}{M_Z}\right)\left(s - \frac{M_Z^2 - iM_Z\Gamma_Z}{1 + \frac{\Gamma_Z^2}{M_Z^2}}\right) \tag{3.11}$$

$$= \left(1 + i\frac{\Gamma_Z}{M_Z}\right)\left(s - \tilde{M}_Z^2 + i\tilde{M}_Z\tilde{\Gamma}_Z\right), \tag{3.12}$$

with

$$\tilde{M}_Z = \frac{M_Z}{\sqrt{1 + \frac{\Gamma_Z^2}{M_Z^2}}} \approx M_Z - \frac{\Gamma_Z^2}{2M_Z} = M_Z - 34\,\text{MeV}, \tag{3.13}$$

$$\tilde{\Gamma}_Z = \frac{\Gamma_Z}{\sqrt{1 + \frac{\Gamma_Z^2}{M_Z^2}}} \approx \Gamma_Z - \frac{\Gamma_Z^3}{2M_Z^2} = \Gamma_Z - 0.9\,\text{MeV}. \tag{3.14}$$

With this the s-dependence of the cross section becomes:

$$\sigma \propto ((s - \tilde{M}_Z^2)^2 + \tilde{\Gamma}_Z^2\tilde{M}_Z^2)^{-1}. \tag{3.15}$$

3.1 Pseudo-observables

The Born matrix element for the e^+e^- annihilation into two fermions has the form

$$\begin{aligned}\mathcal{M} = {} & \frac{e^2}{s}Q_eQ_f\bar{v}(q_1)\gamma^\mu u(q_2)\bar{u}(p_2)\gamma_\mu v(p_1) \\ & + \frac{e^2}{s - \tilde{M}_Z^2 + i\tilde{M}_Z\tilde{\Gamma}_Z}\bar{v}(q_1)(\gamma^\mu v_e^B - \gamma^\mu\gamma_5 a_e^B)u(q_2) \\ & \bar{u}(p_2)(\gamma_\mu v_f^B - \gamma_\mu\gamma_5 a_f^B)v(p_1).\end{aligned} \tag{3.16}$$

We include the Z-exchange, as well as the photon-exchange diagrams. The Z-boson propagator is used in the on-shell scheme. In the energy regime $s \approx \tilde{M}_Z^2$ we can neglect the light fermion masses in the final state and the differential cross section takes the form

$$\frac{\mathrm{d}\sigma^B}{\mathrm{d}\cos\vartheta} = \frac{\pi\alpha^2}{2s}c_f((1 + \cos^2\vartheta)G_1(s) + 2\cos\vartheta G_2(s)), \tag{3.17}$$

with

$$
\begin{aligned}
G_1(s) &= Q_e^2 Q_f^2 + 2Q_e Q_f v_e^B v_f^B \Re e\, \frac{s}{s-\tilde{M}_Z^2+i\tilde{M}_Z\tilde{\Gamma}_Z} \\
&\quad +(a_e^{B\,2}+v_e^{B\,2})(a_f^{B\,2}+v_f^{B\,2})\left|\frac{s}{s-\tilde{M}_Z^2+i\tilde{M}_Z\tilde{\Gamma}_Z}\right|^2, \qquad (3.18)\\
G_2(s) &= 2Q_e Q_f a_e^B a_f^B \Re e\, \frac{s}{s-\tilde{M}_Z^2+i\tilde{M}_Z\tilde{\Gamma}_Z} \\
&\quad +(2a_e^B v_e^B)(2a_f^B v_f^B)\left|\frac{s}{s-\tilde{M}_Z^2+i\tilde{M}_Z\tilde{\Gamma}_Z}\right|^2. \qquad (3.19)
\end{aligned}
$$

Symmetric or anti-symmetric integration over $\cos\vartheta$ allows to determine the two independent contributions related to G_1 and G_2. One of them is the total cross section,

$$
\begin{aligned}
\sigma_T^B &\equiv \int_{-1}^{1} d\cos\vartheta\, \frac{d\sigma^B}{d\cos\vartheta} \qquad (3.20)\\
&\overset{s\approx M_Z^2}{\approx} \frac{4\pi\alpha^2}{3s}c_f\left|\frac{s}{s-\tilde{M}_Z^2+i\tilde{M}_Z\tilde{\Gamma}_Z}\right|^2 \left(a_e^{B\,2}+v_e^{B\,2}\right)\left(a_f^{B\,2}+v_f^{B\,2}\right) \sim \Gamma_e^B\Gamma_f^B, \qquad (3.21)
\end{aligned}
$$

and the other one the forward-backward asymmetry,

$$
\begin{aligned}
\sigma_{FB}^B &\equiv \left[\int_0^1 - \int_{-1}^0\right] d\cos\vartheta\, \frac{d\sigma^B}{d\cos\vartheta} \qquad (3.22)\\
&\overset{s\approx M_Z^2}{\approx} \frac{\pi\alpha^2}{s}c_f\left|\frac{s}{s-\tilde{M}_Z^2+i\tilde{M}_Z\tilde{\Gamma}_Z}\right|^2 (2a_e^B v_e^B)\,(2a_f^B v_f^B), \qquad (3.23)\\
A_{FB}^B &\equiv \frac{\sigma_{FB}^B}{\sigma_T^B} = \frac{3}{4}\,\frac{2a_e^B v_e^B}{a_e^{B\,2}+v_e^{B\,2}}\,\frac{2a_f^B v_f^B}{a_f^{B\,2}+v_f^{B\,2}} \equiv \frac{3}{4}\,A_e^B\,A_f^B. \qquad (3.24)
\end{aligned}
$$

We observe the factorization of σ_T^B into the product of two partial widths,

$$
\Gamma_f^B = \frac{\alpha\tilde{M}_Z}{3}c_f\left(a_f^{B\,2}+v_f^{B\,2}\right), \qquad (3.25)
$$

and of A_{FB}^B into the product of two asymmetry parameters,

$$
A_f^B = \frac{2a_f^B v_f^B}{a_f^{B\,2}+v_f^{B\,2}}. \qquad (3.26)
$$

In Born approximation $a_f^B = \pm\frac{1}{2}$, $Q_e = -1$, c_f the color factor, and

$$
\frac{v_f^B}{a_f^B} = 1 - 4|Q_f|\sin^2\theta_W. \qquad (3.27)
$$

It is discussed in length how to relate pseudo-observables in a strict way to the loop corrections in Ref. [41, 42, 43, 44, 45, 46]. To include the electroweak corrections the most general ansatz is the matrix element with the four effective coupling

constants κ_e, κ_f, κ_{ef} and ρ_{ef} from [44], Eq. (3.3.1) therein:

$$\begin{aligned}\mathcal{M}_Z(s,\cos\vartheta) &= \frac{G_F a_e a_f \rho_{ef}(s,\cos\vartheta)\tilde{M}_Z^2\sqrt{2}}{s-\tilde{M}_Z^2+i\tilde{M}_Z\tilde{\Gamma}_Z}(L^\beta\otimes L_\beta \\ &\quad -4|Q_e|\sin^2\theta_W\kappa_e(s,\cos\vartheta)L^\beta\otimes\gamma_\beta \\ &\quad -4|Q_f|\sin\theta_W\kappa_f(s,\cos\vartheta)\gamma^\beta\otimes L_\beta \\ &\quad +16|Q_eQ_f|\sin^4\theta_W\kappa_{ef}(s,\cos\vartheta)\gamma^\beta\otimes\gamma_\beta), \end{aligned} \tag{3.28}$$

with

$$A^\beta\otimes B_\beta = (\bar{v}_e A^\beta u_e)(\bar{u}_f B_\beta v_f), \tag{3.29}$$

and

$$L_\beta = \gamma_\beta(1-\gamma_5). \tag{3.30}$$

We can rewrite the Eq. (3.28) in terms of the effective couplings $\bar{a}$, $\bar{v}$

$$\begin{aligned}\mathcal{M}_Z(s,\cos\vartheta) = \frac{G_F\rho_{ef}(s,\cos\vartheta)\tilde{M}_Z^2\sqrt{2}}{s-\tilde{M}_Z^2+i\tilde{M}_Z\tilde{\Gamma}_Z}&(\bar{a}_e\bar{a}_f\gamma^\beta\gamma_5\otimes\gamma_\beta\gamma_5-\bar{v}_e\bar{a}_f\gamma^\beta\otimes\gamma_\beta\gamma_5 \\ &-\bar{a}_e\bar{v}_f\gamma^\beta\gamma_5\otimes\gamma_\beta+\bar{v}_{ef}\gamma^\beta\otimes\gamma_\beta), \end{aligned} \tag{3.31}$$

with

$$\bar{a}_f = I_f^3, \tag{3.32}$$

$$\bar{v}_f = \bar{a}_f(1-4|Q_f|\sin^2\theta_W\kappa_f(s,\cos\vartheta)), \tag{3.33}$$

$$\bar{v}_{ef} = \bar{a}_e\bar{v}_f+\bar{v}_e\bar{a}_f-\bar{a}_e\bar{a}_f(1-16|Q_eQ_f|\sin^4\theta_W\kappa_{ef}(s,\cos\vartheta)), \tag{3.34}$$

or

$$\frac{\bar{v}_{ef}}{\bar{a}_e\bar{a}_f} = \frac{\bar{v}_e\bar{v}_f}{\bar{a}_e\bar{a}_f}+\Delta_{ef}, \tag{3.35}$$

$$\Delta_{ef} = 16|Q_eQ_f|\sin^4\theta_W(\kappa_{ef}-\kappa_e\kappa_f). \tag{3.36}$$

We get the Z-boson Born matrix element if we set, $\kappa=1$, $\rho_{ef}=4\cos^2\theta_W\sin^2\theta_W$ and $\bar{v}_{ef}=v_ev_f$, if the form factors $(\kappa_{ef}-\kappa_e\kappa_f)$ exactly cancel. Factorization $\bar{v}_{ef}=\bar{v}_e\bar{v}_f$ is broken by photonic corrections and by box diagrams, while it is respected by weak vertex corrections and self-energies. Note that the radiative corrections to the axial couplings are contained in ρ_{ef}, thus by construction the axial couplings remain Born like.

The form factors, as we have introduced them here may be used to define the effective Fermi constant and three effective weak mixing angles:

$$G_F^{\text{eff}} = \rho_{ef}(s,t)\,G_F, \tag{3.37}$$

$$\sin^2\theta_{W,e}^{\text{eff}} = \kappa_e(s,t)\,\sin^2\theta_W, \tag{3.38}$$

$$\sin^2\theta_{W,f}^{\text{eff}} = \kappa_f(s,t)\,\sin^2\theta_W, \tag{3.39}$$

$$\sin^2\theta_{W,ef}^{\text{eff}} = \sqrt{\kappa_{ef}(s,t)}\,\sin^2\theta_W, \tag{3.40}$$

where

$$\sin^2\theta_W \equiv 1-\frac{\tilde{M}_W^2}{\tilde{M}_Z^2}. \tag{3.41}$$

With the new effective amplitude we calculate next the $2 \to 2$ cross section. For unpolarized scattering one gets [42]:

$$\frac{d\sigma^{\rm eff}}{d\cos\vartheta} = \frac{\pi\alpha^2}{2s}\left(\frac{G_F^{\rm eff}\tilde{M}_Z^2}{\sqrt{2}2\pi\alpha}\right)^2 c_f\left[(1+\cos^2\vartheta)\bar{G}_1 + 2\cos\vartheta\bar{G}_2\right]. \tag{3.42}$$

Neglecting the photonic part the symmetric part depends on

$$\begin{aligned}\bar{G}_1 &= \left|\frac{s}{s-\tilde{M}_Z^2+i\tilde{M}_Z\tilde{\Gamma}_Z}\right|^2\left[|\bar{a}_e\bar{a}_f|^2+|\bar{v}_e\bar{a}_f|^2+|\bar{a}_e\bar{v}_f|^2+|\bar{v}_{ef}|^2\right] &(3.43)\\ &= \left|\frac{s}{s-\tilde{M}_Z^2+i\tilde{M}_Z\tilde{\Gamma}_Z}\right|^2|\bar{a}_e|^2|\bar{a}_f|^2\left[(1+|\frac{\bar{v}_e}{\bar{a}_e}|^2)(1+|\frac{\bar{v}_f}{\bar{a}_f}|^2)+\Delta_T\right], &(3.44)\end{aligned}$$

with

$$\Delta_T = |\Delta_{ef}|^2 + 2\Re e\left(\frac{\bar{v}_e}{\bar{a}_e}\frac{\bar{v}_f}{\bar{a}_f}\Delta_{ef}^*\right). \tag{3.45}$$

Assuming factorization $\bar{v}_{ef} = \bar{v}_e\bar{v}_f$, this becomes

$$\bar{G}_1 = \left|\frac{s}{s-\tilde{M}_Z^2+i\tilde{M}_Z\tilde{\Gamma}_Z}\right|^2\left[(|\bar{a}_e|^2+|\bar{v}_e|^2)(|\bar{a}_f|^2+|\bar{v}_f|^2)\right], \tag{3.46}$$

and finally, neglecting additionally the imaginary parts of $\bar{v}_e$ and $\bar{v}_f$ (and of Δ_T):

$$\bar{G}_1 = \left|\frac{s}{s-\tilde{M}_Z^2+i\tilde{M}_Z\tilde{\Gamma}_Z}\right|^2\left[(\bar{a}_e^2+\bar{v}_e^2)(\bar{a}_f^2+\bar{v}_f^2)\right]. \tag{3.47}$$

This is the formula usually applied to analyses.

Similarly, for the anti-symmetric cross section part:

$$\begin{aligned}\bar{G}_2 &= \left|\frac{s}{s-\tilde{M}_Z^2+i\tilde{M}_Z\tilde{\Gamma}_Z}\right|^2 2\bar{a}_e\bar{a}_f\Re e(\bar{v}_e\bar{v}_f^*+\bar{v}_{ef}) &(3.48)\\ &= \left|\frac{s}{s-\tilde{M}_Z^2+i\tilde{M}_Z\tilde{\Gamma}_Z}\right|^2\bar{a}_e^2\bar{a}_f^2\left(2\Re e\left[\frac{\bar{v}_e}{\bar{a}_e}\right]\,2\Re e\left[\frac{\bar{v}_f}{\bar{a}_f}\right]+\Delta_{FB}\right), &(3.49)\end{aligned}$$

with

$$\Delta_{FB} = 2\Re e\Delta_{ef}, \tag{3.50}$$

and after again neglecting non-factorizing terms and imaginary parts:

$$\bar{G}_2 = \left|\frac{s}{s-\tilde{M}_Z^2+i\tilde{M}_Z\tilde{\Gamma}_Z}\right|^2(2\bar{a}_e\bar{v}_e)\,(2\bar{a}_f\bar{v}_f). \tag{3.51}$$

For unpolarized particles the cross section formula in Eq. (3.42) is the exact result from the squared amplitude.

Assuming that the form factors κ_e, κ_f and κ_{ef} are independent of the scattering angle, we get for the total cross section and the forward-backward asymmetry in analogy to the Born approximation, see Eq. (3.20) and Eq. (3.22):

$$\sigma_T^{\text{eff}} = \frac{4\pi\alpha^2}{3s}\left(\frac{G_F^{\text{eff}}\rho_{ef}\tilde{M}_Z^2}{\sqrt{2}2\pi\alpha}\right)^2 c_f\bar{G}_1, \tag{3.52}$$

$$\sigma_{FB}^{\text{eff}} = \frac{\pi\alpha^2}{s}\left(\frac{G_F^{\text{eff}}\tilde{M}_Z^2}{\sqrt{2}2\pi\alpha}\right)^2 c_f\bar{G}_2, \tag{3.53}$$

$$A_{FB}^{\text{eff}} = \frac{\sigma_{FB}^{\text{eff}}}{\sigma_T^{\text{eff}}} = \frac{3}{4}\frac{\bar{G}_2}{\bar{G}_1}. \tag{3.54}$$

If the form factors κ_e, κ_f and κ_{ef} depend on the scattering angles, as it is the case for corrections from box diagrams, one has to study the numerical effect of that.

Since the ansatz in Eq. (3.28) is general, further observables may be introduced for polarized scattering, where the amplitude in Eq. (3.28) is taken between helicity projected states. More details may be found for example in Ref. [42].

In the following we give the definition for the asymmetry parameter A_f, see Eq. (3.26), this time containing the radiative corrections which are set in relation to the pseudo-observables containing the radiative corrections at $s \approx \tilde{M}_Z^2$, in terms of the angular integrals $\sigma_{FB}^{\text{eff}}, \sigma_T^{\text{eff}}$ as defined in (3.52) and (3.53):

$$A_{FB}^{\bar{f}f} = \frac{\sigma_{FB}^{\text{eff}}}{\sigma_T^{\text{eff}}} \tag{3.55}$$

$$\approx \frac{3}{4}\frac{\Re e[2\bar{a}_e\bar{v}_e\, 2\bar{a}_b\bar{v}_b + 4\sin^2\theta_W|Q_eQ_b|^2(\kappa_{eb} - \kappa_e\kappa_b)]}{|\bar{a}_e\bar{a}_b|^2 + |\bar{v}_e\bar{a}_b|^2 + |\bar{a}_e\bar{v}_b|^2 + |\bar{v}_{eb}|^2} \tag{3.56}$$

$$\approx \frac{3}{4}\frac{2\bar{a}_e\bar{v}_e}{\bar{a}_e^2 + \bar{v}_e^2}\frac{2\bar{a}_f\bar{v}_f}{\bar{a}_f^2 + \bar{v}_f^2} \tag{3.57}$$

$$= \frac{3}{4}\, A_e\, A_f. \tag{3.58}$$

From Eq. (3.55) to Eq. (3.56) we neglect the angular dependence of the form factors and from Eq. (3.56) to Eq. (3.57) we neglect the non-factorizable and imaginary parts.

According to its definition, A_f is a function of one variable only; for bottom quarks:

$$A_b \equiv \frac{2\Re e\,\frac{\bar{v}_b}{\bar{a}_b}}{1 + (\Re e\,\frac{\bar{v}_b}{\bar{a}_b})^2} \tag{3.59}$$

$$= \frac{1 - 4|Q_b|\sin^2\theta_{\text{eff}}^b}{1 - 4|Q_b|\sin^2\theta_{\text{eff}}^b + 8Q_b^2\left(\sin^2\theta_{\text{eff}}^b\right)^2}.$$

The so far best measurement is due to LEP 1 measurements [1]:

$$A_b = 0.899 \pm 0.013. \tag{3.60}$$

For the effective weak mixing angle, this corresponds to:

$$\sin^2\theta_{\text{eff}}^b = 0.281 \pm 0.016. \tag{3.61}$$

The experimental accuracy amounts to 5.7 %.

3.2 Pole-scheme

As discussed in detail in [5, 47], the Z-boson is unstable and cannot be described as an asymptotic state, and the decay process $Z \to f\bar{f}$ is ill defined in the usual formalism of perturbation theory. The idea is to consider the amplitude for $e^+e^- \to f\bar{f}$ near the Z-pole as a Laurent expansion around the complex pole $s_0 = m_Z^2 - im_Z\Gamma'_Z$

$$\mathcal{M}[e^+e^- \to f\bar{f}] = \frac{R}{s - s_0} + S + (s - s_0)S' + \ldots, \tag{3.62}$$

where m_Z and Γ'_Z are the pole mass and width of the Z-boson, respectively. This was studied in detail in [48, 49] and it has been shown that the coefficients $R, S, S', \ldots$ and the pole location s_0 are individually gauge-invariant, ultraviolet and infrared finite, when soft and collinear real photon and gluon emission is included. Furthermore, it can been shown, see for example Ref. [50], that the pole mass and and the width agree with the on-shell mass and width up to terms of $\mathcal{O}(\alpha^3)$ and $\mathcal{O}(\alpha^4)$ respectively. How one can construct cross sections to the process in Eq. (1.1) from the ansatz in Eq. (3.62) has been studied in Ref. [51, 52, 53]

3.3 Definition of the weak mixing angle at the next-to-next-to-leading order

In the energy region $s \approx m_Z^2$ near the Z-pole $(s - s_0)$, α and Γ'_Z are of the same order. For next-to-next-to-leading electroweak corrections we need to expand in Eq. (3.62) R up to α^2, S up to α and we need S' at tree level.

In the pole scheme the effective weak mixing angle $\sin^2\theta^f_{\text{eff}}$ is contained in the residue R in Eq. (3.62). The following notations for the vertices

$$\Gamma[Z_\mu f\bar{f}] = z_{f,\mu}(s) = i\gamma_\mu(v_f(s) + a_f(s)\gamma_5), \tag{3.63}$$
$$\Gamma[\gamma_\mu f\bar{f}] = g_{f,\mu}(s) = i\gamma_\mu(q_f(s) + p_f(s)\gamma_5), \tag{3.64}$$

are introduced, where we consider the one-particle irreducible loop contributions. The effect of $Z - \gamma$ mixing is given by:

$$\hat{z}_{f,\mu}(s) = i\gamma_\mu(\hat{v}_f(s) + \hat{a}_f(s)\gamma_5) \tag{3.65}$$
$$= i\gamma_\mu(v_f(s) + a_f(s)\gamma_5) - i\gamma_\mu(q_f(s) + p_f(s)\gamma_5)\frac{\Sigma_{\gamma Z}(s)}{s + \Sigma_{\gamma\gamma}(s)}, \tag{3.66}$$

With these definitions, the residue R up to next-to-next-to-leading order can be cast

into the form [5, 49]:

$$
\begin{aligned}
R = \; & z_e^{(0)}\, R_{ZZ}\, z_f^{(0)} + \left[\hat{z}_e^{(1)}(\tilde{M_Z}^2)\, z_f^{(0)} + z_e^{(0)}\, \hat{z}_f^{(1)}(\tilde{M_Z}^2)\right] \left[1 + \Sigma_{ZZ}^{(1)\prime}(\tilde{M_Z}^2)\right] \\
& + \hat{z}_e^{(2)}(\tilde{M_Z}^2)\, z_f^{(0)} + z_e^{(0)}\, \hat{z}_f^{(2)}(\tilde{M_Z}^2) + \hat{z}_e^{(1)}(\tilde{M_Z}^2)\, \hat{z}_f^{(1)}(\tilde{M_Z}^2) \\
& - i\tilde{M_Z}\Gamma_Z \left[\hat{z}_e^{(1)\prime}(\tilde{M_Z}^2)\, z_f^{(0)} + z_e^{(0)}\, \hat{z}_f^{(1)\prime}(\tilde{M_Z}^2)\right], \qquad (3.67) \\
R_{ZZ} = \; & 1 - \Sigma_{ZZ}^{(1)\prime}(\tilde{M_Z}^2) \\
& - \Sigma_{ZZ}^{(2)\prime}(\tilde{M_Z}^2) + \left(\Sigma_{ZZ}^{(1)\prime}(\tilde{M_Z}^2)\right)^2 + i\tilde{M_Z}\Gamma_Z\, \Sigma_{ZZ}^{(1)\prime\prime}(\tilde{M_Z}^2) \\
& - \frac{1}{\tilde{M_Z}^4}\left(\Sigma_{\gamma Z}^{(1)}(\tilde{M_Z}^2)\right)^2 + \frac{2}{\tilde{M_Z}^2}\, \Sigma_{\gamma Z}^{(1)}(\tilde{M_Z}^2)\, \Sigma_{\gamma Z}^{(1)\prime}(\tilde{M_Z}^2). \qquad (3.68)
\end{aligned}
$$

Here the Lorentz indices have been suppressed.

We come now back to the definition of the effective weak mixing angle:

$$
\sin^2\theta_{\text{eff}}^f \;\equiv\; \sin^2\theta_W\, \Re e\, \kappa_f = \frac{1}{4|Q_f|}\left(1 - \Re e\, \frac{\hat{v}_f}{\hat{a}_f}\right). \qquad (3.69)
$$

This means also

$$
\sin^2\theta_{\text{eff}}^f \;=\; \left(1 - \frac{\tilde{M}_W^2}{\tilde{M}_Z^2}\right)(1 + \Delta\kappa_f)\,. \qquad (3.70)
$$

Based on the definition of $\sin^2\theta_{\text{eff}}^f$ in Eq. (3.69), the electroweak effective weak mixing angle is derived from R as:

$$
\begin{aligned}
\sin^2\theta_{\text{eff}}^f \;&=\; \left(1 - \frac{\tilde{M}_W^2}{\tilde{M}_Z^2}\right) \Re e\,(1 + \Delta\kappa_Z^f(\tilde{M}_Z^2)) \qquad (3.71) \\
&=\; \left(1 - \frac{\tilde{M}_W^2}{\tilde{M}_Z^2}\right) \Re e\,(1 + \left.\frac{\hat{a}_f^{(1)} v_f^{(0)} - \hat{v}_f^{(1)} a_f^{(0)}}{a_f^{(0)}(a_f^{(0)} - v_f^{(0)})}\right|_{s=\tilde{M}_Z^2} \\
&+\; \left.\frac{\hat{a}_f^{(2)} v_f^{(0)} a_f^{(0)} - \hat{v}_f^{(2)}(a_f^{(0)})^2 - (\hat{a}_f^{(1)})^2 v_f^{(0)} + \hat{a}_f^{(1)}\hat{v}_f^{(1)} a_f^{(0)}}{(a_f^{(0)})^2(a_f^{(0)} - v_f^{(0)})}\right|_{s=\tilde{M}_Z^2}), \qquad (3.72)
\end{aligned}
$$

where the two-loop predictions are contained in the last line.

3.4 Renormalization

In this work we use the renormalization conditions which define the renormalized squared mass as the real part of the propagator poles. It has been shown in Ref. [54] that this definition yields a gauge invariant definition up to all orders in the perturbation theory. This definition equals to the on-shell scheme up to the terms of $\mathcal{O}(\alpha^3)$, which is used in the experimental analysis. The external fields are renormalized to unity at the position of the poles. The renormalization condition

for the electromagnetic charge is defined as the coupling strength of the electromagnetic vertex in the Thomson limit. The determination of the renormalization constants for the two-loop electroweak precision observables has been discussed in Ref. [55, 56, 57, 58, 59, 60, 61, 62]. All infrared divergences and collinear divergences in the calculation of the loop corrections drop out in the quantity $\sin^2\theta^f_{\rm eff}$.

3.5 Two-loop vertex Feynman diagrams

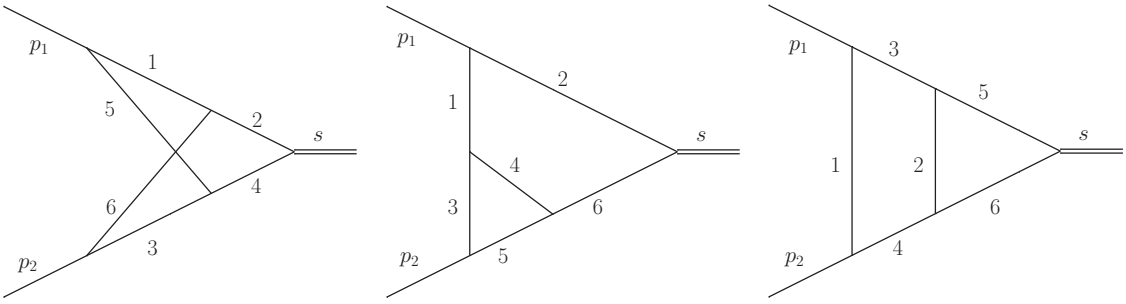

Figure 3.1: Two-loop vertex Feynman diagrams with 6 internal lines. The left figure with the two internal lines crossing each other is a non-planar Feynman diagram and the middle and the right figure are planar Feynman diagrams.

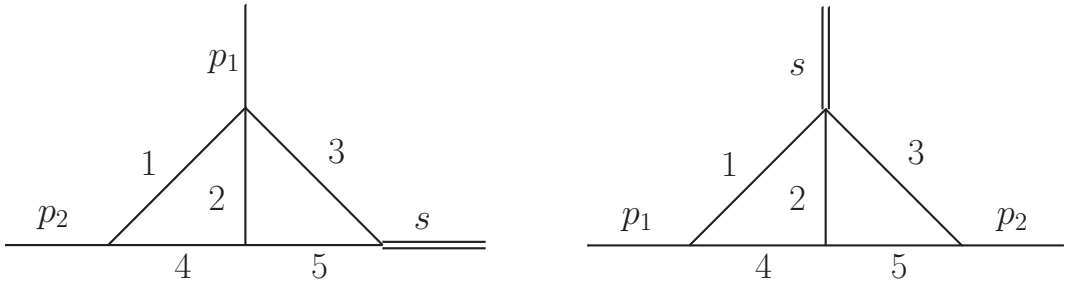

Figure 3.2: Two-loop planar vertex Feynman diagrams with 5 internal lines.

For the calculation of the next-to-next-to-leading electroweak corrections the Yukawa couplings and masses of all fermions but the top quark are neglected and the quark mixing matrix is assumed to be diagonal. In the determination of the *bosonic* electroweak two-loop corrections to $\sin^2\theta^b_{\rm eff}$ [17] the missing ingredient was the computation of *bosonic* two-loop vertex Feynman integrals including massive particles.

These Feynman integrals are projected with the following operators

$$\hat{v}_f(s) = \frac{1}{2(2-D)s}\mathrm{tr}(\gamma^\mu \not{p}_1 \hat{z}_{f,\mu}(s) \not{p}_2), \tag{3.73}$$

$$\hat{a}_f(s) = \frac{1}{2(2-D)s}\mathrm{tr}(\gamma_5\gamma^\mu \not{p}_1 \hat{z}_{f,\mu}(s) \not{p}_2), \tag{3.74}$$

Table 3.1: Reference values used in the numerical analysis, from Ref. [63].

Parameters	**Values**	**Ranges**
$\tilde{M}_Z$	91.1876 GeV	± 0.0042 GeV
$\tilde{\Gamma}_Z$	2.4952 GeV	
$\tilde{M}_W$	80.385 GeV	± 0.030 GeV
$\tilde{\Gamma}_W$	2.085 GeV	
$\tilde{M}_H$	125.1 GeV	± 5.0 GeV
$\tilde{m}_t$	173.2 GeV	± 4.0 GeV
$\alpha_{\rm s}$	0.1184	± 0.0050
$\Delta\alpha$	0.0590	± 0.0005

Table 3.2: Integrals with common mass scale dependence are grouped together.

Mass scales	**Integral classes**
$\tilde{M}_Z$	0h0w
$\tilde{M}_H$	xh0w
$\tilde{M}_H$, $\tilde{M}_W$	xhxw0z
$\tilde{M}_H$, $\tilde{M}_W$, $\tilde{M}_Z$	xhxwxz
$\tilde{M}_W$, $\tilde{m}_t$	0hxwxt0z
$\tilde{M}_W$, $\tilde{m}_t$, $\tilde{M}_Z$	0hxwxtxz

where $D = 4 - 2\epsilon$ is the space-time dimension and $p_{1,2}$ are the momenta of the external fermions. Here $\hat{v}_f(s)$ and $\hat{a}_f(s)$ are the vector and the axial components of the vertex $\hat{z}_{f,\mu}$. After the projection we end up with scalar Feynman integrals with non trivial scalar products in the numerator, depending on the loop-momenta. These integrals depend on the following invariants:

$$p_1^2 = 0, \tag{3.75}$$
$$p_2^2 = 0, \tag{3.76}$$
$$k^2 = 2p_1p_2 = s = \tilde{M}_Z^2, \tag{3.77}$$

and input parameters in Tab. 3.1. All external momenta p_1, p_2 and k are incoming. The calculation of the *bosonic* electroweak two-loop corrections depends on four mass scales. However, each Feynman integral depends at most on three different mass scales. In comparison to that the electroweak *fermionic* two-loop corrections [64] depend on the same number of mass scales, but contain no non-planar diagrams and less diagrams with six internal lines.

In this thesis we compute two-loop vertex Feynman integrals, see Fig. 3.1 and 3.2 in Minkowskian regions see Eq. (3.77) and Tab. 3.1. Feynman integrals which depend on the same mass scales are grouped together, see Tab. 3.2.

Chapter 4

Feynman integrals

First we define a loop-momenta representation for general scalar and tensor integrals and afterwards introduce the Feynman parameter representation. In this work the loop-momentum integral representation is used to define several integrals which we encounter in the integral classes defined in Tab. 3.2. The Feynman parameter representation is needed for the sector decomposition and Mellin-Barnes integral approach methods which are used to calculate these integrals. We demonstrate that it is possible to find a suitable Feynman parameter representation for a general tensor integral of any rank. Furthermore, we rescale all massive parameters by one mass scale.

4.1 loop-momentum integral representation

To fix the notations used in this work we start with a brief review of multi-loop integrals as encountered in perturbative calculations in quantum field theory. Applying within a concrete model the Feynman rules to calculate quantum mechanical scattering matrix elements leads to multi-loop tensor integrals of the form

$$G_L[T(k)] = \int \prod_{j=1}^{L} \frac{\mathrm{d}^D k_j}{i\pi^{D/2}} \, \frac{T(k)}{P_1^{\nu_1} \dots P_j^{\nu_j} \dots P_{N_G}^{\nu_{N_G}}}. \tag{4.1}$$

The numerator $T(k)$ is a tensor in the loop-momenta (integration variables):

$$T(k) = 1, k_l^\nu, k_l^\nu k_n^\mu, \dots. \tag{4.2}$$

The functions $P_j^{\nu_j}$ in the denominator are expressed in terms of the L loop-momenta k_l which are not fixed through momentum conservation at each vertex and the $E+1$ linearly independent external momenta p_e:

$$P_i = q_i^2 - m_i^2 + i\delta = \left(\sum_{l=1}^{L} a_{il} k_l + \sum_{e=1}^{E} b_{ie} p_e \right)^2 - m_i^2 + i\delta, \; a_{il}, \; b_{ie} \in \{-1, 0, 1\}, \tag{4.3}$$

where the m_i denote the masses of the corresponding virtual particles. The $i\delta$ is the Feynman prescription which we ignore for the sake of abbreviation and reconstruct or recall where needed.

Within dimensional regularization, $D = 4 - 2\epsilon$ denotes the dimension of space-time. As usual $D \neq 4$ is used to regularize infrared or ultraviolet divergences. Using projectors or a Feynman/Schwinger type parameterization the multi-loop tensor integrals can be reduced to scalar multi-loop integrals. The Feynman/Schwinger type parameterization will introduce scalar integrals with shifted dimensions and indices. The projectors will generate scalar integrals with auxiliary propagators, which represent irreducible scalar products in the numerator. The required number of auxiliary propagators is easily calculated. The number of scalar products involving the loop-momenta is given by

$$N = EL + \frac{L(L+1)}{2}. \tag{4.4}$$

However, N_G scalar products can be expressed in terms of linear combinations of the N_G propagators. The number of auxiliary propagators is thus given by $(N - N_G)$. The occurring integrals can thus be cast in the form

$$I(\nu_1, \ldots, \nu_{N_G}, \nu_{N_G+1}, \ldots, \nu_N) = \int \prod_{j=1}^{L} \frac{\mathrm{d}^D k_j}{i\pi^{D/2}} \frac{1}{P_1^{\nu_1} \ldots P_{N_G}^{\nu_{N_G}} P_{N_G+1}^{\nu_{N_G+1}} \ldots P_N^{\nu_N}}, \tag{4.5}$$

where the powers ν_i of the auxiliary propagators (i.e. $i = N_G + 1 \ldots N$) may only take non-positive values. Note that the auxiliary propagators $P_{N_G+1} \ldots P_N$ are not uniquely fixed. They are constrained only by the requirement that together with the first N_G propagators all scalar products involving the loop-momenta are expressible as linear combinations of the N propagators. We stress that in this notation scalar integrals refer to integrals which can also contain a scalar product or a propagator in the numerator. This of course differs from the usual notation where scalar integrals are referred to as loop-momentum integrals without a numerator. To avoid confusion we work with the definitions in Eq. (4.1) and Eq. (4.5).

Reducible and irreducible scalar products

In this work the projectors defined in Eq. (3.73) and in Eq. (3.74) generate two-loop vertex integrals with up to three scalar products in the numerator. We call a scalar product in the numerator reducible if it is a linear combination of the propagators in the denominator and can thus be canceled. An irreducible scalar product can not be expressed as a linear combination of the propagators.

Example After the application of the projectors one of the scalar two-loop integrals with one irreducible numerator is:

$$I_{\text{0h0w4}}(1,1,1,1,1,-1,0) = \int \frac{\mathrm{d}^D k_1}{i\pi^{D/2}} \frac{\mathrm{d}^D k_2}{i\pi^{D/2}} \frac{P_6^1}{P_1^1 P_2^1 P_3^1 P_4^1 P_5^1 P_7^0}. \tag{4.6}$$

The corresponding Feynman diagram is shown in Fig. 4.1. This integral has only 5 propagators left in the denominator after the proper cancellation of all reducible scalar products:

$$\begin{aligned} P_1 &= k_1^2, & P_4 &= (k_2 + p_1)^2 - \tilde{M}_Z^2 \\ P_2 &= (k_1 - k_2)^2, & P_5 &= (k_1 - p_2)^2, \\ P_3 &= k_2^2, \end{aligned} \tag{4.7}$$

where $P_6 = k_1 p_1$ is the irreducible scalar product in the numerator. We have added one additional auxiliary propagator $P_7 = (k_2 - p_2)^2$, to complete the definition of the scalar loop integral, note Eq. (4.4). In this work the auxiliary propagator will play a role as a technical trick, which will allow us to use the integration-by-parts identities [65, 66].

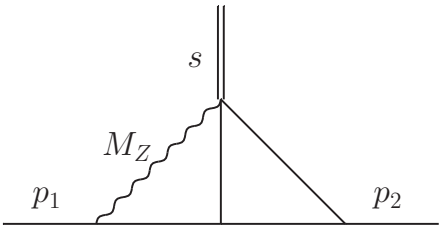

Figure 4.1: All external momenta are incoming and $p_1^2 = p_2^2 = 0$, $k^2 = s$. Wiggle line denotes massive particle. Simple solid lines represent massless particles. This Feynman diagram corresponds to the scalar Feynman integral $I_{\text{0h0w4}}(1,1,1,1,1,0,0)$.

4.2 General Feynman parameter representation

Using [67] and [68] we introduce the Feynman parameters:

$$\frac{(-1)^\nu}{\prod_{j=1}^{N}(-P_j)^{\nu_j}} = \frac{\mathcal{N}(\nu)}{\mathcal{D}^\nu}, \quad \nu = \sum_{j=1}^{N}\nu_j, \tag{4.8}$$

with the denominator function:

$$\mathcal{D} = \sum_{j=1}^{N} -x_j P_j = \sum_{j=1}^{N} x_j(-q_j^2 + m_j^2 - i\delta) = -k_l^\mu M_{ll'} k_{l'\mu} + 2k_l^\mu Q_{l\mu} + J - i\delta, \tag{4.9}$$

where

$$M_{ll'} = \sum_{j=1}^{N} a_{jl} a_{jl'} x_j, \tag{4.10}$$

is an $L \times L$ symmetric matrix,

$$Q_l^\nu = -\sum_{j=1}^{N} x_j a_{jl} \sum_{e=1}^{E} b_{je} p_e^\nu, \tag{4.11}$$

is a vector with L components and

$$J = -\sum_{j=1}^{N} x_j (\sum_{e=1}^{E} b_{je} p_e^\mu \sum_{e'=1}^{E} p_{e'}^\nu b_{je'} g_{\mu\nu} - m_j^2). \tag{4.12}$$

The coefficients a_{ij} and b_{ij} may take only the values $-1, 0, 1$ if we define the propagators like in Eq. (4.3). Also note that to each propagator P_j one Feynman parameter x_j is associated. The new numerator function reads

$$\mathcal{N}(\nu) = (-1)^{\nu}\Gamma(\nu)\left(\prod_{j=1}^{N}\tilde{n}_j\right)\delta(1-\sum_{j=1}^{N_G}x_j). \tag{4.13}$$

Note that for a multi-loop integral N and N_G may differ, see Eq. (4.5). Γ is the Euler's Γ-function. In this work it is convenient to define $\sum_{j=1}^{N_G} x_j$ as a function in the Feynman parameters x_j which are not associated with $\nu_j = -m$, $m \in \mathbb{N}_0$. If not stated otherwise we always respect this. The writing $\tilde{n}_j$ is defined as:

$$\tilde{n}_j[x_j]\phi(\vec{x}) = \begin{cases} \int\limits_{\{x_j\geq 0\}} \frac{\mathrm{d}x_j\, x_j^{\nu_j-1}}{\Gamma(\nu_j)}\phi(\vec{x}), & \nu_j \neq -m, \\ (-1)^{\nu_j}\phi^{(-\nu_j)}(0, x_{i\neq j}), & \nu_j = -m, \end{cases} \qquad m \in \mathbb{N}_0, \tag{4.14}$$

where $\phi^{-\nu_j}(0, x_{i\neq j})$ means to take $(-\nu_j)$ derivative in x_j and then set x_j to zero [69, 70].

Introducing the Feynman parameters the scalar integral becomes

$$G_L[1] = \int\left(\frac{\mathrm{d}^D k}{i\pi^{D/2}}\right)^L \frac{\mathcal{N}(\nu)}{\mathcal{D}^{\nu}}. \tag{4.15}$$

To perform the integration over the loop-momenta several small steps are involved.

Complete the square To complete the square we shift every loop-momentum $k_a^{\mu} = K_a^{\mu} + M_{ab}^{-1}Q_b^{\mu}$ which yields, where we use the translational invariance of the D-dimensional loop integral:

$$\mathcal{D} = -K_l^{\mu}M_{ll'}K_{l'\mu} + Q_l^{\mu}M_{ll'}^{-1}Q_{l'\mu} + J. \tag{4.16}$$

Diagonalizing M In a multi-loop case we need to disentangle the loop-momenta in the denominator $\mathcal{D}$ such, that $\mathcal{D}$ is linear in the loop-momenta squared. M is real and symmetric, thus we can diagonalize it $M = PDP^{-1} = PDP^T$, where P is an orthogonal matrix. $K_l^{\mu}M_{ll'}K_{l'\mu}$ is cast into $\tilde{K}_l^{\mu}D_{ll'}\tilde{K}_{l'\mu}$ with $\tilde{K}_l^{\mu} = P_{ll'}K_{l'}^{\mu}$ and $\tilde{K}_{l\mu} = P_{l'l}^T K_{l'\mu}$.

Wick rotation Later we use the integral representation of the Euler's Beta-function to perform the loop-momentum integral. Performing a Wick rotation (which is dictated by the Feynman prescription $i\delta$)

$$\int\frac{\mathrm{d}^D\tilde{K}}{i}f(-\tilde{K}) = \int\mathrm{d}^D\hat{K}f(\hat{K}), \tag{4.17}$$

and the scalar integral becomes

$$G_L[1] = \int \prod_{j=1}^{L} \frac{\mathrm{d}^D \hat{K}_j}{\pi^{D/2}} \frac{\mathcal{N}(\nu)}{\hat{\mathcal{D}}^\nu}, \tag{4.18}$$

$$\hat{\mathcal{D}} = \hat{K}_l^2 \lambda_l + Q_l^\mu M_{ll'}^{-1} Q_{l'\mu} + J, \quad \hat{K}_l^2 \lambda_l = \hat{K}_l^\mu D_{ll'} \hat{K}_{l'\mu}, \tag{4.19}$$

where λ_l are the eigenvalues of the matrix M.

Spherical coordinates Finally we transform the D-dimensional loop-momenta to spherical coordinates

$$\hat{K}_0 = R\cos\theta_1, \tag{4.20}$$

$$\hat{K}_1 = R\sin\theta_1\cos\theta_2, \tag{4.21}$$

$$\ldots, \tag{4.22}$$

$$\hat{K}_{D-2} = R\sin\theta_1 \ldots \sin\theta_{D-2}\cos\theta_{D-1}, \tag{4.23}$$

$$\hat{K}_{D-1} = R\sin\theta_1 \ldots \sin\theta_{D-2}\sin\theta_{D-1}, \tag{4.24}$$

where we get one radial component R, $D-2$ polar angles θ_j $(1 \leq j < D-2)$ and one azimuthal angle θ_{D-1}. The measure becomes:

$$\int \mathrm{d}^D \hat{K} = \int_0^\infty R^{D-1} \mathrm{d}R\, \mathrm{d}\Omega_D, \tag{4.25}$$

$$\int \mathrm{d}\Omega_D = \frac{2\pi^{D/2}}{\Gamma(D/2)}. \tag{4.26}$$

The advantage of this transformation is that we get a finite integration region times an analytic function in D. With $2R\mathrm{d}R = \mathrm{d}R^2$ the scalar integral is written as

$$G_L[1] = \int_0^\infty \frac{\mathrm{d}R_1^2 (R_1^2)^{(D-2)/2}}{\Gamma(D/2)} \cdots \int_0^\infty \frac{\mathrm{d}R_L^2 (R_L^2)^{(D-2)/2}}{\Gamma(D/2)} \frac{\mathcal{N}(\nu)}{(R_l^2\lambda_l + Q_l^\mu M_{ll'}^{-1} Q_{l'\mu} + J)^\nu}. \tag{4.27}$$

Euler's Beta-function The integration over the R_l^2 is an iterative application of the integral representation of Euler's Beta-function:

$$B(x,y) = \int_0^\infty \frac{t^{x-1}}{(1+t)^{x+y}} \mathrm{d}t, \quad \Re e\, x > 0,\ \Re e\, y > 0 \tag{4.28}$$

which can be expressed in terms of Euler's Γ-functions:

$$B(x,y) = \frac{\Gamma(x)\Gamma(y)}{\Gamma(x+y)}. \tag{4.29}$$

In the first iteration we recognize the integral representation of Euler's Beta-function with the substitution $t = R_1^2 / \left(\sum_{l \neq 1} \frac{R_l^2 \lambda_l}{\lambda_1} + \frac{Q_l^\mu M_{ll'}^{-1} Q_{l'\mu} + J}{\lambda_1} \right)$:

$$G_L[1] = \int_0^\infty \prod_{l=2}^{L} \frac{\mathrm{d}R_l^2 (R_l^2)^{(D-2)/2}}{\Gamma(D/2)} \frac{\Gamma(\nu - D/2)\mathcal{N}(\nu)}{\Gamma(\nu)\lambda_1^\nu \left(\sum_{l \neq 1} \frac{R_l^2 \lambda_l}{\lambda_1} + \frac{Q_l^\mu M_{ll'}^{-1} Q_{l'\mu} + J}{\lambda_1} \right)^{\nu - D/2}}. \tag{4.30}$$

The last Lth iteration yields the Feynman parameter integral we have sought for:

$$G_L[1] = \frac{\mathcal{N}(\nu)\Gamma(\nu - LD/2)}{\Gamma(\nu)(\prod_{l=1}^{L} \lambda_l)^{D/2} \left(Q_l^\mu M_{ll'}^{-1} Q_{l'\mu} + J - i\delta \right)^{\nu - LD/2}}. \tag{4.31}$$

Symanzik Polynomials We recognize in Eq. (4.31) $\prod_{l=1}^{L} \lambda_l = \det M$. The Feynman parameter representation of the scalar integral is:

$$G_L[1] = (-1)^\nu \Gamma(\nu - LD/2) \left(\prod_{j=1}^{N} \tilde{n}_j \right) \delta(1 - \sum_{j=1}^{N_G} x_j) \frac{\mathcal{U}^{\nu - (L+1)D/2}}{\mathcal{F}^{\nu - LD/2}}, \tag{4.32}$$

where

$$\mathcal{U} = \det M, \tag{4.33}$$
$$\mathcal{F} = \mathcal{U}(Q_l^\mu M_{ll'}^{-1} Q_{l'\mu} + J - i\delta). \tag{4.34}$$

From these definitions it follows that the functions $\mathcal{F}$ and $\mathcal{U}$ are homogeneous in the Feynman parameters x_i. The function $\mathcal{U}$ is of degree L and the function $\mathcal{F}$ is of degree $L+1$ (remember the definition of M, Q and J in Eqs. (4.10, 4.11, 4.12)). The functions $\mathcal{U}$ and $\mathcal{F}$ are also known as Symanzik polynomials.

4.3 Homogeneous functions

Like in Ref. [68] we have explicitly derived a Feynman parameter integrand to be homogeneous in the Feynman parameters if we ignore for now the δ-function:

$$G_L[1] = \left(\prod_{j=1}^{N} \tilde{n}_j \right) G_L(\vec{x}) \delta(1 - \sum_{j=1}^{N_G} x_j), \tag{4.35}$$
$$\text{degree} \prod_{j=1}^{N_G} \mathrm{d}x_j = N_G, \tag{4.36}$$
$$\text{degree} \prod_{j=1}^{N_G} x_j^{\nu_j - 1} = \nu - N_G, \tag{4.37}$$
$$\text{degree}\, \mathcal{U}^{\nu - (L+1)D/2} = L(\nu - (L+1)D/2) = L\nu - L^2 D/2 - LD/2, \tag{4.38}$$
$$\text{degree}\, 1/\mathcal{F}^{\nu - LD/2} = -(L+1)(\nu - LD/2) = -\text{degree}\, \mathcal{U}^{\nu - (L+1)D/2} - \nu, \tag{4.39}$$

which leads to

$$\text{degree}\left(\prod_{j=1}^{N}\tilde{n}_j\right)G_L(\vec{x})=0. \tag{4.40}$$

This is very convenient because it will give us a self consistency check for the derived Feynman parameter representations of tensor Feynman integrals $G_L(T(k))$, in addition it provides the possibility to use the methods of projective space, see for example a similar application also in Ref. [71]. We derive Mellin-Barnes integral representations by exploiting the possibility of applying the so called Cheng-Wu theorem see Ref. [72, 73, 74], which relies on the Eq. (4.40).

Example

Applieng Eq. (4.9) to the integral I_{0h0w4} in Eq. (4.6) we obtain:

$$\begin{aligned}\mathcal{D}_{\text{0h0w4}} &= -k_1^2x_1-k_1^2x_2+2k_1k_2x_2-k_2^2x_2-k_2^2x_3-k_2^2x_4+\tilde{M}_Z^2x_4\\ &\quad -2k_2p_1x_4-k_1^2x_5+2k_1p_2x_5-k_1p_1x_6,\end{aligned} \tag{4.41}$$

where we have already used $p_1^2=0$, $p_2^2=0$ and $2p_1p_2=s$. The symmetric 2 times 2 matrix M becomes:

$$M_{11} = x_1+x_2+x_5, \tag{4.42}$$
$$M_{12} = M_{21}=-x_2, \tag{4.43}$$
$$M_{22} = x_2+x_3+x_4. \tag{4.44}$$

The vector Q of length 2 is:

$$Q_1=p_2x_5-p_1x_6/2,\quad Q_2=-p_1x_4. \tag{4.45}$$

The scalar J is:

$$J=\tilde{M}_Z^2x_4. \tag{4.46}$$

The Feynman parameter integral representation for the integral I_{0h0w4} reads

$$I_{\text{0h0w4}}[1]=(-1)^4\Gamma(4-D)\left(\prod_{j=1}^{7}\tilde{n}_j\right)\delta(1-\sum_{j=1}^{5}x_j)\frac{\mathcal{U}_{\text{0h0w4}}^{4-3D/2}}{\mathcal{F}_{\text{0h0w4}}^{4-D}}, \tag{4.47}$$

with the Symanzik graph polynomials in Eq. (4.33) and Eq. (4.34) are now

$$\mathcal{U}_{\text{0h0w4}} = x_1x_2+x_1x_3+x_2x_3+x_1x_4+x_2x_4+x_2x_5+x_3x_5+x_4x_5, \tag{4.48}$$
$$\mathcal{F}_{\text{0h0w4}} = \tilde{M}_Z^2x_4\mathcal{U}_{\text{0h0w4}}-sx_2x_4x_5-\frac{s}{2}(x_6x_2x_5+x_6x_3x_5+x_6x_4x_5). \tag{4.49}$$

Note if x_6 is set to zero we simply get the corresponding $\mathcal{F}$ and $\mathcal{U}$ functions for a scalar integral I_{0h0w4} without the scalar product (k_1p_1) in the numerator.

4.4 Rescaling

J depends on the masses of the particles and the kinematic invariants of a Feynman diagram, Q depends on the external momenta, thus the $\mathcal{F}$ function depends on a mass scale. At this point it is straightforward to rescale all massive parameters in a Feynman integral by one mass scale. In this thesis work we rescale all massive input parameters, see Tab. 3.1 by $\tilde{M}_Z^2$, which leads to the definition of new input parameters:

$$\begin{aligned} x &= s/\tilde{M}_Z^2 + i\,\delta = 1 + i\,\delta, \\ M_Z &= \tilde{M}_Z/\tilde{M}_Z = 1, \\ M_W &= \tilde{M}_W/\tilde{M}_Z = 401925/455938, \\ m_t &= \tilde{m}_t/\tilde{M}_Z = 433000/227969, \\ M_H &= \tilde{M}_H/\tilde{M}_Z = 312750/227969. \end{aligned} \tag{4.50}$$

Here we have used the kinematics defined in Eq. (3.77). If we take for example the $\mathcal{F}_{\text{0h0w4}}$ function in Eq. (4.49) we see that $\tilde{M}_Z^2 > 0$ and $s > 0$. Thus we explicitly attach the Feynman prescription $i\delta$ to the mass scale s. This is true for all integrals shown in Tab. 3.2.

Calculating the two-loop vertex Feynman integrals in the new input parameters instead of in the original input parameters, see Tab. 3.1, an additional pre factor must be taken into account:

$$I(\tilde{M}_Z, \tilde{M}_W, \tilde{M}_H, \tilde{m}_t, s) = (\tilde{M}_Z^2)^{D-\nu} I(M_Z, M_W, M_H, m_t, x), \tag{4.51}$$

where I is a two-loop Feynman integral with the same ν as in $(\tilde{M}_Z^2)^{D-\nu}$.

4.5 Feynman parameter representation for tensor integrals

To derive the Feynman parameter representation for tensor integrals we start off with the following identity:

$$G_L[T(k)] = \int \prod_{j=1}^{L} \frac{\mathrm{d}^D k_j}{i\pi^{D/2}} \prod_{i=1}^{N_T} \frac{\partial}{2\partial Q_{r_i\nu_i}} \frac{\mathcal{N}(\nu - N_T)}{(-k_l^\mu M_{ll'} k_{l'\mu} + 2k_l^\mu Q_{l\mu} + J)^{\nu - N_T}}, \tag{4.52}$$

$$= \int \prod_{j=1}^{L} \frac{\mathrm{d}^D k_j}{i\pi^{D/2}} \frac{\prod_{i=1}^{N_T} k_{r_i}^{\nu_i}}{P_1^{\nu_1} \dots P_{N_G}^{\nu_{N_G}} P_{N_G+1}^{\nu_{N_G+1}} \dots P_N^{\nu_N}}. \tag{4.53}$$

We recognize in the last line the definition of a tensor loop-momentum integral in section 4.1. In this section we allow the coexistence of scalar products in the numerator with the tensor function $T(k) = \prod_{i=1}^{N_T} k_l^\mu \delta_{r_i l} g_\mu^{\nu_i}$, where N_T is the rank of the tensor. From Eq. (4.52) to Eq. (4.53) we exploit the identity for the Γ-function:

$$\Gamma(\nu)\nu = \Gamma(\nu + 1). \tag{4.54}$$

Tensor integral with differentiation operator In Eq. (4.52) the derivative with respect to the $Q_{r_i\nu_i}$ and the loop-momenta measure can be interchanged, which yields:

$$\begin{aligned} G_L[T(k)] &= \prod_{i=1}^{N_T} \frac{\partial}{2\partial Q_{r_i\nu_i}} \int \prod_{j=1}^{L} \frac{\mathrm{d}^D k_j}{i\pi^{D/2}} \frac{\mathcal{N}(\nu - N_T)}{\mathcal{D}^{\nu - N_T}}, \qquad (4.55) \\ &= \prod_{i=1}^{N_T} \frac{\partial}{2\partial Q_{r_i\nu_i}} (-1)^{\nu - N_T} \Gamma(\nu - \frac{LD}{2} - N_T) \prod_{j=1}^{N} \tilde{n}_j \delta(1 - \sum_{j=1}^{N_G} x_j) \\ &\quad \frac{\mathcal{U}^{\nu - \frac{(L+1)D}{2} - N_T}}{\mathcal{F}^{\nu - \frac{LD}{2} - N_T}} \qquad (4.56) \\ &= (-1)^{\nu} \Gamma\left(\nu - \frac{LD}{2}\right) \left(\prod_{j=1}^{N} \tilde{n}_j\right) \delta(1 - \sum_{j=1}^{N_G} x_j) \frac{\mathcal{U}^{\nu - \frac{(L+1)D}{2}}}{\mathcal{F}^{\nu - \frac{LD}{2}}} R_L(T). \qquad (4.57) \end{aligned}$$

To go from Eq. (4.55) to Eq. (4.56) we need to repeat the steps from Sec. 4.2. The definition of $\mathcal{U}$ and $\mathcal{F}$ is again given in Eq. (4.33) and in Eq. (4.34). Note that $\mathcal{F}$ explicitly depends on $Q_{r_i\nu_i}$. The derivatives in Eq. (4.56) give a rational function $R_L(T)$ in the Feynman parameters. The task is now to derive the general representation of the $R_L(T)$ functions. It will become convenient to define the adjugate of the matrix M, see Eq. (4.10):

$$\tilde{M} = \mathcal{U} M^{-1}, \qquad (4.58)$$

which is of degree $L-1$ in the Feynman parameters. $\mathcal{U}$ is defined in Eq. (4.33).

The general $R_L(T)$ function for tensor T of rank 1 is given by:

$$R_L[k_{r_1}^{\mu_1}] = Q_l^{\mu_1} \frac{\tilde{M}_{r_1 l}}{\mathcal{U}}, \qquad (4.59)$$

for tensor T of rank 2:

$$R_L[k_{r_1}^{\mu_1} k_{r_2}^{\mu_2}] = \frac{1}{\mathcal{U}^2} Q_l^{\mu_1} \tilde{M}_{l r_1} Q_{l'}^{\mu_2} \tilde{M}_{l' r_2} + \frac{\Gamma(\nu - \frac{LD}{2} - 1)}{\Gamma(\nu - \frac{LD}{2})} \left(\frac{\mathcal{F}}{-2\mathcal{U}^2}\right) \tilde{M}_{r_1 r_2} g^{\mu_1 \mu_2}, \qquad (4.60)$$

and for tensor T of rank 3 we get:

$$\begin{aligned} R_L[k_{r_1}^{\mu_1} k_{r_2}^{\mu_2} k_{r_3}^{\mu_3}] &= \frac{1}{\mathcal{U}^3} Q_l^{\mu_1} \tilde{M}_{l r_1} Q_{l'}^{\mu_2} \tilde{M}_{l' r_2} Q_{l''}^{\mu_3} \tilde{M}_{l'' r_3} \\ &+ \frac{\Gamma(\nu - \frac{LD}{2} - 1)}{\Gamma(\nu - \frac{LD}{2})} \left(\frac{\mathcal{F}}{-2\mathcal{U}^2}\right) \frac{\tilde{M}_{r_1 r_2} g^{<\mu_1 \mu_2} Q_{l'}^{\mu_3>} \tilde{M}_{l' r_3}}{2\mathcal{U}}. \qquad (4.61) \end{aligned}$$

Here we have used a shorthand notation $< \mu_1 \dots \mu_{N_T} >$ for a sum of all possible permutations of the set of pairs: $\{\mu_i, r_i\}$, for example:

$$\frac{\tilde{M}_{r_1 r_2} g^{<\mu_1 \mu_2} Q_l^{\mu_3>} \tilde{M}_{l r_3}}{2} = \tilde{M}_{r_1 r_2} g^{\mu_1 \mu_2} Q_l^{\mu_3} \tilde{M}_{l r_3} + \tilde{M}_{r_1 r_3} g^{\mu_1 \mu_3} Q_l^{\mu_2} \tilde{M}_{l r_2} + \tilde{M}_{r_2 r_3} g^{\mu_2 \mu_3} Q_l^{\mu_1} \tilde{M}_{l r_1}, \qquad (4.62)$$

in addition we use $1/\mathcal{S} = 1/2$, the so called symmetry factor, which is calculated as follows:

$$1/\mathcal{S}(N_Q) = \frac{\binom{N_T}{N_Q} \prod_{i=1}^{\frac{N_T - N_Q}{2}} \binom{N_T - N_Q - (i-1)2}{2}}{\left(\frac{N_T - N_Q}{2}\right)!} \frac{1}{N_T!}, \qquad (4.63)$$

where N_Q is the number of $Q_l^{\mu_i}\tilde{M}_{l_{r_i}}$ in the respective tensor:

$$N_Q = \begin{cases} 0,2,4,\ldots, & N_T \text{ even}, \\ 1,3,5,\ldots, & N_T \text{ odd}. \end{cases} \tag{4.64}$$

The general tensor Feynman integral consists of building blocks of the following kind:

$$Q_l^{\mu_1}\tilde{M}_{l_{r_1}}\ldots Q_l^{\mu_{N_Q}}\tilde{M}_{l_{r_{N_Q}}} g^{\mu_{N_Q+1}\mu_{N_Q+2}}\tilde{M}_{r_{N_Q+1}r_{N_Q+2}}\ldots g^{\mu_{N_T-1}\mu_{N_T}}\tilde{M}_{r_{N_T-1}r_{N_T}}. \tag{4.65}$$

The first binomial factor in Eq. (4.63) comes from the possibility to distribute N_T set of pairs $\{\mu_i, r_i\}$ in the tensor $Q_l^{\mu_1}\tilde{M}_{l_{r_1}}\ldots Q_l^{\mu_{N_Q}}\tilde{M}_{l_{r_{N_Q}}}$ of rank N_Q in Eq. (4.65). The remaining binomials account for the possibility to distribute all remaining sets of pairs $\{\mu_i, r_i\}$ (which are not taken into account previously) to the remaining tensor $g^{\mu_{N_Q+1}\mu_{N_Q+2}}\tilde{M}_{r_{N_Q+1}r_{N_Q+2}}\ldots g^{\mu_{N_T-1}\mu_{N_T}}\tilde{M}_{r_{N_T-1}r_{N_T}}$ of rank $N_T - N_Q$ in Eq. (4.65). The first factorial in the denominator in Eq. (4.63) takes into account the number of symmetric tensors $g^{\mu_i\mu_j}\tilde{M}_{r_ir_j}$. The second factorial in the denominator is the number of all maximum possible permutations of the set of pairs $\{\mu_i, r_i\}$, $i = 1,\ldots,N_T$ for a general tensor of rank N_T.

The rational function $R_L(T)$ for a general tensor integral of an odd rank $N_T \geq 5$ can be put in the following formula:

$$\begin{aligned}
R_L[T(k)] &= \tilde{M}_{r_1r_2}g^{<\nu_1\nu_2}\ldots\tilde{M}_{r_{N_T-2}r_{N_T-1}}g^{\nu_{N_T-2}\nu_{N_T-1}}Q_l^{\nu_{N_T}>}\tilde{M}_{lr_{N_T}}\left(\frac{\mathcal{F}}{-2\mathcal{U}^2}\right)^{\frac{N_T-1}{2}} \\
&\quad \left.\frac{\Gamma(\nu-\frac{DL}{2}-\frac{N_T-1}{2})}{\mathcal{U}\mathcal{S}(1)\Gamma(\nu-\frac{DL}{2})}\right|_{N_Q=1} \\
&+ \sum_{N_Q=3,2}^{N_T-4}\left(\frac{\mathcal{F}}{-2\mathcal{U}^2}\right)^{\frac{N_T-N_Q}{2}}\tilde{M}_{r_1r_2}g^{<\nu_1\nu_2}\ldots\tilde{M}_{r_{N_T-N_Q-1}r_{N_T-N_Q}}g^{\nu_{N_T-N_Q-1}\nu_{N_T-N_Q}} \\
&\quad Q_l^{\nu_{N_T-N_Q+1}}\tilde{M}_{lr_{N_T-N_Q+1}}\ldots Q_l^{\nu_{N_T}>}\tilde{M}_{lr_{N_T}}\frac{\Gamma(\nu-\frac{DL}{2}-\frac{N_T-N_Q}{2})}{\mathcal{U}^{N_Q}\mathcal{S}(N_Q)\Gamma(\nu-\frac{DL}{2})} \\
&+ \left(\frac{\mathcal{F}}{-2\mathcal{U}^2}\right)\tilde{M}_{r_1r_2}g^{<\nu_1\nu_2}Q_l^{\nu_3}\tilde{M}_{lr_3}\ldots Q_l^{\nu_{N_T}>}\tilde{M}_{lr_{N_T}} \\
&\quad \left.\frac{\Gamma(\nu-\frac{DL}{2}-1)}{\mathcal{U}^{N_Q}\mathcal{S}(N_Q)\Gamma(\nu-\frac{DL}{2})}\right|_{N_Q=N_T-2} \\
&+ \left.Q_l^{\nu_1}\tilde{M}_{lr_1}\ldots Q_l^{\nu_{N_T}}\tilde{M}_{lr_{N_T}}\frac{1}{\mathcal{U}^{N_T}}\right|_{N_Q=N_T}.
\end{aligned} \tag{4.66}$$

And the rational function $R_L(T)$ for a general tensor integral of an even rank $N_T \geq 4$

can be put in the following formula:

$$
\begin{aligned}
R_L[T] &= \tilde{M}_{r_1 r_2} g^{<\nu_1\nu_2} \dots \tilde{M}_{r_{N_T-1} r_{N_T}} g^{\nu_{N_T-1}\nu_{N_T}>} \left(\frac{\mathcal{F}}{-2\mathcal{U}^2}\right)^{\frac{N_T}{2}} \frac{\Gamma(\nu - \frac{DL}{2} - \frac{N_T}{2})}{\mathcal{S}(0)\Gamma(\nu - \frac{DL}{2})}\Bigg|_{N_Q=0} \\
&+ \sum_{N_Q=2,2}^{N_T-4} \tilde{M}_{r_1 r_2} g^{<\nu_1\nu_2} \dots \tilde{M}_{r_{N_T-N_Q-1} r_{N_T-N_Q}} g^{\nu_{N_T-N_Q-1}\nu_{N_T-N_Q}} \left(\frac{\mathcal{F}}{-2\mathcal{U}^2}\right)^{\frac{N_T-N_Q}{2}} \\
&\quad Q_l^{\nu_{N_T-N_Q+1}} \tilde{M}_{l r_{N_T-N_Q+1}} \dots Q_l^{\nu_{N_T}>} \tilde{M}_{l r_{N_T}} \frac{\Gamma(\nu - \frac{DL}{2} - \frac{N_T-N_Q}{2})}{\mathcal{U}^{N_Q}\mathcal{S}(N_Q)\Gamma(\nu - \frac{DL}{2})} \\
&+ \left(\frac{\mathcal{F}}{-2\mathcal{U}^2}\right) \tilde{M}_{r_1 r_2} g^{<\nu_1\nu_2} Q_l^{\nu_3} \tilde{M}_{l r_3} \dots Q_l^{\nu_{N_T}>} \tilde{M}_{l r_{N_T}} \\
&\quad \frac{\Gamma(\nu - \frac{DL}{2} - 1)}{\mathcal{U}^{N_Q}\mathcal{S}(N_Q)\Gamma(\nu - \frac{DL}{2})}\Bigg|_{N_Q=N_T-2} \\
&+ Q_l^{\nu_1} \tilde{M}_{l r_1} \dots Q_l^{\nu_{N_T}} \tilde{M}_{l r_{N_T}} \frac{1}{\mathcal{U}^{N_T}}\Bigg|_{N_Q=N_T} . \qquad (4.67)
\end{aligned}
$$

Here the notation $N_Q = 2,2$ and $N_Q = 3,2$ means that the sums start with $N_Q = 2$ and $N_Q = 3$ and go in steps of 2, see Eq. (4.64).

In the formulas above we observe several kinds of tensors which differ in the number of $Q_l^{\mu_i} \tilde{M}_{l r_i}$. Each tensor integral of even rank N_T in the loop-momenta is thus a linear combination of $\frac{N_T+2}{2}$ different kinds of tensors see Eq. (4.65). A tensor integral of odd rank N_T in the loop-momenta is a linear combination of $\frac{N_T+1}{2}$ different kinds of tensors.

It is important to observe that the tensor structure is homogeneous and of degree zero in the Feynman parameters, that means each term preserves the projective space of each Feynman parameter integral. As we will see this is a crucial property in deriving a Mellin-Barnes integral representation for a general Feynman integral with a general tensor structure.

The tensor integral in the Feynman parameter space depends only on the Lorentz structure of the underlying external momenta (which are the building blocks of $Q_l^{\nu_l}$, see Eq. (4.11)) and the metric tensor $g_{\mu\nu}$, which can be factored out from the Feynman parameter integral.

Multiple terms, see the last column of Tab. 4.1, are generated in Eq. (4.66) and Eq. (4.67). Each of these tensors is a polynomial in the Feynman parameters, because $Q_l^{\nu_l}$, see Eq. (4.11) and $\tilde{M}$ in Eq. (4.58) are polynomials in the Feynman parameters. In the case of the sector decomposition technique which we discuss later in Chap. 5 one may treat integrals with polynomial functions in the numerator. In the case of the Mellin-Barnes integral representations which we study later in Chap. 6, we need to expand these polynomials and treat each term as a new integral.

Each term in the function $R_L[T(k)]$ has a common factor in the denominator $\frac{1}{\mathcal{U}^{N_T}}$, which is the only polynomial in the denominator and the degree of the denominator in the Feynman parameter is thus LN_T. Since the function $R_L[T(k)]$ is homogeneous and of degree zero in the Feynman parameters each term in the numerator in $R_L[T(k)]$ is of degree LN_T in the Feynman parameters. As in Ref. [75] we may absorb the functions $\mathcal{U}$ and $\mathcal{F}$ in the Feynman parameter representations which will be

interpreted as a dimension shift in $D+(N_T+N_Q)$, see third column in Tab. 4.1, if we would convert this integral back to a loop-momentum integral. A polynomial remains of degree $\frac{(1+L)(N_Q-N_T)}{2}+LN_T$ in the Feynman parameters, see fourth column in Tab.4.1. Each term of this polynomial can be absorbed in the measure $\tilde{n}$ of the corresponding Feynman parameter integral. If we convert the Feynman parameter integral back into the loop-momenta representation this would introduce additional dots (which are raised powers of the propagators in the denominator of the loop-momentum integral). What happens is that a loop-momentum integral of tensor rank N_T, which corresponds to N_T scalar products in the numerator of the loop-momentum integral is converted to a a loop-momentum integral with maximum of LN_T dots.

Table 4.1: The first column gives the loop number L. The second column is the tensor rank N_T of a loop-momenta Feynman integral. If we transform each scalar coefficient in the general tensor Feynman parameter integral to scalar Feynman loop-momentum integrals then we can calculate how big is the dimension shift $D+(N_T+N_Q)$ see third column and how many dots occur see fourth column. The last column gives the number of terms due to the Lorentz structure.

$\boldsymbol{L}$	$\boldsymbol{N_T}$	$\boldsymbol{N_T+N_Q}$	$\frac{\boldsymbol{(1+L)(N_Q-N_T)}}{\boldsymbol{2}}+\boldsymbol{LN_T}$	$\sum_{N_Q,2}\frac{\boldsymbol{N_T!}}{\boldsymbol{S(N_Q)}}$
1	1	2	1	1
	2	{2,4}	{0,2}	2
	3	{4,6}	{1,3}	4
	4	{4,6,8}	{0,2,4}	10
	5	{6,8,10}	{1,3,5}	26
2	1	2	2	1
	2	{2,4}	{1,4}	2
	3	{4,6}	{3,6}	4
	4	{4,6,8}	{2,5,8}	10
	5	{6,8,10}	{4,7,10}	26

For completeness, we give the recipe to convert back from the Feynman parameter representation to a loop-momentum integral. For each term of tensor rank N_T and with N_Q Q-vectors, we get a Feynman integral with $D+N_T+N_Q$ dimension shift and a product of $\frac{(1+L)(N_Q-N_T)}{2}+LN_T$ Feynman parameters in the numerator in the Feynman parameter representation. Each Feynman parameter which is left after absorbing all $\mathcal{U}$ and $\mathcal{F}$ functions corresponds to an additional dot in the loop-momenta representation:

$$x_i^{n_i}=(i^+)^{n_i}\frac{\Gamma(\nu_i+1)}{\Gamma(\nu_i)}(-1)^{n_i}, \tag{4.68}$$

where we denote $(i^+)^{n_i}$ as simply raising the power of the ith propagator by n_i. This procedure of trading the scalar products in the numerator of the loop-momentum integral for dots and a dimension shift is the so called Davydychev tensor reduction [75].

Example

The idea how the derivation of tensor Feynman parameter integrals works is illustrated. In addition to that an alternative approach to derive a Feynman parameter representation for a tensor loop-momentum integral is shown. Remember the integral I_{0h0w4} in Eq. (4.6) has in the numerator one irreducible scalar product $(k_1 p_1)$. In the first example we treat this integral as a tensor rank 1 integral $R[k_1^\mu]$ and contract it later with $p_1^\nu g_{\mu\nu}$. The general formula for a tensor rank 1 integral Eq. (4.59) gives

$$\begin{aligned} p_1^\nu g_{\mu\nu} R[k_1^\mu] &= p_1^\nu g_{\mu\nu}(-p_1^\mu x_2 x_4 + p_2^\mu x_2 x_5 + p_2^\mu x_3 x_5 + p_2^\mu x_4 x_5)/\mathcal{U}'_{\text{0h0w4}} && (4.69)\\ &= \frac{s}{2}(x_2 x_5 + x_3 x_5 + x_4 x_5)/\mathcal{U}'_{\text{0h0w4}}, && (4.70)\end{aligned}$$

and we use the functions $\mathcal{U}'_{\text{0h0w4}} = \mathcal{U}_{\text{0h0w4}}|_{x_6=0}$ and $\mathcal{F}'_{\text{0h0w4}} = \mathcal{F}_{\text{0h0w4}}|_{x_6=0}$ in Eq. (4.48) and Eq. (4.49). Thus the Feynman parameter integral is due to Eq. (4.56):

$$\begin{aligned} p_{1\mu} G_2[k_1^\mu]^{\text{0h0w4}} &= (-1)\Gamma(5-D) \int\limits_{\{x_i \geq 0\}} \left(\prod_{j=1}^{5} \mathrm{d}x_j\right) \delta(1 - \sum_{j=1}^{5} x_j) \frac{\mathcal{U}'^{4-\frac{3D}{2}}_{\text{0h0w4}}}{\mathcal{F}'^{5-D}_{\text{0h0w4}}} \\ &\quad \frac{s}{2}(x_2 x_5 + x_3 x_5 + x_4 x_5). && (4.71)\end{aligned}$$

The corresponding scalar loop-momentum integrals are:

$$\begin{aligned} p_{1\mu} G_2[k_1^\mu]^{\text{0h0w4}} &= (-1)^5 \Gamma(7-(D+2)) \left(\prod_{j=1}^{5} \int\limits_{\{x_j \geq 0\}} \mathrm{d}x_j\right) \delta(1 - \sum_{j=1}^{5} x_j) \frac{\mathcal{U}'^{7-\frac{3(D+2)}{2}}_{\text{0h0w4}}}{\mathcal{F}'^{7-(D+2)}_{\text{0h0w4}}} \\ &\quad \frac{s}{2}(x_2 x_5 + x_3 x_5 + x_4 x_5), && (4.72)\\ &= I_{\text{0h0w4}}(D+2,1,2,1,1,2,0,0,s) \\ &+ I_{\text{0h0w4}}(D+2,1,1,2,1,2,0,0,s) \\ &+ I_{\text{0h0w4}}(D+2,1,1,1,2,2,0,0,s), && (4.73)\\ &= I_{\text{0h0w4}}(D,1,1,1,1,1,-1,0,s). && (4.74)\end{aligned}$$

We observe in the loop-momentum integral representation that one integral with a numerator in Eq. (4.74) is replaced by three loop-momentum integrals with two dots and one dimension shift $D+2$, see Eq. (4.73). Here we used the prescription of Eq. (4.68) and $\Gamma(1) = \Gamma(2) = 1$.

In the second example we use the definition for a Feynman parameter integral with negative indices, which correspond to the scalar products in the numerator of the loop-momentum integrals. Instead of using the Feynman parameter integral representation derived in Eq. (4.47) let us use for the integral I_{0h0w4} the $\mathcal{G}$-polynomial

parameter integral (see App. B):

$$G_L^{\mathcal{G}}[p_1 k_1] = \frac{(-1)^4 \Gamma(D/2)}{\Gamma(\frac{3D}{2} - 4)} \left(\prod_{j=1}^{6} \tilde{n}_j \right) \mathcal{G}_{\text{0h0w4}}^{-D/2}, \quad \mathcal{G}_{\text{0h0w4}} = \mathcal{F}_{\text{0h0w4}} + \mathcal{U}_{\text{0h0w4}}. \tag{4.75}$$

The derivative $\tilde{n}_6 = (-1)\phi^{(1)}(0)$ with respect to x_6 yields:

$$G_L^{\mathcal{G}}[p_1 k_1] = \frac{(-1)^5(-\Gamma\left(\frac{D+2}{2}\right))}{\Gamma\left(\frac{3(D+2)}{2} - 7\right)} \left(\prod_{j=1}^{5} \int_{\{x_i \geq 0\}} \mathrm{d}x_j \right) \mathcal{G}_{\text{0h0w4}}^{-\frac{D+2}{2}} \frac{-s}{2} (x_2 x_5 + x_3 x_5 + x_4 x_5), \tag{4.76}$$

where we have used:

$$\Gamma\left(\frac{3D}{2} - 4\right) = \Gamma\left(\frac{3(D+2)}{2} - 7\right), \tag{4.77}$$

$$(-1)^4 \left(-\frac{D}{2}\right) \Gamma\left(\frac{D}{2}\right) (-1) = (-1)^5(-\Gamma\left(\frac{D+2}{2}\right)). \tag{4.78}$$

Note the result in Eq. (4.76) equals that in Eq. (4.72) if we convert the $\mathcal{G}$-polynomial representation to the Feynman parameter representation (see App. B).

4.5.1 One-loop tensor Feynman integrals

The general formulas for tensor Feynman parameter integrals simplify considerably for one-loop tensor Feynman integrals because of $M = 1$ and $\det M = 1 = \tilde{M}$. For example we have:

$$R_L[k^{\mu_1}] = \frac{Q^{\mu_1}}{\mathcal{U}}, \tag{4.79}$$

$$R_L[k^{\mu_1} k^{\mu_2}] = \frac{Q^{\mu_1} Q^{\mu_2}}{\mathcal{U}^2} + \frac{\Gamma(\nu - \frac{D}{2} - 1)}{\Gamma(\nu - \frac{D}{2})} \left(\frac{\mathcal{F}}{-2\mathcal{U}^2} \right) g^{\mu_1 \mu_2}, \tag{4.80}$$

$$R_L[k^{\mu_1} k^{\mu_2} k^{\mu_3}] = \frac{Q^{\mu_1} Q^{\mu_2} Q^{\mu_3}}{\mathcal{U}^3} + \frac{\Gamma(\nu - \frac{D}{2} - 1)}{\Gamma(\nu - \frac{D}{2})} \left(\frac{\mathcal{F}}{-2\mathcal{U}^2} \right) \frac{g^{<\mu_1 \mu_2} Q^{\mu_3>}}{2\mathcal{U}}. \tag{4.81}$$

The one-loop tensor Feynman integrals are used in the derivation of the Mellin-Barnes integral representation with the loop-by-loop approach, which we study later in section 6.1.

4.6 Divergences of Feynman integrals

We should stress that the integrals in loop-momenta representation in Eq. (4.5) and in the Feynman parameter representation in Eq. (4.32) may be ill defined and divergent in $D = 4$. In dimensional regularization, which is used in this thesis work, going away from the dimension $D = 4$ will regularize the divergences. We consider the integrals in $D = 4 - 2\epsilon$. The integrals have a Laurent expansion in ϵ. The poles of the Laurent expansion parameterize the divergences of the original integrals in $D = 4$.

In the Feynman parameter representation we identify three kinds of divergences. First the overall factor $\Gamma(\nu - DL/2)$, if divergent, corresponds to the overall ultraviolet divergence. This happens if the argument of the Γ-function is zero or takes negative integer numbers in the limit $\epsilon \to 0$.

The $\mathcal{U}$-function is positive semi-definite in the Feynman parameters and each coefficient is +1. The $\mathcal{U}$-function may only vanish on the boundary of the integration region. It follows that the quantity $\mathcal{U}^{\nu - D(L+1)/2}$ may diverge and develop poles in ϵ only if the Feynman parameters take zero values. These poles are related to ultraviolet sub-divergences.

If all invariants in the $\mathcal{F}$-function, which are formed from the external momenta, are negative and all internal masses are positive, then such an integral is called Euclidean. The $\mathcal{F}$-function in Euclidean integrals is also positive semi-definite in the Feynman parameters. The $\mathcal{F}$-function may only vanish on the boundary of the integration region. If the quantity $\mathcal{F}^{\nu - DL/2}$ diverges then this may lead to poles in ϵ which are related to the infrared divergences.

In this thesis work it is interesting to study the $\mathcal{F}$-function when we allow that the integral is no longer restricted to the Euclidean region (for example invariants, which are formed from the external momenta are positive) which we call in this work the Minkowski region. In this context the $\mathcal{F}$-function may vanish inside the integration region. These poles are related to the Landau singularities and are integrable except if the singularity is the leading Landau singularity. These leading Landau singularities are related to the threshold behavior of the integrals. The necessary condition for the occurrences of Landau singularities is that the $\mathcal{F}$-function vanishes for a given subset S of variables $\{x_1, \ldots, x_{N_G}\}$ such that

$$x_i = 0, \quad i \in S, \tag{4.82}$$

$$\frac{\partial}{\partial x_j}\mathcal{F} = 0, \text{ for } j \in \{1, \ldots, N_G\} \backslash S. \tag{4.83}$$

Here we consider only the Feynman parameters which are related to the propagators in the denominator of the loop-momenta representation (this of course assumes that we completed the tensor reduction already).

We are interested in the numerical evaluation of Feynman integrals. In this case only two methods are known to resolve infrared and ultraviolet singularities in a systematic way for a general Feynman integral with fully automatized algorithms. Namely the sector decomposition technique and the Mellin-Barnes integral approach.

Chapter 5

Sector decomposition

In this chapter we review a strategy to factor out the endpoint singularities from the $\mathcal{U}$- and the $\mathcal{F}$-functions, which correspond to a Feynman integral regularized in the dimensional regularization. The singularities are then resolved as a Laurent expansion around $\epsilon = 0$ were the coefficients are finite integrals. This technique is called sector decomposition [76, 21, 22, 77, 78, 79].

In this thesis work the sector decomposition is based on the Feynman parameter integrals which we have derived in the previous section. We illustrate the basic steps of the application of the sector decomposition technique for one simple example: On-shell scalar one-loop box-diagram I_{box} with all internal masses set to zero. The $\mathcal{U}$ and the $\mathcal{F}$-functions are:

$$\mathcal{U}_{\text{box}} = x_1 + x_2 + x_3 + x_4, \tag{5.1}$$

$$\mathcal{F}_{\text{box}} = -s x_1 x_3 - t x_2 x_4, \tag{5.2}$$

where $s = (p_1 + p_2)^2$, $t = (p_1 + p_3)^2$ with $p_1^2 = p_2^2 = p_3^2 = p_4^2 = 0$ and all external momenta incoming see Fig. 5.1.

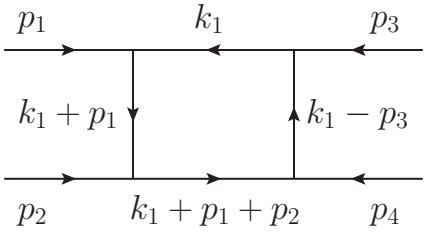

Figure 5.1: On-shell one-loop box-diagram with all internal masses set to zero.

Primary sector decomposition In this section we follow the guideline in Ref. [79]. First the so called primary sector decomposition is applied. Here the Feynman integral is decomposed into N_G primary sectors:

$$\int_0^\infty \mathrm{d}^{N_G} x = \sum_{l=1}^{N_G} \int_0^\infty \mathrm{d}^{N_G} x \prod_{k=1, k\neq l}^{N_G} \theta(x_l \geq x_k). \tag{5.3}$$

The different integration domains of the initial Feynman Parameter integral G^{SD} are now split into N_G parts each corresponding to an integral G_l^{SD}:

$$G^{\text{SD}} = \frac{\Gamma\left(\nu - D\frac{L}{2}\right)(-1)^{\nu}}{\prod_{i=1}^{N_G}\Gamma(\nu_i)} \sum_{l=1}^{N_G} G_l^{\text{SD}}. \tag{5.4}$$

Note that in this section we treat the coefficients in the tensor Feynman parameter integral with $\nu_i > 0$.

Next for each integral G_l^{SD} the integration variables are rescaled :

$$x_i = \begin{cases} x_l x_i', & l > i, \\ x_l, & l = i, \\ x_l x_{i-1}', & l < i. \end{cases} \tag{5.5}$$

The functions $\mathcal{U}$ and $\mathcal{F}$ are homogeneous in the Feynman parameters of degree L and $L+1$ respectively. Thus the rescaling of each integral G_l^{SD} yields:

$$\begin{aligned}
\mathcal{U}^{\nu-(L+1)\frac{D}{2}} &= \mathcal{U}_l{}^{\nu-(L+1)\frac{D}{2}} x_l^{-L\nu-L\frac{D(L+1)}{2}}, && (5.6)\\
\mathcal{F}^{\nu-L\frac{D}{2}} &= \mathcal{F}_l{}^{\nu-L\frac{D}{2}} x_l^{-L\nu-L\frac{D(L+1)}{2}-\nu}, && (5.7)\\
x_i^{\nu_i-1} &= x_i'^{\nu_i-1} x_l^{\nu_i-1}, \quad l > i, && (5.8)\\
x_i^{\nu_i-1} &= x_{i-1}'^{\nu_i-1} x_l^{\nu_i-1}, \quad l < i, && (5.9)\\
x_i^{\nu_i-1} &= x_l^{\nu_l-1}, \quad i = l, && (5.10)
\end{aligned}$$

for each $l = i, \ldots, N_G$. The Jacobian is $x_l^{N_G-1}$. Combining the above all together and using the identity:

$$1 = \int_0^{\infty} \frac{\mathrm{d}x_l}{x_l}\, \delta(1 - x_l(1 + \sum_{i=1}^{N_G-1} x_i')), \tag{5.11}$$

and for ease of notation relabeling the ν_i lexicographically, we find:

$$G_l^{\text{SD}} = \int_0^1 \mathrm{d}^{N_G-1}x' \prod_{i=1}^{N_G-1} x_i'^{\nu_i-1} \frac{\mathcal{U}_l^{\nu-D(L+1)/2}}{\mathcal{F}_l^{\nu-LD/2}}. \tag{5.12}$$

For our example integral I_{box} we find after the primary sector decomposition the integral G_4 with

$$\begin{aligned}
\mathcal{U}_4 &= (1 + x_1' + x_2' + x_3'), && (5.13)\\
\mathcal{F}_4 &= (-s x_1' x_3' - t x_2'), && (5.14)
\end{aligned}$$

where the poles come from regions where a set of parameters x_i' goes to zero. Thus the aim is to factorize these singularities by the following procedure.

Iterated sector decomposition

1. Determine a minimal set S of parameters $\{x_1, \ldots, x_{N_G}\}$ for which at least one of the functions $\mathcal{U}$ or $\mathcal{F}$ becomes zero. One subset contains r elements. We discuss later that this subset is not unique.

2. Decompose the integration region in an r-cube, such that each unity integration is decomposed in r sub sectors:

$$\prod_{j=1}^{r} \theta(1 \geq x_{\alpha_j} \geq 0) = \sum_{k=1}^{r} \prod_{j=1, j\neq k}^{r} \theta(x_{\alpha_k} \geq x_{\alpha_j} \geq 0). \tag{5.15}$$

3. Remap the r variables in each sub sector back to an integration over a hypercube:

$$x_{\alpha_j} = \begin{cases} x_{\alpha_k} x_{\alpha_j}, \text{ for } x_{\alpha_k} \neq x_{\alpha_j}, \\ x_{\alpha_k}, \text{ for } x_{\alpha_k} = x_{\alpha_j}. \end{cases} \tag{5.16}$$

   The Jacobian is thus $x_{\alpha_k}^{r-1}$.

4. Repeat each step for all sub sectors until the $\mathcal{U}$ or the $\mathcal{F}$-functions contain one constant term.

After the iterated sector decomposition terminates, the initial integral is decomposed in M terms, where each has the following form:

$$G_{l,k} = \int_0^1 \left(\prod_{i=1}^{N_G - 1} \mathrm{d}x_i \, x_i^{a_i - b_i \epsilon} \right) \frac{\mathcal{U}_{l,k}^{\nu - D\frac{(L+1)}{2}}}{\mathcal{F}_{l,k}^{\nu - D\frac{L}{2}}}, \tag{5.17}$$

where k counts all possible sub sectors in a primary sector l.

For our example integral I_{box} the $\mathcal{U}_4$-function contains a constant term and is already finite. Of course at one-loop no ultraviolet sub divergences exist. The $\mathcal{F}_4$-function becomes zero if the variables x_1' and x_2' simultaneously go to zero, which forms one subset $X_6 = \{x_1', x_2'\}$. This generates with the iterated sector decomposition two sub sectors $x_1' \geq x_2'$ and $x_2' \geq x_1'$. The second sub sector will be treated according to the above prescription:

$$G_{4,2} = \int_0^1 \mathrm{d}x_1' \mathrm{d}x_2' \mathrm{d}x_3' \, {x_2'}^{-1-\epsilon} \frac{(1 + x_1'x_2' + x_2' + x_3')^{2\epsilon}}{(-s x_1' x_3' - t)^{2-\epsilon}}, \tag{5.18}$$

where we used $D = 4 - 2\epsilon$.

Resolving the poles The divergent part is factored out from the functions $\mathcal{U}$ and $\mathcal{F}$. These factors $x_i^{a_i - b_i\epsilon}$ are treated as follows:

$$G_{lki} = \int_0^1 \mathrm{d}x_i \, x_i^{a_i - b_i\epsilon} \mathcal{I}_{lk}(x_i, \{x_{i\neq j}\}, \epsilon), \tag{5.19}$$

where the function $\mathcal{I}_{lk} = \mathcal{U}_{lk}^{\nu - D\frac{L+1}{2}} / \mathcal{F}_{lk}^{\nu - D\frac{L}{2}}$. If $a_i > -1$ then the integration does not lead to an ϵ-pole. If $a_i \leq -1$ then we expand $\mathcal{I}_{lk}(x_i, \{x_{i\neq j}\}, \epsilon)$ in a Taylor series around $x_i = 0$ which leads to:

$$\mathcal{I}_{lk}(x_i, \{x_{i\neq j}\}, \epsilon) = \sum_{j=0}^{-a_i-1} \mathcal{I}_{lk}(0, \{x_{i\neq j}\}, \epsilon)^{(j)} \frac{x_i^j}{j!} + R(\{x_i\}, \epsilon), \tag{5.20}$$

where

$$\mathcal{I}_{lk}(0, \{x_{i\neq j}\}, \epsilon)^{(j)} = \frac{\partial^j \mathcal{I}_{lk}(x_i, \{x_{i\neq j}\}, \epsilon)}{\partial x_i^j}\Big|_{x_i=0}. \tag{5.21}$$

According to this the poles in ϵ are subtracted:

$$G_{lki} = \sum_{j=0}^{-a_i-1} \frac{1}{a_i - b_i\epsilon + j + 1} \frac{\mathcal{I}_{lk}(0, \{x_{i\neq j}\}, \epsilon)^{(j)}}{j!} + \int_0^1 \mathrm{d}x_i \, x_i^{a_i - b_i\epsilon} R(\{x_j\}, \epsilon). \tag{5.22}$$

The special case for $a_i = -1$ is

$$G_{lki} = \frac{1}{-b_i\epsilon} \mathcal{I}_{lk}(0, \{x_{i\neq j}\}, \epsilon) + \int_0^1 \mathrm{d}x_i \, x_i^{-1-b_i\epsilon} (\mathcal{I}_{lk}(x_i, \{x_{i\neq j}\}, \epsilon) - \mathcal{I}_{lk}(0, \{x_{i\neq j}\}, \epsilon)). \tag{5.23}$$

For our example integral I_{box} this yields the following:

$$G_{42} = \int_0^1 \mathrm{d}x_1 \mathrm{d}x_3 \, \frac{1}{-\epsilon} \frac{(1+x_3)^{2\epsilon}}{(-s x_1 x_3 - t)^{2+\epsilon}} \tag{5.24}$$

$$+ \int_0^1 \mathrm{d}x_1 \mathrm{d}x_3 \mathrm{d}x_2 \, x_2^{-1-\epsilon} \frac{(1 + x_1 x_2 + x_2 + x_3)^{2\epsilon} - (1+x_3)^{2\epsilon}}{(-s x_1 x_3 - t)^{2+\epsilon}}. \tag{5.25}$$

This integral can now be expanded in a Laurent series around $\epsilon = 0$. In Euclidean regions the coefficients in ϵ are finite integrals:

$$G_{42} = \int_0^1 \mathrm{d}x_1 \mathrm{d}x_3 \, \frac{-\frac{1}{\epsilon} - 2\log(1+x_3) + \log(-t - s x_1 x_3)}{(t + s x_1 x_3)^2} + \mathcal{O}(\epsilon). \tag{5.26}$$

Integration in Minkowskian regions As long as all internal masses and kinematic invariants are real the $\mathcal{F}$-function will exhibit integrable singularities which are related to the kinematic thresholds. Here the singularities will be avoided by making use of Cauchy's theorem by deforming the integration contour into the complex plane, where the $+i\delta$ prescription stemming from the propagators dictates the allowed contour deformations into the complex plane. Each term after the iterated sector decomposition is treated separately with the following ansatz:

$$\vec{z}(\vec{x}) = \vec{x} - i\vec{\tau}(\vec{x}), \quad \tau_k = \lambda x_k (1 - x_k) \frac{\partial \mathcal{F}(\vec{x})}{\partial x_k}. \tag{5.27}$$

The motivation behind this choice becomes clear if we look at the $\mathcal{F}$-function in terms of the new variables and expand it in λ:

$$\mathcal{F}(\vec{z}(\vec{x})) = \mathcal{F}(\vec{x}) - i\lambda \sum_{k=1}^{N_G} x_k(1-x_k)(\frac{\partial \mathcal{F}(\vec{x})}{\partial x_k})^2 + \mathcal{O}(\lambda^2). \tag{5.28}$$

Due to Eq. (5.27) the first order expansion in λ leads to $(\frac{\partial \mathcal{F}(\vec{x})}{\partial x_k})^2$ which is convenient since it guarantees that the imaginary part is always negative if we choose positive λ. The task of a sector decomposition program will be to pick out a λ for which the above is true (for example the terms of $\mathcal{O}(\lambda^3)$ do not dominate). For this dedicated studies and numerical implementations are found in Ref. [28]. The contour deformation leads to a new integral:

$$\int_0^1 \prod_{i=1}^{N_G} \mathrm{d}x_i \mathcal{I}(\vec{x}) = \int_0^1 \prod_{i=1}^{N_G} \mathrm{d}x_i \left| \left(\frac{\partial z_l(\vec{x})}{x_k} \right) \right| \mathcal{I}(\vec{z}(\vec{x})), \tag{5.29}$$

where $\left| \left(\frac{\partial z_l(\vec{x})}{x_k} \right) \right|$ is understood as a determinant of a squared $(N_G \times N_G)$ matrix and $\mathcal{I}$ is the integrand in the Feynman parameters after the iterative sector decomposition.

Infinite recursion The primary goal of the iterated sector decomposition is to get the least number of integrals. Which is referred in the implementation of the sector decomposition programs as the strategy. An important feature of Feynman integrals is that as soon as massive internal lines are present, a naive strategy such as iterated sector decomposition may lead to infinite recursions. One can illustrate the problem with the following toy example (see Ref. [79]):

$$f(x_1, x_2, x_3) = x_1^2 + x_2^2 x_3. \tag{5.30}$$

We apply the above discussed algorithm of iterated sector decomposition and choose as a subset of variables $\{x_1, x_3\}$ which, if simultaneously going to zero, will lead to $f = 0$. For the sub sector $x_3 > x_1$ this leads with the replacement $x_1 = x_3 x_1$ to $f = x_3(x_3 x_1 + x_2)$. The next iteration, while choosing as a subset $\{x_3, x_2\}$ and with the substitution $x_2 = x_2 x_3$ in the corresponding sub sector $x_2 > x_3$, gives back the same functional form as we have started off with. So we end up with an infinite recursion. To avoid infinite recursion a suitable choice would be to begin with a subset $\{x_1, x_2\}$, which would lead to a termination of the iterated sector decomposition algorithm. Such heuristic choices were made in Ref. [21, 79].

In contrast to the naive strategy the sector decomposition algorithms in Ref. [80, 81] guarantee to avoid the infinite recursion. The best algorithm which guarantees to terminate and provides the least number of sub sectors seems to be the geometric strategy in Ref. [82, 70].

In this section we have recapitulated a well established technique, namely sector decomposition, which we use in this project to calculate the relevant two-loop vertex Feynman integrals. We use the publicly available programs, see Ref. [70, 83].

Since we are dealing in this work with divergent integrals in Minkowskian regions, the convergence of the integrals is often not assured to be fast or even stable,

see for example Ref. [84]. Here the authors studied the Mellin-Barnes integral approach together with the sector decomposition approach and they have found out that a systematic uncertainty of 10 sigma for the Monte Carlo uncertainty is justified in their application of sector decomposition technique. We show in Chap. 9 that the Mellin-Barnes integral approach is complementary to the sector decomposition approach for the calculation of the two-loop vertex Feynman integrals, which have been projected with Eq. (3.73) and Eq. (3.74) and summarized in Tab. 3.2.

Chapter 6

Construction of Mellin-Barnes integral representation

In this thesis work we show how to evaluate Feynman integrals in Minkowskian regions with the help of the so called Mellin-Barnes integral approach. First we discuss an automatic way to construct these Mellin-Barnes integral representations. Fortunately this is well studied and implemented in a public tool `AMBRE` [85]. In addition to the derivation of the Mellin-Barnes integral representations we focus on the asymptotic behavior of the resulting integrals.

The main relation, the Mellin-Barnes master formula [86] is

$$\frac{1}{(A+B)^\nu} = \frac{B^{-\nu}}{2\pi i\Gamma(\nu)} \int\limits_{-i\infty}^{i\infty} \mathrm{d}z\, A^z B^{-z} \Gamma(-z)\Gamma(\nu+z), \quad |\arg A - \arg B| < \pi \tag{6.1}$$

where the integration contour separates the poles of the Γ-functions. ν is a finite complex value and $\nu \neq 0, -1, -2, \ldots$. We apply the master formula iteratively in the following as:

$$\frac{1}{\left(\sum\limits_{k=1}^{N_M+1} A_k\right)^\nu} = \frac{1}{(2\pi i)^{N_M}\Gamma(\nu)} \int\limits_{-i\infty}^{i\infty} \left(\prod_{k=1}^{N_M} \mathrm{d}z_k\right) M(A_1, \ldots, A_{N_M+1}) \tag{6.2}$$

$$M(A_1, \ldots, A_{N_M+1}) = \left(\prod_{k=1}^{N_M} A_k^{z_k}\Gamma(-z_k)\right) A_{N_M+1}^{-\nu-\sum\limits_{k=1}^{N_M} z_k} \Gamma\left(\nu + \sum_{k=1}^{N_M} z_k\right), \tag{6.3}$$

where N_M is the number of integration variables. Observe that the following relation holds for the product of all Γ-functions: $\prod\limits_l \Gamma(a_l)$ in Eq. (6.3):

$$\sum_l \frac{\partial a_l}{\partial z_k} = 0. \tag{6.4}$$

6.1 Loop-by-loop approach

In Chap. 4 we reviewed how to write down a general L-loop-momentum integral of tensor rank N_T in terms of scalar Feynman parameter integrals. The loop-by-loop

approach [85] is applied to these scalar Feynman parameter integrals to derive the Mellin-Barnes integral representations.

In the loop-by-loop approach the main idea is to find the Feynman parameter representation to all propagators which contain one common loop-momentum and to apply the Mellin-Barnes master formula to each term in the resulting $\mathcal{F}$-function. Finally, the Feynman parameters are integrated out by an iterative application of the integral representation of the Beta-function in Eq. (4.28). These steps are repeated until all loop-momenta and Feynman parameters are integrated out. The remaining integral is a multi-dimensional Mellin-Barnes integral. As an example we derive a Mellin-Barnes integral representation with the loop-by-loop approach for the Feynman integral I_{0h0w4} in Eq. (4.6).

The loop-momentum integral with one numerator is rewritten as a tensor rank 1 loop-momentum integral

$$I_{\text{0h0w4}} = p_1^\nu g_{\mu\nu} G_1[k_1^\mu] = \int \frac{\mathrm{d}^D k_2}{i\pi^{D/2}} \frac{S[k_1^\mu] p_1^\nu g_{\mu\nu}}{((k_2+p_1)-\tilde{M}_Z^2)k_2^2}, \tag{6.5}$$

$$S^{k_1}[k_1^\mu](k_2,p_1,p_2,D) = \int \frac{\mathrm{d}^D k_1}{i\pi^{D/2}} \frac{k_1^\mu}{k_1^2(k_1-k_2)^2(k_1-p_2)^2}. \tag{6.6}$$

The first loop-by-loop iteration will be applied to the function $S^{k_1}[k_1^\mu]$. Here this function is a tensor rank 1 one-loop integral with $\mathcal{F}$ and $\mathcal{U}$ functions as follows:

$$\begin{aligned} S^{k_1}[k_1^\mu] &= (-1)^3\Gamma(3-\frac{D}{2}) \int \mathrm{d}x_1\mathrm{d}x_2\mathrm{d}x_3 \delta(1-\mathcal{U}_{k_1}) \frac{\mathcal{U}_{k_1}^{3-1-D}}{\mathcal{F}_{k_1}^{3-\frac{D}{2}}} \\ &\quad (k_2^\mu x_2 + p_2^\mu x_3), \end{aligned} \tag{6.7}$$

$$\mathcal{U}_{k_1} = x_1 + x_2 + x_3, \tag{6.8}$$

$$\mathcal{F}_{k_1} = -k_2^2 x_2 x_1 - (k_2-p_2)^2 x_2 x_3, \tag{6.9}$$

where we have used the tensor formula for the one-loop-momentum integrals in Eq. (4.79). We apply the Mellin-Barnes master formula only to the $\mathcal{F}_{k_1}$-function explicitly. Since we have chosen $\delta(1-\mathcal{U}_{k_1})$ in the Feynman parameter representation, the $\mathcal{U}_{k_1}$-function becomes trivial:

$$\begin{aligned} S^{k_1}[k_1^\mu] &= (-1)^{\frac{D}{2}} \int_{-i\infty}^{i\infty} \frac{\mathrm{d}z_1}{2\pi i} \frac{\Gamma(-z_1)\Gamma(3-\frac{D}{2}+z_1)}{((k_2-p_2)^2)^{z_1+3-\frac{D}{2}}(k_2^2)^{-z_1}} \int \mathrm{d}x_1\mathrm{d}x_2\mathrm{d}x_3 \\ &\quad \delta(1-\mathcal{U}_{k_1}) \mathcal{U}_{k_1}^{3-1-D} x_1^{z_1} x_2^{-3+\frac{D}{2}} x_3^{-3+\frac{D}{2}-z_1} (k_2^\mu x_2 + p_2^\mu x_3). \end{aligned} \tag{6.10}$$

After the iterative application of the Mellin-Barnes formula to the $\mathcal{F}$-function the resulting integrand is at most a polynomial in the Feynman parameters in the numerator times a $\mathcal{U}$-function and times $\delta(1-\mathcal{U})$. At this point an iterative use of the integral representation of the Beta-function in Eq. (4.28) is trivial:

$$\prod_{j=1}^{N} \int_{\{x_j \geq 0\}} \mathrm{d}x_j\, x_j^{\nu_j-1} \delta(1-\sum_{i=1}^{N} x_i) = \frac{\Gamma(\nu_1)\ldots\Gamma(\nu_N)}{\Gamma\left(\sum_{i=1}^{N}\nu_i\right)}. \tag{6.11}$$

The iterative use of the integral representation of the Beta-function in the integral in Eq. (6.10) yields:

$$\begin{aligned} S^{k_1}[k_1^\mu] &= k_2^\mu \int\limits_{-i\infty}^{i\infty} \frac{\mathrm{d}z_1}{2\pi i} \frac{(-1)^{\frac{D}{2}}\Gamma(-z_1)\Gamma(3-\frac{D}{2}+z_1)}{((k_2-p_2)^2)^{z_1+3-\frac{D}{2}}(k_2^2)^{-z_1}} \\ &\quad \frac{\Gamma(z_1+1)\Gamma(\frac{D}{2}-1)\Gamma(\frac{D}{2}-z_1-2)}{\Gamma(D-2)} \\ &+ p_2^\mu \int\limits_{-i\infty}^{i\infty} \frac{\mathrm{d}z_1}{2\pi i} \frac{(-1)^{\frac{D}{2}}\Gamma(-z_1)\Gamma(3-\frac{D}{2}+z_1)}{((k_2-p_2)^2)^{z_1+3-\frac{D}{2}}(k_2^2)^{-z_1}} \\ &\quad \frac{\Gamma(z_1+1)\Gamma(\frac{D}{2}-2)\Gamma(\frac{D}{2}-z_1-1)}{\Gamma(D-2)}. \end{aligned} \tag{6.12}$$

The example integral I_{0h0w4} is now prepared for the second iteration in the loop-by-loop approach:

$$\begin{aligned} G_1[k_1^\mu] &= \int\limits_{-i\infty}^{i\infty} \frac{\mathrm{d}z_1}{2\pi i} (-1)^{\frac{D}{2}}\Gamma(-z_1)\Gamma(3-\frac{D}{2}+z_1)\Gamma(z_1+1) \\ &\quad \frac{(S^{k_2}[k_2^\mu]\Gamma(\frac{D}{2}-1)\Gamma(\frac{D}{2}-z_1-2)+S^{k_2}[p_2^\mu]\Gamma(\frac{D}{2}-2)\Gamma(\frac{D}{2}-z_1-1))}{\Gamma(D-2)}, \end{aligned} \tag{6.13}$$

$$S^{k_2}[T(k)] = \int \frac{\mathrm{d}^D k_2}{i\pi^{D/2}} \frac{T(k)}{((k_2+p_1)-\tilde{M}_Z^2)k_2^2((k_2-p_2)^2)^{z_1+3-\frac{D}{2}}(k_2^2)^{-z_1}}. \tag{6.14}$$

We apply a Feynman parameter representation to the propagators containing the second loop-momentum k_2:

$$\begin{aligned} S^{k_2}[T(k)] &= (-1)^{5-\frac{D}{2}} \int\limits_{\{x_i\geq 0\}} \mathrm{d}x_1\mathrm{d}x_2\mathrm{d}x_3 \frac{\Gamma(5-D)x_1^{z_1+2-\frac{D}{2}}x_2^{-z_1}}{\Gamma(z_1+3-D/2)\Gamma(-z_1+1)} \\ &\quad \delta(1-\mathcal{U}_{k_2})\frac{\mathcal{U}_{k_2}^{5-\frac{3D}{2}}}{\mathcal{F}_{k_2}^{5-D}} R[T(k)], \end{aligned} \tag{6.15}$$

$$\mathcal{U}_{k_2} = x_1+x_2+x_3, \tag{6.16}$$

$$\mathcal{F}_{k_2} = -sx_1x_3+\tilde{M}_Z^2x_3(x_1+x_2+x_3), \tag{6.17}$$

$$R[p_2^\mu] = p_2^\mu, \tag{6.18}$$

$$R[k_2^\mu] = (p_2^\mu x_1 - p_1^\mu x_3)/\mathcal{U}_{k_2}, \tag{6.19}$$

where we used already the kinematics, $p_1^2 = p_2^2 = 0$, $2p_1p_2 = s$. Next we apply the Mellin-Barnes master formula to the $\mathcal{F}_{k_2}$-function,

$$\frac{1}{\mathcal{F}_{k_2}^{5-D}} = \int\limits_{-i\infty}^{i\infty} \frac{\mathrm{d}z_2}{2\pi i} \frac{(-sx_1x_3)^{-5+D-z_2}(\tilde{M}_Z^2x_3\mathcal{U}_{k_2})^{z_2}}{\Gamma(5-D)}\Gamma(-z_2)\Gamma(5-D+z_2), \tag{6.20}$$

and perform the Feynman parameter integral with the formula in Eq. (6.11)

$$
\begin{aligned}
p_{1\mu} S^{k_2}[p_2^\mu] &= (-1)^{5-\frac{D}{2}} \int\limits_{-i\infty}^{i\infty} \frac{\mathrm{d}z_2}{2\pi i} \frac{\Gamma(-z_2)\Gamma(5-D+z_2)\Gamma(D-4)}{\Gamma(z_1+3-\frac{D}{2})\Gamma(-5-z_2+\frac{3D}{2})} \\
&\quad (\tilde{M}_Z^2)^{z_2} (-s)^{-5+D-z_2} \Gamma(-2-z_2-z_1+D_2) \frac{s}{2}, \qquad (6.21) \\
p_{1\mu} S^{k_2}[k_2^\mu] &= (-1)^{5-\frac{D}{2}} \int\limits_{-i\infty}^{i\infty} \frac{\mathrm{d}z_2}{2\pi i} \frac{\Gamma(-z_2)\Gamma(5-D+z_2)\Gamma(D-4)}{\Gamma(z_1+3-\frac{D}{2})\Gamma(-4-z_2+\frac{3D}{2})} \\
&\quad (\tilde{M}_Z^2)^{z_2} (-s)^{-5+D-z_2} \Gamma(-1-z_2-z_1+D_2) \frac{s}{2}. \qquad (6.22)
\end{aligned}
$$

The example integral I_{0h0w4} becomes a two-dimensional Mellin-Barnes integral:

$$
\begin{aligned}
p_{1\mu} G_1[k_1^\mu] &= \int\limits_{-i\infty}^{i\infty} \frac{\mathrm{d}z_1}{2\pi i} \int\limits_{-i\infty}^{i\infty} \frac{\mathrm{d}z_2}{2\pi i} (-s)^{D-4} \left(\frac{\tilde{M}_Z}{-s}\right)^{z_2} \Gamma(D-4)\Gamma(-2-z_2+z_1+\frac{D}{2}) \\
&\quad \frac{\Gamma(-z_1)\Gamma(z_1+1)\Gamma(\frac{D}{2}-2)\Gamma(\frac{D}{2}-z_1-1)\Gamma(-z_2)\Gamma(5-D+z_2)}{2\Gamma(D-2)\Gamma(-5-z_2+\frac{3D}{2})} \\
&+ \int\limits_{-i\infty}^{i\infty} \frac{\mathrm{d}z_1}{2\pi i} \int\limits_{-i\infty}^{i\infty} \frac{\mathrm{d}z_2}{2\pi i} (-s)^{D-4} \left(\frac{\tilde{M}_Z}{-s}\right)^{z_2} \Gamma(D-4)\Gamma(-1-z_2+z_1+\frac{D}{2}) \\
&\quad \frac{\Gamma(-z_1)\Gamma(z_1+1)\Gamma(\frac{D}{2}-1)\Gamma(\frac{D}{2}-z_1-2)\Gamma(-z_2)\Gamma(5-D+z_2)}{2\Gamma(D-2)\Gamma(-4-z_2+\frac{3D}{2})}. \qquad (6.23)
\end{aligned}
$$

Barnes' first Lemma We can apply to the Mellin-Barnes integral over z_1 the Barnes' first Lemma:

$$
\int\limits_{-i\infty}^{+i\infty} \frac{\mathrm{d}z}{2\pi i} \Gamma(a+z)\Gamma(b+z)\Gamma(c-z)\Gamma(d-z) = \frac{\Gamma(a+c)\Gamma(a+d)\Gamma(b+c)\Gamma(b+d)}{\Gamma(a+b+c+d)}, \qquad (6.24)
$$

which yields for the integral I_{0h0w4} a one-dimensional Mellin-Barnes integral:

$$
\begin{aligned}
p_{1\mu} G_1[k_1^\mu] &= \int\limits_{-i\infty}^{i\infty} \frac{\mathrm{d}z_2}{2\pi i} (-s)^{D-4} \left(\frac{\tilde{M}_Z}{-s}\right)^{z_2} \frac{\Gamma(\frac{D}{2}-2-z_2)\Gamma(D-3-z_2)\Gamma(\frac{D}{2}-2)\Gamma(\frac{D}{2})}{\Gamma(D-2-z_2)} \\
&\quad \frac{\Gamma(-z_2)\Gamma(5-D+z_2)\Gamma(D-4)}{2\Gamma(D-2)\Gamma(-5-z_2+\frac{3D}{2})} \\
&+ \int\limits_{-i\infty}^{i\infty} \frac{\mathrm{d}z_2}{2\pi i} (-s)^{D-4} \left(\frac{\tilde{M}_Z}{-s}\right)^{z_2} \frac{\Gamma(\frac{D}{2}-1-z_2)\Gamma(D-3-z_2)\Gamma(\frac{D}{2}-1)^2}{\Gamma(D-2-z_2)} \\
&\quad \frac{\Gamma(-z_2)\Gamma(5-D+z_2)\Gamma(D-4)}{2\Gamma(D-2)\Gamma(-4-z_2+\frac{3D}{2})}. \qquad (6.25)
\end{aligned}
$$

We are left to evaluate the remaining one-dimensional Mellin-Barnes integral. In this work we focus on the numerical evaluation.

6.2 Global approach

The other possibility is to derive a Mellin-Barnes integral starting from an L-loop Feynman parameter representation [87]. In this approach the Mellin-Barnes formula is applied to the $\mathcal{U}$- and $\mathcal{F}$-functions until the integral representation of the Beta-function can be used to integrate out the Feynman parameters. As an example we take again the integral I_{0h0w4} in Eq. (4.6) without its numerator $(k_1 p_1)$ in the loop-momenta representation or simply by setting $x_6 = 0$ in the Feynman parameter representation in Eq. (4.48) and in Eq. (4.49) and we call this integral in this context a scalar integral whose Feynman parameter integral representation is

$$I_{\text{scalar}} = (-1)^5 \Gamma(5-D) \prod_{i=1}^{5} \int_{x_i \geq 0} \mathrm{d}x_i \, \delta(1 - \sum_{j=1}^{5} x_j) \frac{\mathcal{U}_{\text{scalar}}^{5-D\frac{3}{2}}}{\mathcal{F}_{\text{scalar}}^{5-D}}. \tag{6.26}$$

The $\mathcal{U}$ and $\mathcal{F}$-functions read:

$$\mathcal{U}_{\text{scalar}} = x_1x_2 + x_1x_3 + x_2x_3 + x_1x_4 + x_2x_4 + x_2x_5 + x_3x_5 + x_4x_5, \tag{6.27}$$

$$\mathcal{F}_{\text{scalar}} = \tilde{M}_Z^2 x_5 \mathcal{U}_{\text{scalar}} - s x_2 x_4 x_5. \tag{6.28}$$

Cheng-Wu theorem The integrand of the Feynman parameter integral, without the δ-function, is a homogeneous function of degree zero in the Feynman parameters. So we may change the δ-function under the integral in the simplest case as follows:

$$\int \mathrm{d}^N x H(x) \delta(1 - \sum_{i=1}^{N} x_i) = \int \mathrm{d}^N x H(x) \delta(1 - \sum_{\Omega_i} x_i), \tag{6.29}$$

where $\sum\limits_{\Omega_i} x_i$ is an arbitrary linear combination of the Feynman parameters with coefficient +1 and $H(x)$ represents a homogeneous function in the Feynman parameters. This is known in mathematics as the method of projective space and we call the relation above simply the Cheng-Wu theorem [72, 73].

Furthermore, we can add to the integral identities like:

$$1 = \int_0^\infty \mathrm{d}u_j \, \delta(u_j - \sum_{\Omega_i} x_i), \tag{6.30}$$

which makes variable transformations more straightforward.

Factorization of a two-loop Feynman integral Introduce additional δ-functions in such a way that the $\mathcal{U}$-function factorizes properly leading to less terms. For our example integral I_{scalar} we use

$$\begin{aligned} \int \mathrm{d}^5 x \, \delta(1 - \sum_{i=1}^{5} x_i) f(\{x_i\}) &= \int \mathrm{d}^5 x \, \mathrm{d}^3 u \, \delta(u_1 - x_1 - x_5) \delta(u_2 - x_3 - x_4) \delta(u_3 - x_2) \\ &\quad \delta(1 - u_1 - u_2 - u_3) f(\{u_i\}, \{x_i\}). \end{aligned} \tag{6.31}$$

The following rescaling of the Feynman parameters

$$\begin{aligned}
\mathcal{D} &= -x_1 k_1^2 && x_1 = x_1' u_1, \\
&- x_5 (k_1 - p_2)^2 && x_5 = x_5' u_1, \\
&- x_3 k_2^2 && x_3 = x_3' u_2, \\
&- x_4 (k_2 + p_1)^2 + x_4 \tilde{M}_Z^2 && x_4 = x_4' u_2, \\
&- x_2 (k_1 - k_2)^2 && x_2 = x_2' u_3,
\end{aligned} \tag{6.32}$$

where we have explicitly recovered Eq. (4.9), will lead to less terms in the $\mathcal{U}_{\text{scalar}}$-function. The $\mathcal{U}$- and $\mathcal{F}$-function representation change:

$$\mathcal{U}'_{\text{scalar}} = u_1 u_2 + u_1 u_3 + u_2 u_3, \tag{6.33}$$

$$\mathcal{F}'_{\text{scalar}} = \mathcal{U}'_{\text{scalar}} x_4' u_2 \tilde{M}_Z^2 - s x_2' x_4' x_5' u_1 u_2 u_3, \tag{6.34}$$

and the Jacobian is $u_1 u_2$. The integral in our example is now cast in the following form:

$$\begin{aligned}
\mathcal{I}_{\text{scalar}} &= -\Gamma(5-D) \int \mathrm{d}^5 x' \mathrm{d}^3 u \, u_1 u_2 \delta(1 - u_1 - u_2 - u_3) \\
&\quad \delta(1 - x_1' - x_5') \delta(1 - x_3' - x_4') \delta(1 - x_2') \frac{\mathcal{U}'^{5-D\frac{3}{2}}_{\text{scalar}}}{\mathcal{F}'^{5-D}_{\text{scalar}}}.
\end{aligned} \tag{6.35}$$

Explanation: We have introduced a new variable u_i for each group of Feynman parameters which are associated with the same kind of loop-momenta flow in the propagators, see Eq. (6.32). Afterwards we have rescaled each Feynman parameter with the corresponding new variable. Note that for two-loop integrals only 3 kinds of propagator flows exist. The first 2 kinds contain only one loop-momentum k_1 or k_2. The third kind contains a linear combination of two loop-momenta k_1 and k_2. For a two-loop integral we will always be able to factorize the $\mathcal{U}$-function into 3 monomials.

Which brings us to the first application of the Cheng-Wu theorem. In our example we replace one δ-function by using the above identity in Eq. (6.29):

$$\int\limits_{\{u_i \geq 0\}} \mathrm{d}^3 u \, \delta(1 - u_1 - u_2 - u_3) f(\{u_i\}) = \int\limits_0^\infty \mathrm{d}u_3 \int\limits_{\{u_i \geq 0\}} \mathrm{d}u_1 \mathrm{d}u_2 \, \delta(1 - u_1 - u_2) f(\{u_i\}). \tag{6.36}$$

This allows us to simplify the $\mathcal{U}'_{\text{scalar}}$-function:

$$\mathcal{U}'_{\text{scalar}} = u_3 + u_1 u_2. \tag{6.37}$$

From here on we apply the Mellin-Barnes master formula only to the $\mathcal{F}$-function until we can explicitly apply the integral representation of the Beta-function in u_3, u_2, u_1, x_5', x_4', x_3' and x_1'. In our example we need only one application of the Mellin-Barnes master formula which yields

$$\frac{1}{(\mathcal{F}'_{\text{scalar}})^{5-D}} = \int\limits_{-i\infty}^{i\infty} \frac{\mathrm{d}z}{2\pi i} \frac{(\mathcal{U}'_{\text{scalar}} x_4' u_2 \tilde{M}_Z^2)^z (-s x_2' x_4' x_5' u_1 u_2 u_3)^{-z-5+D} \Gamma(-z) \Gamma(z + 5 - D)}{\Gamma(5 - D)}. \tag{6.38}$$

This allows us to apply the integral representation of the Beta-function to Eq. (6.35) for all variables $\{u_i\}$ and $\{x'_i\}$,

$$\int\limits_0^\infty \mathrm{d}u_3 \, (u_1u_2+u_3)^{5-D\frac{3}{2}+z} u_3^{-z-5+D} = (u_1u_2)^{1-\frac{D}{2}} \frac{\Gamma(D-4-z)\Gamma(\frac{D}{2}-1)}{\Gamma(D\frac{3}{2}-z-5)}, \tag{6.39}$$

$$\int\limits_{\{u_i\geq 0\}} \mathrm{d}u_1\mathrm{d}u_2 \, u_1^{-3+\frac{D}{2}-z} u_2^{-3+\frac{D}{2}} \delta(1-u_1-u_2) = \frac{\Gamma(\frac{D}{2}-2-z)\Gamma(\frac{D}{2}-2)}{\Gamma(D-4-z)}, \tag{6.40}$$

$$\int\limits_{\{x'_i\geq 0\}} \mathrm{d}x'_1\mathrm{d}x'_5 \delta(1-x'_1-x'_5) x'^{1-1}_1 x'^{-5+D-z}_5 = \frac{\Gamma(1)\Gamma(D-4-z)}{\Gamma(D-3-z)}, \tag{6.41}$$

$$\int\limits_{\{x'_i\geq 0\}} \mathrm{d}x'_3\mathrm{d}x'_4 \delta(1-x'_3-x'_4) x'^{1-1}_3 x'^{-5+D}_4 = \frac{\Gamma(1)\Gamma(D-4)}{\Gamma(D-3)}. \tag{6.42}$$

The integral I_{scalar} becomes a one-dimensional Mellin-Barnes integral:

$$\begin{aligned} \mathcal{I}_{\text{scalar}} = -\int\limits_{-i\infty}^{i\infty} \frac{\mathrm{d}z}{2\pi i} & \frac{(\frac{\tilde{M}_Z^2}{-s})^z (-s)^{-5+D} \Gamma(-z)\Gamma(z+5-D)\Gamma(D-4)}{\Gamma(D-3-z)\Gamma(D\frac{3}{2}-z-5)\Gamma(D-3)} \\ & \Gamma(\frac{D}{2}-2)\Gamma(\frac{D}{2}-2-z)\Gamma(D-4-z)\Gamma(\frac{D}{2}-1). \end{aligned} \tag{6.43}$$

A second example is the integral I_{0h0w4} in Eq. (4.72). Here we would apply the same steps as in the case of the scalar integral. Derive an L-loop Feynman parameter representation, rescale the Feynman parameters and apply the Cheng-Wu theorem:

$$\begin{aligned} I^{\text{global}}_{\text{0h0w4}} &= -\int\limits_{-i\infty}^{i\infty} \frac{\mathrm{d}z}{2\pi i} \frac{(\frac{\tilde{M}_Z^2}{-s})^z (-s)^{-5+D} s\Gamma(-z)\Gamma(z+5-D)\Gamma(D-4)}{2\Gamma(D-2-z)\Gamma(D\frac{3}{2}-z-4)\Gamma(D-3)} \\ &\quad \Gamma(\frac{D}{2}-2)\Gamma(\frac{D}{2}-1)\Gamma(\frac{D}{2}-1-z)\Gamma(D-3-z) \\ &\quad - \int\limits_{-i\infty}^{i\infty} \frac{\mathrm{d}z}{2\pi i} \frac{(\frac{\tilde{M}_Z^2}{-s})^z (-s)^{-5+D} s\Gamma(-z)\Gamma(z+5-D)\Gamma(D-4)}{2\Gamma(D-2-z)\Gamma(D\frac{3}{2}-z-4)\Gamma(D-3)} \\ &\quad \Gamma(\frac{D}{2}-2)\Gamma(\frac{D}{2})\Gamma(\frac{D}{2}-2-z)\Gamma(D-3-z). \end{aligned} \tag{6.44}$$

We achieved again a one-dimensional Mellin-Barnes integral for a tensor like integral I_{0h0w4}. Observe that both Mellin-Barnes representations derived with different methods (loop-by-loop approach and global approach) differ in their representations, but the sum will give the same result if these Mellin-Barnes integrals are evaluated.

With the global approach one gets Mellin-Barnes integrals, where in the derivation no Barnes Lemma or its generalizations are needed. We observe that non-planar diagrams give less dimensional Mellin-Barnes integral representations with the global approach, compared to the loop-by-loop approach. In the derivation of

the Mellin-Barnes integral representations we use the tools `AMBREv2` [88] which implements the loop-by-loop approach and `AMBREv3` [87] which implements the global approach in an automatic way. Both programs work with planar and non-planar Feynman diagrams. The Mellin-Barnes integrals with the least number of integration variables are then treated with `MB.m` [26] and `MBnumerics.m`, which has been developed in this work.

Recently, a new method was developed to derive Mellin-Barnes integral representations which is based on the method of brackets [89, 90, 91] and is implemented in an algorithm discussed in Ref. [92]. This algorithm is dedicated to find the best factorization of the $\mathcal{U}$ and the $\mathcal{F}$ polynomial functions similar to the global approach discussed here.

6.3 Analytic continuation

In the derivation of a Mellin-Barnes integral representation we started with a general Feynman parameter integral and applied either the Mellin-Barnes master formula in Eq. (6.2) or the integral representation of the Beta-function in Eq. (6.11). Note that the integral representation of the Beta-function if used is only valid if all arguments of the Γ-functions have positive real part. The Mellin-Barnes master formula only states that the contour needs to separate the right handed and the left handed poles of the Γ-functions.

For simplicity we restrict in this work *all* arguments of the Γ-functions to have positive real part for *all* Mellin-Barnes integrals. This guarantees at the same time the applicability of the integral representation of the Beta-function and allows to choose a straight integration contour parallel to the imaginary axis, which properly separates all right and left handed poles. In this approach we do not need to pay attention to the imaginary part of the variables: ϵ, $\{z_i\}$, $\{\nu_j\}$, which play a role in the argument of the $\Gamma(\epsilon, \{z_i\}, \{\nu_j\})$-functions. Here ν_i are the propagator exponents in the loop-momenta representation, z_i the Mellin-Barnes integration variables and ϵ comes from the dimensional regularization $D = 4 - 2\epsilon$.

The Mellin-Barnes integral with the above assumptions is equal to the initial Feynman integral. If these conditions cannot be satisfied with $\epsilon = 0$ then the initial integral may develop divergences. After the analytic continuation with $\epsilon \to 0$ the divergences are resolved in the Laurent expansion around $\epsilon = 0$.

An algorithmic way to achieve the analytic continuation is proposed in Ref. [24, 26, 27]. We assume a straight integration contour exists which for some ϵ, $\{z_i\}$, $\{\nu_j\}$ separates all poles of the Γ-functions. The analytic continuation itself is then the accounting for all residues taken in the poles, which get crossed by the integration contour during the evaluation $\epsilon \to 0$ and if needed $\nu_j = \nu_j^I + \delta_{\nu_j}$ with $\delta_{\nu_j} \to 0$, where ν_j^I is the initial value in the loop-momenta representation for the propagator exponents ν_j and δ_{ν_j} is an infinitesimal small parameter.

As soon as it is satisfied that all arguments of the Γ-functions are positive with some initial values for $\epsilon, \{z_i\}, \{\nu_j\}$ the above mentioned algorithm is guaranteed to terminate. In practical calculations we keep $\{z_i\}$ fixed and analytically continue $\epsilon, \{\nu_j\}$ to the desired values.

We illustrate the procedure for the Mellin-Barnes integral in Eq. (6.44). Here we

focus on the first term in this Mellin-Barnes integral representation. The arguments of the Γ-functions need to satisfy

$$\Re e\,(-2\epsilon) > 0, \tag{6.45}$$
$$\Re e\,(-\epsilon) > 0, \tag{6.46}$$
$$\Re e\,(1-\epsilon) > 0, \tag{6.47}$$
$$\Re e\,(1+2\epsilon+z) > 0, \tag{6.48}$$
$$\Re e\,(1-\epsilon-z) > 0, \tag{6.49}$$
$$\Re e\,(1-2\epsilon-z) > 0, \tag{6.50}$$
$$\Re e\,(-z) > 0, \tag{6.51}$$

where we used $D = 4 - 2\epsilon$. The suitable choice for ϵ is easy to read off, if we rewrite the above relations as:

$$0 > \Re e\,(\epsilon) > -1/2, \tag{6.52}$$
$$-1 - 2\Re e\,(\epsilon) < \Re e\,(z) < 0, \tag{6.53}$$
$$-1 - 2\Re e\,(\epsilon) < \Re e\,(z) < 1 - \Re e\,(\epsilon), \tag{6.54}$$
$$-1 - 2\Re e\,(\epsilon) < \Re e\,(z) < 1 - 2\Re e\,(\epsilon). \tag{6.55}$$

It is important to note that the Feynman integral is divergent from the start which is related to $\Gamma(-\epsilon)$ in the Mellin-Barnes integral representation. But we can find an existing integral I_{0h0w4} if we choose $\epsilon = -\frac{1}{4}$ and $\Re e\, z = -\frac{1}{8}$. Thus we define a straight integration contour to be $z = -\frac{1}{8} + it$, $t \in [-\infty, \infty]$. In this example, if we continue ϵ to zero, no pole will cross the contour of our choice. Thus we can safely expand our integrand of the Mellin-Barnes integral into a Laurent series around $\epsilon = 0$.

Sign of the residues During the analytic continuation of a Mellin-Barnes integral

$$I = \left(\prod_j^{N_M} \int_{-i\infty+\Re e\, z_j}^{i\infty+\Re e\, z_j} \frac{\mathrm{d}z_j}{2\pi i} \right) \mathcal{I}(\{c_i z_i\}, \{\nu_j\}, c_\epsilon \epsilon)), \tag{6.56}$$

in the multi-dimensional case, say the $\Gamma(f(\{c_i z_i\}, \{\nu_j\}, c_\epsilon \epsilon'))$-function is responsible for the poles located at $f(\{c_i z_i\}, \{\nu_j\}, \epsilon') = -m$, $m \in \mathbb{N}_0$ which cross the fixed contour. The residue is taken at $z_i = -\frac{f(\{c_j z_j \neq c_i z_i\}, \{\nu_j\}, c_\epsilon \epsilon')}{c_i}$, while z_i may be chosen arbitrary from a set $\{z_i\}$ as long as it is also an argument of the function f. Depending on the choice of z_i, the point ϵ' which is responsible for the pole and the point ϵ_0 which is desired to be reached after the analytic continuation, will dictate the overall sign of the taken residue:

$$I' = \left(\prod_{j\neq i}^{N_M} \int_{-i\infty+\Re e\, z_j}^{i\infty+\Re e\, z_j} \frac{\mathrm{d}z_j}{2\pi i} \right) \mathrm{sign}(c_i)\mathrm{sign}(c_\epsilon \epsilon' - c_\epsilon \epsilon_0) \mathrm{res}_{z_i = -\frac{f(\{c_j z_j \neq c_i z_i\}, \{\nu_j\}, c_\epsilon \epsilon')}{c_i}} \mathcal{I}. \tag{6.57}$$

As expected during the analytic continuation additional integrals like I' are collected with less integration variables, which also need to be continued, since the dependence on ϵ is retained.

Continuation of the residues For this toy example:

$$I_{\text{toy}} = \int \frac{\mathrm{d}z_1}{2\pi i} \int \frac{\mathrm{d}z_2}{2\pi i} \Gamma(-z_1)\Gamma(-z_2)\Gamma(\epsilon + z_1)\Gamma(-z_1 + z_2)/\Gamma(-z_1 + 1), \tag{6.58}$$

to ensure that the arguments of all Γ-functions are positive they need to satisfy the following relations:

$$\Re e\,(\epsilon) > 0, \tag{6.59}$$
$$-\Re e\,(\epsilon) < \Re e\,(z_1) < 0, \tag{6.60}$$
$$\Re e\,(z_1) < \Re e\,(z_2) < 0, \tag{6.61}$$
$$-\Re e\,(\epsilon) < \Re e\,(z_2). \tag{6.62}$$

The integral I_{toy} exists with $\epsilon = \frac{3}{2}$, $z_1 = -\frac{1}{2}$, $z_2 = -\frac{1}{4}$. Next we continue this integral in ϵ to $\epsilon_0 = 0$. The poles of the Γ-functions are crossed by fixed contours when the integrand is modified during the $\epsilon \to 0$ continuation. The equations which determine the pole crossings in our example are

$$\epsilon + z_1|_{z_1=-1/2} = -n, \quad n \in \mathbb{N}_0. \tag{6.63}$$

Going from $\epsilon = 3/2$ to ϵ_0 the above equation is only true at $\epsilon' = \frac{1}{2}$ for $n = 0$. Thus we need to collect only one residue at the point $z_1 = -\epsilon - n|_{n=0}$:

$$I_{\text{ResToy}} = \int \frac{\mathrm{d}z_2}{2\pi i} \Gamma(\epsilon)\Gamma(-z_2)\Gamma(\epsilon + z_2)/\Gamma(1 + \epsilon). \tag{6.64}$$

The sign with which we need to multiply the residue is trivially calculated where the coefficient of z_1 is $c_1 = 1$ and the coefficient of ϵ is $c_\epsilon = 1$, which gives

$$\text{sign}(c_1)\text{sign}(\epsilon' - \epsilon_0) = +1. \tag{6.65}$$

In this example the residue must be analytically continued now starting from $\epsilon' = \frac{1}{2}$ to ϵ_0. The following equations dictate which poles of the Γ-functions will cross the fixed contour of the integral I_{ResToy}

$$\epsilon + z_2|_{z_2=-1/4} = -n, \quad n \in \mathbb{N}_0. \tag{6.66}$$

The equation is true for $\epsilon'' = \frac{1}{4}$ and $n = 0$. Thus we take the residue $z_2 = -\epsilon - n|_{n=0}$

$$I_{\text{Res2toy}} = \Gamma(\epsilon)^2/\Gamma(1 + \epsilon), \tag{6.67}$$

where again the sign which needs to multiply the residue equals +1. At this point all three integrals are analytic in ϵ and contain $\epsilon_0 = 0$. Thus we may expand all three integrals in a Laurent series around ϵ_0. We refer to the last residue I_{Res2toy} as a zero-dimensional Mellin-Barnes integral.

We have now created a basis to derive and analytically continue the Mellin-Barnes integrals. These integrals are in general well behaved in Euclidean regions. So far it was not clear how to evaluate numerically in general the Mellin-Barnes integral representation of Feynman integrals including massive particles in the Minkowskian regions. In this thesis work we cover this issue and show how to evaluate these integrals numerically with the help of `MBnumerics.m`, which involves the study of the asymptotic behavior of the Mellin-Barnes integrals.

Chapter 7

Asymptotic behavior of Mellin-Barnes integrals

This chapter contains some of the most essential results of this thesis. We assume the integration contour of the Mellin-Barnes integrals to be parallel to the imaginary axis in the complex plane. The reason is that the integrals are well defined if we treat them the same way as in Sec. 6.3. First we address the problems which appear if we want to evaluate numerically Mellin-Barnes integral representation of Feynman integrals including massive particles in Minkowskian regions. To do this we first need to study the asymptotic behavior of the integrands of the Mellin-Barnes integrals if the integration variables approach $|z| \to \infty$.

7.1 Asymptotic behavior of Euler's Γ-function

From this section on we make use of the well known Stirling formula

$$\lim_{|z|\to\infty} \frac{\Gamma(z)}{z^{z-1/2}e^{-z}} = \sqrt{2\pi}, \quad |\arg z| < \pi. \tag{7.1}$$

Thus the following approximation is valid:

$$\Gamma(z) \underset{|z|\to\infty}{\approx} z^{z-1/2}e^{-z}\sqrt{2\pi}, \quad |\arg z| < \pi. \tag{7.2}$$

If we apply this approximation to each Γ-function in the Mellin-Barnes master formula, then each $\exp(-z_k)$ will cancel due to the Eq. (6.4). Thus from now on we do not pay attention to this factor. We also neglect the $\sqrt{2\pi}$ factor for brevity, since we are only interested if the asymptotic behavior of the Mellin-Barnes integral is polynomial or exponentially in z.

Applying the parameter representation

$$z_k = x_k + ih_k t, \;\; x_k,\; h_k \in \mathbb{R}, \tag{7.3}$$

for a general Γ-function we have:

$$\Gamma\left(\sum_{k=1}^{N_M} b_k z_k + \beta\right) \underset{|z|\to\infty}{\to} \left(\sum_{k=1}^{N_M} b_k(x_k + ih_k t) + \beta\right)^{\sum_{k=1}^{N_M} b_k(x_k+ih_k t)+\beta-1/2}, \tag{7.4}$$

$$= \exp\left(\left(\sum_{k=1}^{N_M} b_k(x_k + ih_k t) + \beta - 1/2\right) \log\left(\sum_{k=1}^{N_M} b_k(x_k + ih_k t) + \beta\right)\right), \tag{7.5}$$

where $b_k,\ \beta \in \mathbb{R}$ and N_M is again the number of all Mellin-Barnes integration variables.

x_k is a constant and $t \in [0, \infty]$. This parameterization gives an integration contour parallel to the imaginary axis which is already used in Sec. 6.3 about analytic continuation. The Jacobian is simply $\prod_k ih_k$.

Here we neglect the phase factor of the Γ-functions, which is responsible for the oscillatory behavior of the Γ-function. Usually the oscillatory behavior of an integrand is exponentially damped for $|z| \to \infty$ in Euclidean regions. In Minkowskian regions this is for most Mellin-Barnes integrals not the case if we assume a contour in Eq. (7.3). In this chapter we show the origin for the cancellation of the exponential damping factor. In a recent paper [93] the authors show how to evaluate one-dimensional Mellin-Barnes integrals with the help of the method of the steepest descent in Minkowskian regions. In this work we show that one-dimensional integrals can also be treated by just studying the absolute value of the Γ-functions in the asymptotic limit $|z| \to \infty$. In Sec. 8.4 we introduce a technique which we call the shifts to treat multi-dimensional Mellin-Barnes integrals. For the application of the shifts we need to study the polynomial asymptotic behavior of the Mellin-Barnes integrals in the asymptotic limit $|z| \to \infty$. In this work the relevant relation to study the asymptotic behavior of a Mellin-Barnes integral is Eq. (7.5):

$$\left|\exp\left[\left(\sum_k b_k(x_k + ih_k t) + \beta - 1/2\right) \log\left(\sum_k b_k(x_k + ih_k t) + \beta\right)\right]\right| \tag{7.6}$$

$$\underset{t\to\infty}{\approx} \exp\left[\left(i\sum_k b_k h_k t\right) i \arg\left(\sum_k b_k(x_k + ih_k t) + \beta\right)\right.$$
$$\left. + \left(\sum_k b_k x_k + \beta - 1/2\right) \log\left|\sum_k b_k(x_k + ih_k t) + \beta\right|\right] \tag{7.7}$$

$$\approx \exp\left[\left(-t\sum_k b_k h_k\right) \arg\left(it\sum_k b_k h_k\right)\right.$$
$$\left. + \left(\sum_k b_k x_k + \beta - 1/2\right) \frac{1}{2} \log\left(t^2 \left(\sum_k b_k h_k\right)^2 + c_i\right)\right] \tag{7.8}$$

$$\underset{t\to\infty}{\approx} \exp\left(-\frac{\pi}{2} t \left|\sum_k b_k h_k\right|\right) \left(t^2 \left(\sum_k b_k h_k\right)^2 + c_i\right)^{\frac{1}{2}\left(\sum_k b_k x_k + \beta - 1/2\right)} \tag{7.9}$$

$$\underset{t\to\infty}{\approx} \quad \exp\left(-\frac{\pi}{2}t\left|\sum_k b_k h_k\right|\right)\left(t\left|\sum_k b_k h_k\right|(1+c_i\mathcal{O}(\frac{1}{t^2}))\right)^{\left(\sum_k b_k x_k+\beta-1/2\right)}, \quad (7.10)$$

where c_i is a constant in the asymptotic limit $t\to\infty$. Note that $\sum_k b_k h_k$ may sum up to zero. In this case the Γ-function does not contribute to the exponential damping factor in the asymptotic limit $t\to\infty$. The only contribution to the exponential damping factor is coming from $\arg(it\sum_k b_k h_k)$, which either is $\frac{\pi}{2}$ or $-\frac{\pi}{2}$ for $\sum_k b_k h_k > 0$ or $\sum_k b_k h_k < 0$ in the asymptotic limit $t\to\infty$ respectively, see Eq. (7.10). We explicitly keep the polynomial dependence in the study of the asymptotic behavior in the asymptotic limit $t\to\infty$, which is the second factor in Eq. (7.10).

7.2 Asymptotic behavior of the Mellin-Barnes master formula

Now we are ready to study the asymptotic behavior of a multi-dimensional Mellin-Barnes integral. Collecting all Γ-functions in the Mellin-Barnes master formula, see Eq. (6.2), gives the following asymptotic behavior in the limit $t\to\infty$, where we use Eq. (7.3):

$$\exp\left[-t\frac{\pi}{2}\left(\sum_{k=1}^{N_M}|h_k|+\left|\sum_{k=1}^{N_M}h_k\right|\right)\right]t^{\sum_{i=1}^{N_M}\alpha_i+\beta},\ t>0, \quad (7.11)$$

with:

$$\alpha_i = \begin{cases}(-x_i-\frac{1}{2}), & \text{if } h_i^2\neq 0,\\ 0, & \text{else,}\end{cases} \quad (7.12)$$

$$\beta = \begin{cases}(\sum_{l=1}^{N_M}x_l)-\frac{1}{2}+\nu, & \text{if } (\sum_{l=1}^{N_M}h_l)^2\neq 0,\\ 0, & \text{else,}\end{cases} \quad (7.13)$$

where we neglect again the phase factor. Note that in the Mellin-Barnes master formula so far $|b_k|=1$ is satisfied. This result states that for any set of variables $\{h_k\}\backslash\{0\}$ the combination of Γ-functions in Eq. (6.2) will always give rise to an exponential damping factor.

In a one dimensional Mellin-Barnes integral the polynomial asymptotic behavior $t^{\sum_{i=1}^{N_M}\alpha_i+\beta}$ in the asymptotic limit $t\to\infty$ will never depend on the position x_i of the Mellin-Barnes integration contour in the complex plane. In the case of a multi-dimensional Mellin-Barnes integral with $N_M>1$ the polynomial asymptotic behavior $t^{\sum_{i=1}^{N_M}\alpha_i+\beta}$ may explicitly depend on the position x_i of the straight integration contours in the complex plane. We can verify this already in the case of a two-dimensional Mellin-Barnes integral if we take $h_1=1$ and $h_2=-1$.

For ease of notation we introduce additional variables $z_{N_M+1} = -\sum_{i=1}^{N_M} z_i$ and $h_{N_M+1} = -\sum_{i=1}^{N_M} h_i$. The asymptotic behavior of the Mellin-Barnes master formula in Eq. (6.2) depends additionally on the following exponential function if at least one of the objects A_k has the property $\Re e\, A_k < 0$, $k = 1, \dots N_M + 1$:

$$|\lim_{\delta\downarrow 0}(A_k \pm i\delta)^{z_k}| = |\lim_{\delta\downarrow 0}\exp(z_k \log(A_k \pm i\delta))|, \tag{7.14}$$

$$= |\lim_{\delta\downarrow 0}\exp((x_k + ih_k t)(\log|A_k \pm i\delta| + i\arg(A_k \pm i\delta)))|, \tag{7.15}$$

$$= |\exp((x_k + ih_k t)(\log|A_k| \pm i\pi))|, \tag{7.16}$$

$$\underset{t\to\infty}{\approx} \exp(\mp h_k t\pi), \quad t > 0. \tag{7.17}$$

The exponential behavior from the factors $A_k^{z_k}$ depend on the sign of the respective h_k and the infinitesimal imaginary part $i\delta$. Thus this factor might enhance the already generated damping factor in the Γ-functions or even cancel.

By multiplying Eq. (7.11) with Eq. (7.17) the asymptotic behavior for $t \to \infty$ of the Mellin-Barnes master formula in Eq. (6.2) reads for $\Re e\,(A_l \pm i\delta) < 0$, $l = 1, \dots, N_M$:

$$-t\frac{\pi}{2}\left(\sum_{k=1}^{N}|h_k| + \left|\sum_{k=1}^{N}h_k\right|\right) - th_l\pi \;=\; 0, \;\; h_{k\neq l} = 0, \;\; h_l < 0 \text{ for } +i\delta, \tag{7.18}$$

$$-t\frac{\pi}{2}\left(\sum_{k=1}^{N}|h_k| + \left|\sum_{k=1}^{N}h_k\right|\right) + th_l\pi \;=\; 0, \;\; h_{k\neq l} = 0, \;\; h_l > 0 \text{ for } -i\delta, \tag{7.19}$$

$$-t\frac{\pi}{2}\left(\sum_{k=1}^{N}|h_k| + \left|\sum_{k=1}^{N}h_k\right|\right) \mp th_l\pi \;<\; 0, \;\; \text{else, for } \pm i\delta, \tag{7.20}$$

where we simply show the argument of the resulting exponential damping factor. If the parameter $\Re e\,(A_{N_M+1} \pm i\delta) < 0$ appears then we may treat it in the asymptotic limit $t \to \infty$ after the linear transformation $z_l \to -\sum_{i\neq l} z_i - \nu$ the same way as the parameters $A_l \pm i\delta < 0$, $l = 1, \dots, N_M$ above .

Observe that in the Mellin-Barnes master formula due to Eq. (7.18) and Eq. (7.19) the exponential damping factor in the asymptotic limit $t \to \infty$ always cancels exactly for the variables $\Re e\,(A_l \pm i\delta) < 0$, for one specific set of parameters $\{h_k\}\backslash\{0\}$. This case is related to the Minkowskian regions. The cancellation of the exponential damping factor in the limit $t \to \infty$ will be never observed if we take Euclidean regions ($\forall \Re e\, A_l > 0$).

If multiple A_l are negative we may repeat the calculation and will again find that the damping factor is canceled for a specific set of variables $\{h_k\}\backslash\{0\}$.

Only if all A_l, $l = 1, \dots, N_M + 1$ are negative no cancellation of a damping factor exists, because the $\mathcal{F}$-function is then positive semidefinite.

7.3 Asymptotic behavior of Euler's Beta-function

In general the A_l, $l = 1, N_M + 1$ may contain Feynman parameters. In the loop-by-loop approach and in the global approach we made use of the integral representa-

tion of the Beta-function in Eq. (6.11) to integrate out the Feynman parameters. Thus we study the asymptotic behavior of the Beta-function, written down as a product of Γ-functions, as follows:

$$\int\limits_{x_i \geq 0} \mathrm{d}^{N_F} x\, \delta(1 - \sum_{i=1}^{N_F} x_i) \prod_{l=1}^{N_M} (A_l^{z_l}) A_{N_M+1}^{-\nu-\sum\limits_{i=1}^{N_M} z_l} \prod_{i=1}^{N_F} x_i^{a_i} \tag{7.21}$$

$$= \frac{\prod\limits_{l=1}^{N_M} ((A_l^0)^{z_l}) (A_{N_M+1}^0)^{-\nu-\sum\limits_{i=1}^{N_M} z_l} \prod\limits_{i=1}^{N_F} \Gamma(\sum\limits_{l=1}^{N_M} z_l (b_{il} - b_{i(N_M+1)}) - b_{i(N_M+1)}\nu + a_i + 1)}{\Gamma\left(\sum\limits_{i=1}^{N_F} \left(\sum\limits_{l=1}^{N_M} z_l (b_{il} - b_{i(N_M+1)}) - b_{i(N_M+1)}\nu + a_i\right) + N_F\right)},$$

where N_M gives the total number of Mellin-Barnes integration variables and N_F gives the total number of the Feynman parameters.

The Feynman parameters which are building blocks of the $A_l = A_l^0 \left(\prod\limits_{j=1}^{N_F} x_j^{b_{jl}}\right)$ come from the application of the Mellin-Barnes master formula to the $\mathcal{U}$- and the $\mathcal{F}$-functions, where A_l^0 do not depend on the Feynman parameters. Some Feynman parameters come from the Jacobians (for example if we rescale the Feynman parameters in order to use the Cheng-Wu theorem). Feynman parameters stemming from the measure $\int \mathrm{d}x_i\, x_i^{\nu_i - 1}$ of the Feynman parameter integral itself are collected in $\prod\limits_{i=1}^{N_F} x_i^{a_i}$, where a_i are some complex valued constants with $\Re e\, a_i > 0$. Note that the above formula is valid if the real parts of all arguments of the Γ-functions are positive.

The asymptotic behavior of Eq. (7.21) in the limit $t \to \infty$ with the parameterization in Eq. (7.3) is given by

$$\exp\left[-\frac{\pi}{2} t \sum_{i=1}^{N_F} \left|\sum_{l=1}^{N_M} (b_{il} - b_{i(N_M+1)}) h_l\right| + \frac{\pi}{2} t \left|\sum_{i=1}^{N_F} \sum_{l=1}^{N_M} (b_{il} - b_{i(N_M+1)}) h_l\right|\right] t^{\sum\limits_{i=1}^{N_F} \gamma_i + \delta}, \tag{7.22}$$

with

$$\gamma_i = \begin{cases} \sum\limits_{l=1}^{N_M} (b_{il} - b_{i(N_M+1)}) x_l + a_i + 1 - \frac{1}{2}, & \text{if } \sum\limits_{l=1}^{N_M} (b_{il} - b_{i(N_M+1)}) h_l \neq 0, \\ 0, & \text{else}, \end{cases} \tag{7.23}$$

$$\delta = \begin{cases} \sum\limits_{i=1}^{N_F} (\sum\limits_{l=1}^{N_M} (b_{il} - b_{i(N_M+1)}) x_l - a_i) + \frac{1}{2} - N_F, & \text{if } \sum\limits_{i=1}^{N_F} \sum\limits_{l=1}^{N_M} (b_{il} - b_{i(N_M+1)}) h_l \neq 0, \\ 0, & \text{else}. \end{cases} \tag{7.24}$$

where the use of the integral representation of the Beta-function to the Feynman parameters will at most generate coefficients $|b_{il}| = \{0, 1, 2\}$ as long as we derive the Mellin-Barnes integral representation from the Feynman parameter representation by the loop-by-loop approach or the global approach.

We observe that for $N_M > 1$ and if in the set $\{h_l\}$ at least one $h_j = 0$ and $h_k \neq 0$, then the polynomial asymptotic behavior may again depend explicitly on the position of x_i of the Mellin-Barnes integration contour in the complex plane.

In the asymptotic behavior of the Beta-function the exponential damping factor dependence may also vanish for example if all coefficients $(b_{il} - b_{i(N_M+1)}) > 0$ and $\forall h_l \geq 0$ or $\forall h_l \leq 0$. Thus if we observe a cancellation of the exponential damping factor in the asymptotic behavior in the limit $t \to \infty$ of the Mellin-Barnes master formula in Eq. (7.18) or in Eq. (7.19), then the use of the integral representation of the Beta-function to the Feynman parameters may not change the fact that the exponential damping factor disappeared in the Mellin-Barnes integral. In this case the asymptotic behavior in the limit $t \to \infty$ of the Mellin-Barnes integral is dictated by the polynomial asymptotic behavior t^α generated by individual Γ-functions, see the second factor in Eq. (7.10). For Feynman integrals including massive particles this is always the case. All integrals which we encounter in the integral classes in Tab. 3.2 exhibit a non-trivial cancellation of the exponential damping factor in the asymptotic limit $t \to \infty$ in Minkowskian regions.

One known example where no cancellation of the exponential damping factor in Minkowskian regions appears is the on-shell massless box which we have introduced in Chap. 5.

If the exponent in the polynomial asymptotic behavior t^α is $\alpha \geq -1$ then the integral is not absolutely convergent. If the asymptotic behavior of the integrand depends on oscillations then the integral may still formally converge but is not treatable with standard numerical methods, which do not take into account oscillations. If the exponent is $\alpha < -1$ then the integrand is absolutely convergent but is numerically very poor convergent. It is possible to restore the exponential damping factor for one-dimensional Mellin-Barnes integrals with a suitable deformation of the integration contours, see Sec. 8.1. But there is no known general recipe to restore the exponential damping factor in a multi-dimensional Minkowski case. In the Sec. 8.4 we show how to treat a general multi-dimensional Mellin-Barnes integral algorithmically with the help of the contour shifts. The algorithm for the application of the contour shifts is greatly improved if we know the polynomial asymptotic behavior in the limit $t \to \infty$.

7.4 Determining the polynomial asymptotic behavior

In this work we test the cancellation of the exponential damping factors for a fixed subset H of values for $\{h_1, \ldots, h_{N_M}\}$, stemming from requiring the straight integration contour $z_k = x_k + ith_k$. We allow that $\{h_i\}$ may take values from the set of $\{-n, \ldots, -i, \ldots, -2, -1, 0, 1, 2, \ldots, i, \ldots, n\}$, $i \in \mathbb{N}_0$. n depends on the dimensionality of the Mellin-Barnes integral and the number of masses appearing in the propagators in the loop-momenta representation. In practice $n = 2$ appeared to be enough to classify the integrals good enough for further numerical treatment. For each subset $H_j = \{h'_k\}$ where a cancellation of the exponential factors in the asymptotic behavior in the limit $t \to \infty$ appears we calculate the polynomial asymptotic behavior dependence in the same subset H_j.

The asymptotic behavior of a multi-dimensional Mellin-Barnes integral may depend on different polynomial asymptotic behavior for different subsets H_j. The test which we are going to introduce can not tell if the cancellation of the exponential damping factors of the Mellin-Barnes integral in the asymptotic limit $t \to \infty$ is point

like (one-dimensional integration region) or is valid for a multi-dimensional integration region.

Example We study the following two-dimensional Mellin-Barnes integral also in Sec. 8.4:

$$I_{\text{soft721}} = \int\limits_{-\frac{1}{3}-i\infty}^{-\frac{1}{3}+i\infty} \frac{\mathrm{d}z_1}{2\pi i} \int\limits_{-\frac{1}{3}-i\infty}^{-\frac{1}{3}+i\infty} \frac{\mathrm{d}z_2}{2\pi i} \mathcal{I}_{\text{soft721}}, \tag{7.25}$$

$$\mathcal{I}_{\text{soft721}} = -\frac{\left(\frac{M_W^2}{m_t^2}\right)^{z_1} \left(-\frac{s}{m_t^2}\right)^{z_2} \Gamma(2-z_1)\Gamma(-z_1)\Gamma(-z_2)\Gamma(1+z_2)}{2m_t^2\Gamma(3+z_2)^2} \Gamma(1+z_1+z_2)^2. \tag{7.26}$$

In this example $A_1 = \frac{M_W^2}{m_t^2}$ and $A_2 = -\frac{s}{m_t^2}$. We apply Eq. (7.17) and Eq. (7.10) to the integrand in Eq. (7.26) and assume that $s = s_0 + i\delta$, with $s_0 > 0$, $m_t > 0$, $M_W > 0$ and $\delta > 0$, where δ is infinitesimally small. If we use the kinematics defined above then A_2 is the Minkowski parameter (generates additional exponential asymptotic behavior in the asymptotic limit $|z| \to \infty$). Applying the parametrization given in Eq. (7.3), the result for the asymptotic behavior in the limit $t \to \infty$ is:

$$e^{+\pi t h_2} e^{-\pi t(|h_1|+|h_1+h_2|)} (t|h_1|+c_1)^{-2\Re e\, z_1+1} (t|h_1+h_2|+c_2)^{2\Re e\, z_1+2\Re e\, z_2+1} (t|h_2|+c_3)^{-2\Re e\, z_2-5}. \tag{7.27}$$

The first exponential factor comes from A_2, the second from the Γ-functions. The first 2 polynomial functions come from the Γ-functions in the numerator, the last polynomial function comes from the Γ-function in the denominator. The constants c_1, c_2, c_3 in the polynomial functions control that if the sum $\sum b_k h_k = 0$, then the polynomial function disappears in the respective asymptotic limit.

Let us fix $n = 2$ and test all appearing cancellations of the exponential damping factors. The resulting subsets which all individually lead in Eq. (7.27) to the cancellation of the exponential damping factor are $H_1 = (0, 1)$, $H_2 = (-1, 1)$, $H_3 = (-1, 2)$. The sets $H_4 = (0, 2)$ and $H_5 = (-2, 2)$ lead also to a cancellation of the exponential damping factor but are redundant. For the given sets H_i we calculate the polynomial asymptotic behavior of the Mellin-Barnes integral in the asymptotic limit $t \to \infty$:

$$H_1 : \quad t^{2\Re e\, z_1-4}, \tag{7.28}$$

$$H_2 : \quad t^{-2\Re e\, z_1-2\Re e\, z_2-4}, \tag{7.29}$$

$$H_3 : \quad t^{-3}. \tag{7.30}$$

In this example $\Re e\, z_1$ is x_1 and $\Re e\, z_2$ is x_2. We see for the first time the cancellation of the exponential damping factors for a Mellin-Barnes integral in Minkowskian regions. Finally we should keep in mind that the polynomial asymptotic behavior is connected to the arguments of the Γ-functions. In Sec. 8.4 we use the fact that the polynomial asymptotic behavior may depend on $\Re e\, z_i$.

Chapter 8

Integration of Mellin-Barnes integrals in Minkowskian regions

This chapter contains some of the most essential results of this thesis. In the following we introduce several techniques to evaluate numerically one- and multi-dimensional Mellin-Barnes integrals in Minkowskian regions. We illustrate how these techniques work by calculating Feynman integrals numerically, which are known in literature analytically. The program `MBnumerics.m`, which is developed in this thesis, automatically generates Mellin-Barnes integrands suitable for Minkowskian regions by applying these techniques also to non-trivial examples.

8.1 One-dimensional Mellin-Barnes integrals

Our starting point will be the QED one-loop vertex integral including massive particles with $p_1^2 = p_2^2 = m^2$. The problem has been discussed initially in [26]:

$$V(s) = \frac{e^{\epsilon\gamma_E}}{i\pi^{D/2}} \int \frac{\mathrm{d}^D k}{((k+p_1)^2 - m^2)k^2((k-p_2)^2 - m^2)} = \frac{V_{-1}(s)}{\epsilon} + V_0(s) + \cdots . \quad (8.1)$$

In the above equation the Laurent series expansion of the integral around $\epsilon = 0$, $D = 4 - 2\epsilon$ is given. We look at the leading divergent integral $V_{-1}(s)$, which takes for $m = 1$, $s = (p_1 + p_2)^2$ the following form

$$V_{-1}(s) = -\frac{1}{2s} \int\limits_{-\frac{1}{2}-i\infty}^{-\frac{1}{2}+i\infty} \frac{\mathrm{d}z}{2\pi i} (-s)^{-z} \frac{\Gamma^3(-z)\Gamma(1+z)}{\Gamma(-2z)}. \quad (8.2)$$

Summing up residues of Eq. (8.2) we get

$$V_{-1}(s) = \frac{1}{2} \sum_{n=0}^{\infty} \frac{s^n}{\binom{2n}{n}(2n+1)} = \frac{2\arcsin(\sqrt{s}/2)}{\sqrt{4-s}\sqrt{s}}. \quad (8.3)$$

So, we can test numerically some basic ideas of numerical integration. For instance, taking $s = 2$, Eq. (8.3) gives an exact result (which is purely real)

$$V_{-1}(2)|_{\text{analyt.}} = \frac{\pi}{4} = 0.78539816339744830961566084581987572104\ldots . \quad (8.4)$$

For s = 4, the integral $V_{-1}(s)$ is divergent. This divergency is the leading Landau singularity of the integral, encoded in $1/\sqrt{1-4/s}$.

8.1.1 Prototype Mellin-Barnes integral

Now if one attempts to numerically integrate this Mellin-Barnes integral in Eq. (8.2) with the publicly available `Mathematica` package `MB.m` [26] one will not succeed. To get an idea how to automatically numerically integrate such an integral we consider a general function, which is a prototype for a one-dimensional Mellin-Barnes integral

$$I \equiv \int \mathrm{d}z\, \mathcal{I}(z) = \int \mathrm{d}z\, (-s)^{-z\left(\sum_i a_i - \sum_k c_k\right)} F(z), \tag{8.5}$$

$$F(z) = \frac{\prod_i^{i_{\max}} \Gamma(a_i z + \alpha_i) \prod_j^{j_{\max}} \Gamma(-b_j z + \beta_j)}{\prod_{k=1}^{k_{\max}} \Gamma(c_k z + \gamma_k) \prod_l^{l_{\max}} \Gamma(-d_l z + \delta_l)}, \tag{8.6}$$

where a_i, b_j, c_k, d_l are positive real numbers and α_i, β_j, γ_k, δ_l are real numbers. We call $(-s)^{-z\left(\sum_i a_i - \sum_k c_k\right)}$ the s-dependent part of the Mellin-Barnes integral. By construction, these integrals satisfy the following equation, see Eq. (6.4):

$$\sum_i a_i - \sum_j b_j - \left(\sum_k c_k - \sum_l d_l\right) = 0. \tag{8.7}$$

Next we need the asymptotic expansion of the Γ-function for large arguments. The Stirling formula in Eq. (7.2) applied to Eq. (8.6) yields:

$$\lim_{|z|\to\infty} F(z) = e^{G(z)}, \tag{8.8}$$

$$G(z) = z\Big(A_1 \ln(z) - A_2 \ln(-z)\Big) + z(A_3 + A_4) + \ln(z) A_5 + \ln(-z) A_6. \tag{8.9}$$

The coefficients A_i in Eq. (8.9) are:

$$A_1 = \sum_i^{i_{\max}} a_i - \sum_k^{k_{\max}} c_k, \tag{8.10}$$

$$A_2 = \sum_j^{j_{\max}} b_j - \sum_l^{l_{\max}} d_l, \tag{8.11}$$

$$A_3 = \sum_i^{i_{\max}} a_i \ln a_i - \sum_j^{j_{\max}} b_j \ln b_j - \sum_k^{k_{\max}} c_k \ln c_k + \sum_l^{l_{\max}} d_l \ln d_l, \tag{8.12}$$

$$A_4 = -\sum_i^{i_{\max}} a_i + \sum_j^{j_{\max}} b_j + \sum_k^{k_{\max}} c_k - \sum_l^{l_{\max}} d_l, \tag{8.13}$$

$$A_5 = -\frac{i_{\max} - k_{\max}}{2} + \sum_i^{i_{\max}} \alpha_i - \sum_k^{k_{\max}} \gamma_k, \tag{8.14}$$

$$A_6 \;=\; -\frac{j_{\max}-l_{\max}}{2}+\sum_j^{j_{\max}}\beta_j-\sum_l^{l_{\max}}\delta_l. \tag{8.15}$$

It follows that A_1=A_2 and $A_4=0$.

Relation $\ln(z)-\ln(-z)=i\pi\,\mathrm{sign}(\Im m\,z)$ and Eq. (8.7) applied to Eq. (8.9) gives:

$$G(z)=z\,A_1 i\pi\,\mathrm{sign}(\Im m\,(z))+z\,A_3+\ln(z)A_5+\ln(-z)A_6. \tag{8.16}$$

Parametrizing

$$z=it+f(t), \tag{8.17}$$

where $f(t)$ is a real function in $t\in[-\infty,\infty]$ and Jacobian is given by:

$$(i+f'(t)). \tag{8.18}$$

Applied to Eq. (8.16) this parameterization yields

$$\begin{aligned}\Re e\,G(it+f(t)) &= -\pi A_1|t|+f(t)A_3+1/2\ln(t^2+f(t)^2)(A_5+A_6), &(8.19)\\ \Im m\,G(it+f(t)) &= \pi A_1\,\mathrm{sign}(t)f(t)+tA_3+\arg(it+f(t))A_5\\ &\quad+\arg(-it-f(t))A_6. &(8.20)\end{aligned}$$

We parameterize also the s-dependent part of Eq. (8.5) with Eq. (8.17) and we use $s=s_0+i\delta$, where s_0 is real and $i\delta$ follows from the Feynman prescription

$$\begin{aligned}\lim_{\delta\downarrow 0}(-(s_0+i\delta))^{-(it+f(t))A_1} &= e^{(-\pi t-f(t)\ln(s_0))\,A_1}e^{i(\pi f(t)-t\ln(s_0))\,A_1},\quad s_0>0, &(8.21)\\ \lim_{\delta\downarrow 0}(-(s_0+i\delta))^{-(it+f(t))A_1} &= e^{(-f(t)\ln(-s_0))\,A_1}e^{(-it\ln(-s_0))\,A_1},\quad s_0<0. &(8.22)\end{aligned}$$

The integral in Eq. (8.5) is studied in Euclidean region for $s_0<0$ and in Minkowskian region for $s_0>0$.

If we choose $f(t)=0$, the asymptotic behavior of the Mellin-Barnes integrand in Eq. (8.5) in Euclidean region is

$$\mathcal{I}(it)=e^{-\pi A_1|t|+1/2\ln(t^2)(A_5+A_6)}e^{i(tA_3+\mathrm{sign}(t)\frac{1}{2}\pi(A_5-A_6)-t\ln(-s_0))},\quad s_0<0. \tag{8.23}$$

We observe an overall exponential damping factor as long as $A_1>0$.

If we choose $f(t)=0$, the asymptotic behavior of the Mellin-Barnes integrand in Eq. (8.5) in Minkowskian region is

$$\mathcal{I}(it)=e^{-\pi A_1(t+|t|)+1/2\ln(t^2)(A_5+A_6)}e^{i(tA_3+\mathrm{sign}(t)\frac{1}{2}\pi(A_5-A_6)\mathrm{sign}(t)-t\ln(s0))},\quad s_0>0. \tag{8.24}$$

The exponential damping factor is canceled for $t<0$.

This time the Mellin-Barnes integrand in Eq. (8.5) in Minkowskian region depends explicitly on the function $f(t)$:

$$\begin{aligned}\mathcal{I}(it+f(t)) &= e^{-(\pi t+f(t)\ln(s_0))\,A_1}e^{i(\pi f(t)-t\ln(s_0))\,A_1}e^{-\pi A_1|t|+f(t)A_3+1/2\ln(t^2+f(t)^2)(A_5+A_6)}\\ &\quad e^{i(\pi A_1\,\mathrm{sign}(t)f(t)+tA_3+\arg(it+f(t))A_5+\arg(-it-f(t))A_6)}e^{\ln(f'(t))},\quad s_0>0. &(8.25)\end{aligned}$$

Here we combined Eqs. (8.18, 8.19, 8.20, 8.21).

We show that it is possible to generate a damping factor for a Mellin-Barnes integrand in Minkowskian region by choosing appropriate functions $f(t)$ in Eq. (8.25). The real part of the argument in the exponential function in Eq. (8.25) is

$$f(t)(A_3 - \ln(s_0)), \quad t < 0, \tag{8.26}$$
$$f(t)(A_3 - \ln(s_0)) - 2\pi t A_1, \quad t > 0, \tag{8.27}$$

which is responsible for the exponential damping factor. We collected only terms which are proportional to $f(t)$ and t. The generation of the exponential damping factor depends explicitly on $A_3 - \ln(s_0)$, A_1 and $f(t)$. If $(A_3 - \ln(s_0)) > 0$, than

$$f(t) < \begin{cases} 0 & t < 0, \\ \frac{2\pi t A_1}{A_3 - \ln(s_0)} & t > 0, \end{cases} \tag{8.28}$$

and if $(A_3 - \ln(s_0)) < 0$, than

$$f(t) > \begin{cases} 0 & t < 0, \\ \frac{2\pi t A_1}{A_3 - \ln(s_0)} & t > 0. \end{cases} \tag{8.29}$$

Satisfying these relations will generate the exponential damping factor. Note that the choice of the function $f(t)$ depends on the s-dependent part of the Mellin-Barnes integral. We observe that the exponential damping factor can not be restored in the case, where $A_3 - \ln(s_0) = 0$.

We look for two suitable functions $f(t)$, and apply the relations in Eq. (8.28) and in Eq. (8.29). In this discussion we assume that $A_1 > 0$.

Ansatz 1: $f(t) = \theta t$

For $(A_3 - \ln(s_0)) > 0$, Eq. (8.28), leads to

$$\theta t < \begin{cases} 0 & t < 0, \\ \frac{2\pi t A_1}{A_3 - \ln(s_0)} & t > 0, \end{cases} \tag{8.30}$$

which yields

$$0 < \theta < \frac{2\pi A_1}{A_3 - \ln(s_0)}, \tag{8.31}$$

and for $(A_3 - \ln(s_0)) < 0$, Eq. (8.29), leads to

$$\theta t > \begin{cases} 0 & t < 0, \\ \frac{2\pi t A_1}{A_3 - \ln(s_0)} & t > 0, \end{cases} \tag{8.32}$$

which yields

$$\frac{2\pi A_1}{A_3 - \ln(s_0)} < \theta < 0. \tag{8.33}$$

Ansatz 2: $f(t) = \theta t^2$

For the second example $f(t) = \theta t^2$ and $(A_3 - \ln(s_0)) > 0$, Eq. (8.28), leads to

$$\theta t^2 < \begin{cases} 0 & t < 0, \\ \frac{2\pi t A_1}{A_3 - \ln(s_0)} & t > 0, \end{cases} \tag{8.34}$$

which yields

$$\theta < 0. \tag{8.35}$$

and for $(A_3 - \ln(s_0)) < 0$, Eq. (8.29), leads to

$$\theta t^2 > \begin{cases} 0 & t < 0, \\ \frac{2\pi t A_1}{A_3 - \ln(s_0)} & t > 0, \end{cases} \tag{8.36}$$

which yields

$$\theta > 0. \tag{8.37}$$

Both $f(t) = \theta t$ and $f(t) = \theta t^2$ are straightforward to implement in a computer program. The function $f(t) = \theta t^2$ is implemented in `MBnumerics.m`, which is developed in this thesis, with a suitable choice $\theta = -1, 1$. We illustrate this choice with the next example.

8.1.2 Example: One-loop vertex integral in Minkowskian regions

We apply Eq. (8.25) to derive the asymptotic behavior with the parametrization $z = it + f(t)$ for the Mellin-Barnes integrand in Eq. (8.2) in Minkowskian regions:

$$\begin{aligned} (-s)^{-z} \frac{\Gamma^3(-z)\Gamma(1+z)}{\Gamma(-2z)} &= e^{1/2i(-2\arg(-it-f(t))+\arg(it+f(t)))} \\ &\quad \frac{e^{\ln(4/s_0)f(t)} e^{i\ln(4/s_0)t}}{\sqrt[4]{t^2+f(t)^2}}, \quad t < 0, \quad s_0 > 0, \end{aligned} \tag{8.38}$$

$$\begin{aligned} (-s)^{-z} \frac{\Gamma^3(-z)\Gamma(1+z)}{\Gamma(-2z)} &= e^{1/2i(-2\arg(-it-f(t))+\arg(it+f(t))+4\pi f(t))} \\ &\quad \frac{e^{-2\pi t} e^{\ln(4/s_0)f(t)} e^{i\ln(4/s_0)t}}{\sqrt[4]{t^2+f(t)^2}}, \quad t > 0, \quad s_0 > 0. \end{aligned} \tag{8.39}$$

If we choose $f(t) = 0$, then the asymptotic behavior of the Mellin-Barnes integrand in Eq. (8.2) in Minkowskian regions becomes:

$$-\frac{(1+i)}{\sqrt{2}} \frac{e^{i\ln(4/s_0)t}}{\sqrt{-t}}, \quad t < 0, \tag{8.40}$$

$$-\frac{(1-i)}{\sqrt{2}} \frac{e^{-2\pi t} e^{i\ln(4/s_0)t}}{\sqrt{t}}, \quad t > 0. \tag{8.41}$$

The exponential damping factor disappeared for $t < 0$ and the integrand is not absolutely convergent due to $1/\sqrt{-t}$. Let us focus from now on only on the exponential damping factor in the asymptotic behavior of Eq. (8.2).

Contour deformation 1. For $f(t) = \theta t$ we find:

$$\frac{e^{\theta \ln(4/s_0) t}}{\sqrt{-t}\sqrt[4]{1+\theta^2}}, \quad t < 0, \tag{8.42}$$

$$\frac{e^{-2\pi t + \theta \ln(4/s_0) t}}{\sqrt{t}\sqrt[4]{1+\theta^2}}, \quad t > 0. \tag{8.43}$$

To evaluate $V_{-1}^{f(t)=\theta t}(2)$ we choose $\theta = 1$ from

$$0 < \theta < \frac{2\pi}{\ln(2)}. \tag{8.44}$$

The results are:

$$V_{-1}^{f(t)=t}(2) = 0.7853981633974483\boldsymbol{9}606, \tag{8.45}$$

$$V_{-1}^{f(t)=t}(2) = 0.7853981633974483096156608458198\boldsymbol{7}721, \tag{8.46}$$

$$V_{-1}^{(\text{analyt.})}(2) = 0.7853981633974483096156608458198757210 4\ldots . \tag{8.47}$$

For this and all the following calculations we have performed explicitly the limit $\lim_{\delta \downarrow 0}$.

Contour deformation 2. For $f(t) = \theta t^2$ we have derived:

$$\frac{e^{\theta \ln(4/s_0) t^2}}{\sqrt[4]{t^2+\theta^2 t^4}}, \quad t < 0, \tag{8.48}$$

$$\frac{e^{-2\pi t + \theta \ln(4/s_0) t^2}}{\sqrt[4]{t^2+\theta^2 t^4}}, \quad t > 0. \tag{8.49}$$

To evaluate $V_{-1}^{f(t)=\theta t^2}(2)$ we choose $\theta = -1$:

$$V_{-1}^{f(t)=-t^2}(2) = 0.7853981633974483\boldsymbol{9}518, \tag{8.50}$$

$$V_{-1}^{f(t)=-t^2}(2) = 0.7853981633974483096156608458198\boldsymbol{7}726, \tag{8.51}$$

$$V_{-1}^{(\text{analyt.})}(2) = 0.7853981633974483096156608458198757210 4\ldots . \tag{8.52}$$

To get the numerical results in Eq. (8.45) and in Eq. (8.50) we have used `NIntegrate` routine from `Mathematica` with the options:
`WorkingPrecision → 16,`
`AccuracyGoal → 16,`
`PrecisionGoal → Infinity.`
To get the numbers in Eq. (8.46) and in Eq. (8.51) we have used `NIntegrate` routine with the options:
`WorkingPrecision → 32,`
`AccuracyGoal → 32,`
`PrecisionGoal → Infinity.`
The achieved numerical accuracy in Eqs. (8.45, 8.50, 8.46, 8.51) with `NIntegrate` routine is marked with bold text. The error estimate is extracted with the help of the builtin `Mathematica` interface: `IntegrationMonitor`.

The Mellin Barnes integral in this example can not be evaluated at $s = 4$, because it is divergent. This behavior is the leading Landau singularity of this integral.

8.1.3 Example: Two-loop vertex integral in Minkowskian regions

As a further example we work with the Mellin-Barnes integral representation in Eq. (6.25) which we have derived for the integral I_{0h0w4} in Eq. (4.6) with the loop-by-loop approach. After the analytic continuation in $\epsilon \to 0$, see Sec. 6.3, we expand this Mellin-Barnes integral in a Laurent series around $\epsilon = 0$. The divergences of the integral are resolved in the $1/\epsilon$ poles:

$$\frac{1}{\Gamma(1+\epsilon)^2} I^{\text{MB}}_{\text{0h0w4}} = \tilde{M}_Z^{2(-2\epsilon)} \sum_{i=-2}^{0} B_i \epsilon^i, \tag{8.53}$$

where we have rescaled the Feynman integral with $(\tilde{M}_Z^2)^{D-\nu}$, see Eq. (4.51). Next we evaluate numerically the coefficients B_i, which are again Mellin-Barnes integrals and use the input parameters of Eq. (4.50) and perform the limit $\lim_{\delta \downarrow 0}$ first.

In Minkowskian regions different Mellin-Barnes integrals may exhibit different polynomial asymptotic behavior, see Sec. 7.4. Since the polynomial asymptotic behavior is connected to the arguments of the Γ-functions in the integrand of the Mellin-Barnes integral we group all Mellin-Barnes integrals with the same Γ-functions and evaluate each group separately. For example in the case of one-dimensional integrals it might appear that we need different contour deformations for different Mellin-Barnes integrals belonging to the same coefficient B_i.

In the following we find the explicit coefficients B_i which appear in Eq. (8.53):

$$B_{-2} = \frac{(-\frac{M_Z^2}{x})^{z_2}\Gamma(-z_2)^2\Gamma(1+z_2)}{4\Gamma(2-z_2)}, \tag{8.54}$$

$$\begin{aligned} B_{-1} = & -\frac{(-\frac{M_Z^2}{x})^{z_2}\Gamma(1-z_2)^2\Gamma(-z_2)\Gamma(1+z_2)}{4\Gamma(2-z_2)^2} \\ & + \frac{(-\frac{M_Z^2}{x})^{z_2}\Gamma(-z_2)^2\Gamma(1+z_2)}{4\Gamma(2-z_2)} (1 + 4\gamma_E - 2\log(-x) \\ & + \Psi(1-z_2) + 2\Psi(2-z_2) - \Psi(-z_2) + 2\Psi(1+z_2)) \end{aligned} \tag{8.55}$$

$$\begin{aligned} B_0 = & -\frac{(-\frac{M_Z^2}{x})^{z_2}\Gamma(1-z_2)^2\Gamma(-z_2)\Gamma(1+z_2)}{4\Gamma(2-z_2)^2} (2 + 4\gamma_E \\ & -2\log(-x) - 3\Psi(1-z_2) + 5\Psi(2-z_2) + 2\Psi(1+z_2)) \\ & + \frac{(-\frac{M_Z^2}{x})^{z_2}\Gamma(-z_2)^2\Gamma(1+z_2)}{8\Gamma(2-z_2)} (4 + 8\gamma_E + 16\gamma_E^2 \\ & -4\log(-x) - 16\gamma_E \log(-x) + 4\log(-x)^2 \\ & +2\Psi(1-z_2) + 8\gamma_E\Psi(1-z_2) - 4\log(-x)\Psi(1-z_2) \\ & +\Psi(1-z_2)^2 + 4\Psi(2-z_2) + 16\gamma_E\Psi(2-z_2) - \\ & 8\log(-x)\Psi(2-z_2) + 4\Psi(1-z_2)\Psi(2-z_2) + \\ & 4\Psi(2-z_2)^2 - 2\Psi(-z_2) - 8\gamma_E\Psi(-z_2) \\ & +4\log(-x)\Psi(-z_2) - 2\Psi(1-z_2)\Psi(-z_2) \\ & -4\Psi(2-z_2)\Psi(-z_2) + \Psi(-z_2)^2 + 4\Psi(1+z_2) \\ & +16\gamma_E\Psi(1+z_2) - 8\log(-x)\Psi(1+z_2) \end{aligned}$$

$$
\begin{aligned}
&+4\Psi(1-z_2)\Psi(1+z_2)+8\Psi(2-z_2)\Psi(1+z_2)\\
&-4\Psi(-z_2)\Psi(1+z_2)+4\Psi(1+z_2)^2-5\Psi'(1-z_2)\\
&-4\Psi'(2-z_2)+\Psi'(-z_2)+4\Psi'(1+z_2)),
\end{aligned}
\tag{8.56}
$$

where the integration measure $\int_{-1/2-it}^{-1/2+it} \frac{\mathrm{d}z_2}{2\pi i}$ was omitted for brevity. The function Ψ (PolyGamma) and its derivatives are defined as:

$$
\Psi(z) = \frac{\partial \log \Gamma(z)}{\partial z}, \tag{8.57}
$$

$$
\Psi'(z) = \frac{\partial \Psi(z)}{\partial z}, \tag{8.58}
$$

$$
\Psi^{(i)}(z) = \frac{\partial^{(i)} \Psi(z)}{\partial z^{(i)}}. \tag{8.59}
$$

Analytic calculation to verify the numerical results

In this thesis we use the software package `Kira` [94], which is an implementation of the Laporta algorithm to reduce scalar multi-loop integrals to a set of master integrals, by using an additional algorithm based on modular arithmetic to remove linearly dependent equations from the system of equations arising from integration-by-parts identities.

With the software package `Kira`, the needed integration-by-parts reduction of the integral I_{0h0w4} in Eq. (4.6) was performed to a set of known master integrals which can be found in the literature [95]:

$$
\begin{aligned}
&-2M_Z^2(D-4)^2 I_{\text{0h0w4}}(1,1,1,1,1,-1,0) =\\
&+(M_Z^2)^2(D-4)^2 x\, I_{\text{0h0w4}}(1,1,1,1,1,0,0)\\
&-M_Z^2\,(D-2)\,(D-3)\,I_{\text{0h0w4}}(0,1,1,1,1,0,0)\\
&+(D-2)\,(D-3)\,I_{\text{0h0w4}}(1,1,0,1,0,0,0).
\end{aligned}
\tag{8.60}
$$

The analytic results in terms of the harmonic polylogarithms (HPL) [96] for the master integrals can be read off in Ref. [95], which are Eqs. (119, 573, 643) therein. We multiply the integrals $I_{\text{0h0w4}}(1,1,1,1,1,0,0)$ and $I_{\text{0h0w4}}(1,1,0,1,0,0,0)$ by an additional factor (-1). The reason is that in this work we defined the loop-momenta representation for the integrals with the metric in the more plus convention, but in Ref. [95] the authors use the metric with the more minus convention.

The Laurent series around $\epsilon = 0$ with the coefficients in terms of the harmonic polylogarithms reads

$$
\frac{1}{\Gamma(1+\epsilon)^2} I_{\text{0h0w4}}^{\text{Ana}} = \tilde{M}_Z^{2(-2\epsilon)} \sum_{i=-2}^{0} A_i \epsilon^i, \tag{8.61}
$$

and the coefficients read:

$$A_{-2} = \left(\frac{1}{4x}+\frac{1}{4}\right)\text{HPL}(\{-1\},x) - \frac{1}{4}, \tag{8.62}$$

$$\begin{aligned} A_{-1} &= \left(\frac{1}{4x}+\frac{1}{4}\right)\text{HPL}(\{-2\},x) + \left(\frac{1}{x}+1\right)\text{HPL}(\{-1\},x) \\ &\quad + \left(-\frac{1}{x}-1\right)\text{HPL}(\{-1,-1\},x) - \frac{5}{4}, \end{aligned} \tag{8.63}$$

$$\begin{aligned} A_0 &= \left(\frac{1}{4x}+\frac{1}{4}\right)\text{HPL}(\{-3\},x) + \left(\frac{1}{x}+\frac{3}{2}\right)\text{HPL}(\{-2\},x) \\ &\quad + \left(\frac{\frac{7}{2}+\frac{\pi^2}{12}}{x}+\frac{\pi^2}{12}+\frac{7}{2}\right)\text{HPL}(\{-1\},x) + \left(-\frac{1}{x}-1\right) \\ &\quad \text{HPL}(\{-2,-1\},x) + \left(-\frac{3}{2x}-\frac{3}{2}\right)\text{HPL}(\{-1,-2\},x) \\ &\quad + \left(-\frac{4}{x}-4\right)\text{HPL}(\{-1,-1\},x) \\ &\quad + \left(\frac{4}{x}+4\right)\text{HPL}(\{-1,-1,-1\},x) - \frac{\pi^2}{12} - \frac{19}{4}. \end{aligned} \tag{8.64}$$

In order to evaluate numerically the analytic result in Eq. (8.61) we have used the function `HPLConvertToKnownFunctions`, which is part of the package `HPL.m` [97], to express all coefficients in Eqs. (8.62, 8.63, 8.64) in terms of logarithms and polylogarithms.

Numerical evaluation of one-dimensional Mellin-Barnes integrals

The integral I_{0h0w4} is evaluated in two different kinematic points: First we evaluate the coefficients A_i in Eq. (8.61) and B_i in Eq. (8.53) at the original kinematic point of Eq. (4.50), where $x = 1 + i\delta$ and $M_Z = 1$, see Tab. 8.2. Next we evaluate these coefficients at the new kinematic point $x = \left(\frac{455938}{401925}\right)^2 + i\delta$ and $M_Z = 1$, see Tab. 8.1. Furthermore, we apply the contour deformation $z_2 = -\frac{1}{2} + (i+\theta)t^2$, $t \in [-\infty, \infty]$, where θ is the contour deformation parameter and $2(i+\theta)t$ the Jacobian. The numerical evaluation was done with the `NIntegrate` routine in `Mathematica` and we have used the options:

```
WorkingPrecision → 32,
AccuracyGoal → 32,
PrecisionGoal → Infinity.
```

The effect of the contour deformation is best illustrated with simpler integrands:

$$\mathcal{I}_1 = \frac{(-\frac{M_Z^2}{x})^{z_2}\Gamma(1-z_2)^2\Gamma(-z_2)\Gamma(1+z_2)}{\Gamma(2-z_2)^2}, \tag{8.65}$$

$$\mathcal{I}_2 = \frac{(-\frac{M_Z^2}{x})^{z_2}\Gamma(-z_2)^2\Gamma(1+z_2)}{\Gamma(2-z_2)}, \tag{8.66}$$

which we also find as building blocks in the coefficients B_i in Eqs. (8.54, 8.55, 8.56).

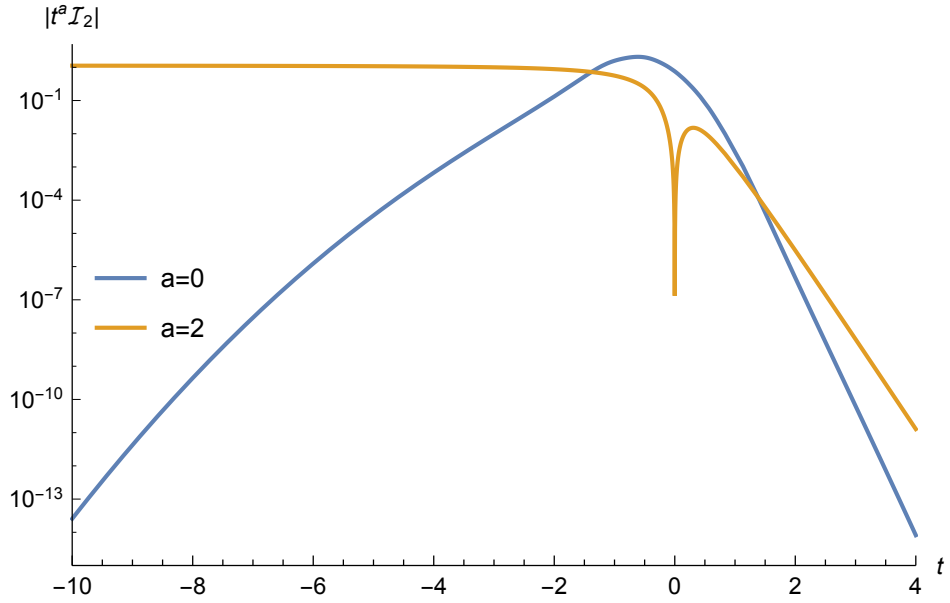

Figure 8.1: Logarithmic plot illustrates the asymptotic behavior of the integrand $\mathcal{I}_2$ in Eq. (8.66) with (blue curve) and without contour deformation (orange curve). The contour deformation generates an overall exponential damping factor. The asymptotic behavior is polynomial $1/t^2$ for the integrand without the contour deformation. We have used the input parameters: $x = \left(\frac{455938}{401925}\right)^2 + i\delta$ and $M_Z = 1$, while taking the limit $\lim_{\delta \downarrow 0}$ first.

The asymptotic behavior in the limit $|z_2| \to \infty$ is given by:

$$|\mathcal{I}_{1,2}| \underset{t\to-\infty}{\approx} \frac{\left(\frac{M_Z^2}{x}\right)^{\theta t^2}}{\theta^2 t^4 + t^2}, \tag{8.67}$$

$$|\mathcal{I}_{1,2}| \underset{t\to\infty}{\approx} \frac{e^{-2\pi t}\left(\frac{M_Z^2}{x}\right)^{\theta t^2}}{\theta^2 t^4 + t^2}. \tag{8.68}$$

In Minkowskian regions, see Eq. (4.50), we see the cancellation of the exponential damping factor for a straight integration contour $\theta = 0$ in the asymptotic limit $t \to -\infty$. The choice of $\theta = 1$ generates an exponential damping factor for the kinematic point $x = \left(\frac{455938}{401925}\right)^2 + i\delta$, see blue curve in Fig. 8.1. The exponential damping factor is not generated for the kinematic point $x = 1 + i\delta$, but the asymptotic behavior is improved to $1/t^3$ for $\theta = 1$ (blue curve) instead of $1/t^2$ for $\theta = 0$ (orange curve) for $t \to -\infty$, see Fig 8.2.

For the same accuracy the integrator is forced to evaluate the integrand with polynomial asymptotic behavior in a bigger integration region, than the integrand with an overall exponential damping factor. Since the Mellin-Barnes integrands include Γ-functions, which growth factorial, we convert in `MBnumerics.m`, developed in this thesis, all products of Γ-functions as a sum of $\log\Gamma$-funcitons:

$$\prod_i \Gamma_i \to \exp\left(\sum_i \log\Gamma_i\right). \tag{8.69}$$

Table 8.1: Results are presented for the coefficients B_i in Eqs. (8.54, 8.55, 8.56) and for the coefficients A_i in Eqs. (8.62, 8.63, 8.64). We have used the input parameters: $x = \left(\frac{455938}{401925}\right)^2 + i\delta$ and $M_Z = 1$, while taking the limit $\lim_{\delta \downarrow 0}$ first. The contour deformation $f(t) = \theta t^2$ is applied in `MBnumerics.m`. The numerical results are shown for $\theta = 1$ and $\theta = 0$, which effectively switches the contour deformation on and off. The significant digits are highlighted.

Coefficient in $1/\epsilon^2$	**Numerics**
Eq. (8.62)	-0.319591958678431917727445157765957
	-0.175063069196677755853271916418687722 i
Eq. (8.54) with $\theta = 1$	-0.319591958678431917727445157765956
	-0.175063069196677755853271916418687725 i
Eq. (8.54) with $\theta = 0$	-0.319**6**1 - 0.175**0**8 i
Coefficient in $1/\epsilon$	**Numerics**
Eq. (8.63)	-0.726411782273487251253818743982**1**017
	-1.618918492235158369941841060118**2**7374 i
Eq. (8.55) with $\theta = 1$	-0.726411782273487251253818743982**1**019
	-1.618918492235158369941841060118**2**7370 i
Eq. (8.55) with $\theta = 0$	-0.72**6**4 - 1.61**9**4 i
Finite coefficient	**Numerics**
Eq. (8.64)	0.671705063623169826581999831588940**4**
	-6.534329693981888746794185343393382 i
Eq. (8.56) with $\theta = 1$	0.671705063623169826581999831588942
	-6.534329693981888746794185343393388 i
Eq. (8.56) with $\theta = 0$	0.6**6**1 - 6.5**2**5 i

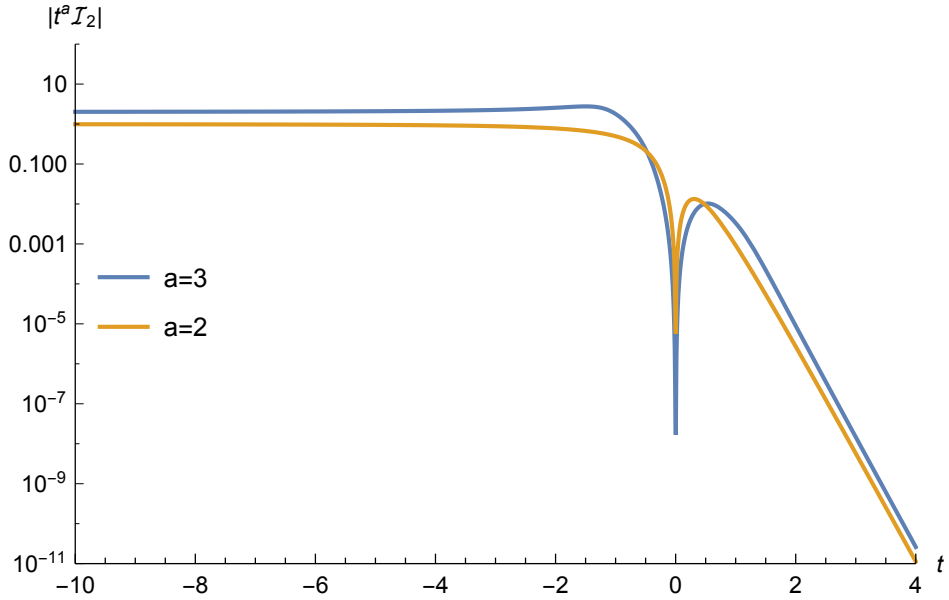

Figure 8.2: Logarithmic plot illustrates the asymptotic behavior of the integrand $\mathcal{I}_2$ in Eq. (8.66) with (blue curve) and without contour deformation (orange curve). The contour deformation does not generate an overall exponential damping factor, but the polynomial asymptotic behavior is improved to $1/t^3$. Without the contour deformation the asymptotic behavior is polynomial $1/t^2$ for the same integrand. We have used the input parameters: $x = 1 + i\delta$ and $M_Z = 1$, while taking the limit $\lim_{\delta \downarrow 0}$ first.

It is important to stress that we evaluate a function representation for $\log\Gamma$-function instead of taking a logarithm of the Γ-function [98]. The calculation of one-dimensional Mellin-Barnes integrals in this work will be at most of the complexity as the integral $I_{0\text{h}0\text{w}4}$, discussed in this section. In the program `MBnumerics.m`, which is developed in this thesis, the contour deformation $f(t) = \theta t^2$ and the transformation in Eq. (8.69) is implemented.

8.1.4 Asymptotic behavior of the Ψ-function

After the expansion in ϵ in Eq. (8.53) we see for the first time the presence of the Ψ-function in Eq. (8.57) and its derivatives [98] in the Mellin-Barnes integrals. They exhibit the same poles as the Γ-functions. The asymptotic behavior of the Ψ-function for large arguments is logarithmic:

$$\Psi(z) \underset{|z|\to\infty}{\approx} \log(z). \tag{8.70}$$

The asymptotic behavior stemming from the Ψ-functions is suppressed in the presence of an exponential damping factor in a Mellin-Barnes integrand in the asymptotic limit $|z| \to \infty$, but if the exponential damping factor cancels, the asymptotic behavior in the limit $|z| \to \infty$ is a polynomial function. In this case due to the presence of logarithmic asymptotic behavior the overall asymptotic behavior in the limit $|z| \to \infty$ gets worse.

Table 8.2: Results are presented for the coefficients B_i in Eqs. (8.54, 8.55, 8.56) and for the coefficients A_i in Eqs. (8.62, 8.63, 8.64). We have used the input parameters: $x = 1 + i\delta$ and $M_Z = 1$, while taking the limit $\lim_{\delta \downarrow 0}$ first. The contour deformation $f(t) = \theta t^2$ is applied in `MBnumerics.m`. The numerical results are shown for $\theta = 1$ and $\theta = 0$, which effectively switches the contour deformation on and off. The significant digits are highlighted.

Coefficient in $1/\epsilon^2$	**Numerics**
Eq. (8.62)	-1/4
Eq. (8.54) with $\theta = 1$	-0.250000000000000000000000000000***0***2
Eq. (8.54) with $\theta = 0$	-0.250000000000000000000000000000***0***0
Coefficient in $1/\epsilon^1$	**Numerics**
Eq. (8.63)	-5/4
Eq. (8.55) with $\theta = 1$	-1.250000000000000000000000000***0***0
Eq. (8.55) with $\theta = 0$	-1.249999999999***8***8
Finite coefficient	**Numerics**
Eq. (8.64)	-6.3949340668482264364724151666460***2***5
Eq. (8.56) with $\theta = 1$	-6.394934066848226436472415***5***2
Eq. (8.56) with $\theta = 0$	-6.39493406684***4***6

The derivatives of the Ψ-functions are harmless because they enhance the polynomial asymptotic behavior in the asymptotic limit $|z| \to \infty$:

$$\frac{\partial^a \Psi(z)}{\partial z^a} \underset{|z|\to\infty}{\propto} \frac{1}{z^a}. \tag{8.71}$$

8.2 Mapping of infinities

It is important to note that the package `MB.m` was not designed to treat Mellin-Barnes integrals in Minkowskian regions. This is mentioned in the manual [26] and can be concluded from the implemented logarithmic mapping therein.

We use for the integration of multi-dimensional Mellin-Barnes integrals publicly available libraries which calculate in machine precision. Explicitly we use the `CUBA` [99][100] library. This library contains a Monte Carlo algorithm, `Vegas`, but also an algorithm which applies deterministic curbature rules, `Cuhre`. We use both, `Vegas` for five or more dimensional Mellin-Barnes integrals and `Cuhre` for four or less dimensional Mellin-Barnes integrals. To automatically generate the `Fortran` code for the numerical integration in `MBnumerics.m` a modified code is used stemming originally from `MB.m`. Furthermore, to evaluate numerically the functions like $\log \Gamma$

and Ψ in Eq. (8.57) and its derivatives in `Fortran` we use the `CernLib` library [101, 98, 102].

Since the library `CUBA` assumes an integration region over a finite hypercube, we want to apply an integrand mapping in such a way that the integration ranges are $d \in [0,1]$ instead of $t \in [-\infty, \infty]$. Here we use the parameterization $z_i = x_i + it_i$, with $x_i \in \mathbb{R}$ a constant and $t_i \in [-\infty, \infty]$.

We test two different mappings at a one-dimensional integral level. We have seen that the one-dimensional Mellin-Barnes integrands in Minkowskian regions with a contour $f(t) = 0$ have an asymptotic behavior like $1/t^a$, $a \in \mathbb{R}$. The logarithmic works well for Mellin-Barnes integrals in Euclidean regions whose asymptotic behavior is an overall exponential damping factor for large values of t. The logarithmic mapping $t = \ln[\frac{d}{1-d}]$ applied to a polynomial function gives

$$\frac{1}{t^a} = \frac{1}{\ln[\frac{d}{1-d}]^a}, \tag{8.72}$$

and the Jacobian is $\frac{1}{d(1-d)}$. The limits $d = 0, 1$ for the logarithmic mapping times the Jacobian give in the case of polynomial asymptotic behavior:

$$\lim_{d\to 0, d\to 1} \frac{1}{d(1-d)} \frac{1}{\ln(\frac{d}{1-d})^a} = \frac{1}{0}, \ \forall\, a. \tag{8.73}$$

Such a mapping introduces in the Mellin-Barnes integrands in Minkowskian regions an integrable singularity at the borders $d = 0, 1$. In the Minkowskian regions the exponential damping factor is only canceled either for $t < 0$ or for $t > 0$. Thus the singularity is either in $d = 0$ or in $d = 1$.

The cotangent mapping $t = \frac{1}{\tan(-\pi d)}$ when applied to the polynomial function gives

$$\frac{1}{t^a} = \tan(-\pi d)^a, \tag{8.74}$$

where the Jacobian is $\frac{\pi}{\sin(\pi d)^2}$. The polynomial asymptotic behavior times the Jacobian gives

$$\frac{\pi \tan(-\pi d)^a}{\sin(\pi d)^2} = \begin{cases} \frac{1}{0}, & a < 2, \\ \pi, & a = 2, \\ 0, & a > 2, \end{cases} \tag{8.75}$$

thus the cotangent mapping does not generate a domain with a singularity at the boundaries for $a \geq 2$. And is suitable for the numerical integration of Mellin-Barnes integrals.

Again we convert all products of Γ-functions into a sum of $\log\Gamma$-functions, see Eq. (8.69). This is mandatory, since Γ-functions growth very fast if its argument is mapped with cotangent.

8.2.1 Example: One-dimensional Mellin-Barnes integral

We study the integrand $\mathcal{I}_1$ in Eq. (8.65). In this example the contour deformation $f(t) = \theta t^2$ does not restore the damping factor if we take the kinematic point of

Eq. (4.50), $x = 1 + i\delta$ and $M_Z = 1$. The asymptotic behavior is a polynomial function $1/t^2$, see Eq. (8.67) for $\theta = 0$, similar to the integrand $\mathcal{I}_2$ in Eq. (8.66) . Thus the above analysis would yield that the logarithmic mapping in Eq. (8.72) gives ∞ at $d = 0$, see orange curve in Fig. 8.3 and for cotangent mapping gives a constant at $d = 0$, see blue curve in Fig. 8.3.

This one-dimensional Mellin-Barnes integral was just a toy example, because we do not apply any mappings to one-dimensional integrals. `NIntegrate` a routine in `Mathematica` maps the boundaries $t \in [-\infty, \infty]$ automatically.

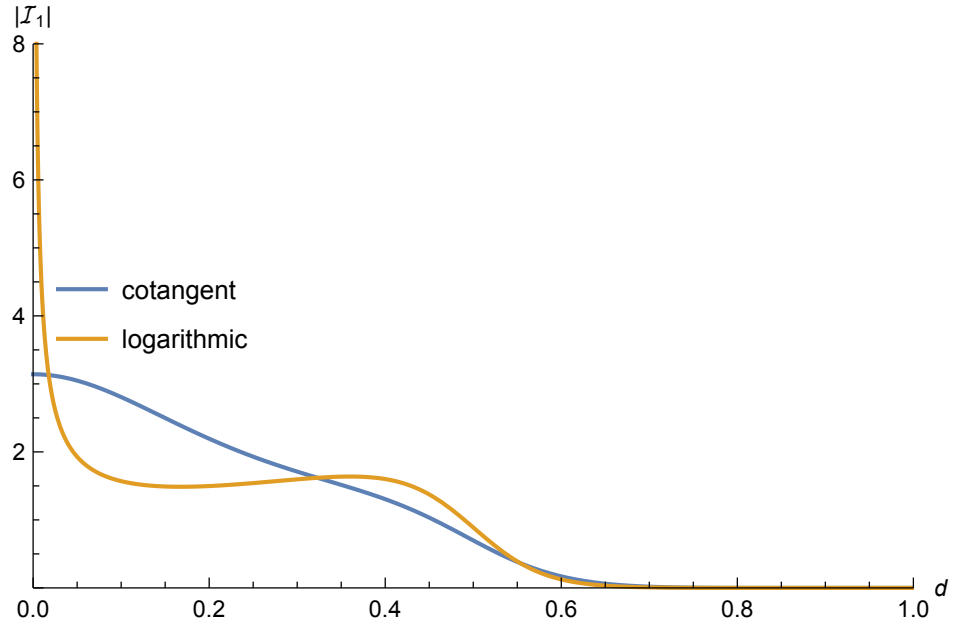

Figure 8.3: The absolute value of the integrand $\mathcal{I}_1$ in Eq. (8.65) is plotted for different mappings. The logarithmic mapping in Eq. (8.72) (orange curve) and cotangent mapping in Eq. (8.74) (blue curve) are illustrated.

8.2.2 Example: Two-dimensional Mellin-Barnes integral

To illustrate the procedure of integrand mappings to multi-dimensional integrals it is sufficient to study the following two-dimensional Mellin-Barnes integral in Minkowskian regions. The loop-momenta representation is

$$I_{0\text{h}0\text{w}14}(1,1,1,1,1,-1,0) = \int \frac{\mathrm{d}^D k_1}{i\pi^{D/2}} \frac{\mathrm{d}^D k_2}{i\pi^{D/2}} \frac{1}{P_1^1 P_2^1 P_3^1 P_4^1 P_5^1 P_6^{-1} P_7^0}, \tag{8.76}$$

where the propagators are $P_1 = k_1^2,\ P_2 = ((k_1 - k_2)^2 - \tilde{M}_Z^2),\ P_3 = k_2^2,\ P_4 = ((k_2 + p_1)^2 - \tilde{M}_Z^2),\ P_5 = (k_1 + p_1 + p_2)^2,\ P_6 = k_1 p_1,\ P_7 = k_2 p_2$, see Fig. 8.4. This integral $I_{0\text{h}0\text{w}14}(1,1,1,1,1,-1,0)$ has one irreducible scalar product in the numerator, $(k_1 p_1)$,.

The Mellin-Barnes integral representation for the integral $I_{0\text{h}0\text{w}14}$ after the ana-

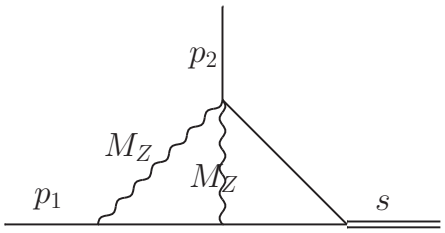

Figure 8.4: Wiggle lines denote propagators including massive particles. The simple solid lines are massless. This Feynman diagram corresponds to the scalar Feynman integral $I_{\text{0h0w14}}(1,1,1,1,1,0,0)$.

lytic continuation in $\epsilon \to 0$ reads:

$$I^{\text{MB}}_{\text{0h0w14}} = -M'^{2(-2\epsilon)}_Z B^{\text{0h0w14}}_0, \tag{8.77}$$

$$\begin{aligned} B^{\text{0h0w14}}_0 = & \frac{\Gamma(-z_1)\Gamma(-z_2)\Gamma(z_2+1)\Gamma(-\epsilon-z_1)\Gamma(2\epsilon+z_1+1)\left(-\frac{M_Z^2}{x}\right)^{z_1}}{2\Gamma(1-z_2)\Gamma(-3\epsilon-z_1+2)\Gamma(-2\epsilon-2z_1-z_2)} \\ & (-x)^{-2\epsilon}\,\Gamma(-2\epsilon-z_1-z_2)^2\Gamma(-\epsilon-z_1-z_2)\Gamma(\epsilon+z_1+z_2+1), \end{aligned} \tag{8.78}$$

where the contour is parallel to the imaginary axis at $\Re e\, z_1 = \Re e\, z_2 = -1/3$ and for brevity omitted integral measure is $\int \frac{\mathrm{d}z_1}{2\pi i}\frac{\mathrm{d}z_2}{2\pi i}$. The expansion in ϵ yields:

$$\begin{aligned} B^{\text{0h0w14}}_0 = & -\frac{\Gamma(-z_1)^2\Gamma(z_1+1)\Gamma(-z_2)\Gamma(z_2+1)\left(-\frac{M_Z^2}{x}\right)^{z_1}\Gamma(-z_1-z_2)^3\Gamma(z_1+z_2+1)}{2\Gamma(2-z_1)\Gamma(1-z_2)\Gamma(-2z_1-z_2)} \\ & +\mathcal{O}(\epsilon). \end{aligned} \tag{8.79}$$

This integral is finite in the ϵ expansion. In the further discussion we neglect terms of higher orders in ϵ.

If we use contours parallel to the imaginary axis $z_1 = -\frac{1}{3} + i h_1 t$ and $z_2 = -\frac{1}{3} + i h_2 t$, with $t > 0$, then the polynomial asymptotic behavior (see Sec. 7.4) for this Mellin-Barnes integral in Minkowskian regions reads in the limit $t \to \infty$:

$$H_1 = (-1, 1), \quad t^{-2+2\Re e\, z_1 + 2\Re e\, z_2}. \tag{8.80}$$

The polynomial asymptotic behavior depends on the real parts of the integration variables z_1, z_2.

Rotation of the coordinate system

It is possible to rotate the original coordinate system $(h_1 t, h_2 t)$ such that the polynomial asymptotic behavior is along one integration axis $(h_1 t)$ or $(h_2 t)$. For this example we simply apply a linear transformation:

$$z_2 \to z_2 - z_1, \tag{8.81}$$

and the Mellin-Barnes integral in Eq. (8.79) is now cast into:

$$\begin{aligned} B^{\text{0h0w14r}}_0 = & -\frac{(-\frac{M_Z^2}{x})^{z_1}\Gamma(-z_1)^2\Gamma(1+z_1)\Gamma(z_1-z_2)\Gamma(-z_2)^3\Gamma(1+z_2)}{2\Gamma(2-z_1)\Gamma(-z_1-z_2)\Gamma(1+z_1-z_2)} \\ & \Gamma(1-z_1+z_2), \end{aligned} \tag{8.82}$$

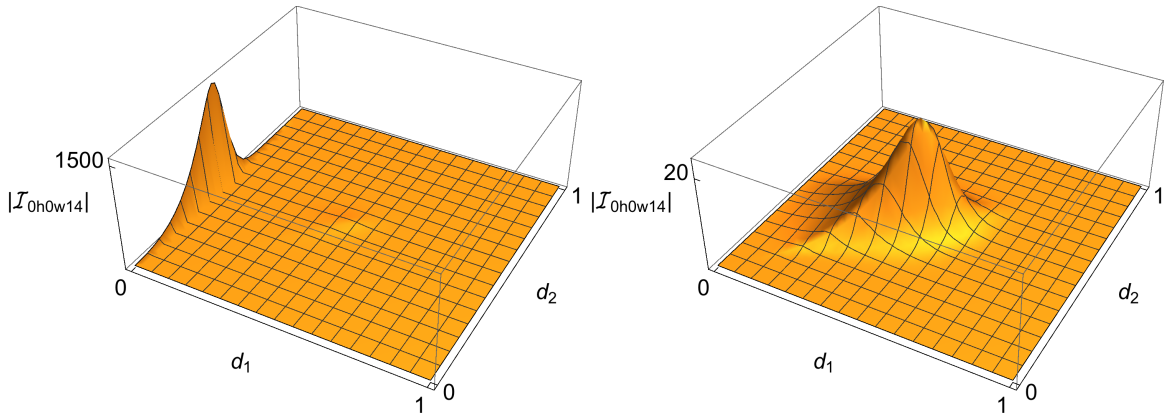

Figure 8.5: The absolute value of the integrand in Eq. (8.82) of the integral I_{0h0w14} with two different mappings is shown. We have applied logarithmic mapping in Eq. (8.72), see left figure and the cotangent mapping in Eq. (8.74), see right figure.

where the integration contour is parallel to the imaginary axis at $z_1 = -\frac{1}{3} + ih_1 t,\ z_2 = -\frac{2}{3} + ih_2 t$. The new polynomial asymptotic behavior depends on the real part of the integration variable z_2 only:

$$H_1 = (-1, 0), \quad t^{-2+2\Re e\, z_2}. \tag{8.83}$$

If we set $\Re e\, z_2 = -\frac{2}{3}$ in Eq. (8.83) we get $t^{-\frac{10}{3}}$, where obviously $-10/3 < -2$. In case of the logarithmic mapping $h_i t = \ln[\frac{d_i}{1-d_i}]$, $i = 1, 2$ the integrand should have an integrable singularity at $d_1 \to 0$, see left figure in Fig. 8.5. In case of cotangent mapping $h_i t = \frac{1}{\tan(-\pi d_i)}$, $i = 1, 2$, the integrand should give zero at $d_1 \to 0$, see right figure in Fig. 8.5.

Analytic calculation to verify the numerical results

To study the numerical effects for the different mappings we derive an analytic representation for the integral I_{0h0w14} in terms of the harmonic polylogarithms (HPL). First the integration-by-parts reduction is performed with `Kira` resulting in a set of known master integrals:

$$\begin{aligned}
&I_{0h0w14}(1,1,1,1,1,-1,0) = \\
&\frac{I^{\text{crossed}}_{0h0w14}(0,0,1,1,0,0,0)\,((6D^2-38D+64)\,M_Z^2+(D^2-5D+6)\,x)}{8(D-5)(D-3)M_Z^6} \\
&-\frac{I_{0h0w14}(1,1,0,1,1,0,0)\,(4(2D-7)M_Z^2+(3D-10)x)}{2(D-2)M_Z^2} \\
&-\frac{xI_{0h0w14}(2,1,0,1,1,0,0)\,(4M_Z^2+x)}{(D-2)M_Z^2} \\
&-\frac{I_{0h0w14}(1,1,0,0,1,0,0)}{M_Z^2} \\
&+\frac{I^{\text{crossed}}_{0h0w14}(1,1,1,1,0,0,0)\,(M_Z^2+x)}{2M_Z^2}
\end{aligned}$$

$$+\frac{2I^{\text{crossed}}_{\text{0h0w14}}(1,1,1,1,-1,0,0)}{M_Z^2}$$
$$+\frac{I^{\text{crossed}}_{\text{0h0w14}}(1,1,0,1,0,0,0)}{2M_Z^2}. \tag{8.84}$$

Additional integrals are defined as:

$$I^{\text{crossed}}_{\text{0h0w14}}(a_1,a_2,a_3,a_4,a_5,a_6,a_7) = \int \frac{\mathrm{d}^D k_1}{i\pi^{D/2}} \frac{\mathrm{d}^D k_2}{i\pi^{D/2}} \frac{1}{P_1^{a_1} P_2^{a_2} P_3^{a_3} P_4^{a_4} P_5^{a_5} P_6^{a_6} P_7^{a_7}}, \tag{8.85}$$

where the propagators are $P_1 = (p_2+k_1)^2,\ P_2 = ((p_1-k_1+k_2)^2),\ P_3 = (k_1^2-\tilde{M}_Z^2),\ P_4 = ((k_2)^2-\tilde{M}_Z^2),\ P_5 = k_2p_2,\ P_6 = k_2p_1,\ P_7 = k_1p_1$. Here the propagator P_5 will appear as the irreducible numerator, P_6 and P_7 play an auxiliary role. Note that the integral $I^{\text{crossed}}_{\text{0h0w14}}$ is a possible loop representation of the integral I_{0h0w14} with some shrinked lines. The non trivial symmetries which are needed to map the integral $I^{\text{crossed}}_{\text{0h0w14}}$ to I_{0h0w14} are automatically sought for by `Kira`.

The master integrals $I_{\text{0h0w14}}(1,1,0,1,1,0,0)$, $I_{\text{0h0w14}}(2,1,0,1,1,0,0)$ are taken from Ref. [103], see Eqs. (74, 75) therein, where the second integral is multiplied with (-1). The master integrals $I^{\text{crossed}}_{\text{0h0w14}}(1,1,0,1,0,0,0)$, $I_{\text{0h0w14}}(1,1,0,0,1,0,0)$ are taken from Ref. [95], see Eqs. (105, 126) therein and both are multiplied with (-1). The master integrals $I^{\text{crossed}}_{\text{0h0w14}}(1,1,1,1,0,0,0)$, $I^{\text{crossed}}_{\text{0h0w14}}(1,1,1,1,-1,0,0)$ are taken from the Ref. [104], see the Eqs. (145, 150) therein, where the second integral is multiplied with (-1).

Note that in our loop-momenta representation we use the metric with the more plus convention, but the results for the master integrals in the Ref. [95, 103, 104] are listed for the metric with the more minus convention in the loop-momenta representation. Thus each master integral was multiplied with a factor (-1) if the number of the propagators in the master integral is odd.

A product of the tadpole integral is calculated to give:

$$I^{\text{crossed}}_{\text{0h0w14}}(0,0,1,1,0,0,0) = \left(\frac{4\tilde{M}_Z^2}{(D-4)(D-2)}\right)^2. \tag{8.86}$$

The complete analytic result in terms of harmonic polylogarithms for the integral I_{0h0w14} in Eq. (8.76) reads:

$$I_{\text{0h0w14}} = (M'^2_Z)^{-2\epsilon} A_0^{\text{0h0w14}} \epsilon^0, \tag{8.87}$$

with the coefficient:

$$\begin{aligned} A_0^{\text{0h0w14}} \;=\; & \left(-\frac{4M_Z^2}{x}-2\right) \text{HPL}\left(\{-3\}, \frac{\sqrt{-x}-\sqrt{-4M_Z^2-x}}{\sqrt{-4M_Z^2-x}+\sqrt{-x}}\right) \\ & + \left(\frac{2\sqrt{-x}\sqrt{-4M_Z^2-x}}{x}-2\right) \text{HPL}\left(\{-2\}, \frac{\sqrt{-x}-\sqrt{-4M_Z^2-x}}{\sqrt{-4M_Z^2-x}+\sqrt{-x}}\right) \\ & -8\text{HPL}\left(\{-1\}, \frac{\sqrt{-x}-\sqrt{-4M_Z^2-x}}{\sqrt{-4M_Z^2-x}+\sqrt{-x}}\right) \end{aligned}$$

$$
\begin{aligned}
&+\left(\frac{\pi^2 M_Z^2}{3x}+\frac{\pi^2}{6}+4\right)\mathrm{HPL}\left(\{0\},\frac{\sqrt{-x}-\sqrt{-4M_Z^2-x}}{\sqrt{-4M_Z^2-x}+\sqrt{-x}}\right)\\
&+4\mathrm{HPL}\left(\{-1,-1\},\frac{\sqrt{-x}-\sqrt{-4M_Z^2-x}}{\sqrt{-4M_Z^2-x}+\sqrt{-x}}\right)\\
&-2\mathrm{HPL}\left(\{-1,0\},\frac{\sqrt{-x}-\sqrt{-4M_Z^2-x}}{\sqrt{-4M_Z^2-x}+\sqrt{-x}}\right)\\
&+\left(1-\frac{\sqrt{-x}\sqrt{-4M_Z^2-x}}{x}\right)\mathrm{HPL}\left(\{0,0\},\frac{\sqrt{-x}-\sqrt{-4M_Z^2-x}}{\sqrt{-4M_Z^2-x}+\sqrt{-x}}\right)\\
&+\left(\frac{2M_Z^2}{x}+1\right)\mathrm{HPL}\left(\{0,0,0\},\frac{\sqrt{-x}-\sqrt{-4M_Z^2-x}}{\sqrt{-4M_Z^2-x}+\sqrt{-x}}\right)\\
&-\mathrm{HPL}\left(\{-2\},-\frac{x}{M_Z^2}\right)+\left(1-\frac{M_Z^2}{x}\right)\mathrm{HPL}\left(\{-1\},-\frac{x}{M_Z^2}\right)\\
&+3\mathrm{HPL}\left(\{0\},-\frac{x}{M_Z^2}\right)+\left(\frac{\pi^2 M_Z^2}{12x}+\frac{\pi^2}{12}\right)\mathrm{HPL}\left(\{1\},-\frac{x}{M_Z^2}\right)\\
&-\mathrm{HPL}\left(\{0,0\},-\frac{x}{M_Z^2}\right)+\left(-\frac{M_Z^2}{x}-1\right)\mathrm{HPL}\left(\{1,-2\},-\frac{x}{M_Z^2}\right)\\
&-\frac{4M_Z^2\zeta(3)}{x}-\frac{\pi^2\sqrt{-x}\sqrt{-4M_Z^2-x}}{6x}-2\zeta(3)+\frac{\pi^2}{12}. \qquad (8.88)
\end{aligned}
$$

We express the coefficient A_0 in Eq. (8.88) in terms of logarithms and polylogarithms with the routine `HPLConvertToKnownFunctions` provided by the package `HPL.m` [97].

Numerical evaluation of two-dimensional Mellin-Barnes integrals

We observe that the Mellin-Barnes integral in Eq. (8.82) is better suited for numerical treatment than the Mellin-Barnes integral in Eq. (8.79). The numeric results produced with the logarithmic mapping in Eq. (8.72) have very poor accuracy in comparison to the application of the cotangent mapping in Eq. (8.74). The program `MBnumerics.m`, which is developed in this thesis, implements the cotangent integrand mapping. The achieved accuracy with `MBnumerics.m` is in perfect agreement with the analytic result, see Tab. 8.3.

The analytic result is prepared with high accuracy in Tab. 8.3, because we will show in Subsec. 8.4.4 that `MBnumerics.m` is able to evaluate this Mellin-Barnes integral in Eq. (8.82) with even higher accuracy than what we achieved here so far.

8.3 Contour deformations (rotations)

To apply a multi-dimensional contour deformation we work with the parameterization

$$z_k = x_k + i t_k + f(t_k), \quad k = 1, \ldots, N_M, \qquad (8.89)$$

Table 8.3: Results are presented for the numerical evaluation of the Mellin-Barnes integrals B_0^{0h0w14} in Eq. (8.79) and $B_0^{0h0w14r}$ in Eq. (8.82) with different mappings. The significant digits reported by the integrator `Cuhre` from the library `CUBA` are marked with bold text. We have used the routine `HPLConvertToKnownFunctions` provided by the package `HPL.m` to express the coefficient A_0^{0h0w14} in Eq. (8.88) in terms of logarithms and polylogarithms. We have used the input parameters of Eq. (4.50).

Methods	**Results**
Eq. (8.79), logarithmic mapping,	0.***3***96
	+0.***7***45 i
Eq. (8.79), cotangent mapping,	0.3923***8***3
default in `MBnumerics.m`	+0.7456***3***9 i
Eq. (8.82), logarithmic mapping,	0.392***3***96
(200000 function evaluations)	+0.74***5***637 i
Eq. (8.82), cotangent mapping,	0.39238285888***7***8
default in `MBnumerics.m`,	+0.74563885366***3***1 i
(150000 function evaluations)	
Analytic result in Eq. (8.88)	0.392382858885785670637465846526***6***8
	+0.74563885366131762208398242444403***5***9 i

where N_M is the number of all Mellin-Barnes integration variables, x_k is a constant, $t_k \in [-\infty, \infty]$ and $f(t_k) \in \mathbb{R}$. Usually the Mellin-Barnes integrals in Minkowskian regions with $f(t_k) = 0$ exhibit a polynomial asymptotic behavior like $1/t^a$, $a > 0$. In general it is a non-trivial task to generate an overall exponential damping factor with the help of contour deformation for multi-dimensional Mellin-Barnes integrals. The main difficulty is, that the contour deformation will produce singularities in a multi-dimensional integral due to the appearance of the Γ-functions in the integrand. One trivial exception, which was studied also in Ref. [29], is the so called multi-dimensional rotation

$$f(t_k) = \theta t_k, \quad k = 1, \ldots, N_M, \tag{8.90}$$

where θ is the same parameter for all integration variables.

In order to study the parameterization in Eq. (8.89) with $f(t_k) = \theta t_k$ we introduce general spherical coordinates for t_k with the radial component r, the polar angles ϕ_i, $i = 1, \ldots, N-2$ and the azimuthal angle ϕ_{N-1}. The asymptotic behavior of a Mellin-Barnes integral in Minkowskian regions $I_{\text{Minkowski}}$ reads

$$I_{\text{Minkowski}} \underset{|z|\to\infty}{\approx} \exp(r\eta(\{\phi_i\}, \theta)), \tag{8.91}$$

where $\eta(\{\phi_i\},\theta)$ is ideally negative for $\forall\{\phi_i\}$ in the asymptotic limit $r \to \infty$ for one fixed θ. In this case the overall exponential damping factor exists. Else, if no fixed θ exists to satisfy $\eta(\{\phi_i\},\theta) < 0$, $\forall\{\phi_i\}$, then the multi-dimensional rotation $f(t_k) = \theta t_k$ failed to restore the exponential damping factor. We give one example where the multi-dimensional rotation is used to generate an overall exponential damping factor. And in the next example we show where the contour deformation $f(t_k) = \theta t_k$ fails.

8.3.1 Example where multi-dimensional contour rotation works

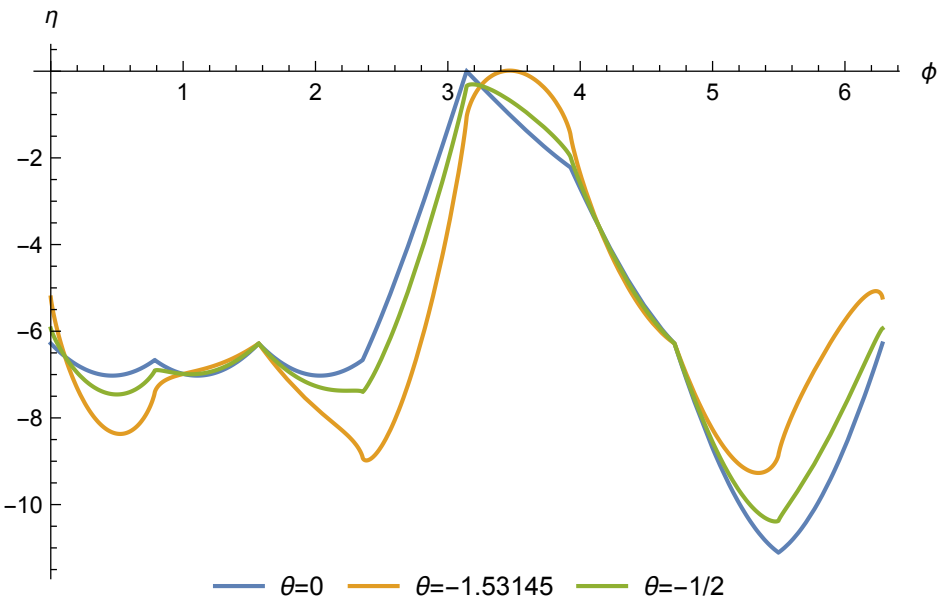

Figure 8.6: Function $\eta(\phi,\theta)$ in Eq. (8.92) is plotted for $\phi = [0, 2\pi]$ for different values θ. The blue curve with $\theta = 0$, the green curve with $\theta = -1/2$ and the orange curve with $\theta = -1.53145$ are related to the integral B_0^{0h0w14r} and the kinematic point $x = 2 + i\delta$ and $M_Z = 1$.

First we use the polar coordinate system $t_1 = r\cos\phi$, $t_2 = r\sin\phi$, with $r > 0$ and $\phi \in [0, 2\pi]$ to parametrize the two-dimensional Mellin-Barnes integral B_0^{0h0w14r} in Eq. (8.82). The Jacobian is r. In these new coordinates the exponential damping factor depends on the radial component r, the azimuthal angle ϕ and the parameter θ. If we set $\theta = 0$, then this will reproduce the integration over the straight contours where the exponential damping factor cancels exactly at $\phi = \pi$, see blue curve in Fig. 8.6.

The exponential damping factor in the asymptotic behavior depends now explicitly on the rotation parameter θ

$$B_0^{\text{0h0w14r}} \underset{r\to\infty}{\approx} \exp(r\eta(\phi,\theta)), \tag{8.92}$$

$$\eta(\phi,\theta)|_{\phi=\pi} = \frac{\theta}{2}(-2\log(M_Z^2) + \Re e\,(\log(x^2))). \tag{8.93}$$

If we evaluate this integral at $x = 2 + i\delta$ and take the limit $\lim_{\delta\downarrow 0}$ first we find that

an overall exponential damping factor is generated for $\theta \in]0, -1.53145[$. The green curve shows the asymptotic behavior for one fixed value of $\theta = -\frac{1}{2}$ and the orange curve shows the asymptotic behavior for $\theta = -1.53145$ in Fig. 8.6. Thus the method of contour rotation works for the kinematic point $x = 2 + i\delta$ and $M_Z = 1$.

On the other hand If we evaluate this integral B_0^{0h0w14r} at $x = 1 + i\delta$, $M_Z = 1$ and take the limit $\lim_{\delta \downarrow 0}$ first no θ can be found to satisfy $\eta(\phi, \theta)|_{\phi=\pi} < 0$ at all. This shows that kinematic regions exists where no exponential damping factor can be generated with the help of contour rotation.

8.3.2 Example where multi-dimensional contour rotation fails

For the two-dimensional Mellin-Barnes integral in Minkowskian regions I_{soft721} in Eq. (7.25) the multi-dimensional rotation fails to generate the exponential damping factor. To illustrate the problem we use again the polar coordinate system $t_1 = r\cos\phi$, $t_2 = r\sin\phi$, with $r > 0$ and $\phi \in [0, 2\pi]$ and the contour deformation $f(t_k) = \theta t_k$. The exponential damping factor is canceled for $\theta = 0$ in the region from $\pi/2$ to π. For arbitrary θ we find in analogy to the example in Subsec. 8.3.1:

$$\eta(\pi, \theta) = \theta \log(50/39), \tag{8.94}$$

$$\eta(\pi/2, \theta) = -\theta \log(18/5), \tag{8.95}$$

where we have used the input parameters of Eq. (4.50). Due to these equations no suitable choice can be found for one fixed θ to generate an *overall* exponential damping factor.

Furthermore, we can probe numerically that the exponential damping factor disappears for the angle $\phi' = 3.1187148434371776$ for one fixed $\theta = 1$. Next we can numerically study the θ dependence by fixing $\phi = \phi'$:

$$\eta(\phi', \theta) = 1.1\theta \log(1 + \theta^2) 10^{-16}, \tag{8.96}$$

thus no θ can be found to restore an overall exponential damping factor. The program `MBnumerics.m`, which is developed in this thesis, checks numerically if the application of contour rotation works and whenever possible uses the contour rotation to evaluate numerically the Mellin-Barnes integrals.

8.4 Contour shifts

A very promising technique to evaluate the Mellin-Barnes integrals in Minkowskian regions is the application of the contour shifts. It is a technique which allows to exchange the original Mellin-Barnes integrals by Mellin-Barnes integrals with improved asymptotic behavior in a controlled manner, see for example Ref. [27], here the authors sketch the idea without going into the details. Technically the contour shifts help to regularize the Mellin-Barnes integrals, see Sec. 6.3 or in a similar context see Ref. [105].

In the following we introduce this technique with the two-dimensional Mellin-Barnes integral B_0^{0h0w14r} in Eq. (8.82). Here the exponential damping factor is canceled for straight integration contours in Minkowskian regions. In this case we de-

rive the polynomial asymptotic behavior, which reads: $H_1 = (-1, 0), \quad t^{-2+2\Re e\, z_2}$, see Eq. (8.83). We have used the input parameters of Eq. (4.50).

The first important observation is that the polynomial asymptotic behavior depends explicitly on the real part of the integration variable z_2. In the following it will become convenient to treat Mellin-Barnes integrals in Minkowskian regions as discrete functions in their real parts of the integration variables. For ease of notation the initial integration variables are written as

$$z_k = x_k + (i + \theta)h_k t, \quad h_k \in \mathbb{R},\ t \in [0, \infty], \tag{8.97}$$

and the shifted integration variables are written as:

$$z'_k = z_k + n_k, \quad n_k \in \mathbb{R}. \tag{8.98}$$

For simplicity we set $\theta = 0$ if not stated otherwise. The parameters n_k may take any real value as long as every Γ-function in the numerator of the integrand is well defined. The values for x_k were usually generated during the analytic continuation of the Mellin-Barnes integral.

In our example the Mellin-Barnes integral B_0^{0h0w14r} in Eq. (8.82) becomes a discrete function in n_1 and n_2, $B_0^{\text{0h0w14r}}(n_1, n_2)$. If we set $n_1 = n_2 = 0$ we get our initial Mellin-Barnes integral. With this the polynomial asymptotic behavior depends explicitly on the shift n_2, $t^{-2+2x_2+2n_2}$. Thus taking a negative value for n_2 will improve the convergence of the new shifted integral. Changing n_2 is the same as shifting the straight integration contour along the real axis.

8.4.1 One-dimensional shift

In the case of a one-dimensional shift $n_k \neq 0$ and $\forall n_{l\neq k} = 0$ all poles which get passed during the contour shift are coming from the Γ-functions or the Ψ-functions in Eq. (8.57) of the new shifted Mellin-Barnes integral. The residue theorem states that the initial integral equals the sum of residues for each crossed pole between the new and the old contour plus the original integral with the shifted contour. If the poles are to the right of the new contour, then we add up the residues taken in these poles or we subtract them if they are to the left of the new contour.

In the following example the function is called the shifted integral $B_0^{\text{0h0w14r}}(0, -1)$.

Two Γ-functions will develop poles during the shift going from $B_0^{\text{0h0w14r}}(0, 0) \to B_0^{\text{0h0w14r}}(0, -1)$: $\Gamma(1 + z_2 + n_2)$ and $\Gamma(1 - z_1 + z_2 + n_1 + n_2)$. The following equations collect all possible poles:

$$z_2 + 1 + n_2 = -k, \quad k \in \mathbb{N}_0, \tag{8.99}$$

$$z_2 - z_1 + 1 + n_2 + n_1 = -k, \quad k \in \mathbb{N}_0. \tag{8.100}$$

For fixed values $z_2 = -\frac{2}{3}$, $z_1 = -\frac{1}{3}$, $n_1 = 0$ each of the above equations will give only one solution at $k = 0$ for $n_2 \in [-1, 0]$. Thus we collect the residues in the poles $z_2 + 1 - z_1 = 0$ and $z_2 + 1 = 0$. We can write the initial Mellin-Barnes integral as a sum of the shifted integral and the residues:

$$B_0^{\text{0h0w14r}}(0, 0) = B_0^{\text{0h0w14r}}(0, -1) + \underset{z_2=-1+z_1}{\tilde{\text{res}}}\, B_0^{\text{0h0w14r}}(0, 0) + \underset{z_2=-1}{\tilde{\text{res}}}\, B_0^{\text{0h0w14r}}(0, 0), \tag{8.101}$$

where we have added up the residues since their poles are to the right of the new contour $z_2' = \frac{1}{3} + it_2$ of $B_0^{\text{0h0w14r}}(0,-1)$. Here we use the following notation:

$$\underset{z_i=z_i^*}{\tilde{\text{res}}}\, I(0,\dots,0) = \int \left(\prod_{j\neq i}^{N_M} \frac{\mathrm{d}z_j}{2\pi i}\right) \underset{z_i=z_i^*}{\text{res}}\, \mathcal{I}(\{z_k\}), \tag{8.102}$$

where $\mathcal{I}$ is the integrand of the N_M-dimensional Mellin-Barnes integral. The residue $\underset{z_i=z_i^*}{\text{res}}\, \mathcal{I}(\{z_k\})$-function is defined as the $1/z_i$ coefficient in the Laurent expansion of the function $\mathcal{I}(\{z_k\})$ at the pole location $z_i = z_i^*$.

We observe that Eq. (8.101) enables us to write the initial Mellin-Barnes integral $B_0^{\text{0h0w14r}}(0,0)$ with the polynomial asymptotic behavior t^{-2+2x_2} as a Mellin-Barnes integral $B_0^{\text{0h0w14r}}(0,-1)$ with improved asymptotic behavior t^{-2+2x_2-2} plus two residues, which are one-dimensional Mellin-Barnes integrals. It is important to stress, that in general the residues are also Mellin-Barnes integrals but with exactly one dimension less.

8.4.2 Multi-dimensional shift

In the following we generalize the procedure of a one-dimensional shift to multi-dimensional shift. The simplest definition of a multi-dimensional shift is to apply the one-dimensional shifts iteratively:

$$\begin{aligned}
I(0,\dots,0) &= c(n_1) \sum_{i=\{\text{poles}_1\}} \underset{z_1=i}{\tilde{\text{res}}}\, I(0,\dots,0) \\
&+ c(n_2) \sum_{i=\{\text{poles}_2\}} \underset{z_2=i}{\tilde{\text{res}}}\, I(n_1,0,\dots,0) \\
&+ c(n_3) \sum_{i=\{\text{poles}_3\}} \underset{z_3=i}{\tilde{\text{res}}}\, I(n_1,n_2,0,\dots,0) \\
&+ \dots \\
&+ c(n_{N_M}) \sum_{i=\{\text{poles}_{N_M}\}} \underset{z_{N_M}=i}{\tilde{\text{res}}}\, I(n_1,n_2,n_{N_M-1},0) \\
&+ I(n_1,n_2,\dots,n_{N_M-1},n_{N_M}),
\end{aligned} \tag{8.103}$$

where $c(n_k)$ is defined as:

$$c(n_k) = \begin{cases} 1, & \text{if } n_k < 0, \\ -1, & \text{if } n_k > 0. \end{cases} \tag{8.104}$$

The writing $\{\text{poles}_k\}$ collects all poles which are located between the initial contour z_k belonging to the integral $I(n_1,\dots,n_{k-1},0\dots,0)$ and the shifted contour $z_k' = z_k + n_k$ belonging to the integral $I(n_1,\dots,n_{k-1},n_k,0,\dots,0)$.

8.4.3 Avoiding singularities with shifts

For the example integral $B_0^{\text{0h0w14r}}(n_1,n_2)$, if we take $n_1 = 0$ and $n_2 = 43/60$, the polynomial asymptotic behavior reads $t^{-2+2x_2+86/60}$. With $x_2 = -\frac{2}{3}$ we get $t^{-19/10}$,

where $-19/10 > -2$. If we use cotangent mapping as discussed in the previous Sec. 8.2 the domain of the integration should develop a singularity at the borders. More explicitly if we map $h_1 t = \frac{1}{\tan(-\pi d_1)}$ and $h_2 t = \frac{1}{\tan(-\pi d_2)}$, the singularity is at the border $d_1 = 0$ and $d_2 \in [0, 1]$. Which is absent in the initial integral with the same mapping see right figure in Fig. 8.5.

To use the cotangent mapping we should try to improve the polynomial asymptotic behavior to be better than t^{-2}.

8.4.4 Improving asymptotic behavior with shifts

In the following we calculate all two-dimensional integrals with the same integrator `Cuhre` which is part of the `CUBA` library.

Table 8.4: Results are presented for $B_0^{0\text{h}0\text{w}14\text{r}}(n_1, n_2)$ for 50000 function evaluations for different values of n_1 and n_2 and with the explicit limit $\lim_{\delta \downarrow 0}$ taken first. The bold digits are the last significant digits reported by the integrator `Cuhre` from the library `CUBA` for two-dimensional integrals and the `Mathematica` routine `NIntegrate` for one-dimensional integrals. We have used the input parameters of Eq. (4.50).

Shifts	**Results**
no shifts	0.3923828588
$B_0^{0\text{h}0\text{w}14\text{r}}(0, 0)$	+ 0.7456388566 i
$B_0^{0\text{h}0\text{w}14\text{r}}(0, -1)$	0.1079010833**2**6
	+ 0.3149036025**8**8 i
$B_0^{0\text{h}0\text{w}14\text{r}}(0, -100)$	0.000894879786**8**31324
	+ 0.004802121701**9**52021 i
$B_0^{0\text{h}0\text{w}14\text{r}}(-3, -1)$	0.000211116684**7**637598 + 0 i
$B_0^{0\text{h}0\text{w}14\text{r}}(-23, -14)$	$-3.8234343402\mathbf{5}514710^{-22}$+ 0 i
(100000 function evaluations)	
residues: 38 one-dimensional	0.392382858885785670637848189960893603
Mellin-Barnes integrals	+ 0.7456388536613176220839824244440**3**965 i
$B_0^{0\text{h}0\text{w}14\text{r}}(0, 0) =$	0.392382858885785670637465846526**8**80
$B_0^{0\text{h}0\text{w}14\text{r}}(-23, -14)$ + residues	+ 0.745638853661317622083982424444**0**359 i

If we evaluate numerically the integral $B_0^{0\text{h}0\text{w}14\text{r}}(0, -1)$, then we will get two digits of better accuracy in comparison to the evaluation of the original integral $B_0^{0\text{h}0\text{w}14\text{r}}(0, 0)$. Computing the two missing residues in Eq. (8.101) and adding them to the numeric result $B_0^{0\text{h}0\text{w}14\text{r}}(0, -1)$ recovers the result for $B_0^{0\text{h}0\text{w}14\text{r}}(0, 0)$.

The result for the real and imaginary parts of $B_0^{\text{0h0w14r}}(0,-1)$ is just a little bit smaller than the real and imaginary parts of $B_0^{\text{0h0w14r}}(0,0)$ see Tab. 8.4. If we instead evaluate the integral $B_0^{\text{0h0w14r}}(0,-100)$ and compare it to the initial integral, then it has a 3 orders of magnitude smaller real part and a 2 orders of magnitude smaller imaginary part and it is overall better convergent. If we calculate all 200 residues in the 200 crossed poles due to the shift of the contour we would again restore the result in $B_0^{\text{0h0w14r}}(0,0)$, see Tab. 8.4. In this example the calculation of the 200 one-dimensional integrals is not problematic since we have learned how to correctly treat them in Minkowskian regions, see Sec. 8.1, but the calculation does not seem to be economical if we would like to integrate Mellin-Barnes integrals with more than two dimensions.

8.4.5 Change the order of magnitude of a Mellin-Barnes Integral with shifts

A much more economical shift appears if we focus on the reduction of the order of magnitude of the integral $B_0^{\text{0h0w14r}}(n_1,n_2)$. For example, the integral $B_0^{\text{0h0w14r}}(-3,-1)$ is smaller than the initial integral B_0^{0h0w14r} by 3 orders of magnitude. We apply the algorithm in Eq. (8.103) in order to calculate the resulting residues due to the shift. If we first calculate the residues in the poles due to the shift $n_1=-3$, then take the shifted integral $I(-3,0)$ and calculate the residues in the poles which got passed due to the next shift in $n_2=-1$, we get in total 5 residues, which are 5 one-dimensional Mellin-Barnes integrals.

If we first shift in $n_2=-1$ and then in $n_1=-3$, we get 7 residues, but 2 of the residues differ only by sign. Thus in total we have again 5 residues to calculate. The origin for the appearance of two residues with opposite sign is that the same poles may be passed multiple times by the different shifted contours. These integrals might differ even in the integration variables. In this simple example the integrals can be mapped on each other by relabeling the integration variables and straightforward linear transformations. In a more general case in a multi-dimensional integral this is not straightforward anymore. Algorithmically we evaluate each residue in a simple kinematic point which guarantees high accuracy, typically an Euclidean kinematic point, and compare all results with each other. If we find two residues which agree numerically with high accuracy with an opposite sign, then we remove them from the evaluation queue.

The previously mentioned change of the order of magnitude can be used algorithmically to push the shifted integral to be negligible compared to the desired accuracy of the original integral. To verify the method of the shifts we compare the numerical results to the given analytic result in Tab. 8.3. We compute the integral $I(-23,-14)$ and collect the residues due to the poles which got passed first by the shift n_1 and then by the shift n_2, which will give 38 residues, see Tab. 8.4. The one dimensional integrals were computed in `Mathematica` with the routine `NIntegrate` with the options:

```
AccuracyGoal → 33,
PrecisionGoal → Infinity,
WorkingPrecision → 35.
```

Before calculating the 38 one-dimensional integrals we convert all products of Γ-

functions into a sum of $\log\Gamma$-functions, see Eq. (8.69). We can successfully verify the numerical result in Tab. 8.4 with the analytic result in Tab. 8.3.

In this thesis the direct calculation of a Mellin-Barnes integral is reformulated as the calculation of its shifted integral plus the corresponding residues due to the shifts. In the program `MBnumerics.m`, which is developed in this thesis, the method of shifts is algorithmically realized, see App. C.

8.4.6 Analyzing the asymptotic behavior

To enhance the algorithms which are implemented in `MBnumerics.m` it is useful to compare the polynomial asymptotic behavior, see Sec. 7.4, stemming from different Mellin-Barnes integrals with equal dimension. For better illustration we work with the following example integral

$$I_{\text{soft7}} = \exp(2\gamma_E\epsilon)(\tilde{M}_Z^2)^{-1-2\epsilon} \int \frac{\mathrm{d}^D k_1}{i\pi^{\frac{D}{2}}} \frac{\mathrm{d}^D k_2}{i\pi^{\frac{D}{2}}} \frac{D_7}{D_1 D_2 D_3 D_4 D_5 D_6}, \tag{8.105}$$

where $D_1 = k_1^2,\ D_2 = (k_1 - k_2)^2 - m_t^2,\ D_3 = k_2^2 - M_W^2,\ D_4 = (k_1 + p_1)^2,\ D_5 = (k_2 + p_1)^2 - m_t^2,\ D_6 = (k_1 + p_1 + p_2)^2,\ D_7 = k_2 p_2$, see Fig. 8.7. The integral I_{soft7} is

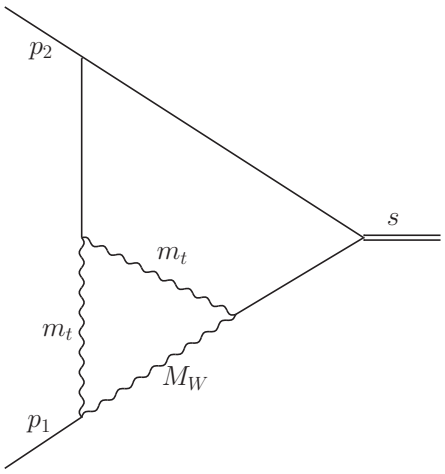

Figure 8.7: Wiggle lines denote propagators including massive particles. The simple solid lines are massless. This Feynman diagram corresponds to the scalar Feynman integral $I_{\text{soft7}}(1,1,1,1,1,1,0)$.

divergent. Using the loop-by-loop approach (see Sec. 6.1), analytic continuation (see Sec. 6.3) and the Laurent expansion of the resulting Mellin-Barnes integrals around $\epsilon = 0$ the result can be cast in:

$$I_{\text{soft7}} = (\tilde{M}_Z^2)^{-1-2\epsilon} \sum_{i=-2}^{0} C_i \epsilon^i. \tag{8.106}$$

This integral is not known analytically, yet, which makes it a non-trivial example.

Here we give explicitly the Mellin-Barnes integral representation for the $1/\epsilon$ coefficient for the Feynman integral I_{soft7}:

$$
\begin{aligned}
C_{-1} &= I_{\text{soft721}} + I_{\text{soft722}} + I_{\text{soft711}}, && (8.107)\\
I_{\text{soft721}} &= -\int \mathrm{d}z_1 \int \mathrm{d}z_2 \, \frac{\left(\frac{M_W^2}{m_t^2}\right)^{z_1} \left(-\frac{x}{m_t^2}\right)^{z_2} \Gamma(2-z_1)\Gamma(-z_1)\Gamma(-z_2)\Gamma(1+z_2)}{2m_t^2\Gamma(3+z_2)^2} \\
&\quad \Gamma(1+z_1+z_2)^2, \\
I_{\text{soft722}} &= -\int \mathrm{d}z_4 \int \mathrm{d}z_5 \, \frac{\left(\frac{M_W^2}{m_t^2}\right)^{z_4} \left(-\frac{x}{m_t^2}\right)^{z_5} \Gamma(2-z_4)\Gamma(-z_4)\Gamma(-z_5)\Gamma(z_5)}{m_t^2\Gamma(3+z_5)^2} \\
&\quad \Gamma(1+z_4+z_5)^2, \\
I_{\text{soft711}} &= -\int \mathrm{d}z_3 \, \frac{1}{8m_t^2} \left(\frac{M_W^2}{m_t^2}\right)^{z_3} \Gamma(2-z_3)\Gamma(-z_3)\Gamma(1+z_3)^2[-5+4\log(-x) \\
&\quad -\log(-\frac{x}{m_t^2}) + 2\Psi(2-z_3) - 2\Psi(1+z_3)], && (8.108)
\end{aligned}
$$

where $z_1 = -\frac{1}{3} + n_1 + (i+\theta)h_1 t$, $z_2 = -\frac{1}{3} + n_2 + (i+\theta)h_2 t$, $z_3 = -\frac{1}{2} + n_3 + (i+\theta)h_3 t$, $z_4 = -\frac{2}{3} + n_4 + (i+\theta)h_4 t$ and $z_5 = \frac{1}{3} + n_5 + (i+\theta)h_5 t$. Again we set $\theta = 0$ for simplicity.

The polynomial asymptotic behavior for the first Mellin-Barnes integral I_{soft721} reads:

$$
\begin{aligned}
H_1 : &\quad t^{2\Re e\, z_1 - 4}, && (8.109)\\
H_2 : &\quad t^{-2\Re e\, z_1 - 2\Re e\, z_2 - 4}, && (8.110)\\
H_3 : &\quad t^{-3}. && (8.111)
\end{aligned}
$$

and for the second Mellin-Barnes integral I_{soft722}:

$$
\begin{aligned}
H_1 : &\quad t^{2\Re e\, z_4 - 5}, && (8.112)\\
H_2 : &\quad t^{-2\Re e\, z_4 - 2\Re e\, z_5 - 5}, && (8.113)\\
H_3 : &\quad t^{-4}, && (8.114)
\end{aligned}
$$

where for both integrals the sets $H_1 = (0,1)$, $H_2 = (-1,1)$ and $H_3 = (-1,2)$ are identical. Next we fix the real parts of the integration variables z_1, z_2, z_4, z_5 for both Mellin-Barnes integrals:

$$
\begin{aligned}
H_1 : &\quad t^{-14/3}, && (8.115)\\
H_2 : &\quad t^{-8/3}, && (8.116)\\
H_3 : &\quad t^{-3}, && (8.117)
\end{aligned}
$$

and

$$
\begin{aligned}
H_1 : &\quad t^{-19/3}, && (8.118)\\
H_2 : &\quad t^{-13/3}, && (8.119)\\
H_3 : &\quad t^{-4}. && (8.120)
\end{aligned}
$$

In this example the two two-dimensional Mellin-Barnes integrals I_{soft721} and I_{soft722} have similar asymptotic behavior, because the polynomial asymptotic behavior of

both integrals depend on the same integration variables times their numeric coefficients (if we relabel $z_4 \to z_1$ and $z_5 \to z_2$, see Eqs. (8.109-8.114)), but the asymptotic behavior is not identical because it differs numerically see Eqs. (8.115-8.120).

Finally to be able to tell which polynomial asymptotic behavior for both integrals I_{soft721} and I_{soft722} is better we apply the following ordering.

Two Mellin-Barnes integrals I and I' with the respective similar polynomial asymptotic behavior $\{H_i\}$ and $\{H_i'\}$ are given. we study each polynomial asymptotic behavior t^{a_i} and $t^{a_i'}$ which are associated with H_i and H_i':

1 First we compare lexicographically a_i and a_i' which do not depend on the integration variables. If for one $a_i < a_i'$ then the integral I has better polynomial asymptotic behavior than the integral I'.

2 All a_i and a_i' are evaluated numerically by fixing the real parts of the integration variables. If $\sum_i a_i < \sum_i a_i'$ then the integral I has better polynomial asymptotic behavior than the integral I'.

3 All a_i and a_i' are evaluated numerically again by fixing the real parts of the integration variables and are compared lexicographically. If for one $a_i < a_i'$ then the integral I has better polynomial asymptotic behavior than the integral I'.

4 Else we treat both integrals as if theiy were of equal complexity.

For our example the integral I_{soft722} has better polynomial asymptotic behavior than the integral I_{soft721}. This information is crucial for the algorithm presented in App. C.

8.4.7 First non-trivial two-dimensional Mellin-Barnes integral

Table 8.5: Results are presented for the two-dimensional integral I_{soft721}. We treat this integral as a discrete function $I_{\text{soft721}}(n_1, n_2)$ in the shifts n_1 and n_2. The bold digits are the last significant digits reported by the integrator `Cuhre` from the library `CUBA`. We have used the input parameters of Eq. (4.50).

Shifts	**Results**
$I_{\text{soft721}}(0,0)$	-0.03084**4**1
$I_{\text{soft721}}(-16,16)$	$-\boldsymbol{0}.20 * 10^{-33}$
residues: 32	-0.0308405851800568934368777396592**4**28

We calculate the C_{-1} coefficient of the Feynman integral I_{soft7}. This coefficient in the Mellin-Barnes integral representation contains three integrals. One is one-dimensional and two are two-dimensional Mellin-Barnes integrals in Minkowkian regions.

Table 8.6: Results are presented for the two-dimensional integral I_{soft722}. We treat this integral as a discrete function $I_{\text{soft722}}(n_1, n_2)$ in the shifts n_1 and n_2. The bold digits are the last significant digits reported by the integrator `Cuhre` from the library `CUBA`. We have used the input parameters of Eq. (4.50).

Shifts	**Results**
$I_{\text{soft722}}(0,0)$	-0.001381**9**5
$I_{\text{soft722}}(-15,15)$	$-0.\mathbf{0}9 * 10^{-33}$
residues: 30	-0.00138119608874042986300517868840**0**69

The one-dimensional integral I_{soft711} is evaluated with the help of the contour deformation, see Sec. 8.1:

$$\begin{aligned} I_{\text{soft711}} &= 0.000709292234085281115460467899290\mathbf{1} \\ &\quad +0.189332751427338069100111019640807\mathbf{4}i \end{aligned} \tag{8.121}$$

The final result for the coefficient C_{-1} is a sum of the numerically evaluated two-dimensional integrals, see in Tab. 8.5 and Tab. 8.6, and of the numerically evaluated one-dimensional integral, see Eq. (8.121):

$$\begin{aligned} C_{-1}^{\text{MB}} &= -0.03151248903471204218442245044835\mathbf{9}6 \\ &\quad +0.189332751427338069100111019640807\mathbf{4}i \end{aligned} \tag{8.122}$$

To verify this numerical result we give a second numerical calculation with the program `SecDec` [70] which applies sector decomposition:

$$C_{-1}^{\text{SD}} = -0.0315124\mathbf{8}16 + 0.1893327\mathbf{6}9i. \tag{8.123}$$

The calculation with the program `SecDec` was performed with 90 million function evaluations. In the case of sector decomposition approach the coefficient C_{-1} is at most four-dimensional integral and in the case of Mellin-Barnes integral approach the same coefficient is at most a two-dimensional Mellin-Barnes integral.

In the case were a Mellin-Barnes integral representation is less dimensional than the integral representation in the sector decomposition approach, `MBnumerics.m` usually is better suited for the numerical evaluation of two-loop vertex Feynman integrals in Minkowskian regions.

Chapter 9

Application: The Z-boson resonance

This chapter contains some of the most essential results of this thesis. The computation for the Standard Model two-loop *bosonic* predictions to the effective weak mixing angle for bottom quarks $\sin^2\theta_{\rm eff}^{b,\rm bos}$ consists of two parts: The determination of the renormalization constants, see the discussion in Ref. [55, 56, 57, 58, 59, 60, 61, 62], and the computation of the bare vertex diagrams.

Ayres Freitas, in a common collaboration, has generated the bare diagrams with `FeynArts 3.3` [106] while adding the two-loop renormalization terms by hand, and has used the projectors in Eq. (3.73) and in Eq. (3.74). In total he generated $\mathcal{O}(700)$ two-loop scalar vertex integrals some of them with non-trivial scalar products in the numerator. Most of these integrals contain masses of several virtual particles, which make at present an analytic computation impossible.

We have abandoned the idea to reduce with the help of integration-by-parts identities [65, 66] the $\mathcal{O}(700)$ two-loop scalar vertex integrals with non-trivial scalar products in the numerator to one common set of basis integrals, which in principle is a shorter list of integrals, in this case $\mathcal{O}(100)$. We need to evaluate the original $\mathcal{O}(700)$ integrals in $D = 4 - 2\epsilon$ up to terms in $\mathcal{O}(\epsilon^0)$, but in the case of the $\mathcal{O}(100)$ basis integrals we would need to evaluate several basis integrals at higher order in ϵ.

We rely on two numerical techniques which can resolve the divergences for a general Feynman integral with fully automatized algorithms, namely: Sector decomposition technique and Mellin-Barnes integral approach. In fact there is no general recipe to incorporate the integration-by-parts identities and the numerical methods, sector decomposition and Mellin-Barnes integral approach. In Ref. [107] some ideas in this direction are shown for one scale integrals.

9.1 Numerical evaluation of two-loop vertex Feynman integrals

The Mellin-Barnes integral representations are derived for all $\mathcal{O}(700)$ integrals mentioned above with the publicly available tools `AMBREv2`[88] and `AMBREv3` [87, 108], which apply the loop-by-loop and the global approach. The analytic continuation of the Mellin-Barnes integrals is achieved with the package `MB.m` [26] or alternatively with `MBresolve.m` [109].

In the following we show with selected examples that we can calculate the two-loop vertex Feynman integrals for the Standard Model two-loop *bosonic* predictions to the effective weak mixing angle for bottom quarks $\sin^2\theta_{\rm eff}^{b,\rm bos}$ in an automatic way either with `MBnumerics.m` or with both programs `SecDec` [70] and `Fiesta` [83]. In all programs the library `CUBA` [100, 99] is used which contains the routines `Vegas` and `Cuhre` for numerical integration. The integrator `Vegas` is used for five or more dimensional integrals and `Cuhre` is used for four or less dimensional integrals. In the case of Mellin-Barnes integral approach the library `CernLib` [101, 98, 102] is used for the evaluation of the $\log\Gamma$-functions, ψ-functions and their derivatives. The programs `MBnumerics.m`, `SecDec` and `Fiesta` evaluate multiple integrals separately and finally add the numerical results up. In this case the numerical errors, stemming from the library `CUBA`, are combined in quadrature. In App. D we use bold digits to denote the significant digits in the results reported by the programs `SecDec`, `Fiesta` and `MBnumerics.m`.

The simplest check of the numerical results is to run the programs `Fiesta`, `SecDec` and `MBnumerics.m` and see if the numerical results agree. For Euclidean kinematics we could prove with at least 8 significant digits that the sector decomposition and Mellin-Barnes representations are correctly derived.

If the Mellin-Barnes integral approach is used then the most non trivial cross check is to modify the multi-dimensional integrands by a linear transformation $z_i \to z_i + z_j$. This does not modify the numerical result but it modifies the polynomial asymptotic behavior of the integrands, see for example Subsec. 8.2.2.

If sector decomposition is used, then the calculation with both programs `SecDec` and `Fiesta` was performed. These programs are written by different authors and apply different strategies for the sector decomposition. Furthermore, the contour deformation depends on the contour deformation parameter λ, see Eq. (5.27), which is chosen differently in both programs. This gives again a non trivial check for the numeric results.

All results discussed in this chapter are calculated with the input parameters taken of Eq. (4.50). For all integrals `MBnumeris.m` was used complementary to the programs `SecDec` and `Fiesta` either to verify the analytic results or to calculate the numerical results with two different methods.

9.1.1 Integrals of the type 0h0w0txz

100 Feynman integrals depend on up to one dimensionless parameter $x = \frac{s}{\tilde{M}_Z}$ taken of Eq. (4.50), see App. D.1. With $s = \tilde{M}_Z + i\delta$, the Feynman integrals seem to depend only on one trivial dimensionless parameter $x = 1 + i\delta$, but the Feynman integrals are still evaluated in Minkowskian regions. We neglect the overall prefactor $(\tilde{M}_Z^2)^{D-\nu}$, see Eq. (4.51). Some integrals with 5 propagators, like Eq. (D.19), do not have an internal mass $\tilde{M}_Z$. This happens when reducible numerators appear which cancel the massive propagator in the denominator.

All integrals in this class are at most four-dimensional Mellin-Barnes integrals. All Feynman integrals with 6 propagators are five-dimensional and with 5 propagators four-dimensional integrals in the sector decomposition approach.

We have calculated all 100 integrals in `MBnumerics.m` by requiring that we get

8 digits for the finite part, 12 digits for the $1/\epsilon$ coefficients and 16 digits for the $1/\epsilon^2$ coefficients. With the program `MBnumerics.m` we could have pushed the numerics to a very high accuracy, see for example Tab. 8.2 for the integral in Eq. (D.7) and Tab. 8.4 for the integral in Eq. (D.27). The results in Tab. 8.2 agree with the result in Eq. (D.8) if we expand this latter result with the factor $\frac{\exp(-2\epsilon\gamma_E)}{\Gamma(1+\epsilon)^2}$.

The programs `Fiesta` Ref. [83] and `SecDec` Ref. [70] fail to evaluate only 15 Feynman integrals, with 6 propagators of which one is massive, see Eqs. (D.13, D.29, D.55, D.83, D.85, D.99, D.121, D.147, D.177, D.179, D.185, D.189, D.191, D.195, D.197). But the most recent program `pySecDec`, first introduced in Ref. [110] is able to treat these Feynman integrals numerically.

To validate the numerics we have performed a second calculation where we have applied the integration-by-parts identities to all 100 integrals and reduced them with `Kira` to one set of master integrals, which can be evaluated with the help of the literature [103, 95, 104, 111]. In this work we have presented two examples in Subsec. 8.1.3 and in Subsec. 8.2.2.

9.1.2 Integrals of the type 0hxwxtxz

We studied 6 Feynman integrals defined in Eqs. (D.201-D.206) which were difficult to calculate with both techniques using sector decomposition and Mellin-Barnes integral approach. These integrals are finite. They depend on two dimensionless parameters m_t, M_W taken of Eq. (4.50). We again neglect the overall prefactor $(\tilde{M}_Z^2)^{D-\nu}$, see Eq. (4.51). So far no analytic results were reported for them. In this case the numerical evaluation of these integrals is mandatory. The numerical results are summarized in Tab. D.1.

For all these 6 Feynman integrals a four-dimensional Mellin-Barnes integral representation can be derived. In the case of sector decomposition we need to evaluate five-dimensional integrals. The reported numerical values were calculated with the programs `SecDec` and `MBnumerics.m`. In the Tab. D.1 we label the numerical result which is produced by `SecDec` with 15 Mio, with 90 Mio or with 540 Mio function evaluations with SD–15, SD–90 or SD–540 respectively. With MB–8 we labeled the numerical results which are produced with `MBnumerics.m` by requiring 8 digits. Here we have computed the Mellin-Barnes integrals twice, while the second computation includes a transformation of the integration variables $z_i \to z_i + z_j$.

The results produced with `MBnumerics.m` seem to be accurate in the significant digit. The only discrepancy of 2 sigma arises for the integral in Eq. (D.204). The reported errors by the program `SecDec` are underestimated by 1 or 2 digits for all 6 integrals in Eqs. (D.201-D.206). This leads for example to a 7 sigma discrepancy if we compare two results SD–15 and SD–90 for the integral in Eq. (D.205). It seems that in addition to the Monte Carlo error a systematic error needs to be taken into account. The underestimation of the Monte Carlo error is similar to the work in [84], where the authors mention a 7-10 sigma discrepancy in the sector decomposition results.

The run time for the results labeled with MB–8 and SD–90 is of the same order. Furthermore, we favor the results produced with `MBnumerics.m` which are more accurate. Even if the Mellin-Barnes integral and sector decomposition results are calculated in the same amount of time, `MBnumerics.m` once terminated is by a

factor of 10 faster in preparing a grid in varying the input parameters inside their ranges in Tab. 3.1, see App. C for the description.

9.1.3 Integrals of the type xhxwxz, xhxw0z, xh0w, 0hxwxt0z

We show some example integrals stemming from the classes xhxwxz, xhxw0z, xh0w, 0hxwxt0z which are preferably calculated by the sector decomposition techniques. In this case all integrals are finite. We neglect the overall prefactor $(\tilde{M}_Z^2)^{D-\nu}$, see Eq. (4.51). The integrals in Eq. (9.7) and in Eq. (9.1) are at most four-dimensional integrals in the sector decomposition approach and the integrals in Eqs. (9.4, 9.13, 9.1, 9.10) are at most five-dimensional integrals in the sector decomposition approach.

The integrals in Eq. (9.4) and in Eq. (9.7) are five-dimensional Mellin-Barnes integrals. The integrals in Eq. (9.1) and Eq. (9.10) are three- and six-dimensional Mellin-Barnes integrals. The integral in Eq. (9.13) is eight-dimensional Mellin-Barnes integral.

All integrals belonging to the classes xhxwxz, xhxw0z, xh0w, 0hxwxt0z have been evaluated with `Fiesta` and `SecDec` with at least an agreement in 8 significant digits. In the case of the evaluation of the integrals in the Mellin-Barnes integral representation the accuracy drops down to 5 significant digits for the five-dimensional integrals. And is worse for the eight-dimensional Mellin-Barnes integrals where we at present achieve only from 1 to 3 significant digits. The runtime for all calculations with `SecDec` and `MBnumerics.m` is of the same order. From this short study it is evident that the sector decomposition approach with at most five-dimensional integrals is superior to eight-dimensional Mellin-Barnes integral representations. In the following the `SecDec` results are denoted by $I^{\rm SD}$ and the `MBnumerics.m` results are denoted by $I^{\rm MB}$.

Three-dimensional Mellin-Barnes integral

$$I_{\rm xh0w1} = \int \frac{\mathrm{d}^D k_1}{i\pi^{D/2}} \frac{\mathrm{d}^D k_2}{i\pi^{D/2}} \frac{\exp(2\epsilon\gamma_E)(k_1 p_1)}{X_1(X_2 - M_Z^2)X_3(X_5 - M_Z^2)(X_8 - M_Z^2)}, \tag{9.1}$$

$$I^{\rm SD}_{\rm xh0w1} = (-0.2979430968\boldsymbol{5})\epsilon^0 + \mathcal{O}(\epsilon), \tag{9.2}$$

$$I^{\rm MB}_{\rm xh0w1} = (-0.2979430968\boldsymbol{4}05)\epsilon^0 + \mathcal{O}(\epsilon). \tag{9.3}$$

Five-dimensional Mellin-Barnes integrals

$$I_{\rm xhxwxz1} = \int \frac{\mathrm{d}^D k_1}{i\pi^{D/2}} \frac{\mathrm{d}^D k_2}{i\pi^{D/2}} \frac{\exp(2\epsilon\gamma_E)}{(X_1 - M_H^2)(X_2 - m_t^2)(X_3 - m_t^2)X_4(X_5 - M_W^2)} \frac{1}{(X_6 - M_Z^2)}, \tag{9.4}$$

$$I^{\rm SD}_{\rm xhxwxz1} = 0.133023412\boldsymbol{3}\epsilon^0 + \mathcal{O}(\epsilon), \tag{9.5}$$

$$I^{\rm MB}_{\rm xhxwxz1} = (0.13301 \pm 0.00002)\epsilon^0 + \mathcal{O}(\epsilon). \tag{9.6}$$

$$I_{\text{xhxw0z2}} = \int \frac{\mathrm{d}^D k_1}{i\pi^{D/2}} \frac{\mathrm{d}^D k_2}{i\pi^{D/2}} \frac{\exp(2\epsilon\gamma_E)(k_1 p_2)}{(X_1 - m_t^2)(X_2 - M_H^2)(X_3 - m_t^2)(X_4 - M_W^2)} \frac{1}{(X_5 - M_W^2)}, \tag{9.7}$$

$$I^{\text{SD}}_{\text{xhxw0z2}} = (0.111103806\boldsymbol{6})\epsilon^0 + \mathcal{O}(\epsilon), \tag{9.8}$$

$$I^{\text{MB}}_{\text{xhxw0z2}} = (0.11106 \pm 0.00007)\epsilon^0 + \mathcal{O}(\epsilon). \tag{9.9}$$

Six-dimensional Mellin-Barnes integral

$$I_{\text{xh0w16}} = \int \frac{\mathrm{d}^D k_1}{i\pi^{D/2}} \frac{\mathrm{d}^D k_2}{i\pi^{D/2}} \frac{\exp(2\epsilon\gamma_E)(k_1 p_1)^2}{(X_1 - M_H^2)(X_2 - M_Z^2)(X_3 - M_Z^2)X_{11}} \frac{1}{X_9(X_6 - M_Z^2)}, \tag{9.10}$$

$$I^{\text{SD}}_{\text{xh0w16}} = (0.043616655537\boldsymbol{5})\epsilon^0 + \mathcal{O}(\epsilon), \tag{9.11}$$

$$I^{\text{MB}}_{\text{xh0w16}} = (0.04361 \pm 0.00003)\epsilon^0 + \mathcal{O}(\epsilon). \tag{9.12}$$

Eight-dimensional Mellin-Barnes integrals

$$I_{\text{xhxwxz63}} = \int \frac{\mathrm{d}^D k_1}{i\pi^{D/2}} \frac{\mathrm{d}^D k_2}{i\pi^{D/2}} \frac{\exp(2\epsilon\gamma_E)(k_1 p_1)^2}{(X_1 - M_Z^2)(X_2 - m_t^2)(X_3 - m_t^2)(X_{11} - M_W^2)} \frac{1}{(X_9 - M_W^2)(X_6 - M_H^2)}, \tag{9.13}$$

$$I^{\text{SD}}_{\text{xhxwxz63}} = 0.0031338336\boldsymbol{3}\epsilon^0 + \mathcal{O}(\epsilon), \tag{9.14}$$

$$I^{\text{MB}}_{\text{xhxwxz63}} = (0.0029 \pm 0.0008)\epsilon^0 + \mathcal{O}(\epsilon). \tag{9.15}$$

9.1.4 Sample integrals for infrared divergent integrals

We study 10 Feynman integrals, see Eqs. (D.207-D.216), which were difficult to calculate with the sector decomposition technique. These integrals are Laurent expanded in ϵ to resolve the divergences in ϵ^{-2} and ϵ^{-1} terms. Furthermore, these integrals depend on two dimensionless parameters m_t and M_W, taken of Eq. (4.50) and we neglect the overall prefactor $(\tilde{M}_Z^2)^{D-\nu}$, see Eq. (4.51). Again so far no analytic results were reported for these Feynman integrals with two different internal masses. In this case the numerical evaluation of these integrals is mandatory.

For Feynman integrals in Eqs. (D.207, D.208, D.209, D.210) three-dimensional Mellin-Barnes integral representations and for the integrals in Eqs. (D.211, D.212, D.213, D.214, D.215, D.216) four-dimensional Mellin-Barnes integral representations can be derived.

In the case of sector decomposition we need to evaluate five-dimensional integrals.

The numerical results calculated with `SecDec` and `MBnumerics.m` are summarized in Tab. D.5 for the ϵ^{-2} coefficients, in Tab. D.4 for the ϵ^{-1} coefficients and in

Tab. D.2 and in Tab. D.3 for the finite part. We label numerical results which are produced by `SecDec` with 15 Mio or with 90 Mio function evaluations with SD–15 and SD–90, respectively. The numerical results calculated with `MBnumerics.m` with 8, 10, 11 and 16 significant digits are labeled with MB–8, MB–10, MB–11 and MB–16.

Some results for Mellin-Barnes integrals are reported twice, where the second computation includes a transformation of the integration variables $z_i \to z_i + z_j$.

All results produced with the `MBnumerics.m` package are accurate, that means the second calculation, with the transformation of the integration variables $z_i \to z_i + z_j$, yields at most 1 sigma discrepancy. We have not performed in Tab. D.4 this test for some Mellin-Barnes integrals because these Mellin-Barnes integrals are two-dimensional and are considered as trivial as see for example Sec. 8.4.7 and Eq. (8.122) therein.

The reported errors by the program `SecDec` are underestimated by 1 or 2 digits for some integrals contributing to the finite part. It seems that again in addition to the Monte Carlo error a systematic error needs to be taken into account.

If we compare the runtime of the best results with `MBnumerics.m` and the results SD–90 then `MBnumerics.m` was faster than `SecDec` by a factor of 20 for the finite and the ϵ^{-1} part and by a huge factor of 1000 faster for the ϵ^{-2} part. If we take into account the time difference in both runtime of the programs and compare the achieved accuracy, we see that in this case the Mellin-Barnes integral approach is superior compared to the sector decomposition approach.

9.2 Effective weak mixing angle

We would like to remind that the Standard Model prediction for the effective weak mixing angle in this work is expressed in terms of $\Delta\kappa_b$,

$$\sin^2\theta^b_{\text{eff}} = \frac{1}{4|Q_b|}\left(1 - \Re e\,\frac{\hat{v}_b}{\hat{a}_b}\right) = \left(1 - \frac{M_W^2}{M_Z^2}\right)(1 + \Delta\kappa_b). \tag{9.16}$$

The $\Delta\kappa_b$ contains all contributions to $\sin^2\theta^b_{\text{eff}}$ stemming from the radiative corrections. The calculation includes the aforementioned $\mathcal{O}(700)$ two-loop vertex Feynman integrals and two-loop self-energies stemming from the renormalization constants, but also some trivial two-loop Feynman integrals which factorize into two one-loop Feynman integrals. The numerical cancellation of all ϵ^{-2} terms is varified up to an accuracy of 16 significant digits. The cancellation of ϵ^{-1} terms is safely below the worst numerical result of ten significant digits. The computation of the finite part with the input values in Tab. 3.1, the *bosonic* electroweak two-loop corrections are calculated in this thesis and presented in Ref. [17] to give:

$$\Delta\kappa_b^{(\alpha^2,\text{bos})} = -0.9855 \times 10^{-4}. \tag{9.17}$$

This result is compared in Tab. 9.1 with the already known radiative corrections: one-loop contributions [2, 3], $\mathcal{O}(\alpha\alpha_s)$ QCD corrections [112, 113, 114, 115, 116], [117, 118, 119, 120, 121, 122], partial higher-order corrections of orders $\mathcal{O}(\alpha_t\alpha_s^2)$ [123, 124], $\mathcal{O}(\alpha_t\alpha_s^3)$ [13, 14, 15], $\mathcal{O}(\alpha^2\alpha_t)$ and $\mathcal{O}(\alpha_t^3)$ [11, 12] and *fermionic* electroweak two-loop corrections [16]. Here the result of the *bosonic* electroweak two-loop corrections is

Table 9.1: Comparison of different orders of radiative corrections to $\Delta\kappa_b$, using the input parameters in Tab. 3.1. Where $\alpha_t = \frac{y_t^2}{4\pi}$, y_t being the Yukawa coupling.

Order	**Value [10^{-4}]**	**Order**	**Value [10^{-4}]**
α	468.945	$\alpha_t^2\alpha_\mathrm{s}$	1.362
$\alpha\alpha_\mathrm{s}$	-42.655	α_t^3	0.123
$\alpha_t\alpha_\mathrm{s}^2$	-7.074	α_ferm^2	3.866
$\alpha_t\alpha_\mathrm{s}^3$	-1.196	α_bos^2	-0.986

about a factor of four smaller, but of similar order of magnitude, compared to the *fermionic* electroweak two-loop corrections [16].

In addition the calculation can be repeated for input parameters varying in their ranges see Tab. 3.1. This way the numerical result can be parameterized by the following formula:

$$\Delta\kappa_b^{(\alpha^2,\mathrm{bos})} = k_0 + k_1 c_H + k_2 c_t + k_3 c_t^2 + k_4 c_H c_t + k_5 c_W, \tag{9.18}$$

where

$$\begin{aligned} c_H = \log\left(\frac{M_H}{M_Z}\times\frac{91.1876\ \mathrm{GeV}}{125.1\ \mathrm{GeV}}\right), \quad c_t = \left(\frac{m_t}{M_Z}\times\frac{91.1876\ \mathrm{GeV}}{173.2\ \mathrm{GeV}}\right)^2 - 1, \\ c_W = \left(\frac{M_W}{M_Z}\times\frac{91.1876\ \mathrm{GeV}}{80.385\ \mathrm{GeV}}\right)^2 - 1, \end{aligned} \tag{9.19}$$

with the numerical coefficients:

$$\begin{aligned} k_0 &= -0.98605\times10^{-4}, \quad k_1 = 0.3342\times10^{-4}, \quad k_2 = 1.3882\times10^{-4}, \\ k_3 &= -1.7497\times10^{-4}, \quad k_4 = -0.4934\times10^{-4}, \quad k_5 = -9.930\times10^{-4}. \end{aligned} \tag{9.20}$$

The full calculation is reproduced with maximal deviations of 1.2×10^{-7}, which come solely from the input parameter ranges in Tab. 3.1. Here the numerical errors coming from the evaluation of the Feynman integrals are in the full calculation negligible.

At present the most precise prediction for the effective weak mixing angle $\sin^2\theta_\mathrm{eff}^b$ can be obtained by combining the results in Tab. 9.1. It is:

$$\sin^2\theta_\mathrm{eff}^b = 0.232312. \tag{9.21}$$

Chapter 10

Summary

In this thesis the electroweak two-loop vertex Feynman integrals including massive particles are calculated with the Mellin-Barnes integral approach. The numerical results are collected in App. D. This approach is applicable to any Feynman integral. Its limitations are due to the number of Mellin-Barnes integral dimensions.

The Mellin-Barnes integral approach was used in the calculation of the *bosonic* electroweak two-loop contributions to the $\mathrm{Z\bar{b}b}$ vertex. In the calculation we consider up to four scales, of which three variables encountered are non-trivial: $M_H = \frac{\tilde{M}_H}{\tilde{M}_Z}$, $M_W = \frac{\tilde{M}_W}{\tilde{M}_Z}$, $m_t = \frac{\tilde{m}_t}{\tilde{M}_Z}$. Several integrals are complex in these variables. All Feynman integrals were computed with sufficient accuracy.

To evaluate the Mellin-Barnes integrals numerically we have used the programs: `AMBRE` to generate the Mellin-Barnes integral representations, `MB.m` to analytically continue the integrals to $\epsilon \to 0$, `MBnumerics.m` to generate integrands suitable for Minkowskian regions, `CUBA` to perform multi-dimensional numerical integration in `Fortran` and `Mathematica` to perform one-dimensional numerical integration. In this thesis `MBnumerics.m` was developed. This program takes as input the coefficients of the ϵ-expansion of a regularized Mellin-Barnes integral representation in $D = 4 - 2\epsilon$. In `MBnumerics.m` a combination of several techniques is implemented:

- A parabolic contour deformation is applied to one-dimensional integrals.
- For multi-dimensional integrals the cotangent is used to map an integration region with infinities to a finite interval.
- The simultaneous rotation of all integration contours is utilized.
- Contour shifts are applied.
- The $\prod_i \Gamma_i$, a building block of the Mellin-Barnes integrands, is replaced by $\exp \sum_i \log \Gamma_i$, where the explicit numerical evaluation of the function representation for the logarithm of the Γ-function is considered.

The contour shift replaces the original n-dimensional Mellin-Barnes integral, $n > 1$, by a finite number of less dimensional Mellin-Barnes integrals and a remainder, which is also an n-dimensional Mellin-Barnes integral with enhanced convergence and smaller order of magnitude, than the original n-dimensional Mellin-Barnes integral. The contour shifts, are also applicable to the Feynman integrals in Euclidean

kinematics. In this case `MBnumerics.m` enhances the runtime compared to the `MBintegrate` routine in the package `MB.m`. We have studied vertices, and did not perform any study regarding double box Feynman integrals.

For crosschecks the sector decomposition approach was used to evaluate numerically the two-loop vertex Feynman integrals and in the case where the Mellin-Barnes integral representation had more Mellin-Barnes integral dimensions than the integrals in the sector decomposition approach. In many cases either the Mellin-Barnes integral approach or the sector decomposition approach yield a numerical result with 1-3 significant digits, but in all cases at least one method could give numerical results with 8 significant digits. In cases where the Mellin-Barnes integral approach gives insufficient accuracy, the sector decomposition result was calculated with two different programs `SecDec` and `Fiesta`, which apply different strategies for the sector decomposition and use different values for the contour deformation parameter λ, see Eq. (5.27). Similarly, if the sector decomposition approach gives insufficient accuracy, then the Mellin-Barnes integral approach results are cross checked non trivially by modifying the multi-dimensional integrands with a linear transformation $z_i \to z_i + z_j$. In this sense the two methods are complementary because they either give two non trivial results for a better study of the numerical error estimate or at least one method gives high numerical accuracy, where the other method would fail.

Table 10.1: Last number of the first line relies on this thesis project. Electroweak *fermionic* and *bosonic* two-loop corrections are compared to the experiment uncertainty.

	Experiment uncertainty	$\mathcal{O}(\alpha^2_{\mathrm{ferm}})$	$\mathcal{O}(\alpha^2_{\mathrm{bos}})$
$\sin^2\theta^b_{\mathrm{eff}}[10^{-3}]$	16	0.086	-0.022
$\Gamma_Z[\mathrm{MeV}]$	2.3	8.2	in progress
$\sigma^0_{\mathrm{had}}[\mathrm{pb}]$	37	8.0	in progress
$R_b = \Gamma^b_Z/\Gamma^{\mathrm{had}}_Z[10^{-5}]$	66	-17	in progress
$R_l = \Gamma^l_Z/\Gamma^{\mathrm{had}}_Z[10^{-3}]$	25	-27	in progress

So far the *bosonic* electroweak two-loop corrections to the pseudo-observables Γ_Z, σ^0_{had}, $R_b = \Gamma^b_Z/\Gamma^{\mathrm{had}}_Z$ and $R_l = \Gamma^l_Z/\Gamma^{\mathrm{had}}_Z$ are unknown, see Tab. 10.1. These pseudo-observables depend on the vector and axial couplings of the $Z\bar{f}f$ vertex separately. In the calculation of the missing *bosonic* two-loop corrections new classes of vertex Feynman integrals with more massless lines appear, which are potentially more infrared divergent and are of the same type as integrals in Subsec. 9.1.4 or simpler. In fact all missing two-loop vertex integrals have been computed with sufficient accuracy, 6 significant digits for the finite part, 8 significant digits for the ϵ^{-1} part, 16 significant digits for the ϵ^{-2} part and 16 significant digits for the ϵ^{-3} part, with the complementary numerical methods, mentioned above. We could validate the

cancellation of all $1/\epsilon$ terms at the level of the numerical accuracy. Finally the combination of all terms to collect the finite contributions is in progress.

At present most of the precision observables are in a perfect state, where the theory uncertainty is lower than the measured uncertainty, see Tab. 10.2. The ambitious concepts for the future colliders, ILC/FCC-ee/CEPC [18, 20, 19], aim for an improvement of measurements for the precision observables by one to two significant digits. This will put the Electroweak Standard Model predictions in a situation where the leading three-loop corrections together with the missing *bosonic* two-loop corrections will become mandatory, see Tab. 10.2 and Tab. 10.3.

Table 10.2: Current status for some pseudo observables. The theory uncertainty is taken from Refs. [5, 47, 125] and compared to the current measurement error taken from Ref. [1, 63]. N_f^n denotes bare Feynman diagrams with at least n closed fermion loops.

	Experiment	**Theory uncertainty**	**Main source**
$M_W[\mathrm{MeV}]$	80385 ± 15	4	$N_f^2\alpha^3$, $N_f\alpha^2\alpha_\mathrm{s}$
$\sin^2\theta^l_\mathrm{eff}[10^{-5}]$	23153 ± 16	4.5	$N_f^2\alpha^3$, $N_f\alpha^2\alpha_\mathrm{s}$
$\Gamma_Z[\mathrm{MeV}]$	2495.2 ± 2.3	0.5	α^2_bos, $N_f^2\alpha^3$, $N_f\alpha^2\alpha_\mathrm{s}$, $\alpha\alpha_\mathrm{s}^2$
$R_b = \Gamma_Z^b/\Gamma_Z^\mathrm{had}[10^{-5}]$	21629 ± 66	15	α^2_bos, $N_f^2\alpha^3$, $N_f\alpha^2\alpha_\mathrm{s}$

Table 10.3: The projection to the theory errors in the future assumes that the missing corrections α^2_bos, $\alpha\alpha_\mathrm{s}^2$, $N_f^2\alpha^3$, $N_f\alpha^2\alpha_\mathrm{s}$ will become available. The measurement errors for future e^+e^- colliders are taken from the Refs. [126, 18, 19].

	Experiment uncertainty			**Theory uncertainty**	
	FCC-ee	**ILC**	**CEPC**	**Current**	**Future**
$M_W[\mathrm{MeV}]$	1	3-4	3	4	1
$\sin^2\theta^l_\mathrm{eff}[10^{-5}]$	0.6	1	2.3	4.5	1.5
$\Gamma_Z[\mathrm{MeV}]$	0.1	0.8	0.5	0.5	0.2
$R_b[10^{-5}]$	6	14	17	15	5-10

The study of the numerical application of the combined Mellin-Barnes integral approach and the sector decomposition approach to the three-loop vertex integrals is ongoing [127]. If we consider the bare diagrams corresponding to the electroweak corrections at $\mathcal{O}(\alpha^3)$, then first of all the number of bare diagrams is much bigger than at the two-loop order. This time the use of integration-by-parts identities might be mandatory to find a suitable basis of master integrals. For this task a reduction

program `Kira` is tailored to the class of Feynman integrals including massive particles, which is publicly available and is further developed. The electroweak three-loop Feynman diagrams depend explicitly on all four mass scales compared to the electroweak two-loop Feynman diagrams which depend at maximum on three mass scales. In view of the importance of the numerical methods for this thesis, the program `MBnumerics.m` is planned to be made publicly available for further use and development.

Appendix A

Propagator building blocks

$X_1 = k_1^2$
$X_2 = (k_1 - k_2)^2$
$X_3 = k_2^2$
$X_4 = (k_1 + p_1)^2$
$X_5 = (k_2 + p_1)^2$
$X_6 = (k_1 + p_1 + p_2)^2$
$X_7 = (k_2 + p_1 + p_2)^2$
$X_8 = (k_1 - p_2)^2$
$X_9 = (k_2 + p_2)^2$
$X_{10} = (k_1 + p_2)^2$
$X_{11} = (k_1 - k_2 + p_1)^2$
$X_{12} = (k_1 - p_1)^2$

Appendix B

Alternative parameter representations

Here we picked out some alternatives to the Feynman parameter representations. The following representations are called $\mathcal{G}$-polynomial representation [69]:

$$G_L^{\mathcal{G}}[1] = \frac{(-1)^\nu \Gamma(D/2)}{\Gamma((L+1)D/2-\nu)} \left(\prod_{j=1}^{N} \tilde{n}_j\right) \mathcal{G}^{-D/2}, \quad \mathcal{G} = \mathcal{F} + \mathcal{U}. \tag{B.1}$$

and the Schwinger parameter representation:

$$G_L^{\text{Schwinger}}[1] = (-1)^\nu \left(\prod_{j=1}^{N} \tilde{n}_j\right) \mathcal{U}^{-D/2} \exp\left(-\frac{\mathcal{F}}{\mathcal{U}}\right). \tag{B.2}$$

Here $\mathcal{U}$ and $\mathcal{F}$ are the same functions as in Eq. (4.33) and Eq. (4.34). These representations may be used to crosscheck the derivation of the Feynman parameter integral representation for the tensor loop integrals. These representations are all related to the Feynman parameter integral representation.

To get the Feynman parameter representation in Eq. (4.32) back, the following steps are involved:

- Add $1 = \int\limits_0^\infty \mathrm{d}s\delta(s - \sum\limits_{i=1}^{N_G} x_i)$.
- Rescale $x_i = sx_i'$, $\mathrm{d}x_j = s\mathrm{d}x_j'$, $\quad i = 1, \ldots, N, \quad j = 1, \ldots, N_G$.
- Use $\int\limits_0^\infty \mathrm{d}s\delta(s - s\sum\limits_{i=1}^{N_G} x_i') = \int\limits_0^\infty \mathrm{d}s\frac{1}{s}\delta(1 - \sum\limits_{i=1}^{N_G} x_i')$, $\mathcal{F}(x_i) = s^{L+1}\mathcal{F}(x_i')$, $\mathcal{U}(x_i) = s^L\mathcal{U}(x_i')$.
- Rescale $s = t\mathcal{U}/\mathcal{F}$, $\mathrm{d}s = \mathrm{d}t\mathcal{U}/\mathcal{F}$,

These steps are common for the $\mathcal{G}$-polynomial representation and for the Schwinger representation. For the $\mathcal{G}$-polynomial representation we use the integral representation of the Euler's Beta-function in Eq. (4.28). For the Schwinger parameter representation use the integral representation of the Γ-function:

$$\Gamma(z) = \int\limits_0^\infty \mathrm{d}t\, t^{z-1} \exp(-t). \tag{B.3}$$

Appendix C

MBnumerics.m

The implementation of MBnumerics.m package is sketched as follows:

1 MBnumerics.m takes a list of Mellin-Barnes integrals of different dimensionality (which for example contribute to one coefficient in the Laurent expansion in ϵ of a Feynman integral), the kinematic point K_1 of interest and the desired accuracy.

MBnumerics.m takes one more kinematic point K_2 where these Mellin-Barnes integrals converge fast (in practice it is an Euclidean kinematic point).

2 MBnumerics.m groups integrals which have the same dimensionality D_i in lists I_{D_i}.

These lists are collected together in one bigger list $I = (I_{D_1}, I_{D_2}, \ldots)$, with $D_k < D_l$, $k < l$.

Set i=1.

3 MBnumerics.m will evaluate all integrals in the list I_{D_i} at the kinematic point K_2. All pairs of integrals which agree up to 16 digits of accuracy with opposite sign are removed from the list I_{D_i}.

4 MBnumerics.m groups integrals in lists $I^{a_j}_{D_i}$ with similar polynomial asymptotic behavior (see Subsec. 8.4.6) $I_{D_i} = \{I^{a_1}_{D_i}, I^{a_2}_{D_i}, \ldots\}$, which is now an unordered set. The integrals in the lists $I^{a_j}_{D_i}$ are sorted according to the Subec. 8.4.6.

Set $j = 1$.

5 If $D_i = 1$ evaluate the one-dimensional integrals with the help of contour deformation (see Sec. 8.1) up to the desired accuracy. Collect the numerical result in the list F and move the integrals from the list $I^{a_j}_{D_i}$ to the list R.

If $D_i = 0$, evaluate these null-dimensional Mellin-Barnes integrals up to the desired accuracy. Collect the numerical result in the list F and move the integrals from the list $I^{a_j}_{D_i}$ to the list R.

If $D_i > 1$: MBnumerics.m finds a shift for the first integral in the list $I^{a_j}_{D_i}$ for which the numerical value reaches the desired accuracy. Collect the numerical result in the list F and remove the integral from the list $I^{a_j}_{D_i}$ but collect the shifted integral in the list R. Apply the shift to all remaining integrals in the list $I^{a_j}_{D_i}$. Collect the residues due to the shifted integrals in the list $I_{D_{i-1}}$.

6 If the list $I_{D_i}^{a_j} \neq \{\}$, then repeat step ***5***.

If the list $I_{D_i}^{a_j} = \{\}$, then remove $I_{D_i}^{a_j}$ from the list I_{D_i}.

If the list $I_{D_i} = \{\}$, then remove I_{D_i} from the list I. Relabel all D_i such that the list I is again $I = (I_{D_1}, I_{D_2}, \ldots)$. Repeat step ***3***.

If the list $I_{D_i} \neq \{\}$, then set $j = j + 1$ and repeat step ***5***.

7 The program `MBnumerics.m` terminates and will return two lists, which contain the numerical results (list F) and the integrals which were evaluated to get this result (list R).

It can be verified that the step ***3*** does not modify the calculation by a second calculation which skips the step ***3***.

The numerical results returned by `MBnumerics.m` in the list F are summed up. The error is combined in quadrature.

`MBnumerics.m` returns all Mellin-Barnes integrals which were needed to evaluate the initial integrals in the point K_1 in a list R. We evaluate the list R again at a different point K_1'. This may reduce the total run time in the second `MBnumerics.m` call.

Appendix D

Numerics

D.1 0h0w0txz

$$I_{\text{0h0w1}} = \int \frac{\mathrm{d}^D k_1}{i\pi^{D/2}} \frac{\mathrm{d}^D k_2}{i\pi^{D/2}} \frac{\exp(2\epsilon\gamma_E)}{X_1 X_2 X_3 (X_4 - M_Z^2) X_5 X_6} \tag{D.1}$$

$$\begin{aligned} &= (9.0437097\boldsymbol{7}54 - 1.156762\boldsymbol{7}\boldsymbol{3}54i)\epsilon^0 \\ &\quad +(-0.357958099\boldsymbol{9}\boldsymbol{9}73 - 3.3385502194\boldsymbol{8}\boldsymbol{5}23i)\epsilon^{-1} \\ &\quad -0.82246703342411\boldsymbol{3}\boldsymbol{2}\epsilon^{-2} \\ &\quad +\mathcal{O}(\epsilon) \end{aligned} \tag{D.2}$$

$$I_{\text{0h0w2}} = \int \frac{\mathrm{d}^D k_1}{i\pi^{D/2}} \frac{\mathrm{d}^D k_2}{i\pi^{D/2}} \frac{\exp(2\epsilon\gamma_E)}{X_1 X_2 (X_3 - M_Z^2)(X_4 - M_Z^2) X_5 X_6} \tag{D.3}$$

$$\begin{aligned} &= (-1.199526\boldsymbol{1}\boldsymbol{8}27 + 5.567365\boldsymbol{9}\boldsymbol{0}76i)\epsilon^0 \\ &\quad +\mathcal{O}(\epsilon) \end{aligned} \tag{D.4}$$

$$I_{\text{0h0w3}} = \int \frac{\mathrm{d}^D k_1}{i\pi^{D/2}} \frac{\mathrm{d}^D k_2}{i\pi^{D/2}} \frac{\exp(2\epsilon\gamma_E)(k_2 p_2)}{X_1 X_2 X_3 (X_4 - M_Z^2) X_5} \tag{D.5}$$

$$\begin{aligned} &= 1.085600\boldsymbol{2}\boldsymbol{7}50\epsilon^0 \\ &\quad +0.1875\epsilon^{-1} \\ &\quad +0.125\epsilon^{-2} \\ &\quad +\mathcal{O}(\epsilon) \end{aligned} \tag{D.6}$$

$$I_{\text{0h0w4}} = \int \frac{\mathrm{d}^D k_1}{i\pi^{D/2}} \frac{\mathrm{d}^D k_2}{i\pi^{D/2}} \frac{\exp(2\epsilon\gamma_E)(k_1 p_1)}{X_1 X_2 X_3 (X_5 - M_Z^2) X_8} \tag{D.7}$$

$$\begin{aligned} &= -6.806167\boldsymbol{5}\boldsymbol{8}35\epsilon^0 \\ &\quad -1.25\epsilon^{-1} \\ &\quad -0.25\epsilon^{-2} \\ &\quad +\mathcal{O}(\epsilon) \end{aligned} \tag{D.8}$$

$$I_{\text{0h0w5}} = \int \frac{\mathrm{d}^D k_1}{i\pi^{D/2}} \frac{\mathrm{d}^D k_2}{i\pi^{D/2}} \frac{\exp(2\epsilon\gamma_E)(k_2 p_2)}{X_1 X_2 X_3 (X_5 - M_Z^2) X_8} \tag{D.9}$$

$$\begin{aligned} &= -0.8276092\boldsymbol{9}13\epsilon^0 \\ &\quad -0.32246703342\boldsymbol{4}11\epsilon^{-1} \\ &\quad +\mathcal{O}(\epsilon) \end{aligned} \tag{D.10}$$

$$I_{\text{0h0w6}} = \int \frac{\mathrm{d}^D k_1}{i\pi^{D/2}} \frac{\mathrm{d}^D k_2}{i\pi^{D/2}} \frac{\exp(2\epsilon\gamma_E)(k_1 p_1)}{X_1 X_2 X_3 X_5 (X_8 - M_Z^2)} \tag{D.11}$$

$$\begin{aligned} &= 0.8276092\boldsymbol{9}13\epsilon^0 \\ &\quad +0.32246703342\boldsymbol{4}11\epsilon^{-1} \\ &\quad +\mathcal{O}(\epsilon) \end{aligned} \tag{D.12}$$

$$I_{\text{0h0w7}} = \int \frac{\mathrm{d}^D k_1}{i\pi^{D/2}} \frac{\mathrm{d}^D k_2}{i\pi^{D/2}} \frac{\exp(2\epsilon\gamma_E)}{X_1 X_2 X_3 (X_{10} - M_Z^2) X_9 X_6} \tag{D.13}$$

$$\begin{aligned} &= (9.0437097\boldsymbol{7}54 - 1.1567627\boldsymbol{3}54i)\epsilon^0 \\ &\quad +(-0.357958099\boldsymbol{9}73 - 3.33855021948\boldsymbol{5}23i)\epsilon^{-1} \\ &\quad -0.82246703342411\boldsymbol{2}\epsilon^{-2} \\ &\quad +\mathcal{O}(\epsilon) \end{aligned} \tag{D.14}$$

$$I_{\text{0h0w8}} = \int \frac{\mathrm{d}^D k_1}{i\pi^{D/2}} \frac{\mathrm{d}^D k_2}{i\pi^{D/2}} \frac{\exp(2\epsilon\gamma_E)}{X_1 X_2 (X_3 - M_Z^2)(X_{10} - M_Z^2) X_9 X_6} \tag{D.15}$$

$$\begin{aligned} &= (-1.199526\boldsymbol{8}27 + 5.567365\boldsymbol{9}76i)\epsilon^0 \\ &\quad +\mathcal{O}(\epsilon) \end{aligned} \tag{D.16}$$

$$I_{\text{0h0w9}} = \int \frac{\mathrm{d}^D k_1}{i\pi^{D/2}} \frac{\mathrm{d}^D k_2}{i\pi^{D/2}} \frac{\exp(2\epsilon\gamma_E)(k_2 p_1)}{X_1 X_2 X_3 (X_{10} - M_Z^2) X_9} \tag{D.17}$$

$$\begin{aligned} &= 1.085600\boldsymbol{7}50\epsilon^0 \\ &\quad +0.1875\epsilon^{-1} \\ &\quad +0.125\epsilon^{-2} \\ &\quad +\mathcal{O}(\epsilon) \end{aligned} \tag{D.18}$$

$$I_{\text{0h0w10}} = \int \frac{\mathrm{d}^D k_1}{i\pi^{D/2}} \frac{\mathrm{d}^D k_2}{i\pi^{D/2}} \frac{\exp(2\epsilon\gamma_E)(k_1 p_1)}{X_1 X_2 X_3 X_5 X_6} \tag{D.19}$$

$$\begin{aligned} &= (3.068429\boldsymbol{5}18 + 5.167712\boldsymbol{8}00i)\epsilon^0 \\ &\quad +0.8224670334\boldsymbol{4}11\epsilon^{-1} \\ &\quad +\mathcal{O}(\epsilon) \end{aligned} \tag{D.20}$$

$$I_{\text{0h0w11}} = \int \frac{\mathrm{d}^D k_1}{i\pi^{D/2}} \frac{\mathrm{d}^D k_2}{i\pi^{D/2}} \frac{\exp(2\epsilon\gamma_E)(k_2 p_2)}{X_1 X_2 X_3 X_5 X_6} \tag{D.21}$$

$$\begin{aligned} &= (3.6644652\boldsymbol{6}91 - 2.6862688\boldsymbol{5}39i)\epsilon^0 \\ &\quad +(-0.427532966575\boldsymbol{8}8 - 1.570796326794\boldsymbol{8}9i)\epsilon^{-1} \\ &\quad -0.25\epsilon^{-2} \\ &\quad +\mathcal{O}(\epsilon) \end{aligned} \tag{D.22}$$

$$I_{\text{0h0w12}} = \int \frac{\mathrm{d}^D k_1}{i\pi^{D/2}} \frac{\mathrm{d}^D k_2}{i\pi^{D/2}} \frac{\exp(2\epsilon\gamma_E)(k_1 p_1)}{X_1 (X_2 - M_Z^2) X_3 X_5 X_6} \tag{D.23}$$

$$\begin{aligned} &= (1.821367\boldsymbol{9}95 - 1.582407\boldsymbol{2}86i)\epsilon^0 \\ &\quad -0.60678976350\boldsymbol{8}70i\epsilon^{-1} \\ &\quad +\mathcal{O}(\epsilon) \end{aligned} \tag{D.24}$$

$$I_{\text{0h0w13}} = \int \frac{\mathrm{d}^D k_1}{i\pi^{D/2}} \frac{\mathrm{d}^D k_2}{i\pi^{D/2}} \frac{\exp(2\epsilon\gamma_E)(k_1 p_1)}{X_1 X_2 X_3 (X_5 - M_Z^2) X_6} \tag{D.25}$$

$$\begin{aligned} &= (-0.136519\boldsymbol{1}80 + 1.160964\boldsymbol{2}91i)\epsilon^0 \\ &\quad +\mathcal{O}(\epsilon) \end{aligned} \tag{D.26}$$

$$I_{\text{0h0w14}} = \int \frac{\mathrm{d}^D k_1}{i\pi^{D/2}} \frac{\mathrm{d}^D k_2}{i\pi^{D/2}} \frac{\exp(2\epsilon\gamma_E)(k_1 p_1)}{X_1 (X_2 - M_Z^2) X_3 (X_5 - M_Z^2) X_6} \tag{D.27}$$

$$\begin{aligned} &= (0.392382\boldsymbol{5}88 + 0.745638\boldsymbol{5}36i)\epsilon^0 \\ &\quad +\mathcal{O}(\epsilon) \end{aligned} \tag{D.28}$$

$$I_{\text{0h0w15}} = \int \frac{\mathrm{d}^D k_1}{i\pi^{D/2}} \frac{\mathrm{d}^D k_2}{i\pi^{D/2}} \frac{\exp(2\epsilon\gamma_E)}{X_1 X_2 X_3 (X_{11} - M_Z^2) X_9 X_6} \tag{D.29}$$

$$\begin{aligned} &= (-0.778599\boldsymbol{6}092 - 4.123512\boldsymbol{5}932i)\epsilon^0 \\ &\quad +(-2.8902545096\boldsymbol{7}99 - 3.87578458503\boldsymbol{7}58i)\epsilon^{-1} \\ &\quad -1.2337005501361\boldsymbol{6}0\boldsymbol{2}\epsilon^{-2} \\ &\quad +\mathcal{O}(\epsilon) \end{aligned} \tag{D.30}$$

$$I_{\text{0h0w16}} = \int \frac{\mathrm{d}^D k_1}{i\pi^{D/2}} \frac{\mathrm{d}^D k_2}{i\pi^{D/2}} \frac{\exp(2\epsilon\gamma_E)(k_1 p_1)}{X_1 X_2 X_3 X_9 X_6} \tag{D.31}$$

$$\begin{aligned} &= (3.911797\boldsymbol{3}\boldsymbol{6}68 + 0.798082\boldsymbol{2}\boldsymbol{8}58i)\epsilon^0 \\ &\quad +(0.12701874078\boldsymbol{5}98 - 1.013060063\boldsymbol{2}\boldsymbol{3}\boldsymbol{0}08i)\epsilon^{-1} \\ &\quad -0.161233516712056\boldsymbol{6}09\epsilon^{-2} \\ &\quad +\mathcal{O}(\epsilon) \end{aligned} \tag{D.32}$$

$$I_{\text{0h0w17}} = \int \frac{\mathrm{d}^D k_1}{i\pi^{D/2}} \frac{\mathrm{d}^D k_2}{i\pi^{D/2}} \frac{\exp(2\epsilon\gamma_E)(k_2 p_1)}{X_1 X_2 X_3 X_9 X_6} \tag{D.33}$$

$$\begin{aligned} &= (3.6644652\boldsymbol{6}91 - 2.6862688\boldsymbol{5}39i)\epsilon^0 \\ &\quad +(-0.427532966575\boldsymbol{8}8 - 1.57079632679\boldsymbol{4}89i)\epsilon^{-1} \\ &\quad -0.25\epsilon^{-2} \\ &\quad +\mathcal{O}(\epsilon) \end{aligned} \tag{D.34}$$

$$I_{\text{0h0w18}} = \int \frac{\mathrm{d}^D k_1}{i\pi^{D/2}} \frac{\mathrm{d}^D k_2}{i\pi^{D/2}} \frac{\exp(2\epsilon\gamma_E)(k_1 p_1)}{X_1 (X_2 - M_Z^2) X_3 X_9 X_6} \tag{D.35}$$

$$\begin{aligned} &= (1.6582993\boldsymbol{9}65 - 1.9579418\boldsymbol{8}65i)\epsilon^0 \\ &\quad +(-0.12298125921\boldsymbol{4}01 - 0.6851384315\boldsymbol{3}78i)\epsilon^{-1} \\ &\quad +\mathcal{O}(\epsilon) \end{aligned} \tag{D.36}$$

$$I_{\text{0h0w19}} = \int \frac{\mathrm{d}^D k_1}{i\pi^{D/2}} \frac{\mathrm{d}^D k_2}{i\pi^{D/2}} \frac{\exp(2\epsilon\gamma_E)(k_2 p_1)}{X_1 (X_2 - M_Z^2) X_3 X_9 X_6} \tag{D.37}$$

$$\begin{aligned} &= (1.148976\boldsymbol{4}908 - 1.582407\boldsymbol{2}86i)\epsilon^0 \\ &\quad +(-0.17753296657\boldsymbol{5}88 - 0.60678976350\boldsymbol{8}70i)\epsilon^{-1} \\ &\quad +\mathcal{O}(\epsilon) \end{aligned} \tag{D.38}$$

$$I_{\text{0h0w20}} = \int \frac{\mathrm{d}^D k_1}{i\pi^{D/2}} \frac{\mathrm{d}^D k_2}{i\pi^{D/2}} \frac{\exp(2\epsilon\gamma_E)(k_1 p_1)}{X_1 X_2 X_3 (X_9 - M_Z^2) X_6} \tag{D.39}$$

$$\begin{aligned} &= (0.0508106\boldsymbol{9}20 + 1.3005492\boldsymbol{8}04i)\epsilon^0 \\ &\quad +\mathcal{O}(\epsilon) \end{aligned} \tag{D.40}$$

$$I_{\text{0h0w21}} = \int \frac{\mathrm{d}^D k_1}{i\pi^{D/2}} \frac{\mathrm{d}^D k_2}{i\pi^{D/2}} \frac{\exp(2\epsilon\gamma_E)(k_2 p_1)}{X_1 X_2 X_3 (X_9 - M_Z^2) X_6} \tag{D.41}$$

$$\begin{aligned} &= (0.245172\boldsymbol{7}561 + 1.087674\boldsymbol{4}87i)\epsilon^0 \\ &\quad +\mathcal{O}(\epsilon) \end{aligned} \tag{D.42}$$

$$I_{\text{0h0w22}} = \int \frac{\mathrm{d}^D k_1}{i\pi^{D/2}} \frac{\mathrm{d}^D k_2}{i\pi^{D/2}} \frac{\exp(2\epsilon\gamma_E)(k_1 p_1)}{X_1 (X_2 - M_Z^2) X_3 (X_9 - M_Z^2) X_6} \tag{D.43}$$

$$\begin{aligned} &= (0.490463\boldsymbol{1}190 + 0.764910\boldsymbol{4}\boldsymbol{0}08i)\epsilon^0 \\ &\quad +\mathcal{O}(\epsilon) \end{aligned} \tag{D.44}$$

$$I_{\text{0h0w23}} = \int \frac{\mathrm{d}^D k_1}{i\pi^{D/2}} \frac{\mathrm{d}^D k_2}{i\pi^{D/2}} \frac{\exp(2\epsilon\gamma_E)(k_2 p_1)}{X_1(X_2 - M_Z^2)X_3(X_9 - M_Z^2)X_6} \tag{D.45}$$

$$= (0.4476762\boldsymbol{0}67 + 0.5623921\boldsymbol{6}59i)\epsilon^0 + \mathcal{O}(\epsilon) \tag{D.46}$$

$$I_{\text{0h0w24}} = \int \frac{\mathrm{d}^D k_1}{i\pi^{D/2}} \frac{\mathrm{d}^D k_2}{i\pi^{D/2}} \frac{\exp(2\epsilon\gamma_E)(k_1 p_1)}{X_1 X_2 X_3 X_6 X_7} \tag{D.47}$$

$$= -1.8030853\boldsymbol{5}47\epsilon^0 + \mathcal{O}(\epsilon) \tag{D.48}$$

$$I_{\text{0h0w25}} = \int \frac{\mathrm{d}^D k_1}{i\pi^{D/2}} \frac{\mathrm{d}^D k_2}{i\pi^{D/2}} \frac{\exp(2\epsilon\gamma_E)(k_1 p_1)}{X_1(X_2 - M_Z^2)X_3 X_6 X_7} \tag{D.49}$$

$$= (-0.9015426\boldsymbol{7}71 + 1.2919281\boldsymbol{9}44i)\epsilon^0 + \mathcal{O}(\epsilon) \tag{D.50}$$

$$I_{\text{0h0w26}} = \int \frac{\mathrm{d}^D k_1}{i\pi^{D/2}} \frac{\mathrm{d}^D k_2}{i\pi^{D/2}} \frac{\exp(2\epsilon\gamma_E)(k_1 p_1)}{X_1 X_2(X_3 - M_Z^2)X_5 X_6} \tag{D.51}$$

$$= 1.5707963\boldsymbol{2}67i\epsilon^0 + \mathcal{O}(\epsilon) \tag{D.52}$$

$$I_{\text{0h0w27}} = \int \frac{\mathrm{d}^D k_1}{i\pi^{D/2}} \frac{\mathrm{d}^D k_2}{i\pi^{D/2}} \frac{\exp(2\epsilon\gamma_E)(k_2 p_2)}{X_1 X_2(X_3 - M_Z^2)X_5 X_6} \tag{D.53}$$

$$= (0.2909490\boldsymbol{7}92 + 2.5068121\boldsymbol{7}09i)\epsilon^0 + \mathcal{O}(\epsilon) \tag{D.54}$$

$$I_{\text{0h0w28}} = \int \frac{\mathrm{d}^D k_1}{i\pi^{D/2}} \frac{\mathrm{d}^D k_2}{i\pi^{D/2}} \frac{\exp(2\epsilon\gamma_E)}{X_1 X_2(X_3 - M_Z^2)X_{11} X_9 X_6} \tag{D.55}$$

$$= (-0.7785996\boldsymbol{0}92 - 4.1235125\boldsymbol{9}34i)\epsilon^0 + (-2.89025450965\boldsymbol{9}83 - 3.87578458503\boldsymbol{2}34i)\epsilon^{-1} - 1.2337005501361795\epsilon^{-2} + \mathcal{O}(\epsilon) \tag{D.56}$$

$$I_{\text{0h0w29}} = \int \frac{\mathrm{d}^D k_1}{i\pi^{D/2}} \frac{\mathrm{d}^D k_2}{i\pi^{D/2}} \frac{\exp(2\epsilon\gamma_E)}{X_1 X_2(X_3 - M_Z^2)(X_{11} - M_Z^2)X_9 X_6} \tag{D.57}$$

$$= (-1.2116223\boldsymbol{3}07 + 4.9954503\boldsymbol{1}70i)\epsilon^0 + \mathcal{O}(\epsilon) \tag{D.58}$$

$$I_{\text{0h0w30}} = \int \frac{\mathrm{d}^D k_1}{i\pi^{D/2}} \frac{\mathrm{d}^D k_2}{i\pi^{D/2}} \frac{\exp(2\epsilon\gamma_E)(k_1 p_1)}{X_1 X_2 (X_3 - M_Z^2) X_9 X_6} \tag{D.59}$$

$$= (0.3539849\boldsymbol{8}75 + 2.2055768\boldsymbol{0}93i)\epsilon^0 + \mathcal{O}(\epsilon) \tag{D.60}$$

$$I_{\text{0h0w31}} = \int \frac{\mathrm{d}^D k_1}{i\pi^{D/2}} \frac{\mathrm{d}^D k_2}{i\pi^{D/2}} \frac{\exp(2\epsilon\gamma_E)(k_2 p_1)}{X_1 X_2 (X_3 - M_Z^2) X_9 X_6} \tag{D.61}$$

$$= (0.2909490\boldsymbol{7}92 + 2.5068121\boldsymbol{7}09i)\epsilon^0 + \mathcal{O}(\epsilon) \tag{D.62}$$

$$I_{\text{0h0w32}} = \int \frac{\mathrm{d}^D k_1}{i\pi^{D/2}} \frac{\mathrm{d}^D k_2}{i\pi^{D/2}} \frac{\exp(2\epsilon\gamma_E)(k_2 p_1)}{(X_1 - M_Z^2) X_2 X_3 X_{12} X_9} \tag{D.63}$$

$$= (1.1302774\boldsymbol{2}62 - 2.7433720\boldsymbol{5}77i)\epsilon^0 + (-0.3224670334\boldsymbol{4}11 - 0.6067897635\boldsymbol{0}870i)\epsilon^{-1} + \mathcal{O}(\epsilon) \tag{D.64}$$

$$I_{\text{0h0w33}} = \int \frac{\mathrm{d}^D k_1}{i\pi^{D/2}} \frac{\mathrm{d}^D k_2}{i\pi^{D/2}} \frac{\exp(2\epsilon\gamma_E)(k_2 p_1)}{(X_1 - M_Z^2) X_2 X_3 X_{12} (X_9 - M_Z^2)} \tag{D.65}$$

$$= 0.4505720\boldsymbol{0}27\epsilon^0 + \mathcal{O}(\epsilon) \tag{D.66}$$

$$I_{\text{0h0w34}} = \int \frac{\mathrm{d}^D k_1}{i\pi^{D/2}} \frac{\mathrm{d}^D k_2}{i\pi^{D/2}} \frac{\exp(2\epsilon\gamma_E)(k_1 p_2)}{(X_1 - M_Z^2) X_2 X_3 X_4 (X_5 - M_Z^2)} \tag{D.67}$$

$$= 0.9474670\boldsymbol{3}34\epsilon^0 + \mathcal{O}(\epsilon) \tag{D.68}$$

$$I_{\text{0h0w35}} = \int \frac{\mathrm{d}^D k_1}{i\pi^{D/2}} \frac{\mathrm{d}^D k_2}{i\pi^{D/2}} \frac{\exp(2\epsilon\gamma_E)(k_2 p_2)}{(X_1 - M_Z^2) X_2 X_3 X_4 (X_5 - M_Z^2)} \tag{D.69}$$

$$= 0.6974670\boldsymbol{3}34\epsilon^0 + \mathcal{O}(\epsilon) \tag{D.70}$$

$$I_{\text{0h0w36}} = \int \frac{\mathrm{d}^D k_1}{i\pi^{D/2}} \frac{\mathrm{d}^D k_2}{i\pi^{D/2}} \frac{\exp(2\epsilon\gamma_E)(k_1 p_1)}{(X_1 - M_Z^2) X_2 X_3 X_5 X_8} \tag{D.71}$$

$$= (-1.1302774\boldsymbol{2}62 + 2.7433720\boldsymbol{5}77i)\epsilon^0 + (0.3224670334\boldsymbol{4}11 + 0.6067897635\boldsymbol{0}870i)\epsilon^{-1} + \mathcal{O}(\epsilon) \tag{D.72}$$

$$I_{\text{0h0w37}} = \int \frac{\mathrm{d}^D k_1}{i\pi^{D/2}} \frac{\mathrm{d}^D k_2}{i\pi^{D/2}} \frac{\exp(2\epsilon\gamma_E)(k_2 p_2)}{(X_1 - M_Z^2) X_2 X_3 X_5 X_8} \tag{D.73}$$

$$= (1.1302774\boldsymbol{2}62 - 2.7433720\boldsymbol{5}77i)\epsilon^0 + (-0.3224670334\boldsymbol{4}11 - 0.606789763508\boldsymbol{7}0i)\epsilon^{-1} + \mathcal{O}(\epsilon) \tag{D.74}$$

$$I_{\text{0h0w38}} = \int \frac{\mathrm{d}^D k_1}{i\pi^{D/2}} \frac{\mathrm{d}^D k_2}{i\pi^{D/2}} \frac{\exp(2\epsilon\gamma_E)(k_1 p_1)}{(X_1 - M_Z^2) X_2 X_3 (X_5 - M_Z^2) X_8} \tag{D.75}$$

$$= -0.95057200\boldsymbol{0}27\epsilon^0 + \mathcal{O}(\epsilon) \tag{D.76}$$

$$I_{\text{0h0w39}} = \int \frac{\mathrm{d}^D k_1}{i\pi^{D/2}} \frac{\mathrm{d}^D k_2}{i\pi^{D/2}} \frac{\exp(2\epsilon\gamma_E)(k_2 p_2)}{(X_1 - M_Z^2) X_2 X_3 (X_5 - M_Z^2) X_8} \tag{D.77}$$

$$= 0.45057200\boldsymbol{0}27\epsilon^0 + \mathcal{O}(\epsilon) \tag{D.78}$$

$$I_{\text{0h0w40}} = \int \frac{\mathrm{d}^D k_1}{i\pi^{D/2}} \frac{\mathrm{d}^D k_2}{i\pi^{D/2}} \frac{\exp(2\epsilon\gamma_E)(k_1 p_1)}{(X_1 - M_Z^2) X_2 X_3 X_{10} (X_9 - M_Z^2)} \tag{D.79}$$

$$= 0.9474670\boldsymbol{3}34\epsilon^0 + \mathcal{O}(\epsilon) \tag{D.80}$$

$$I_{\text{0h0w41}} = \int \frac{\mathrm{d}^D k_1}{i\pi^{D/2}} \frac{\mathrm{d}^D k_2}{i\pi^{D/2}} \frac{\exp(2\epsilon\gamma_E)(k_2 p_1)}{(X_1 - M_Z^2) X_2 X_3 X_{10} (X_9 - M_Z^2)} \tag{D.81}$$

$$= 0.6974670\boldsymbol{3}34\epsilon^0 + \mathcal{O}(\epsilon) \tag{D.82}$$

$$I_{\text{0h0w42}} = \int \frac{\mathrm{d}^D k_1}{i\pi^{D/2}} \frac{\mathrm{d}^D k_2}{i\pi^{D/2}} \frac{\exp(2\epsilon\gamma_E)(k_2 p_2)}{X_1 X_2 X_3 (X_4 - M_Z^2) X_5 X_6} \tag{D.83}$$

$$= (-2.1542059\boldsymbol{6}49 + 1.5827797\boldsymbol{1}16i)\epsilon^0 + (0.33876648328\boldsymbol{7}95 + 1.08879304515\boldsymbol{1}80i)\epsilon^{-1} + 0.25\epsilon^{-2} + \mathcal{O}(\epsilon) \tag{D.84}$$

$$I_{\text{0h0w43}} = \int \frac{\mathrm{d}^D k_1}{i\pi^{D/2}} \frac{\mathrm{d}^D k_2}{i\pi^{D/2}} \frac{\exp(2\epsilon\gamma_E)(k_2 p_1)}{X_1 X_2 X_3 (X_4 - M_Z^2) X_6 X_7} \tag{D.85}$$

$$(1.2966269\boldsymbol{4}53 + 1.0444361\boldsymbol{3}15i)\epsilon^0 + \mathcal{O}(\epsilon) \tag{D.86}$$

$$I_{\text{0h0w44}} = \int \frac{\mathrm{d}^D k_1}{i\pi^{D/2}} \frac{\mathrm{d}^D k_2}{i\pi^{D/2}} \frac{\exp(2\epsilon\gamma_E)(k_2 p_1)}{X_1(X_2 - M_Z^2)X_3(X_4 - M_Z^2)X_6 X_7} \tag{D.87}$$

$$= (0.9894379\boldsymbol{8}03 - 0.3806822\boldsymbol{2}76i)\epsilon^0 + \mathcal{O}(\epsilon) \tag{D.88}$$

$$I_{\text{0h0w45}} = \int \frac{\mathrm{d}^D k_1}{i\pi^{D/2}} \frac{\mathrm{d}^D k_2}{i\pi^{D/2}} \frac{\exp(2\epsilon\gamma_E)(k_2 p_2)}{X_1 X_2(X_3 - M_Z^2)(X_4 - M_Z^2)X_5 X_6} \tag{D.89}$$

$$= (0.4263954\boldsymbol{1}32 - 1.9327075\boldsymbol{1}75i)\epsilon^0 + \mathcal{O}(\epsilon) \tag{D.90}$$

$$I_{\text{0h0w46}} = \int \frac{\mathrm{d}^D k_1}{i\pi^{D/2}} \frac{\mathrm{d}^D k_2}{i\pi^{D/2}} \frac{\exp(2\epsilon\gamma_E)(k_1 p_1)^2}{X_1 X_2 X_3(X_5 - M_Z^2)X_8} \tag{D.91}$$

$$= -3.0601253\boldsymbol{4}38\epsilon^0 - 0.546874999\boldsymbol{9}66\epsilon^{-1} - 0.093749999999\boldsymbol{5}69\epsilon^{-2} + \mathcal{O}(\epsilon) \tag{D.92}$$

$$I_{\text{0h0w47}} = \int \frac{\mathrm{d}^D k_1}{i\pi^{D/2}} \frac{\mathrm{d}^D k_2}{i\pi^{D/2}} \frac{\exp(2\epsilon\gamma_E)(k_1 p_1)(k_2 p_2)}{X_1 X_2 X_3(X_5 - M_Z^2)X_8} \tag{D.93}$$

$$= -0.0712448\boldsymbol{0}42\epsilon^0 - 0.026266483287\boldsymbol{9}4\epsilon^{-1} + \mathcal{O}(\epsilon) \tag{D.94}$$

$$I_{\text{0h0w48}} = \int \frac{\mathrm{d}^D k_1}{i\pi^{D/2}} \frac{\mathrm{d}^D k_2}{i\pi^{D/2}} \frac{\exp(2\epsilon\gamma_E)(k1 * p1)^2}{X_1 X_2 X_3 X_5(X_8 - M_Z^2)} \tag{D.95}$$

$$= 0.0234771\boldsymbol{8}52\epsilon^0 + 0.049366758356\boldsymbol{0}2\epsilon^{-1} + \mathcal{O}(\epsilon) \tag{D.96}$$

$$I_{\text{0h0w49}} = \int \frac{\mathrm{d}^D k_1}{i\pi^{D/2}} \frac{\mathrm{d}^D k_2}{i\pi^{D/2}} \frac{\exp(2\epsilon\gamma_E)(k_1 p_1)(k_2 p_2)}{X_1 X_2 X_3 X_5(X_8 - M_Z^2)} \tag{D.97}$$

$$= -0.0712448\boldsymbol{0}42\epsilon^0 - 0.026266483287\boldsymbol{9}4\epsilon^{-1} + \mathcal{O}(\epsilon) \tag{D.98}$$

$$I_{\text{0h0w50}} = \int \frac{\mathrm{d}^D k_1}{i\pi^{D/2}} \frac{\mathrm{d}^D k_2}{i\pi^{D/2}} \frac{\exp(2\epsilon\gamma_E)(k_2 p_1)}{X_1 X_2 X_3 (X_{10} - M_Z^2) X_9 X_6} \tag{D.99}$$

$$\begin{aligned} &= (-2.1542059\boldsymbol{6}49 + 1.5827797\boldsymbol{1}16i)\epsilon^0 \\ &\quad +(0.338766483287\boldsymbol{9}5 + 1.088793045151\boldsymbol{8}0i)\epsilon^{-1} \\ &\quad +0.25\epsilon^{-2} \\ &\quad +\mathcal{O}(\epsilon) \end{aligned} \tag{D.100}$$

$$I_{\text{0h0w51}} = \int \frac{\mathrm{d}^D k_1}{i\pi^{D/2}} \frac{\mathrm{d}^D k_2}{i\pi^{D/2}} \frac{\exp(2\epsilon\gamma_E)(k_2 p_1)}{X_1 X_2 (X_3 - M_Z^2)(X_{10} - M_Z^2) X_9 X_6} \tag{D.101}$$

$$\begin{aligned} &= (0.4263954\boldsymbol{1}32 - 1.9327075\boldsymbol{1}75i)\epsilon^0 \\ &\quad +\mathcal{O}(\epsilon) \end{aligned} \tag{D.102}$$

$$I_{\text{0h0w52}} = \int \frac{\mathrm{d}^D k_1}{i\pi^{D/2}} \frac{\mathrm{d}^D k_2}{i\pi^{D/2}} \frac{\exp(2\epsilon\gamma_E)(k1 * p1)^2}{X_1 X_2 X_3 X_5 X_6} \tag{D.103}$$

$$\begin{aligned} &= (-0.6642990\boldsymbol{0}87 - 1.2919281\boldsymbol{9}50i)\epsilon^0 \\ &\quad -0.20561675835\boldsymbol{6}02\epsilon^{-1} \\ &\quad +\mathcal{O}(\epsilon) \end{aligned} \tag{D.104}$$

$$I_{\text{0h0w53}} = \int \frac{\mathrm{d}^D k_1}{i\pi^{D/2}} \frac{\mathrm{d}^D k_2}{i\pi^{D/2}} \frac{\exp(2\epsilon\gamma_E)(k_1 p_1)(k_2 p_2)}{X_1 X_2 X_3 X_5 X_6} \tag{D.105}$$

$$\begin{aligned} &= (-0.726899\boldsymbol{7}249 - 1.178097\boldsymbol{4}450i)\epsilon^0 \\ &\quad -0.1875\epsilon^{-1} \\ &\quad +\mathcal{O}(\epsilon) \end{aligned} \tag{D.106}$$

$$I_{\text{0h0w54}} = \int \frac{\mathrm{d}^D k_1}{i\pi^{D/2}} \frac{\mathrm{d}^D k_2}{i\pi^{D/2}} \frac{\exp(2\epsilon\gamma_E)(k_2 p_2)^2}{X_1 X_2 X_3 X_5 X_6} \tag{D.107}$$

$$\begin{aligned} &= (-1.192499\boldsymbol{0}27 + 1.358790\boldsymbol{6}\boldsymbol{0}64i)\epsilon^0 \\ &\quad +(0.216258241643\boldsymbol{9}7 + 0.589048622548\boldsymbol{0}8i)\epsilon^{-1} \\ &\quad +0.09375\epsilon^{-2} \\ &\quad +\mathcal{O}(\epsilon) \end{aligned} \tag{D.108}$$

$$I_{\text{0h0w55}} = \int \frac{\mathrm{d}^D k_1}{i\pi^{D/2}} \frac{\mathrm{d}^D k_2}{i\pi^{D/2}} \frac{\exp(2\epsilon\gamma_E)(k_1 p_1)^2}{X_1 (X_2 - M_Z^2) X_3 X_5 X_6} \tag{D.109}$$

$$\begin{aligned} &= (-0.663427\boldsymbol{7}354 + 0.535525\boldsymbol{9}520i)\epsilon^0 \\ &\quad +(-0.01811675835\boldsymbol{6}02 + 0.1963495408\boldsymbol{4}\boldsymbol{9}36i)\epsilon^{-1} \\ &\quad +\mathcal{O}(\epsilon) \end{aligned} \tag{D.110}$$

$$I_{\text{0h0w56}} = \int \frac{\mathrm{d}^D k_1}{i\pi^{D/2}} \frac{\mathrm{d}^D k_2}{i\pi^{D/2}} \frac{\exp(2\epsilon\gamma_E)(k_1 p_1)(k_2 p_2)}{X_1(X_2 - M_Z^2)X_3 X_5 X_6} \tag{D.111}$$

$$\begin{aligned} &= (-0.2398724\boldsymbol{6}16 + 0.3651432\boldsymbol{9}16i)\epsilon^0 \\ &\quad +(0.073476403817\boldsymbol{7}10 + 0.139434065891\boldsymbol{1}20i)\epsilon^{-1} \\ &\quad +\mathcal{O}(\epsilon) \end{aligned} \tag{D.112}$$

$$I_{\text{0h0w57}} = \int \frac{\mathrm{d}^D k_1}{i\pi^{D/2}} \frac{\mathrm{d}^D k_2}{i\pi^{D/2}} \frac{\exp(2\epsilon\gamma_E)(k_1 p_1)^2}{X_1 X_2 X_3(X_5 - M_Z^2)X_6} \tag{D.113}$$

$$\begin{aligned} &= (0.0625000\boldsymbol{0}00 - 0.3480469\boldsymbol{8}17i)\epsilon^0 \\ &\quad +\mathcal{O}(\epsilon) \end{aligned} \tag{D.114}$$

$$I_{\text{0h0w58}} = \int \frac{\mathrm{d}^D k_1}{i\pi^{D/2}} \frac{\mathrm{d}^D k_2}{i\pi^{D/2}} \frac{\exp(2\epsilon\gamma_E)(k_1 p_1)(k_2 p_2)}{X_1 X_2 X_3(X_5 - M_Z^2)X_6} \tag{D.115}$$

$$\begin{aligned} &= (0.2178888\boldsymbol{6}27 - 0.1351235\boldsymbol{2}31i)\epsilon^0 \\ &\quad +0.0625\epsilon^{-1} \\ &\quad +\mathcal{O}(\epsilon) \end{aligned} \tag{D.116}$$

$$I_{\text{0h0w59}} = \int \frac{\mathrm{d}^D k_1}{i\pi^{D/2}} \frac{\mathrm{d}^D k_2}{i\pi^{D/2}} \frac{\exp(2\epsilon\gamma_E)(k_1 p_1)^2}{X_1(X_2 - M_Z^2)X_3(X_5 - M_Z^2)X_6} \tag{D.117}$$

$$\begin{aligned} &= (-0.1140564\boldsymbol{3}47 - 0.2469790\boldsymbol{9}95i)\epsilon^0 \\ &\quad +\mathcal{O}(\epsilon) \end{aligned} \tag{D.118}$$

$$I_{\text{0h0w60}} = \int \frac{\mathrm{d}^D k_1}{i\pi^{D/2}} \frac{\mathrm{d}^D k_2}{i\pi^{D/2}} \frac{\exp(2\epsilon\gamma_E)(k_1 p_1)(k_2 p_2)}{X_1(X_2 - M_Z^2)X_3(X_5 - M_Z^2)X_6} \tag{D.119}$$

$$\begin{aligned} &= (-0.0573093\boldsymbol{7}59 - 0.1226773\boldsymbol{0}15i)\epsilon^0 \\ &\quad +0.0625\epsilon^{-1} \\ &\quad +\mathcal{O}(\epsilon) \end{aligned} \tag{D.120}$$

$$I_{\text{0h0w61}} = \int \frac{\mathrm{d}^D k_1}{i\pi^{D/2}} \frac{\mathrm{d}^D k_2}{i\pi^{D/2}} \frac{\exp(2\epsilon\gamma_E)(k_1 p_1)}{X_1 X_2 X_3(X_{11} - M_Z^2)X_9 X_6} \tag{D.121}$$

$$\begin{aligned} &= (-2.3844933\boldsymbol{7}42 - 0.8260816\boldsymbol{2}31i)\epsilon^0 \\ &\quad +0.645964097506\boldsymbol{3}0i\epsilon^{-1} \\ &\quad +0.2056167583560283\epsilon^{-2} \\ &\quad +\mathcal{O}(\epsilon) \end{aligned} \tag{D.122}$$

$$I_{\text{0h0w62}} = \int \frac{\mathrm{d}^D k_1}{i\pi^{D/2}} \frac{\mathrm{d}^D k_2}{i\pi^{D/2}} \frac{\exp(2\epsilon\gamma_E)(k_1 p_1)^2}{X_1 X_2 X_3 X_9 X_6} \tag{D.123}$$

$$\begin{aligned} &= (-1.3161659\boldsymbol{5}16 - 0.3833849\boldsymbol{6}34i)\epsilon^0 \\ &\quad +(-0.061017612036\boldsymbol{9}6 + 0.3101804907\boldsymbol{5}68i)\epsilon^{-1} \\ &\quad 0.04936675835602\boldsymbol{8}304\epsilon^{-2} \\ &\quad +\mathcal{O}(\epsilon) \end{aligned} \tag{D.124}$$

$$I_{\text{0h0w63}} = \int \frac{\mathrm{d}^D k_1}{i\pi^{D/2}} \frac{\mathrm{d}^D k_2}{i\pi^{D/2}} \frac{\exp(2\epsilon\gamma_E)(k_1 p_1)(k_2 p_1)}{X_1 X_2 X_3 X_9 X_6} \tag{D.125}$$

$$\begin{aligned} &= (-1.159448\boldsymbol{9}03 + 0.361386\boldsymbol{7}27i)\epsilon^0 \\ &\quad +(0.0575164832\boldsymbol{8}794 + 0.39269908169\boldsymbol{8}72i)\epsilon^{-1} \\ &\quad +0.0625\epsilon^{-2} \\ &\quad +\mathcal{O}(\epsilon) \end{aligned} \tag{D.126}$$

$$I_{\text{0h0w64}} = \int \frac{\mathrm{d}^D k_1}{i\pi^{D/2}} \frac{\mathrm{d}^D k_2}{i\pi^{D/2}} \frac{\exp(2\epsilon\gamma_E)(k_2 p_1)^2}{X_1 X_2 X_3 X_9 X_6} \tag{D.127}$$

$$\begin{aligned} &= (-1.192499\boldsymbol{0}27 + 1.358790\boldsymbol{6}\boldsymbol{0}64i)\epsilon^0 \\ &\quad +(0.2162582416\boldsymbol{4}397 + 0.589048622\boldsymbol{5}\boldsymbol{4}\boldsymbol{8}08i)\epsilon^{-1} \\ &\quad +0.09375\epsilon^{-2} \\ &\quad +\mathcal{O}(\epsilon) \end{aligned} \tag{D.128}$$

$$I_{\text{0h0w65}} = \int \frac{\mathrm{d}^D k_1}{i\pi^{D/2}} \frac{\mathrm{d}^D k_2}{i\pi^{D/2}} \frac{\exp(2\epsilon\gamma_E)(k_1 p_1)^2}{X_1 (X_2 - M_Z^2) X_3 X_9 X_6} \tag{D.129}$$

$$\begin{aligned} &= (-0.600903\boldsymbol{1}12 + 0.723292\boldsymbol{3}10i)\epsilon^0 \\ &\quad +(0.03522414631\boldsymbol{9}06 + 0.2355238748\boldsymbol{4}\boldsymbol{6}90i)\epsilon^{-1} \\ &\quad +\mathcal{O}(\epsilon) \end{aligned} \tag{D.130}$$

$$I_{\text{0h0w66}} = \int \frac{\mathrm{d}^D k_1}{i\pi^{D/2}} \frac{\mathrm{d}^D k_2}{i\pi^{D/2}} \frac{\exp(2\epsilon\gamma_E)(k_1 p_1)(k_2 p_1)}{X_1 (X_2 - M_Z^2) X_3 X_9 X_6} \tag{D.131}$$

$$\begin{aligned} &= (-0.308944\boldsymbol{3}\boldsymbol{7}97 + 0.426060\boldsymbol{6}\boldsymbol{7}25i)\epsilon^0 \\ &\quad +(0.05152359618\boldsymbol{2}89 + 0.16396081586\boldsymbol{3}15i)\epsilon^{-1} \\ &\quad +\mathcal{O}(\epsilon) \end{aligned} \tag{D.132}$$

$$I_{\text{0h0w67}} = \int \frac{\mathrm{d}^D k_1}{i\pi^{D/2}} \frac{\mathrm{d}^D k_2}{i\pi^{D/2}} \frac{\exp(2\epsilon\gamma_E)(k_1 p_1)^2}{X_1 X_2 X_3 (X_9 - M_Z^2) X_6} \tag{D.133}$$

$$\begin{aligned} &= (-0.010556\boldsymbol{5}\boldsymbol{8}83 - 0.408968\boldsymbol{9}\boldsymbol{8}68i)\epsilon^0 \\ &\quad +\mathcal{O}(\epsilon) \end{aligned} \tag{D.134}$$

$$I_{\text{0h0w68}} = \int \frac{\mathrm{d}^D k_1}{i\pi^{D/2}} \frac{\mathrm{d}^D k_2}{i\pi^{D/2}} \frac{\exp(2\epsilon\gamma_E)(k_1 p_1)(k_2 p_1)}{X_1 X_2 X_3 (X_9 - M_Z^2) X_6} \tag{D.135}$$

$$= (-0.0542417\boldsymbol{2}40 - 0.3016684\boldsymbol{6}02i)\epsilon^0 + \mathcal{O}(\epsilon) \tag{D.136}$$

$$I_{\text{0h0w69}} = \int \frac{\mathrm{d}^D k_1}{i\pi^{D/2}} \frac{\mathrm{d}^D k_2}{i\pi^{D/2}} \frac{\exp(2\epsilon\gamma_E)(k_1 p_1)^2}{X_1 (X_2 - M_Z^2) X_3 (X_9 - M_Z^2) X_6} \tag{D.137}$$

$$= (-0.1567553\boldsymbol{8}38 - 0.2566148\boldsymbol{7}31i)\epsilon^0 + \mathcal{O}(\epsilon) \tag{D.138}$$

$$I_{\text{0h0w70}} = \int \frac{\mathrm{d}^D k_1}{i\pi^{D/2}} \frac{\mathrm{d}^D k_2}{i\pi^{D/2}} \frac{\exp(2\epsilon\gamma_E)(k_1 p_1)(k_2 p_1)}{X_1 (X_2 - M_Z^2) X_3 (X_9 - M_Z^2) X_6} \tag{D.139}$$

$$= (-0.1236979\boldsymbol{7}03 - 0.1585187\boldsymbol{8}14i)\epsilon^0 + \mathcal{O}(\epsilon) \tag{D.140}$$

$$I_{\text{0h0w71}} = \int \frac{\mathrm{d}^D k_1}{i\pi^{D/2}} \frac{\mathrm{d}^D k_2}{i\pi^{D/2}} \frac{\exp(2\epsilon\gamma_E)(k1 * p1)^2}{X_1 X_2 (X_3 - M_Z^2) X_5 X_6} \tag{D.141}$$

$$= (0.0312499\boldsymbol{9}99 - 0.4908738\boldsymbol{5}21i)\epsilon^0 + \mathcal{O}(\epsilon) \tag{D.142}$$

$$I_{\text{0h0w72}} = \int \frac{\mathrm{d}^D k_1}{i\pi^{D/2}} \frac{\mathrm{d}^D k_2}{i\pi^{D/2}} \frac{\exp(2\epsilon\gamma_E)(k_1 p_1)(k_2 p_2)}{X_1 X_2 (X_3 - M_Z^2) X_5 X_6} \tag{D.143}$$

$$= (0.2759985\boldsymbol{2}90 - 0.4384309\boldsymbol{4}18i)\epsilon^0 + 0.0625i\epsilon^{-1} + \mathcal{O}(\epsilon) \tag{D.144}$$

$$I_{\text{0h0w73}} = \int \frac{\mathrm{d}^D k_1}{i\pi^{D/2}} \frac{\mathrm{d}^D k_2}{i\pi^{D/2}} \frac{\exp(2\epsilon\gamma_E)(k_2 p_2)^2}{X_1 X_2 (X_3 - M_Z^2) X_5 X_6} \tag{D.145}$$

$$= (-0.0819273\boldsymbol{4}38 - 0.9521707\boldsymbol{2}40i)\epsilon^0 + \mathcal{O}(\epsilon) \tag{D.146}$$

$$I_{\text{0h0w74}} = \int \frac{\mathrm{d}^D k_1}{i\pi^{D/2}} \frac{\mathrm{d}^D k_2}{i\pi^{D/2}} \frac{\exp(2\epsilon\gamma_E)(k_1 p_1)}{X_1 X_2 (X_3 - M_Z^2) X_{11} X_9 X_6} \tag{D.147}$$

$$= (4.2447364\boldsymbol{3}24 + 5.7825713\boldsymbol{6}46i)\epsilon^0 + (2.4041138063\boldsymbol{1}928 + 1.9378922925\boldsymbol{1}886i)\epsilon^{-1} + 0.6168502750680\boldsymbol{9}4\epsilon^{-2} + \mathcal{O}(\epsilon) \tag{D.148}$$

$$I_{\text{0h0w75}} = \int \frac{\mathrm{d}^D k_1}{i\pi^{D/2}} \frac{\mathrm{d}^D k_2}{i\pi^{D/2}} \frac{\exp(2\epsilon\gamma_E)(k_1 p_1)}{X_1 X_2 (X_3 - M_Z^2)(X_{11} - M_Z^2) X_9 X_6} \tag{D.149}$$

$$= (0.2841098\boldsymbol{5}01 - 1.5105492\boldsymbol{5}66i)\epsilon^0 + \mathcal{O}(\epsilon) \tag{D.150}$$

$$I_{\text{0h0w76}} = \int \frac{\mathrm{d}^D k_1}{i\pi^{D/2}} \frac{\mathrm{d}^D k_2}{i\pi^{D/2}} \frac{\exp(2\epsilon\gamma_E)(k_1 p_1)^2}{X_1 X_2 (X_3 - M_Z^2) X_9 X_6} \tag{D.151}$$

$$= (-0.1210591\boldsymbol{1}46 - 0.8082640\boldsymbol{9}34i)\epsilon^0 + \mathcal{O}(\epsilon) \tag{D.152}$$

$$I_{\text{0h0w77}} = \int \frac{\mathrm{d}^D k_1}{i\pi^{D/2}} \frac{\mathrm{d}^D k_2}{i\pi^{D/2}} \frac{\exp(2\epsilon\gamma_E)(k_1 p_1)(k_2 p_1)}{X_1 X_2 (X_3 - M_Z^2) X_9 X_6} \tag{D.153}$$

$$= (-0.0908563\boldsymbol{1}03 - 0.8149751\boldsymbol{4}38i)\epsilon^0 + \mathcal{O}(\epsilon) \tag{D.154}$$

$$I_{\text{0h0w78}} = \int \frac{\mathrm{d}^D k_1}{i\pi^{D/2}} \frac{\mathrm{d}^D k_2}{i\pi^{D/2}} \frac{\exp(2\epsilon\gamma_E)(k_2 p_1)^2}{X_1 X_2 (X_3 - M_Z^2) X_9 X_6} \tag{D.155}$$

$$= (-0.0819273\boldsymbol{4}38 - 0.9521707\boldsymbol{2}40i)\epsilon^0 + \mathcal{O}(\epsilon) \tag{D.156}$$

$$I_{\text{0h0w79}} = \int \frac{\mathrm{d}^D k_1}{i\pi^{D/2}} \frac{\mathrm{d}^D k_2}{i\pi^{D/2}} \frac{\exp(2\epsilon\gamma_E)(k_1 p_2)(k_2 p_1)}{(X_1 - M_Z^2) X_2 X_3 X_{12} X_9} \tag{D.157}$$

$$= (0.6035635\boldsymbol{8}78 - 0.5088333\boldsymbol{7}29i)\epsilon^0 + (0.013271338684\boldsymbol{4}84 - 0.139434065891\boldsymbol{2}0i)\epsilon^{-1} + \mathcal{O}(\epsilon) \tag{D.158}$$

$$I_{\text{0h0w80}} = \int \frac{\mathrm{d}^D k_1}{i\pi^{D/2}} \frac{\mathrm{d}^D k_2}{i\pi^{D/2}} \frac{\exp(2\epsilon\gamma_E)(k_2 p_1)^2}{(X_1 - M_Z^2) X_2 X_3 X_{12} X_9} \tag{D.159}$$

$$= (-0.3849670\boldsymbol{3}34 + 0.8835729\boldsymbol{3}38i)\epsilon^0 + (0.093749999\boldsymbol{9}99 + 0.1963495408\boldsymbol{9}36i)\epsilon^{-1} + \mathcal{O}(\epsilon) \tag{D.160}$$

$$I_{\text{0h0w81}} = \int \frac{\mathrm{d}^D k_1}{i\pi^{D/2}} \frac{\mathrm{d}^D k_2}{i\pi^{D/2}} \frac{\exp(2\epsilon\gamma_E)(k_1 p_2)(k_2 p_1)}{(X_1 - M_Z^2) X_2 X_3 X_{12} (X_9 - M_Z^2)} \tag{D.161}$$

$$= 0.1969446\boldsymbol{4}20\epsilon^0 + 0.0625\epsilon^{-1} + \mathcal{O}(\epsilon) \tag{D.162}$$

$$I_{\text{0h0w82}} = \int \frac{\mathrm{d}^D k_1}{i\pi^{D/2}} \frac{\mathrm{d}^D k_2}{i\pi^{D/2}} \frac{\exp(2\epsilon\gamma_E)(k_2 p_1)^2}{(X_1 - M_Z^2) X_2 X_3 X_{12} (X_9 - M_Z^2)} \tag{D.163}$$

$$= -0.1028083\boldsymbol{7}91\epsilon^0 + \mathcal{O}(\epsilon) \tag{D.164}$$

$$I_{\text{0h0w83}} = \int \frac{\mathrm{d}^D k_1}{i\pi^{D/2}} \frac{\mathrm{d}^D k_2}{i\pi^{D/2}} \frac{\exp(2\epsilon\gamma_E)(k_1 p_1)^2}{(X_1 - M_Z^2) X_2 X_3 X_5 X_8} \tag{D.165}$$

$$= (-0.3849670\boldsymbol{3}34 + 0.8835729\boldsymbol{3}38i)\epsilon^0 + (0.093749999999\boldsymbol{9}99 + 0.19634954084\boldsymbol{9}36i)\epsilon^{-1} + \mathcal{O}(\epsilon) \tag{D.166}$$

$$I_{\text{0h0w84}} = \int \frac{\mathrm{d}^D k_1}{i\pi^{D/2}} \frac{\mathrm{d}^D k_2}{i\pi^{D/2}} \frac{\exp(2\epsilon\gamma_E)(k_1 p_1)(k_2 p_2)}{(X_1 - M_Z^2) X_2 X_3 X_5 X_8} \tag{D.167}$$

$$= (0.6035635\boldsymbol{8}78 - 0.5088333\boldsymbol{7}29i)\epsilon^0 + (0.013271338684\boldsymbol{4}84 - 0.139434065891\boldsymbol{2}0i)\epsilon^{-1} + \mathcal{O}(\epsilon) \tag{D.168}$$

$$I_{\text{0h0w85}} = \int \frac{\mathrm{d}^D k_1}{i\pi^{D/2}} \frac{\mathrm{d}^D k_2}{i\pi^{D/2}} \frac{\exp(2\epsilon\gamma_E)(k_2 p_2)^2}{(X_1 - M_Z^2) X_2 X_3 X_5 X_8} \tag{D.169}$$

$$= (-0.3849670\boldsymbol{3}34 + 0.8835729\boldsymbol{3}38i)\epsilon^0 + (0.093749999999\boldsymbol{9}99 + 0.19634954084\boldsymbol{9}36i)\epsilon^{-1} + \mathcal{O}(\epsilon) \tag{D.170}$$

$$I_{\text{0h0w86}} = \int \frac{\mathrm{d}^D k_1}{i\pi^{D/2}} \frac{\mathrm{d}^D k_2}{i\pi^{D/2}} \frac{\exp(2\epsilon\gamma_E)(k_1 p_1)^2}{(X_1 - M_Z^2) X_2 X_3 (X_5 - M_Z^2) X_8} \tag{D.171}$$

$$= -0.3240501\boldsymbol{3}75\epsilon^0 + \mathcal{O}(\epsilon) \tag{D.172}$$

$$I_{\text{0h0w87}} = \int \frac{\mathrm{d}^D k_1}{i\pi^{D/2}} \frac{\mathrm{d}^D k_2}{i\pi^{D/2}} \frac{\exp(2\epsilon\gamma_E)(k_1 p_1)(k_2 p_2)}{(X_1 - M_Z^2) X_2 X_3 (X_5 - M_Z^2) X_8} \tag{D.173}$$

$$= 0.1969446\boldsymbol{4}20\epsilon^0 + 0.0625\epsilon^{-1} + \mathcal{O}(\epsilon) \tag{D.174}$$

$$I_{\text{0h0w88}} = \int \frac{\mathrm{d}^D k_1}{i\pi^{D/2}} \frac{\mathrm{d}^D k_2}{i\pi^{D/2}} \frac{\exp(2\epsilon\gamma_E)(k_2 p_2)^2}{(X_1 - M_Z^2) X_2 X_3 (X_5 - M_Z^2) X_8} \tag{D.175}$$

$$= -0.1028083\boldsymbol{7}91\epsilon^0 + \mathcal{O}(\epsilon) \tag{D.176}$$

$$I_{\text{0h0w89}} = \int \frac{\mathrm{d}^D k_1}{i\pi^{D/2}} \frac{\mathrm{d}^D k_2}{i\pi^{D/2}} \frac{\exp(2\epsilon\gamma_E)(k_2 p_2)^2}{X_1 X_2 X_3 (X_4 - M_Z^2) X_5 X_6} \tag{D.177}$$

$$= (0.7003660\boldsymbol{1}30 - 0.8928644\boldsymbol{8}49i)\epsilon^0 + (-0.180933379178\boldsymbol{0}1 - 0.42389570216\boldsymbol{5}12i)\epsilon^{-1} - 0.09375\epsilon^{-2} + \mathcal{O}(\epsilon) \tag{D.178}$$

$$I_{\text{0h0w90}} = \int \frac{\mathrm{d}^D k_1}{i\pi^{D/2}} \frac{\mathrm{d}^D k_2}{i\pi^{D/2}} \frac{\exp(2\epsilon\gamma_E)(k_2 p_1)^2}{X_1 X_2 X_3 (X_4 - M_Z^2) X_6 X_7} \tag{D.179}$$

$$+ \quad (-0.4393583\boldsymbol{1}39 - 0.3697802\boldsymbol{0}22i)\epsilon^0 + \mathcal{O}(\epsilon) \tag{D.180}$$

$$I_{\text{0h0w91}} = \int \frac{\mathrm{d}^D k_1}{i\pi^{D/2}} \frac{\mathrm{d}^D k_2}{i\pi^{D/2}} \frac{\exp(2\epsilon\gamma_E)(k_2 p_1)(k_2 p_1)}{X_1 (X_2 - M_Z^2) X_3 (X_4 - M_Z^2) X_6 X_7} \tag{D.181}$$

$$= (-0.3303953\boldsymbol{6}75 + 0.1208596\boldsymbol{4}01i)\epsilon^0 + \mathcal{O}(\epsilon) \tag{D.182}$$

$$I_{\text{0h0w92}} = \int \frac{\mathrm{d}^D k_1}{i\pi^{D/2}} \frac{\mathrm{d}^D k_2}{i\pi^{D/2}} \frac{\exp(2\epsilon\gamma_E)(k_2 p_2)^2}{X_1 X_2 (X_3 - M_Z^2)(X_4 - M_Z^2) X_5 X_6} \tag{D.183}$$

$$= (-0.1663502\boldsymbol{6}19 + 0.7538501\boldsymbol{0}03i)\epsilon^0 + \mathcal{O}(\epsilon) \tag{D.184}$$

$$I_{\text{0h0w93}} = \int \frac{\mathrm{d}^D k_1}{i\pi^{D/2}} \frac{\mathrm{d}^D k_2}{i\pi^{D/2}} \frac{\exp(2\epsilon\gamma_E)(k_2 p_1)^2}{X_1 X_2 X_3 (X_{10} - M_Z^2) X_9 X_6} \tag{D.185}$$

$$= (0.7003660\boldsymbol{1}30 - 0.8928644\boldsymbol{8}49i)\epsilon^0 + (-0.180933379178\boldsymbol{0}1 - 0.42389570216\boldsymbol{5}12i)\epsilon^{-1} - 0.09375\epsilon^{-2} + \mathcal{O}(\epsilon) \tag{D.186}$$

$$I_{\text{0h0w94}} = \int \frac{\mathrm{d}^D k_1}{i\pi^{D/2}} \frac{\mathrm{d}^D k_2}{i\pi^{D/2}} \frac{\exp(2\epsilon\gamma_E)(k_2 p_1)^2}{X_1 X_2 (X_3 - M_Z^2)(X_{10} - M_Z^2) X_9 X_6} \tag{D.187}$$

$$= (-0.1663502\boldsymbol{6}19 + 0.7538501\boldsymbol{0}03i)\epsilon^0 + \mathcal{O}(\epsilon) \tag{D.188}$$

$$I_{\text{0h0w95}} = \int \frac{\mathrm{d}^D k_1}{i\pi^{D/2}} \frac{\mathrm{d}^D k_2}{i\pi^{D/2}} \frac{\exp(2\epsilon\gamma_E)(k_1 p_1)^2}{X_1 X_2 X_3 (X_{11} - M_Z^2) X_9 X_6} \tag{D.189}$$

$$= (0.8915269\boldsymbol{0}41 + 0.4125160\boldsymbol{1}04i)\epsilon^0 + (0.043735822448\boldsymbol{8}89 - 0.1835479828\boldsymbol{6}\boldsymbol{1}72i)\epsilon^{-1} - 0.0584251375340424\boldsymbol{6}\epsilon^{-2} + \mathcal{O}(\epsilon) \tag{D.190}$$

$$I_{\text{0h0w96}} = \int \frac{\mathrm{d}^D k_1}{i\pi^{D/2}} \frac{\mathrm{d}^D k_2}{i\pi^{D/2}} \frac{\exp(2\epsilon\gamma_E)(k_1 p_1)^2}{X_1 X_2 (X_3 - M_Z^2) X_{11} X_9 X_6} \tag{D.191}$$

$$= (-3.2860060\boldsymbol{6}23 - 3.8178696\boldsymbol{8}83i)\epsilon^0 + (-1.456264177547\boldsymbol{7}99 - 0.9689461462\boldsymbol{6}\boldsymbol{0}32i)\epsilon^{-1} - 0.308425137534044\boldsymbol{8}\epsilon^{-2} + \mathcal{O}(\epsilon) \tag{D.192}$$

$$I_{\text{0h0w97}} = \int \frac{\mathrm{d}^D k_1}{i\pi^{D/2}} \frac{\mathrm{d}^D k_2}{i\pi^{D/2}} \frac{\exp(2\epsilon\gamma_E)(k_1 p_1)^2}{X_1 X_2 (X_3 - M_Z^2)(X_{11} - M_Z^2) X_9 X_6} \tag{D.193}$$

$$= (-0.092595\boldsymbol{9}581 + 0.565701\boldsymbol{8}\boldsymbol{6}6i)\epsilon^0 + \mathcal{O}(\epsilon) \tag{D.194}$$

$$I_{\text{0h0w98}} = \int \frac{\mathrm{d}^D k_1}{i\pi^{D/2}} \frac{\mathrm{d}^D k_2}{i\pi^{D/2}} \frac{\exp(2\epsilon\gamma_E)(k_1 p_1)^3}{X_1 X_2 X_3 (X_{11} - M_Z^2) X_9 X_6} \tag{D.195}$$

$$= (-0.352235\boldsymbol{6}\boldsymbol{3}73 - 0.178062\boldsymbol{6}\boldsymbol{6}86i)\epsilon^0 + (-0.02219162082\boldsymbol{2}02 + 0.06331625395\boldsymbol{1}84i)\epsilon^{-1} + 0.020154189589007\boldsymbol{0}75\epsilon^{-2} + \mathcal{O}(\epsilon) \tag{D.196}$$

$$I_{\text{0h0w99}} = \int \frac{\mathrm{d}^D k_1}{i\pi^{D/2}} \frac{\mathrm{d}^D k_2}{i\pi^{D/2}} \frac{\exp(2\epsilon\gamma_E)(k_1 p_1)^3}{X_1 X_2 (X_3 - M_Z^2) X_{11} X_9 X_6} \tag{D.197}$$

$$= (2.0897829\boldsymbol{0}64 + 2.2182394\boldsymbol{4}66i)\epsilon^0 + (0.815703589114\boldsymbol{4}17 + 0.484473073129\boldsymbol{9}80i)\epsilon^{-1} + 0.1542125687670224\epsilon^{-2} + \mathcal{O}(\epsilon) \tag{D.198}$$

$$I_{\text{0h0w100}} = \int \frac{\mathrm{d}^D k_1}{i\pi^{D/2}} \frac{\mathrm{d}^D k_2}{i\pi^{D/2}} \frac{\exp(2\epsilon\gamma_E)(k_1 p_1)^3}{X_1 X_2 (X_3 - M_Z^2)(X_{11} - M_Z^2) X_9 X_6} \tag{D.199}$$

$$= (0.0343825\boldsymbol{0}88 - 0.2304144\boldsymbol{9}76i)\epsilon^0 + \mathcal{O}(\epsilon) \tag{D.200}$$

D.2 0hxwxtxz

$$I_{\text{0hxwxtxz1}} = \int \frac{\mathrm{d}^D k_1}{i\pi^{D/2}} \frac{\mathrm{d}^D k_2}{i\pi^{D/2}} \frac{\exp(2\epsilon\gamma_E)}{X_1(X_2 - M_W^2)(X_3 - m_t^2)(X_4 - M_Z^2)(X_5 - M_W^2)X_6} \tag{D.201}$$

$$I_{\text{0hxwxtxz2}} = \int \frac{\mathrm{d}^D k_1}{i\pi^{D/2}} \frac{\mathrm{d}^D k_2}{i\pi^{D/2}} \frac{\exp(2\epsilon\gamma_E)}{X_1(X_2 - m_t^2)(X_3 - M_W^2)(X_4 - M_Z^2)(X_5 - m_t^2)X_6} \tag{D.202}$$

$$I_{\text{0hxwxtxz94}} = \int \frac{\mathrm{d}^D k_1}{i\pi^{D/2}} \frac{\mathrm{d}^D k_2}{i\pi^{D/2}} \frac{\exp(2\epsilon\gamma_E)(k_2 p_2)}{X_1(X_2 - M_W^2)(X_3 - m_t^2)(X_4 - M_Z^2)(X_5 - M_W^2)X_6} \tag{D.203}$$

$$I_{\text{0hxwxtxz96}} = \int \frac{\mathrm{d}^D k_1}{i\pi^{D/2}} \frac{\mathrm{d}^D k_2}{i\pi^{D/2}} \frac{\exp(2\epsilon\gamma_E)(k_2 p_2)}{X_1(X_2 - m_t^2)(X_3 - M_W^2)(X_4 - M_Z^2)(X_5 - m_t^2)X_6} \tag{D.204}$$

$$I_{\text{0hxwxtxz188}} = \int \frac{\mathrm{d}^D k_1}{i\pi^{D/2}} \frac{\mathrm{d}^D k_2}{i\pi^{D/2}} \frac{\exp(2\epsilon\gamma_E)(k_2 p_2)^2}{X_1(X_2 - M_W^2)(X_3 - m_t^2)(X_4 - M_Z^2)(X_5 - M_W^2)X_6} \tag{D.205}$$

$$I_{\text{0hxwxtxz190}} = \int \frac{\mathrm{d}^D k_1}{i\pi^{D/2}} \frac{\mathrm{d}^D k_2}{i\pi^{D/2}} \frac{\exp(2\epsilon\gamma_E)(k_2 p_2)^2}{X_1(X_2 - m_t^2)(X_3 - M_W^2)(X_4 - M_Z^2)(X_5 - m_t^2)X_6} \tag{D.206}$$

Table D.1: We have used the input parameters of Eq. (4.50). Chosen integrals of the integral class 0hxwxtxz. Coefficients in ϵ^0.

Integrals	**Methods**	**Results**	
0hxwxtxz1	MB - 8	0.175898**9**4	+0.708900**2**6 i
	MB - 8	0.175898**9**9	+0.708900**2**8 i
	SD - 90	0.17589**5**1	+0.70889**7**8 i
	SD - 15	0.1757**8**5	+0.7089**7**9 i
0hxwxtxz2	MB - 8	0.129603**0**1	+0.44037843**0** i
	MB - 8	0.129603**9**4	+0.44037843**3** i
	SD - 90	0.12960**6**9	+0.4403801**6** i
	SD - 15	0.12956**0**5	+0.44044**0**1 i
0hxwxtxz94	MB - 8	-0.0601885**2**2	-0.2072560**6**1 i
	MB - 8	-0.0601885**0**8	-0.2072560**6**2 i
	SD - 90	-0.0601882**2**1	-0.2072566**3**5 i
	SD - 15	-0.0601**6**2	-0.2072**8**8 i
0hxwxtxz96	MB - 8	-0.0348955**6**6	-0.1010186**9**8 i
	MB - 8	-0.0348955**3**4	-0.1010186**6**5 i
	SD - 540	-0.034895529**3**	-0.101018681**3** i
	SD - 90	-0.034895**4**29	-0.10101882**6** i
	SD - 15	-0.03489**5**7	-0.1010253**0** i
0hxwxtxz188	MB - 8	0.022761**4**5	+0.0702365**9**7 i
	MB - 8	0.022761**4**8	+0.0702365**9**8 i
	SD - 90	0.0227608**8**8	+0.0702367**2**6 i
	SD - 15	0.02274**9**0	+0.07025**0**1 i
0hxwxtxz190	MB - 8	0.0114355**2**4	+0.0296312**1**5 i
	MB - 8	0.0114355**2**0	+0.0296312**1**3 i
	SD - 90	0.011435503**3**	+0.029631247**7**0 i
	SD - 15	0.01143**4**3	+0.02963**2**7 i

D.3 soft

D.3.1 Three-dimensional Mellin-Barnes integral representations

$$I_{\text{soft1}} = \int \frac{\mathrm{d}^D k_1}{i\pi^{D/2}} \frac{\mathrm{d}^D k_2}{i\pi^{D/2}} \frac{\exp(2\epsilon\gamma_E)}{X_1(X_2 - M_W^2)(X_3 - m_t^2)X_4(-M_W^2 + X_5)X_6} \tag{D.207}$$

$$I_{\text{soft2}} = \int \frac{\mathrm{d}^D k_1}{i\pi^{D/2}} \frac{\mathrm{d}^D k_2}{i\pi^{D/2}} \frac{\exp(2\epsilon\gamma_E)}{X_1(X_2 - m_t^2)(X_3 - M_W^2)X_4(-m_t^2 + X_5)X_6} \tag{D.208}$$

$$I_{\text{soft5}} = \int \frac{\mathrm{d}^D k_1}{i\pi^{D/2}} \frac{\mathrm{d}^D k_2}{i\pi^{D/2}} \frac{\exp(2\epsilon\gamma_E) k_2 p_2}{X_1(X_2 - M_W^2)(X_3 - m_t^2)X_4(-M_W^2 + X_5)X_6} \tag{D.209}$$

$$I_{\text{soft7}} = \int \frac{\mathrm{d}^D k_1}{i\pi^{D/2}} \frac{\mathrm{d}^D k_2}{i\pi^{D/2}} \frac{\exp(2\epsilon\gamma_E) k_2 p_2}{X_1(X_2 - m_t^2)(X_3 - M_W^2)X_4(-m_t^2 + X_5)X_6} \tag{D.210}$$

D.3.2 Four-dimensional Mellin-Barnes integral representations

$$I_{\text{soft6}} = \int \frac{\mathrm{d}^D k_1}{i\pi^{D/2}} \frac{\mathrm{d}^D k_2}{i\pi^{D/2}} \frac{\exp(2\epsilon\gamma_E) k_2 p_1}{X_1(X_2 - M_W^2)(X_3 - m_t^2)X_4 X_6(-m_t^2 + X_7)} \tag{D.211}$$

$$I_{\text{soft8}} = \int \frac{\mathrm{d}^D k_1}{i\pi^{D/2}} \frac{\mathrm{d}^D k_2}{i\pi^{D/2}} \frac{\exp(2\epsilon\gamma_E) k_2 p_1}{X_1(X_2 - m_t^2)(X_3 - M_W^2)X_4 X_6(-M_W^2 + X_7)} \tag{D.212}$$

$$I_{\text{soft11}} = \int \frac{\mathrm{d}^D k_1}{i\pi^{D/2}} \frac{\mathrm{d}^D k_2}{i\pi^{D/2}} \frac{\exp(2\epsilon\gamma_E) (k_2 p_1)^2}{X_1(X_2 - M_W^2)(X_3 - m_t^2)X_4 X_6(-m_t^2 + X_7)} \tag{D.213}$$

$$I_{\text{soft12}} = \int \frac{\mathrm{d}^D k_1}{i\pi^{D/2}} \frac{\mathrm{d}^D k_2}{i\pi^{D/2}} \frac{\exp(2\epsilon\gamma_E) (k_2 p_1)^2}{X_1(X_2 - m_t^2)(X_3 - M_W^2)X_4 X_6(-M_W^2 + X_7)} \tag{D.214}$$

$$I_{\text{soft13}} = \int \frac{\mathrm{d}^D k_1}{i\pi^{D/2}} \frac{\mathrm{d}^D k_2}{i\pi^{D/2}} \frac{\exp(2\epsilon\gamma_E)}{X_1(X_2 - M_W^2)(X_3 - m_t^2)X_4 X_6(-m_t^2 + X_7)} \tag{D.215}$$

$$I_{\text{soft14}} = \int \frac{\mathrm{d}^D k_1}{i\pi^{D/2}} \frac{\mathrm{d}^D k_2}{i\pi^{D/2}} \frac{\exp(2\epsilon\gamma_E)}{X_1(X_2 - m_t^2)(X_3 - M_W^2)X_4 X_6(-M_W^2 + X_7)} \tag{D.216}$$

Table D.2: We have used the input parameters of Eq. (4.50). Chosen integrals of the integral class soft. Coefficients in ϵ^0.

Integrals	**Methods**	**Results**	
soft1	MB - 11	1.5424526284***0***2	+0.2473136618***8***9i
	MB - 11	1.542452628***5***8	+0.2473136619***0***8i
	SD - 90	1.5421***9***7	+0.2472***4***1 i
	SD - 15	1.53***4***6	+0.24***6***5 i
soft2	MB - 11	0.8961247329***0***6	+0.5255129640***1***4i
	MB - 11	0.8961247329***3***6	+0.5255129640***3***5i
	SD - 90	0.89609***8***6	+0.52548***2***4 i
	SD - 15	0.895***5***8	+0.524***7***0 i
soft5	MB - 11	-0.4769530994***7***6	+0.1441368581***2***5 i
	MB - 11	-0.4769530994***7***4	+0.1441368581***2***8 i
	SD - 90	-0.4768***6***9	+0.1441***6***6 i
	SD - 15	-0.473***3***4	+0.144***2***8 i
soft6	MB - 8	-0.19283106***4***	-0.22762897***8*** i
	MB - 8	-0.19283105***3***	-0.22762897***8*** i
	SD - 90	-0.1928287***8***	-0.2276272***8*** i
	SD - 15	-0.1927***8***6	-0.2275***5***7 i
soft7	MB - 11	-0.2282318675***1***1	-0.0882479456***9***1i
	MB - 11	-0.2282318675***5***1	-0.0882479457***3***9i
	SD - 90	-0.2282265***3***	-0.088245***9***6 i
	SD - 15	-0.2281***6***2	-0.0882***0***9 i

Table D.3: We have used the input parameters of Eq. (4.50). Chosen integrals of the integral class soft. Coefficients in ϵ^0.

Integrals	**Methods**	**Results**	
soft8	MB - 8	-0.40729354182	-0.15276147502 i
	MB - 8	-0.40729354132	-0.15276146850 i
	SD - 90	-0.40731353989	-0.15273227134 i
	SD - 15	-0.40834293929	-0.15187297075 i
soft11	MB - 8	0.05105975520	+0.07155072319 i
	MB - 8	0.05105975036	+0.07155071547 i
	SD - 90	0.05105952769	+0.07155053644 i
	SD - 15	0.05105374026	+0.07154136822 i
soft12	MB - 8	0.11906871873	+0.05485236718 i
	MB - 8	0.11906872743	+0.05485236763 i
	SD - 90	0.11907480305	+0.05484490815 i
	SD - 15	0.11943505792	+0.05471644724 i
soft13	MB - 8	0.93453624332	+0.54089756531 i
	MB - 8	0.93453624300	+0.54089756809 i
	SD - 90	0.93449867498	+0.54086830186 i
	SD - 15	0.93427180511	+0.54054950796 i
soft14	MB - 8	1.78963923034	+0.21542764297 i
	MB - 8	1.78963923757	+0.21542764381 i
	SD - 90	1.78966901404	+0.21528457636 i
	SD - 15	1.79535854914	+0.21106548471 i

Table D.4: We have used the input parameters of Eq. (4.50). Chosen integrals of the integral class soft. Coefficients in ϵ^{-1}.

Integrals	**Methods**	**Results**	
soft1	MB - 10	0.1232496327**7**2	-1.0618599225**5**9 i
	SD - 90	0.123250**3**567	-1.061860**2**8805 i
soft2	MB - 10	0.180783316**2**9	-0.6420853985**5**1 i
	SD - 90	0.180783**6**645	-0.642085**5**700 i
soft5	MB - 10	0.030658947**9**9	+0.399220013**4**6 i
	SD - 90	0.030658**6**896	+0.39922**0**07314 i
soft6	MB - 10	-0.0758103636**6**5	+0.097633290**6**7 i
	MB - 10	-0.0758103636**6**5	+0.097633290**6**5 i
	SD - 90	-0.075810358**3**	+0.097633293**3**58 i
soft7	MB - 10	-0.0315124890**3**	+0.189332751**4**2 i
	SD - 90	-0.031512481**6**	+0.189332716**9**6 i
soft8	MB - 10	-0.056775366**4**4	+0.225528015**5**7 i
	MB - 10	-0.056775366**4**9	+0.225528015**5**4 i
	SD - 90	-0.05677568**3**8	+0.2255283**4**353 i
soft11	MB - 10	0.023587409**0**1	-0.022864720**5**6 i
	MB - 10	0.023587408**9**1	-0.022864720**7**7 i
	SD - 90	0.023587408**7**3	-0.022864722**2**4 i
soft12	MB - 10	0.019638671**9**1	-0.060933020**1**1 i
	MB - 10	0.019638671**7**4	-0.060933020**0**5 i
	SD - 90	0.019638**1**039	-0.060933**1**169 i
soft13	MB - 10	0.190113725**6**7	-0.658315756**3**5 i
	MB - 10	0.190113725**6**6	-0.658315756**3**4 i
	SD - 90	0.19011371**5**1	-0.65831575**5**251 i
soft14	MB - 10	0.106022189**8**8	-1.178394541**4**0 i
	MB - 10	0.106022189**4**3	-1.178394541**3**7 i
	SD - 90	0.10602**3**681	-1.17839**0**2291 i

Table D.5: We have used the input parameters of Eq. (4.50). Chosen integrals of the integral class soft. Coefficients in ϵ^{-2}.

Integrals	Methods	Results
soft1	MB - 16	-0.3380005111031239
	SD - 90	-0.338000511
soft2	MB - 16	-0.20438213012131033
	SD - 90	-0.204382131
soft5	MB - 16	0.12707567704860677
	SD - 90	0.1270756775
soft6	MB - 16	0.03107764164424488
	SD - 90	0.0310776416445
soft7	MB - 16	0.06026648655769999
	SD - 90	0.0602664865
soft8	MB - 16	0.07178779696731100
	SD - 90	0.0717877969
soft11	MB - 16	-0.00727806664769188
	SD - 90	-0.007278066645
soft12	MB - 16	-0.01939558267818188
	SD - 90	-0.0193955826775
soft13	MB - 16	-0.20954841348083700
	SD - 90	-0.209548413
soft14	MB - 16	-0.37509463235541333
	SD - 90	-0.375094632

Bibliography

[1] SLD Electroweak Group, DELPHI, ALEPH, SLD, SLD Heavy Flavour Group, OPAL, LEP Electroweak Working Group, L3 Collaboration, S. Schael et al., *Precision electroweak measurements on the Z resonance*, Phys. Rept. **427** (2006) 257–454, arXiv:hep-ex/0509008 [hep-ex].

[2] A. A. Akhundov, D. Yu. Bardin, and T. Riemann, *Electroweak One Loop Corrections to the Decay of the Neutral Vector Boson*, Nucl. Phys. **B276** (1986) 1–13.

[3] W. Beenakker and W. Hollik, *The Width of the Z Boson*, Z. Phys. **C40** (1988) 141.

[4] K. G. Chetyrkin, J. H. Kuhn, and M. Steinhauser, *QCD corrections from top quark to relations between electroweak parameters to order* α_s^2, Phys. Rev. Lett. **75** (1995) 3394–3397, arXiv:hep-ph/9504413 [hep-ph].

[5] M. Awramik, M. Czakon, and A. Freitas, *Electroweak two-loop corrections to the effective weak mixing angle*, JHEP **11** (2006) 048, arXiv:hep-ph/0608099 [hep-ph].

[6] M. Awramik, M. Czakon, A. Freitas, and G. Weiglein, *Towards better constraints on the Higgs boson mass: Two-loop fermionic corrections to* $\sin^2\theta_{\rm eff}^{\rm lept}$, in *Linear colliders. Proceedings, International Conference, LCWS 2004, Paris, France, April 19-23, 2004*. 2004. arXiv:hep-ph/0409142 [hep-ph]. http://lss.fnal.gov/cgi-bin/find_paper.pl?conf-04-199-T.

[7] M. Awramik, M. Czakon, and A. Freitas, *Bosonic corrections to the effective weak mixing angle at O(α^2)*, Phys. Lett. **B642** (2006) 563–566, arXiv:hep-ph/0605339 [hep-ph].

[8] W. Hollik, U. Meier, and S. Uccirati, *The Effective electroweak mixing angle* $\sin^2\theta_{\rm eff}$ *with two-loop fermionic contributions*, Nucl. Phys. **B731** (2005) 213–224, arXiv:hep-ph/0507158 [hep-ph].

[9] W. Hollik, U. Meier, and S. Uccirati, *The Effective electroweak mixing angle* $\sin^2\theta_{\rm eff}$ *with two-loop bosonic contributions*, Nucl. Phys. **B765** (2007) 154–165, arXiv:hep-ph/0610312 [hep-ph].

[10] K. G. Chetyrkin, J. H. Kuhn, and M. Steinhauser, *Three loop polarization function and O(α^2) corrections to the production of heavy quarks*, Nucl. Phys. **B482** (1996) 213–240, arXiv:hep-ph/9606230 [hep-ph].

[11] J. J. van der Bij, K. G. Chetyrkin, M. Faisst, G. Jikia, and T. Seidensticker, *Three loop leading top mass contributions to the rho parameter*, Phys. Lett. **B498** (2001) 156–162, arXiv:hep-ph/0011373 [hep-ph].

[12] M. Faisst, J. H. Kuhn, T. Seidensticker, and O. Veretin, *Three loop top quark contributions to the rho parameter*, Nucl. Phys. **B665** (2003) 649–662, arXiv:hep-ph/0302275 [hep-ph].

[13] Y. Schroder and M. Steinhauser, *Four-loop singlet contribution to the rho parameter*, Phys. Lett. **B622** (2005) 124–130, arXiv:hep-ph/0504055 [hep-ph].

[14] K. G. Chetyrkin, M. Faisst, J. H. Kuhn, P. Maierhofer, and C. Sturm, *Four-Loop QCD Corrections to the Rho Parameter*, Phys. Rev. Lett. **97** (2006) 102003, arXiv:hep-ph/0605201 [hep-ph].

[15] R. Boughezal and M. Czakon, *Single scale tadpoles and O($G_F m_t^2 \alpha_s^3$) corrections to the ρ parameter*, Nucl. Phys. **B755** (2006) 221–238, arXiv:hep-ph/0606232 [hep-ph].

[16] M. Awramik, M. Czakon, A. Freitas, and B. A. Kniehl, *Two-loop electroweak fermionic corrections to* $\sin^2\theta^{b\bar{b}}_{\rm eff}$, Nucl. Phys. **B813** (2009) 174–187, arXiv:0811.1364 [hep-ph].

[17] I. Dubovyk, A. Freitas, J. Gluza, T. Riemann, and J. Usovitsch, *The two-loop electroweak bosonic corrections to* $\sin^2\theta^{b}_{\rm eff}$, Phys. Lett. **B762** (2016) 184–189, arXiv:1607.08375 [hep-ph].

[18] H. Baer, T. Barklow, K. Fujii, Y. Gao, A. Hoang, S. Kanemura, J. List, H. E. Logan, A. Nomerotski, M. Perelstein, et al., *The International Linear Collider Technical Design Report - Volume 2: Physics*, arXiv:1306.6352 [hep-ph].

[19] CEPC-SPPC Study Group, *CEPC-SPPC Preliminary Conceptual Design Report. 1. Physics and Detector*, (2015) .

[20] TLEP Design Study Working Group Collaboration, M. Bicer et al., *First Look at the Physics Case of TLEP*, JHEP **01** (2014) 164, arXiv:1308.6176 [hep-ex].

[21] T. Binoth and G. Heinrich, *An automatized algorithm to compute infrared divergent multiloop integrals*, Nucl. Phys. **B585** (2000) 741–759, arXiv:hep-ph/0004013 [hep-ph].

[22] T. Binoth and G. Heinrich, *Numerical evaluation of multiloop integrals by sector decomposition*, Nucl. Phys. **B680** (2004) 375–388, arXiv:hep-ph/0305234 [hep-ph].

[23] V. A. Smirnov, *Analytical result for dimensionally regularized massless on shell double box*, Phys. Lett. **B460** (1999) 397–404, arXiv:hep-ph/9905323 [hep-ph].

[24] J. B. Tausk, *Nonplanar massless two loop Feynman diagrams with four on-shell legs*, Phys. Lett. **B469** (1999) 225–234, arXiv:hep-ph/9909506 [hep-ph].

[25] G. Heinrich and V. A. Smirnov, *Analytical evaluation of dimensionally regularized massive on-shell double boxes*, Phys. Lett. **B598** (2004) 55–66, arXiv:hep-ph/0406053 [hep-ph].

[26] M. Czakon, *Automatized analytic continuation of Mellin-Barnes integrals*, Comput. Phys. Commun. **175** (2006) 559–571, arXiv:hep-ph/0511200 [hep-ph].

[27] C. Anastasiou and A. Daleo, *Numerical evaluation of loop integrals*, JHEP **10** (2006) 031, arXiv:hep-ph/0511176 [hep-ph].

[28] S. Borowka, J. Carter, and G. Heinrich, *Numerical Evaluation of Multi-Loop Integrals for Arbitrary Kinematics with SecDec 2.0*, Comput. Phys. Commun. **184** (2013) 396–408, arXiv:1204.4152 [hep-ph].

[29] A. Freitas and Y.-C. Huang, *On the Numerical Evaluation of Loop Integrals With Mellin-Barnes Representations*, JHEP **04** (2010) 074, arXiv:1001.3243 [hep-ph].

[30] S. L. Glashow, *Partial Symmetries of Weak Interactions*, Nucl. Phys. **22** (1961) 579–588.

[31] A. Salam, *Weak and Electromagnetic Interactions*, Conf. Proc. **C680519** (1968) 367–377.

[32] S. Weinberg, *A Model of Leptons*, Phys. Rev. Lett. **19** (1967) 1264–1266.

[33] P. W. Higgs, *Broken symmetries, massless particles and gauge fields*, Phys. Lett. **12** (1964) 132–133.

[34] P. W. Higgs, *Broken Symmetries and the Masses of Gauge Bosons*, Phys. Rev. Lett. **13** (1964) 508–509.

[35] F. Englert and R. Brout, *Broken Symmetry and the Mass of Gauge Vector Mesons*, Phys. Rev. Lett. **13** (1964) 321–323.

[36] P. W. Higgs, *Spontaneous Symmetry Breakdown without Massless Bosons*, Phys. Rev. **145** (1966) 1156–1163.

[37] T. W. B. Kibble, *Symmetry breaking in nonAbelian gauge theories*, Phys. Rev. **155** (1967) 1554–1561.

[38] M. Bohm, A. Denner, and H. Joos, *Gauge theories of the strong and electroweak interaction*, Stuttgart, Germany: Teubner 784 p (2001) .

[39] F. J. Dyson, *The S matrix in quantum electrodynamics*, Phys. Rev. **75** (1949) 1736–1755.

[40] D. Yu. Bardin, A. Leike, T. Riemann, and M. Sachwitz, *Energy Dependent Width Effects in e+ e- Annihilation Near the Z Boson Pole*, Phys. Lett. **B206** (1988) 539–542.

[41] D. Yu. Bardin, C. Burdik, P. C. Khristova, and T. Riemann, *Electroweak radiative corrections to deep inelastic scattering at HERA*, Z. Phys. **C42** (1989) 679.

[42] D. Yu. Bardin, M. S. Bilenky, T. Riemann, M. Sachwitz, and H. Vogt, *Dizet: A Program Package for the Calculation of Electroweak One Loop Corrections for the Process e+ e- $\to$ f+ f- Around the Z^0 Peak*, Comput. Phys. Commun. **59** (1990) 303–312.

[43] D. Yu. Bardin et al., *ZFITTER: An Analytical program for fermion pair production in e+ e- annihilation*, arXiv:hep-ph/9412201 [hep-ph]. Report number: CERN-TH-6443-92.

[44] D. Yu. Bardin, P. Christova, M. Jack, L. Kalinovskaya, A. Olchevski, S. Riemann, and T. Riemann, *ZFITTER v.6.21: A Semianalytical program for fermion pair production in e+ e- annihilation*, Comput. Phys. Commun. **133** (2001) 229–395, arXiv:hep-ph/9908433 [hep-ph].

[45] A. B. Arbuzov, M. Awramik, M. Czakon, A. Freitas, M. W. Grunewald, K. Monig, S. Riemann, and T. Riemann, *ZFITTER: A Semi-analytical program for fermion pair production in e+ e- annihilation, from version 6.21 to version 6.42*, Comput. Phys. Commun. **174** (2006) 728–758, arXiv:hep-ph/0507146 [hep-ph].

[46] A. Akhundov, A. Arbuzov, S. Riemann, and T. Riemann, *The ZFITTER project*, Phys. Part. Nucl. **45** no. 3, (2014) 529–549, arXiv:1302.1395 [hep-ph].

[47] A. Freitas, *Higher-order electroweak corrections to the partial widths and branching ratios of the Z boson*, JHEP **04** (2014) 070, arXiv:1401.2447 [hep-ph].

[48] R. G. Stuart, *Gauge invariance, analyticity and physical observables at the Z^0 resonance*, Phys. Lett. **B262** (1991) 113–119.

[49] H. G. J. Veltman, *Mass and width of unstable gauge bosons*, Z. Phys. **C62** (1994) 35–52.

[50] A. Freitas, *Fermionische Zwei-Schleifen-Beiträge zum Myon-Zerfall*, Diplomarbeit, Universitat Karlsruhe, Karlsruhe, 1999. https://www.itp.kit.edu/publications/diploma.

[51] A. Leike, T. Riemann, and J. Rose, *S matrix approach to the Z line shape*, Phys. Lett. **B273** (1991) 513–518, arXiv:hep-ph/9508390 [hep-ph].

[52] T. Riemann, *Cross-section asymmetries around the Z peak*, Phys. Lett. **B293** (1992) 451–456, arXiv:hep-ph/9506382 [hep-ph].

[53] S. Kirsch and T. Riemann, *SMATASY: A program for the model independent description of the Z resonance*, Comput. Phys. Commun. **88** (1995) 89–108, arXiv:hep-ph/9408365 [hep-ph].

[54] P. Gambino and P. A. Grassi, *The Nielsen identities of the SM and the definition of mass*, Phys. Rev. **D62** (2000) 076002, arXiv:hep-ph/9907254 [hep-ph].

[55] A. Freitas, W. Hollik, W. Walter, and G. Weiglein, *Complete fermionic two loop results for the $M_{\rm W}$ - $M_{\rm Z}$ interdependence*, Phys. Lett. **B495** (2000) 338–346, arXiv:hep-ph/0007091 [hep-ph]. [Erratum: Phys. Lett.B570,no.3-4,265(2003)].

[56] A. Freitas, W. Hollik, W. Walter, and G. Weiglein, *Electroweak two loop corrections to the $M_W - M_Z$ mass correlation in the standard model*, Nucl. Phys. **B632** (2002) 189–218, arXiv:hep-ph/0202131 [hep-ph]. [Erratum: Nucl. Phys.B666,305(2003)].

[57] M. Awramik and M. Czakon, *Complete two loop electroweak contributions to the muon lifetime in the standard model*, Physics Letters B **568** no. 1, (2003) 48 – 54.

[58] M. Awramik and M. Czakon, *Complete two loop bosonic contributions to the muon lifetime in the standard model*, Phys. Rev. Lett. **89** (2002) 241801, arXiv:hep-ph/0208113 [hep-ph].

[59] A. Onishchenko and O. Veretin, *Two loop bosonic electroweak corrections to the muon lifetime and $M_{\rm Z}$ - $M_{\rm W}$ interdependence*, Phys. Lett. **B551** (2003) 111–114, arXiv:hep-ph/0209010 [hep-ph].

[60] M. Awramik, M. Czakon, A. Onishchenko, and O. Veretin, *Bosonic corrections to Δr at the two loop level*, Phys. Rev. **D68** (2003) 053004, arXiv:hep-ph/0209084 [hep-ph].

[61] F. Jegerlehner, M. Yu. Kalmykov, and O. Veretin, *MS versus pole masses of gauge bosons: Electroweak bosonic two loop corrections*, Nucl. Phys. **B641** (2002) 285–326, arXiv:hep-ph/0105304 [hep-ph].

[62] F. Jegerlehner, M. Yu. Kalmykov, and O. Veretin, *MS-bar versus pole masses of gauge bosons. 2. Two loop electroweak fermion corrections*, Nucl. Phys. **B658** (2003) 49–112, arXiv:hep-ph/0212319 [hep-ph].

[63] Particle Data Group Collaboration, K. A. Olive et al., *Review of Particle Physics*, Chin. Phys. **C38** (2014) 090001.

[64] A. Freitas and Y.-C. Huang, *Electroweak two-loop corrections to $sin^2\theta^{b\bar{b}}_{eff}$ and R_b using numerical Mellin-Barnes integrals*, JHEP **08** (2012) 050, arXiv:1205.0299 [hep-ph]. [Erratum: JHEP10,044(2013)].

[65] F. V. Tkachov, *A Theorem on Analytical Calculability of Four Loop Renormalization Group Functions*, Phys. Lett. **B100** (1981) 65–68.

[66] K. G. Chetyrkin and F. V. Tkachov, *Integration by Parts: The Algorithm to Calculate beta Functions in 4 Loops*, Nucl. Phys. **B192** (1981) 159–204.

[67] S. Weinzierl, *The Art of computing loop integrals*, in *Universality and renormalization: From stochastic evolution to renormalization of quantum fields. Proceedings, Workshop on 'Percolation, SLE and related topics', Toronto, Canada, September 20-24, 2005, and Workshop on 'Renormalization and universality in mathematical physics', Toronto, Canada, October 18-22, 2005*, pp. 345–395. 2006. arXiv:hep-ph/0604068 [hep-ph].

[68] C. Bogner and S. Weinzierl, *Feynman graph polynomials*, Int. J. Mod. Phys. **A25** (2010) 2585–2618, arXiv:1002.3458 [hep-ph].

[69] R. N. Lee, *LiteRed 1.4: a powerful tool for reduction of multiloop integrals*, J. Phys. Conf. Ser. **523** (2014) 012059, arXiv:1310.1145 [hep-ph].

[70] S. Borowka, G. Heinrich, S. P. Jones, M. Kerner, J. Schlenk, and T. Zirke, *SecDec-3.0: numerical evaluation of multi-scale integrals beyond one loop*, Comput. Phys. Commun. **196** (2015) 470–491, arXiv:1502.06595 [hep-ph].

[71] G. Passarino, *An Approach toward the numerical evaluation of multiloop Feynman diagrams*, Nucl. Phys. **B619** (2001) 257–312, arXiv:hep-ph/0108252 [hep-ph].

[72] H. Cheng and T. T. Wu, *Expanding protons: Scattering at high-energies*, CAMBRIDGE, USA: MIT-PR. 285p (1987) .

[73] K. S. Bjoerkevoll, P. Osland, and G. Faeldt, *Two loop ladder diagram contributions to Bhabha scattering. 2: Asymptotic results for high-energies*, Nucl. Phys. **B386** (1992) 303–342.

[74] V. A. Smirnov, *Feynman integral calculus*, Berlin, Germany: Springer 283 p (2006) .

[75] A. I. Davydychev, *A Simple formula for reducing Feynman diagrams to scalar integrals*, Phys. Lett. **B263** (1991) 107–111.

[76] K. Hepp, *Proof of the Bogolyubov-Parasiuk theorem on renormalization*, Commun. Math. Phys. **2** (1966) 301–326. http://www.projecteuclid.org/euclid.cmp/1103815087.

[77] T. Binoth and G. Heinrich, *Numerical evaluation of phase space integrals by sector decomposition*, Nucl. Phys. **B693** (2004) 134–148, arXiv:hep-ph/0402265 [hep-ph].

[78] A. Denner and S. Pozzorini, *An Algorithm for the high-energy expansion of multi-loop diagrams to next-to-leading logarithmic accuracy*, Nucl. Phys. **B717** (2005) 48–85, arXiv:hep-ph/0408068 [hep-ph].

[79] G. Heinrich, *Sector Decomposition*, Int. J. Mod. Phys. **A23** (2008) 1457–1486, arXiv:0803.4177 [hep-ph].

[80] C. Bogner and S. Weinzierl, *Resolution of singularities for multi-loop integrals*, Comput. Phys. Commun. **178** (2008) 596–610, arXiv:0709.4092 [hep-ph].

[81] A. V. Smirnov and M. N. Tentyukov, *Feynman Integral Evaluation by a Sector decomposiTion Approach (FIESTA)*, Comput. Phys. Commun. **180** (2009) 735–746, arXiv:0807.4129 [hep-ph].

[82] T. Kaneko and T. Ueda, *A Geometric method of sector decomposition*, Comput. Phys. Commun. **181** (2010) 1352–1361, arXiv:0908.2897 [hep-ph].

[83] A. V. Smirnov, *FIESTA 3: cluster-parallelizable multiloop numerical calculations in physical regions*, Comput. Phys. Commun. **185** (2014) 2090–2100, arXiv:1312.3186 [hep-ph].

[84] P. Marquard, A. V. Smirnov, V. A. Smirnov, M. Steinhauser, and D. Wellmann, $\overline{\text{MS}}$*-on-shell quark mass relation up to four loops in QCD and a general* $SU(N)$ *gauge group*, Phys. Rev. **D94** no. 7, (2016) 074025, arXiv:1606.06754 [hep-ph].

[85] J. Gluza, K. Kajda, and T. Riemann, *AMBRE: A Mathematica package for the construction of Mellin-Barnes representations for Feynman integrals*, Comput. Phys. Commun. **177** (2007) 879–893, arXiv:0704.2423 [hep-ph].

[86] E. W. Barnes, *A new development of the theory of the hypergeometric functions*, Proc. Lond. Math. Soc. (2) **6** (1908) 141–177.

[87] I. Dubovyk, J. Gluza, and T. Riemann, *Non-planar Feynman diagrams and Mellin-Barnes representations with AMBRE 3.0*, J. Phys. Conf. Ser. **608** no. 1, (2015) 012070.

[88] J. Gluza, K. Kajda, T. Riemann, and V. Yundin, *Numerical Evaluation of Tensor Feynman Integrals in Euclidean Kinematics*, Eur. Phys. J. **C71** (2011) 1516, arXiv:1010.1667 [hep-ph].

[89] I. Gonzalez and I. Schmidt, *Optimized negative dimensional integration method (NDIM) and multiloop Feynman diagram calculation*, Nucl. Phys. **B769** (2007) 124–173, arXiv:hep-th/0702218 [hep-th].

[90] I. Gonzalez and V. H. Moll, *Definite integrals by the method of brackets. Part 1*, arXiv:0812.3356 [math-ph].

[91] I. Gonzalez, *Method of Brackets and Feynman diagrams evaluation*, Nucl. Phys. Proc. Suppl. **205-206** (2010) 141–146, arXiv:1008.2148 [hep-th].

[92] M. Prausa, *MellinBarnes meets Method of Brackets: a novel approach to MellinBarnes representations of Feynman integrals*, Eur. Phys. J. **C77** no. 9, (2017) 594, arXiv:1706.09852 [hep-ph].

[93] J. Gluza, T. Jelinski, and D. A. Kosower, *Efficient Evaluation of Massive Mellin-Barnes Integrals*, Phys. Rev. **D95** no. 7, (2017) 076016, arXiv:1609.09111 [hep-ph].

[94] P. Maierhöfer, J. Usovitsch, and P. Uwer, *Kira—A Feynman integral reduction program*, Comput. Phys. Commun. **230** (2018) 99–112, arXiv:1705.05610 [hep-ph].

[95] U. Aglietti and R. Bonciani, *Master integrals with one massive propagator for the two loop electroweak form-factor*, Nucl. Phys. **B668** (2003) 3–76, arXiv:hep-ph/0304028 [hep-ph].

[96] E. Remiddi and J. A. M. Vermaseren, *Harmonic polylogarithms*, Int. J. Mod. Phys. **A15** (2000) 725–754, arXiv:hep-ph/9905237 [hep-ph].

[97] D. Maitre, *HPL, a mathematica implementation of the harmonic polylogarithms*, Comput. Phys. Commun. **174** (2006) 222–240, arXiv:hep-ph/0507152 [hep-ph].

[98] Y. L. LUKE, *Chapter i - the gamma function and related functions*, in *Mathematical Functions and their Approximations*, Y. L. LUKE, ed., pp. 1 – 23. Academic Press, 1975. http://www.sciencedirect.com/science/article/pii/B9780124599505500055.

[99] T. Hahn, *Concurrent Cuba*, Comput. Phys. Commun. **207** (2016) 341–349.

[100] T. Hahn, *Concurrent Cuba*, J. Phys. Conf. Ser. **608** no. 1, (2015) 012066, arXiv:1408.6373 [physics.comp-ph].

[101] J. Shiers, *CERN Program Library*. http://cernlib.web.cern.ch/cernlib.

[102] K. Kölbig, *Programs for computing the logarithm of the gamma function, and the digamma function, for complex argument*, Comput. Phys. Commun. **4** no. 2, (1972) 221 – 226.

[103] R. Bonciani, P. Mastrolia, and E. Remiddi, *Master integrals for the two loop QCD virtual corrections to the forward backward asymmetry*, Nucl. Phys. **B690** (2004) 138–176, arXiv:hep-ph/0311145 [hep-ph].

[104] U. Aglietti and R. Bonciani, *Master integrals with 2 and 3 massive propagators for the 2 loop electroweak form-factor - planar case*, Nucl. Phys. **B698** (2004) 277–318, arXiv:hep-ph/0401193 [hep-ph].

[105] J. Gluza and T. Riemann, *A New treatment of mixed virtual and real IR-singularities*, PoS **RADCOR2007** (2007) 007, arXiv:0801.4228 [hep-ph].

[106] T. Hahn, *Generating Feynman diagrams and amplitudes with FeynArts 3*, Comput. Phys. Commun. **140** (2001) 418–431, arXiv:hep-ph/0012260 [hep-ph].

[107] A. von Manteuffel and R. M. Schabinger, *Numerical Multi-Loop Calculations via Finite Integrals and One-Mass EW-QCD Drell-Yan Master Integrals*, JHEP **04** (2017) 129, arXiv:1701.06583 [hep-ph].

[108] I. Dubovyk, *In preparation*. PhD thesis, Universität Hamburg, Hamburg, 2017.

[109] A. V. Smirnov and V. A. Smirnov, *On the Resolution of Singularities of Multiple Mellin-Barnes Integrals*, Eur. Phys. J. **C62** (2009) 445–449, arXiv:0901.0386 [hep-ph].

[110] S. Borowka, G. Heinrich, S. Jahn, S. P. Jones, M. Kerner, J. Schlenk, and T. Zirke, *pySecDec: a toolbox for the numerical evaluation of multi-scale integrals*, Comput. Phys. Commun. **222** (2018) 313–326, arXiv:1703.09692 [hep-ph].

[111] U. Aglietti, R. Bonciani, L. Grassi, and E. Remiddi, *The Two loop crossed ladder vertex diagram with two massive exchanges*, Nucl. Phys. **B789** (2008) 45–83, arXiv:0705.2616 [hep-ph].

[112] A. Djouadi and C. Verzegnassi, *Virtual Very Heavy Top Effects in LEP / SLC Precision Measurements*, Phys. Lett. **B195** (1987) 265–271.

[113] A. Djouadi, *$O(\alpha\alpha_s)$ Vacuum Polarization Functions of the Standard Model Gauge Bosons*, Nuovo Cim. **A100** (1988) 357.

[114] B. A. Kniehl, *Two Loop Corrections to the Vacuum Polarizations in Perturbative QCD*, Nucl. Phys. **B347** (1990) 86–104.

[115] B. A. Kniehl and A. Sirlin, *Dispersion relations for vacuum polarization functions in electroweak physics*, Nucl. Phys. **B371** (1992) 141–148.

[116] A. Djouadi and P. Gambino, *Electroweak gauge bosons selfenergies: Complete QCD corrections*, Phys. Rev. **D49** (1994) 3499–3511, arXiv:hep-ph/9309298 [hep-ph]. [Erratum: Phys. Rev.D53,4111(1996)].

[117] J. Fleischer, O. V. Tarasov, F. Jegerlehner, and P. Raczka, *Two loop $O(\alpha_s G_\mu m_t^2)$ corrections to the partial decay width of the Z^0 into $b\bar{b}$ final states in the large top mass limit*, Phys. Lett. **B293** (1992) 437–444.

[118] G. Buchalla and A. J. Buras, *QCD corrections to the $\bar{s}dZ$ vertex for arbitrary top quark mass*, Nucl. Phys. **B398** (1993) 285–300.

[119] G. Degrassi, *Current algebra approach to heavy top effects in $Z \to b\bar{b}$*, Nucl. Phys. **B407** (1993) 271–289, arXiv:hep-ph/9302288 [hep-ph].

[120] K. G. Chetyrkin, A. Kwiatkowski, and M. Steinhauser, *Leading top mass corrections of order $O(\alpha\alpha_s m_t^2/M_W^2)$ to partial decay rate gamma ($Z \to b\bar{b}$)*, Mod. Phys. Lett. **A8** (1993) 2785–2792.

[121] A. Czarnecki and J. H. Kuhn, *Nonfactorizable QCD and electroweak corrections to the hadronic Z boson decay rate*, Phys. Rev. Lett. **77** (1996) 3955–3958, arXiv:hep-ph/9608366 [hep-ph].

[122] R. Harlander, T. Seidensticker, and M. Steinhauser, *Complete corrections of $O(\alpha\alpha_s)$ to the decay of the Z boson into bottom quarks*, Phys. Lett. **B426** (1998) 125–132, arXiv:hep-ph/9712228 [hep-ph].

[123] L. Avdeev, J. Fleischer, S. Mikhailov, and O. Tarasov, *$\mathcal{O}(\alpha\alpha_s^2)$ correction to the electroweak ρ parameter*, Phys. Lett. **B336** (1994) 560–566, arXiv:hep-ph/9406363 [hep-ph]. [Erratum: Phys. Lett.B349,597(1995)].

[124] K. G. Chetyrkin, J. H. Kuhn, and M. Steinhauser, *Corrections of order $\mathcal{O}(G_F M_t^2 \alpha_s^2)$ to the ρ parameter*, Phys. Lett. **B351** (1995) 331–338, arXiv:hep-ph/9502291 [hep-ph].

[125] M. Awramik, M. Czakon, A. Freitas, and G. Weiglein, *Precise prediction for the W boson mass in the standard model*, Phys. Rev. **D69** (2004) 053006, arXiv:hep-ph/0311148 [hep-ph].

[126] D. d'Enterria, *Physics at the FCC-ee*, in *Proceedings, 17th Lomonosov Conference on Elementary Particle Physics: Moscow, Russia, August 20-26, 2015*, pp. 182–191. 2017. arXiv:1602.05043 [hep-ex].

[127] J. Gluza, *Present status on numerical calculation of complete 2-loop EWPOs and 3-loop prospects*, (2017) . https://indico.cern.ch/event/556692/.

Selbstständigkeitserklärung

Ich erkläre, dass ich die Dissertation selbständig und nur unter Verwendung der von mir gemäß §7 Abs. 3 der Promotionsordnung der Mathematisch-Naturwissenschaftlichen Fakultät, veröffentlicht im Amtlichen Mitteilungsblatt der Humboldt-Universität zu Berlin Nr. 126/2014 am 18.11.2014, angegebenen Hilfsmittel angefertigt habe.

Berlin, Oktober 23, 2017

Johann Usovitsch